Physical and Biochemical Strategies for Improving the Yield and Material Properties of Polyhydroxyalkanoate Biopolymers

A Thesis
SUBMITTED TO THE FACULTY OF
THE UNIVERSITY OF MINNESOTA

John Stephen Francis Barrett

IN PARTIAL FULFILLMENT OF THE REQUIREMENTS
FOR THE DEGREE OF
DOCTOR OF PHILOSOPHY

Friedrich Srienc, Advisor

October-2014

Acknowledgements

Foremost, I gratefully acknowledge the contributions made by the five undergraduate research assistants who helped me in completing the work presented in this thesis: Diego Escalante, Jordan Klussendorf, Caroline Lie, Peng Peng, Mitchell Armstrong, and Malcolm Davidson. While part of their work was funded by two UROP grants, the majority of time they spent was volunteered. Nevertheless, they persisted with me over multiple summers and semesters and even came to collect samples in the late hours of the night and on weekends. Despite their novice status, the consistent effort they provided was a real factor that enabled the depth of study presented in this thesis. On several occasions the insights and effort they provided was critical in the successful outcome of a project. In return, I tried to teach them well, and I think they're all better engineers for it. I hope that the knowledge and advice I provided them was commensurate with the help they provided me.

I also thank my academic advisor, Professor Friedrich Srienc. When I was asked to leave my former academic lab after 4 years of graduate study, I wasn't sure if a Ph.D degree from the University of Minnesota, or from anywhere, could still be salvaged. Obviously, I was anxious how future employers might view my record; nevertheless, Friedrich agreed to give me a chance. Over the years, I observed that this was the approach he took with people in general, saying "yes" more often than "no", which I think is something to be admired. He was infinitely patient with me and respected my scientific opinion when I pursued experimental approaches that were different than his own, i.e. almost enough rope to hang any ambitious graduate student. When I achieved successes, he lauded them more than he criticized my mistakes. Our professional relationship has worked well for me.

In my various life experiences, I have learned that not everyone who is knowledgeable about something wants to teach you what they know, … and that's ok. So, when I do have the privilege of learning from a good teacher, I am truly grateful. My previous advisor, Dr. Jennifer Maynard, who first taught me the basics of molecular cloning, was both a knowledgeable and generous teacher.

I also thank my professional collaborator, Professor Ahmed Abdala, whom I had the privilege to meet when I traveled to the Petroleum Institute in Abu Dhabi, UAE. He is a kind, intelligent, and diligent man and was the impetus for the PHA-graphene nanocomposite study presented in this thesis. As a major contributing author to my very first, manuscript, his expertise in polymer science and hands-on assistance in several of the experiments are especially appreciated.

Furthermore, I acknowledge the contributions of Mr. Dan Rouse, a former graduate of the Srienc lab, who was responsible for the biosynthesis and initial purification of the PHA_{mcl} copolymers used for the PHA-graphene nanocomposites.

I also acknowledge Mr. Hussain Arwani (an undergraduate research assistant at the Petroleum Institute visiting from the University of Waterloo) for his assistance in preparation and characterization of nanocomposite samples, Dr. Fang Zhou of the UMN Characterization Facility who patiently instructed me in use of the cryomicrotome and TEM; and Dr. David Giles of the UMN Polymer Characterization Lab who assisted in the collection of polymer molecular weight data.

I thank my lab-mates, Mr. Dan Rouse, Dr. Pedro Pena, Dr. Luz Perez, and Ms. Gilsinia Lopez, for teaching me, helping me troubleshoot problems, taking early morning samples, and sharing their stock solutions.

In my work with the autotrophic cultivation of *Ralstonia eutropha*, I gratefully acknowledge the contributions by Dr. Luz Perez whose collaboration and knowledge in microbiology were very helpful during the time when we were trying to develop a reliable technique for autotrophic growth and seed transfers. Furthermore, the mathematical model that is used in this thesis to describe the autotrophic metabolism of *R. eutropha* has been extensively researched and verified by Dr. Perez and her predecessor, Ms. Gilsinia Lopez.

For his help in identifying of PHA_{mcl} monomers via GCxGC-TOF mass-spectroscopy, I acknowledged the expertise and patience of Dr. Tom Crick of the Center for Mass-Spectroscopy and Proteomics, at the University of Minnesota.

For their extensive knowledge of microbial cultivations, of which I frequently inquired, and for always turning a blind eye when I had to borrow various tubing

connectors, pump heads, and valves from their stock of spare parts, I acknowledge the staff of the University of Minnesota, Biotechnology Resource Center.

For generously providing the pCDFBB-eGFP cloning vector and developing the modular cloning technique used to generate the pCDFBB-*phaJ* plasmid, I acknowledge the laboratory of Dr. Claudia Schmidt-Dannert.

Both the graphene-nanocomposite study and the study of autotrophic cultivation in *R. eutropha* were financially supported by the Abu Dhabi Minnesota Institute for Research Excellence (ADMIRE).

Lastly, I acknowledge those people whose close, personal support and encouragement made life worth living during the past 9 years: Nichole, Annika, James, Linda, Davetta, William, Mary Florence, Tom, Bhanu, Kay, Bob, Ruth, Dick, and Matt: I love you all.

Dedication

This thesis is dedicated to my mother, Linda Francis, for giving me the curiosity and inspiration to start such big projects, and to my father, James Barrett, for giving me the persistence and encouragement to finish them.

Abstract

Polyhydroxyalkanoates (PHAs) are a diverse class of microbially synthesized biopolymers that are valued for their synthesis from renewable feedstocks and rapid biodegradation. As such, the commercial development of PHA plastics has potential to reduce the environmental impact of many, current polymers, which are non-biodegradable and rely on the use of unsustainable petroleum feedstocks But despite the desirable traits of PHAs, the proliferation of these materials into commercial markets remains slow. Part of this is due to the greater cost of the renewable substrates used for PHA production versus the artificially low cost of petroleum-derived feedstocks. The other part of the challenge of promoting PHA utilization owes to the relatively limited diversity of physical and mechanical properties of PHAs that are currently available. As such, additional work is needed to develop new PHAs, which can satisfy the performance characteristics of many polymers already in use.

Motivated by these two main challenges—1.) to lower the production cost of PHAs and 2.) to broaden the range of unique PHAs materials available, the thesis presented herein details the development of new technologies to increase the substrate-to-product yield of PHA production and to expand the range of physical and mechanical properties of PHA-based materials.In Chapter1 we give a broad introduction to polyhydroxyalkanoates and discuss various aspects of their production and application. In recent years, a new vein of research has opened up, which seeks to apply the technology of block-copolymers to PHAs in order to expand the diversity of properties available. As we highlight in Chapter 2, the application of block-copolymer technology to PHAs presents a rich source for scientific discovery and technological development.

For our experimental studies, we explore PHA production using a varity of organic feedstocks including glucose, glycerol, fatty acids, and CO_2. To achieve these conversions we employ a diversity of biosynthesis capabilities from microorganism including wild-type *Pseudomonas oleovorans,* wild-type *Ralstonia eutropha*, and recombinant *Escherichia coli*. A description of the various methods is given in Chapter 3. The experimental results are given in Chapters 4, 5, and 6, which focus generally upon: 4.) production of PHA copolymers in recombinant *E. coli ,* 5.) fabrication and testing of

PHA-graphene nanocomposites using PHA_{mcl} produced by *P. oleovorans* and 6.) production of PHA copolymers and block-copolymers directly from CO_2 using *Ralstonia eutropha*.

More specifically, we demonstrate two technologies to enhance polymer yield. 1.) by employing mathematical models of cell metabolism to aid in design, we introduce recombinant pathways into *Escherichia coli* to increase product flux and make gene-knockouts within the *E. coli* chromosome to eliminate competing side-reactions, and 2.) by using the mixotrophic capabilities of *Ralstonia eutropha,* we show how mass-spectroscopy-based feed-back control can be used to operate PHA production processes that achieve the CO_2- neutral conversion of a heterotrophic substrate. In this process, energy derived from the co-feeding of hydrogen gas is used by the cells to fix residual CO_2 that is typically emitted as a waste product during purely heterotrophic fermentations.

For the purpose of improving PHA properties, we demonstrate three technologies 1.) Via protein engineering, we expand the substrate specificity of the PHA synthase enzyme from *Pseudomonas oleovronas* to permit the synthesis of novel PHA copolymers containing disparate monomer types of both short-chain-length PHA (PHA_{scl}) and medium-chain-length PHA (PHA_{mcl}), thereby providing a basis for unique PHA copolymers. 2.) By incorporating graphene nanoparticles into elastomeric PHAs produced by *P. oleovorans,* we create composite materials, which show significant improvements in elastic modulus and electrical conductivity. 3.) Using the mixotrophic capabilities of *R. eutropha* we synthesize both random and block-copolymer molecules of PHA using CO_2 as a major substrate. With the use of mass-spectrocopy for real-time monitoring of cellular metabolims, we are able to make precise adjustments to the size and composition of molecular domains within PHA block-copolymers and correlate these with the physical and mechanical properties we observe.

Final conclusions and prospects for future PHA research and developemnt are given in Chapter 7. Taken all together, this thesis provides a solid foundation in theory and practice, for several technological approaches, which have great potential to promote the commercial proliferation of this valuable class of renewable plastics.

Table of Contents

List of Tables

List of Figures

Chapter 1 Polyhydroxyalkanoates

Information in this chapter has been reproduced in part with permission from the following source:

Barrett, J. S. F. and Srienc, F., "Green Chemistry for the Production of Biodegradable, Biorenewable, and Biocompatible Polymers", In Biocatalysis for Green Chemistry and Chemical Process Development, Eds. J. (Alex) Tao and R. Kazlauskas, 2011, John Wiley & Sons, Inc., Hoboken, NJ, USA.

Introduction

Petroleum derived plastics are ubiquitous in human society; however, their production from nonrenewable resources, contribution to greenhouse gas emissions, and permanent presence in the environment after discard demand an alternative solution, which is both environmentally friendly and sustainable. Biodegradable plastics derived from renewable sources offer an attractive alternative. The information contained in this chapter is a broad-scope review discussing the science and technology associated with the production and application of bioplastics. Specifically the review focuses on polyhydroxyalkanoates and polylactide. We discuss the mechanical properties of these plastics, the technologies used to enhance them, and the types of application for which they are suitable. Additionally we detail synthesis routes for creating these materials both *in vivo* and *in vitro*. Because bioplastics are currently more expensive than petroleum derived plastics, we consider the use of alternative feedstocks and processing technologies which may help to reduces costs. Lastly we discuss polymer recovery and purification processes and their impact on product cost and the environment.

Biopolymers

Biopolymers are an exciting topic that sits at the intersection of several areas of study including: biocatalysis, green chemistry, microbiology, and material science. Such compounds are considered desirable for their biodegradability, biocompatibility, and capacity for synthesis from renewable feedstocks. Furthermore biopolymers are aptly named because a biocatalysis step is usually implemented at some point in their production whether it is for the synthesis of feedstocks or the polymerization step itself. Biopolymers are ubiquitous in nature and include such compounds as nucleic acids, polypeptides, and cellulose. Biopolymers for commercial applications as plastics include starch based plastics, poly lactic acid, polyhydroxyalkanoates, polyurethanes from vegetable oil derived polyols, and polyethylene synthesized from bio-derived ethanol. In this chapter we will focus mainly on the polyhydroxyalkanoates (PHA) and their applications. We will also give a short discussion about the synthesis of polylactic acid.

Polyhydroxyalkanoates

Polyhydroxyalkanoates occur naturally and are found in a wide range of microorganisms which use them to store excess carbon and energy in preparation for times of nutrient limitations [1]. The polymers are formed within the cell as large insoluble inclusions surrounded by a lipid monolayer [2]. In the case of PHA, polymerization occurs by the action of a polymerase enzyme which catalytically adds monomers to a growing polymer chain. Commercial production of PHA is carried out by microbial fermentation using a variety of feedstocks.

PHA is a polyester because the monomers that comprise PHA are linked by oxoester bonds. The key enzyme for PHA synthesis is the PHA synthase. This enzyme polymerizes (*R*)-3-hydroxyacyl-CoA thioester monomers into polyhydroxyalkanoate with the release of coenzyme-A[3]. A broad diversity of monomer types exists in nature, and more than 120 have been discovered [4]. Within the broad class of polyhydroxyalkanoates, the polymers are further classified according to the number of carbon atoms within monomer units that comprise them. PHA made of monomers containing 3-5 carbon atoms are referred to as PHA_{scl} (short chain length) while those made of monomers

containing 6-14 carbon atoms are referred to as PHA_{mcl} (medium chain length). PHA_{scl} polymers include polyhydroxybutyrate (PHB) and polyhydroxyvalerate (PHV). PHA_{mcl} polymers include polyhydroxyhexanoate (PHH) and polyhydroxyoctanoate (PHO). See **Figure 1.1**.

The division of PHA into these two subclasses of PHA_{scl} and PHA_{mcl} arises from the substrate specificity of the polymerase enzymes used to synthesize the polymers. For example the organism *Ralstonia eutropha* contains a polymerase enzyme (*phbC)* that accepts (*R)*-3-hydroxyacyl-CoA substrates that contain from 3 to 5 carbons only [5]. In contrast the organism *Pseudomonas oleovorans* contains a different polymerase enzyme (*phaC1*) that has specificity for longer (*R)*-3-hydroxyacyl-CoA substrates containing 6-14 carbon atoms [6]. Furthermore this distinction between monomer specificity is so prevalent that whole classes of synthase genes from various organisms have been catalogued accordingly [3]. While many polymerases fall within these two categories, some polymerases have been identified which demonstrate specificity for both scl and mcl type monomers[7-12].

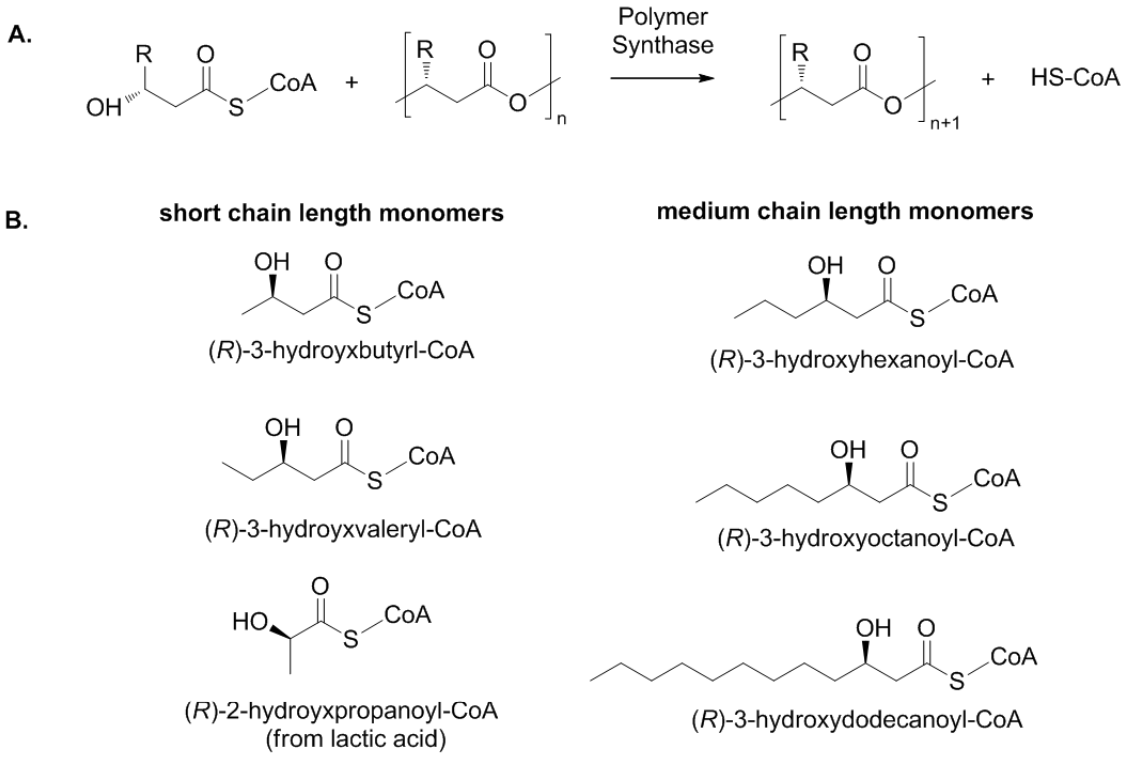

Figure 1.1 Polyhydroxyalkanoate biosynthesis
a. Polymerization via PHA synthase. **b**. Various hydroxyalkanoate monomers. **c**. Polyhydroxyalkanoate granules in Ralstonia eutropha.

Engineering Polymer Properties

Within the field of polymer engineering scientists have created a wide variety of materials exhibiting a range of physical properties, which in turn dictate the types of technological applications for which a polymer is suited. Important physical properties include polymer strength, stiffness, toughness, elasticity, and thermoplasticity. Strong materials can withstand heavy loads before failure. Stiff materials support this load with little or no strain i.e. distortion of shape. Steel is a strong and stiff material. If upon loading the distortion occurs suddenly and causes catastrophic fracture, such materials are considered brittle. Glass is a strong but brittle material. Tough is the opposite of brittle. If sufficient load is applied to a tough material permanent deformation will occur, but the material can undergo significantly more strain before catastrophic failure. Kevlar and Nylon are tough materials. Elastomeric materials can undergo a large strain without permanent deformation. Rubber is an elastomer. Thermoplastic materials easily undergo plastic deformation at high temperature but regain stiffness upon cooling.

For practical applications the distinction between PHA_{scl} and PHA_{mcl} is important, as monomer composition can greatly affect the material properties of the resulting polymer. The properties of polyhydroxyalkanoates are similar to those of conventional petroleum derived polyesters. In general, homopolymers of PHA_{scl} polymers are strong and stiff thermoplastics that are brittle with a high melting temperature. In contrast PHA_{mcl} polymers are more elastomeric, have a lower melting temperature, and are tougher when subjected to shock and shearing stresses. See **Table 1.1** for a comparison of polymer properties.

One factor greatly affecting a polymer's physical performance is molecular weight which correlates directly with polymer chain length. Increasing the molecular weight of a polymer chain usually results in a higher softening temperature and increased toughness [13]. In 1997 Sim et al. observed in recombinant *E. coli* producing PHA that the expression of additional pha synthase molecules was inversely correlated with polymer molecular weight[14] thus providing a tool for controlling polymer properties. In 2002 researchers produced PHB samples of varying molecular weights by controlling the aeration rate to a culture of *Azotobacter chroococcum* 6B. Testing of the polymer

samples showed that tensile strength increased with increasing polymer molecular weight [15].

Table 1.1 Polymer Properties.

Polymer	Melting Temp. (°C)	Young's Modulus (GPa)	Tensile Strength (MPa)	Elong. at Break (%)	Ref. (#)
PHB	175–180	3.5-4	40	3-8	[17-18]
PHB					[15]
MW = 445 kDa	-	-	38	-	
MW = 1000 kDA	-	-	113	-	
MW = 1240 kDA	-	-	215	-	
Poly(3HB-co-3HV)					[19]
0 mol % 3HV	179	3.5	40	-	
3 mol %	170	2.9	38	-	
9 mol %	162	1.9	37	-	
14 mol %	150	1.5	35	-	
20 mol %	145	1.2	32	-	
25 mol %	137	0.7	30	-	
Poly(3HB-co-3HV)					[20-21]
8 mol % 3HV (random)	151	0.260	18	15	
29 mol % 3HV (random)	101	0.210	18	15	
15 mol % 3HV (block)	164	0.210	28	90	
23 mol % 3HV (block)	161	0.150	15	175	
Poly(3HB-co-4HB)					[22-23]
0 mol % 4HB	-	0.860	43	5	
3 mol % 4HB	166	0.850	28	45	
10 mol % 4HB	159	0.560	24	242	
16 mol % 4HB	-	0.271	26	444	
64 mol % 4HB	50	0.030	17	591	
78 mol % 4HB	49	0.024	42	1120	
82 mol % 4HB	52	0.045	58	1320	
90 mol % 4HB	50	0.100	65	1080	
100 mol % 4HB	53	0.149	104	1000	
Polyhydroxyoctanoate (PHO)	61	-	6-10	300-450	[24]
Poly Lactic Acid (PLA)					[25]
L-PLA	145-186	1.2-3.0	28-50	2-6	
L,D-PLA	-	1.9-2.4	29-35	5-6	
Conventional polymers					[26]
Polypropylene (PP)	160-175	1.1-1.6	31-41	100-600	
High density polyethylene (HDPE)	130-137	1.1	22-31	10-1200	
Low density polyethylene (LDPE)	98-115	0.2-0.3	8.2-31	100-650	
Polyethylene terephthalate (PET)	212-265	2.8-4.1	48-72	30-300	
Polycarbonate (PC)	150 (Tg)	2.4	63-72	110-120	
Polystyrene (PS)	74-104 (Tg)	2.3-3.3	36-52	1.2-2.5	
Nylon-66	255-265	1.6-3.4	75.8	150-300	

Adapted from van der Walle etal. [16]

Another common approach for enhancing polymer performance is by blending two different polymers to make a novel compound with hybrid mechanical properties e.g. a polymer that is stiff and strong yet tough against impact and tearing. Polymer blending is a suitable practice when the types and amounts of polymer used readily form a homogeneous solution or are combined in a stable dispersion. Polymer blends containing polyhydroxyalkanoates have been explored with various materials including: starch[27], rubber[28], and polylactide[29-30]. Composite plastics utilizing polyhydroxyalkanoates have also been created using montmorillonite clay [31], single-wall carbon nanotubes[32].

In some cases however the polymers may be chemically dissimilar e.g. containing hydrophobic and hydrophilic moieties which results in phase separation of the two polymers[33]. One way to prevent phase separation is by linking the two different polymers using a covalent bond. These types of molecules are called copolymers. The polymer may consist of short repeats or long repeats of each monomer which may be ordered periodically or randomly e.g. DNA is a copolymer of the nucleotides A, G, C, and T in an irregular order. When a single monomer type occurs in a long repeat followed by long repeat of the alternate polymer such molecules are called block copolymers. Depending on the size of the homogeneous domains within the chain, the copolymer may undergo microphase separation to form periodic mesostructures. This additional level of structural order can be useful for a variety of technical applications. For more common synthetic polymers numerous structures have been observed experimentally and include micelles, vesicles, cylinder arrays, sphere arrays, continuous phase gyroids, and lamellae [34]. Micelles and vesicles are useful for applications in drug delivery and particle encapsulation. Continuous phase gyroids are good for mechanical applications because of their ability to stop crack propagation, similar to how ripstop nylon prevents tears from propagating in fabric. Spherical domains, arrayed on either a body-centered or face-centered lattice, are useful for applications such as photonic crystals. Cylinder arrays and lamellae can serve as templates for patterning other materials with ordered mesostructures. Continuous phase gyroids, cylinder arrays, and lamellae offer useful structures for designing polymer materials with unique transport properties.

PHA Copolymers

In light of the potential benefits of copolymer architecture on material properties and applications much work in the field of polyhydroxyalkanoates has focused on the production of copolymer molecules[6, 35-37]. Such polymers can arise when an organism simultaneously consumes two separate substrates [38] or when successive rounds of metabolic cycles e.g. fatty acid β-oxidation or fatty acid de novo biosynthesis generate multiple monomer types from the same starting material [6]. One example of a PHA copolymer is poly(3-hydroxybutyrate-co-3-hydroxyvalerate) (PHBV) which can be synthesized from *Ralstonia eutropha* via the simultaneous feeding of metabolic precursors fructose and valerate [38]. Synthesis of this particular polymer is possible because the *phbC* synthase accepts both the (R)-3-hydroxybutyrate and (R)-3-hydroxyvalerate substrates which are both scl type monomers. The polymer synthase of *Pseudomonas oleovorans* which is known to have specificity for mcl type monomers produces poly(3-hydroxyhexanoate-co-3-hydroxyoctanoate) (PHBHO) when cultured on octane as the soul carbon source [6]. For the synthesis of copolymers containing both scl and mcl monomer types, researchers have found some enzymes with broader specificity capable of accepting both monomer types and producing such polymers as poly(3-hydroxybutyrate-co-3-hydroxyhexanoate). PHA synthase enzymes with broad substrate specificity have been found in *Aeromonus caviae, Aeromonas hydrophila, Pseudomonus* sp. 61-3*, Pseudomonas stuzteri*, *Nocardia coralline*, and *Bacillus sp.* 88D[7-10]. Furthermore, using the techniques of protein engineering, e.g. random mutagenesis and site-directed mutagenesis, researchers have been able to create novel broad specificity polymerases showing enhanced affinity toward scl type monomers[11-12].

For the types of copolymers described above the sequence of monomers is random; however, as discussed earlier, block-copolymers with their ordered microstructure offer new possibilities for unique technical applications. To achieve the desired block organization some type of sequential substrate feeding is usually employed. In 2006 Pederson et al. synthesized block copolymers of polyhydroxybutyrate and polyhydroxvalerate (PHB-b-PHV) by periodic feeding of pentanoic acid to *Ralstonia eutropha* cultured on fructose as a primary carbon source[21] [21]. Additionally they

demonstrated that measurements of oxygen uptake rate and carbon dioxide evolution rate could be used to indicate the consumption of specific substrates in the batch thereby allowing for feedback control of substrate addition. Later McChalicher and Srienc performed extensive physical testing of these PHB-b-PHV block copolymers and compared them to random copolymers of the same monomers. Upon aging the block copolymers showed superior toughness versus the random copolymers [20] A similar demonstration of block copolymer synthesis via alternate substrate feeding was also made in 2008 by Pereira et al.[39] Recognizing the importance of process control strategies for manipulating polydispersity and copolymer organization, Mantzaris et al. utilized population balance modeling to predict the optimal period for substrate feeding [40]. Later Jurasek and Marchessault created a computer simulation based on a highly mechanistic model of PHB granule assembly. The model was able to predict such statistics of granule size, number, polymer molecular weight, and polydispersity as a function of gene expression levels of polymerase, depolymerases, and phasins[41]. More recently Iadevaia and Mantzaris presented modeling results suggesting that block copolymer organization could be controlled by the use of synthetic gene networks designed to control transient expression of genes necessary for monomer synthesis. In this way both monomers could be transiently produced using a single carbon source. In one network design monomer switching was controlled via the addition of external inducer molecules [42], while an alternate device coupled monomer switching to a genetic device capable of generating stable oscillations[43].

Monomer Supply Pathways in Native PHA Producing Organisms

In addition to studies focused on the polymerization process considerable effort has also been made to uncover the enzymatic pathways involved in the conversion of feedstocks to polymer precursors. These pathways are linked to both catabolic and anabolic processes within the cell. For the synthesis of mcl (*R*)-3-hydroxyacyl-CoA substrates the most direct route is through the catabolism of fatty acids and alkanes. This is accomplished via the β-oxidation pathway which is a primary supply of PHA_{mcl} monomers in *Pseudomonads*. Various intermediates of this pathway can be converted to

PHA monomers [44]. For the production of mcl monomers from unrelated carbon sources such as glucose and gluconate, a *phaG* gene coding for an (*R*)-3-hydroxyacyl transferase (ACP to CoA) has been identified in *Pseudomonas spp.*[45-46]. This enzyme allows the organism to convert (*R*)-3-hydroxyacyl-ACP, an intermediate of fatty acid synthesis, directly to the polymer precursor, (*R*)-3-hydroxyacyl-CoA. For the production of the scl substrate, (*R*)-3-hydroxybutyrl-CoA, the organism, *Ralstonia eutropha,* has developed a particularly direct pathway [47]. This route involves the expression of two additional genes, *phbA,* a β-ketothiolase and *phbB,* an acetoacetyl-CoA reductase, which converts acetyl-CoA to PHB monomers in only two steps.

Metabolic Pathways in Recombinant Escherichia coli

In addition to production of PHAs in native host strains, e.g. *Pseudomonas oleovorans* and *Ralstonia eutropha*, researchers have also investigated PHA synthesis using recombinant systems. The industrial workhorse, *Escherichia coli*, is an ideal candidate for metabolic engineering because of its sequenced genome, well studied metabolism, and rapid growth rate. The capacity to synthesize polyhydroxyalkanoates requires two specific activities: (i) the ability to synthesize monomer precursors from either related or unrelated carbon sources and (ii) the ability to catalyze the formation of oxoester linkages between monomers. Wild type *E. coli* does not naturally produce PHAs and so attempts at recombinant expression have required the inclusion of both a polymerase gene as well as additional metabolic engineering to increase monomer substrate production. A thorough review of polyhydroxyalkanoate production in recombinant *E. coli* is provided by Li et al. [8]. Here we provide a summary of the topic along with relevant figures.

Production of PHB

For the production of PHB researchers have achieved success by cloning the PHB biosynthesis genes from both *Ralstonia eutropha* and *Alcaligenes latus* among others [48-49]. In each case three specific genes are essential: *phbA*, a β-ketothiolase enzyme for the conversion of two acetyl-CoA to a single acetoacetyl-CoA molecule, *phbB,* a reductase enzyme for the conversion of acetoacetyl-CoA to (R)-3-hydroxybutyryl-CoA, and *phbC*,

a polymer synthase enzyme. Alternatively Taguchi et al. produced PHB from glucose using a *phaC* gene from *Aeromonas caviae* along with overexpression of the *E. coli* protein, 3-ketoacyl-ACP synthase III (FabH). The authors proposed that the transacylating activity of the enzyme could convert (*R*)-3-hydroxybutryl-ACP, an intermediate of fatty acid *de novo* synthesis to the proper (*R*)-3-hydroxybutryl-CoA substrate [50]. In an alternate synthesis route Taguchi et al. showed that the native *E. coli* gene, 3-ketoacyl-ACP reductase (FabG) also had activity toward analogous CoA-tagged substrates thus allowing the conversion of the β-oxidation intermediate 3-ketoacyl-CoA to the polymer precursors, (*R*)-3-hydroxyacyl-CoA including scl monomer, (*R*)-3-hydroxybutryl-CoA [51]. **Figure 1.2** shows some of the main metabolic pathways by which PHB can be synthesized.

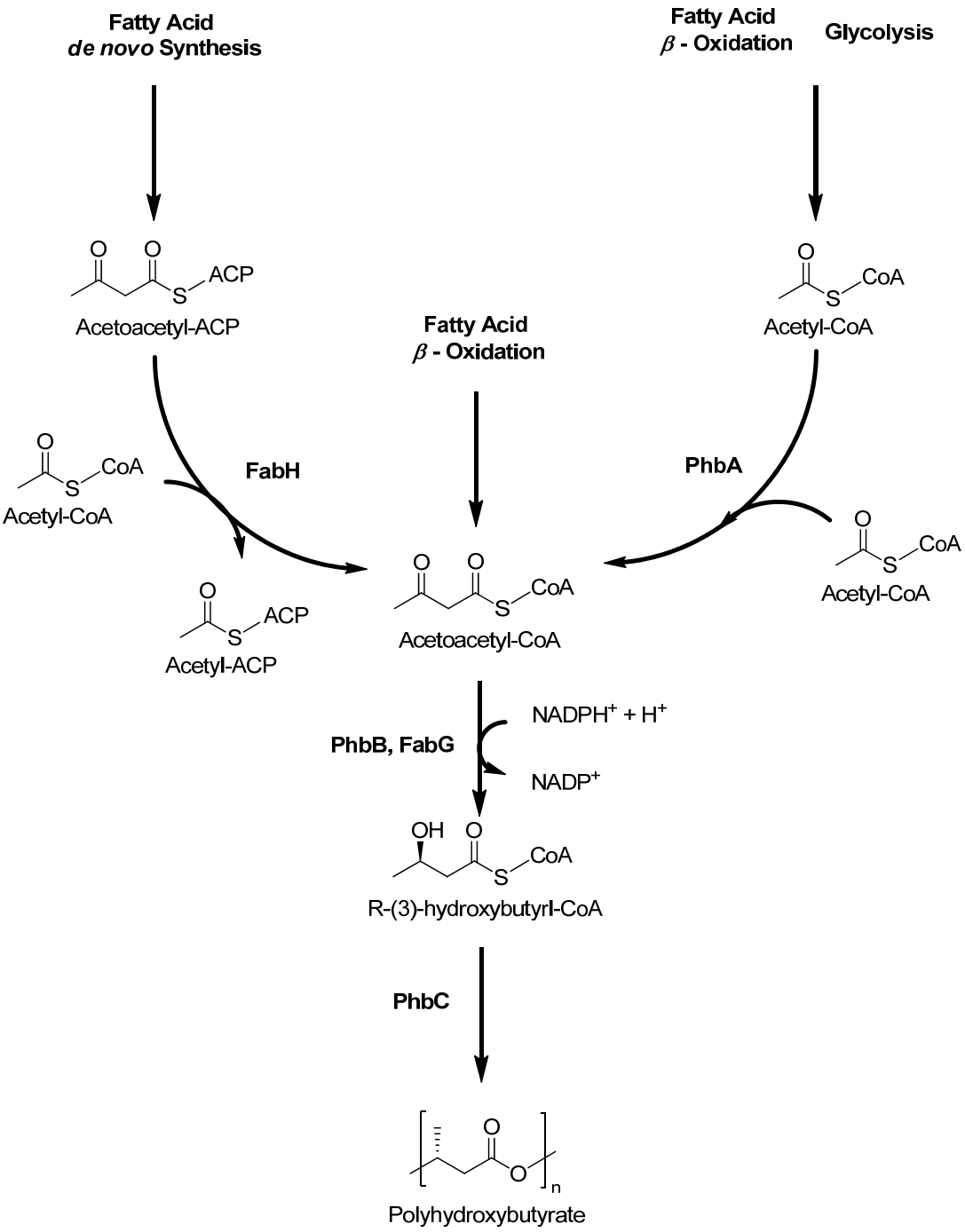

Figure 1.2 Metabolic pathways involved in PHB synthesis
Included are those in native PHA producing organisms and recombinant *E. coli*: FabH, 3-ketoacyl-ACP synthase III, FabG, 3-ketoacyl-ACP reductase, (*E. coli)*; PhbA, β-ketothiolase, PhbB, acetoacetyl-CoA reductase, PhbC, type I polymer synthase (*Ralstonia eutropha).*

Production of PHA$_{mcl}$

For the production of PHA$_{mcl}$ in *E. coli* researchers inserted a type II mcl synthase from *Pseudomonas aeruginosa.* *E. coli* cells harboring only the synthase gene produced minimal PHA$_{mcl}$ [52]; however, when the gene was inserted into a *fadB* mutant deficient in β-oxidation PHA synthesis increased significantly[53-54]. Later the same authors demonstrated that addition of acrylic acid, a know inhibitor of fatty acid β-oxidation, increased the production of PHA$_{mcl}$ [55]. In *E. coli* the *fadB* gene codes for enoyl-CoA hydratase which converts enoyl-CoA to (S)-3-hydroxyacyl-CoA, another intermediate of the β-oxidation cycle; however, the polymer synthase enzyme only accepts (R)-3-hydroxyacyl-CoA substrates. By knocking out this pathway via the *fadB* deletion the conversion of enoyl-CoA was shunted away from the unusable S-enantiomer. In *P. aeruginosa* the production of the usable, *R*-configuration 3-hydroxyacyl-CoA monomers has been attributed to an R-specific enoyl-CoA hydratase (PhaJ1) [56-57]. In *E. coli* a homologous enzyme, MaoC, has been linked to PHA synthesis and is believed to be a new enoyl-CoA hydratase with increased selectivity for producing (R)-3-hydroxyacl-CoA [58] . Furthermore other researchers showed that *P. aeruginosa* contained at least 4 different PhaJ proteins with unique specificities for various enoyl-Co substrates. Individually cloning each *phaJ* gene in recombinant *E. coli* with the *P. sp.* 61-3 synthase produced PHA with varying proportions of even number mcl monomers when the cells were fed with sodium dodecanoate [59]. Additionally Taguchi et al. demonstrated that the *E. coli* gene for 3-ketoacyl-ACP reductase, *fabG*, also showed activity in the conversion of 3-ketoacyl-CoA, another β-oxidation intermediate, to (R)-3-hydroxyacyl-CoA monomers. Overexpression of this gene along with a synthase gene, *phaC1*, form *Pseduomonas sp.* 61-3 in *E. coli* strain HB101 resulted in the accumulation of PHA$_{mcl}$ [51]. In 2001 Rehm et al. engineered *E. coli* to produce PHA$_{mcl}$ via the fatty acid *de novo* biosynthesis pathway from the unrelated carbon source gluconate. This was done by the recombinant expression of the *phaG* gene from *P. putida* coding for a transacylase enzyme capable of converting (R)-3-hydroxyacyl-ACP, a fatty acid *de novo* synthesis intermediate, to (R)-3-hydroxyacyl-CoA monomers [60]. In another attempt to derive mcl monomers from unrelated carbon sources Rehm et al. inserted an acyl-ACP thioesterase from *Umbellularia californica* into *E. coli* mutants deficient in the β-oxidation pathway.

The enzyme which shows enhanced selectivity for ACP thioesters over CoA thioesters, was able to convert lauryl-ACP, a 12 carbon intermediate of the fatty acid *de novo* synthesis directly to lauric acid which was subsequently converted to PHA_{mcl} via truncated fatty acid β-oxidation [61].

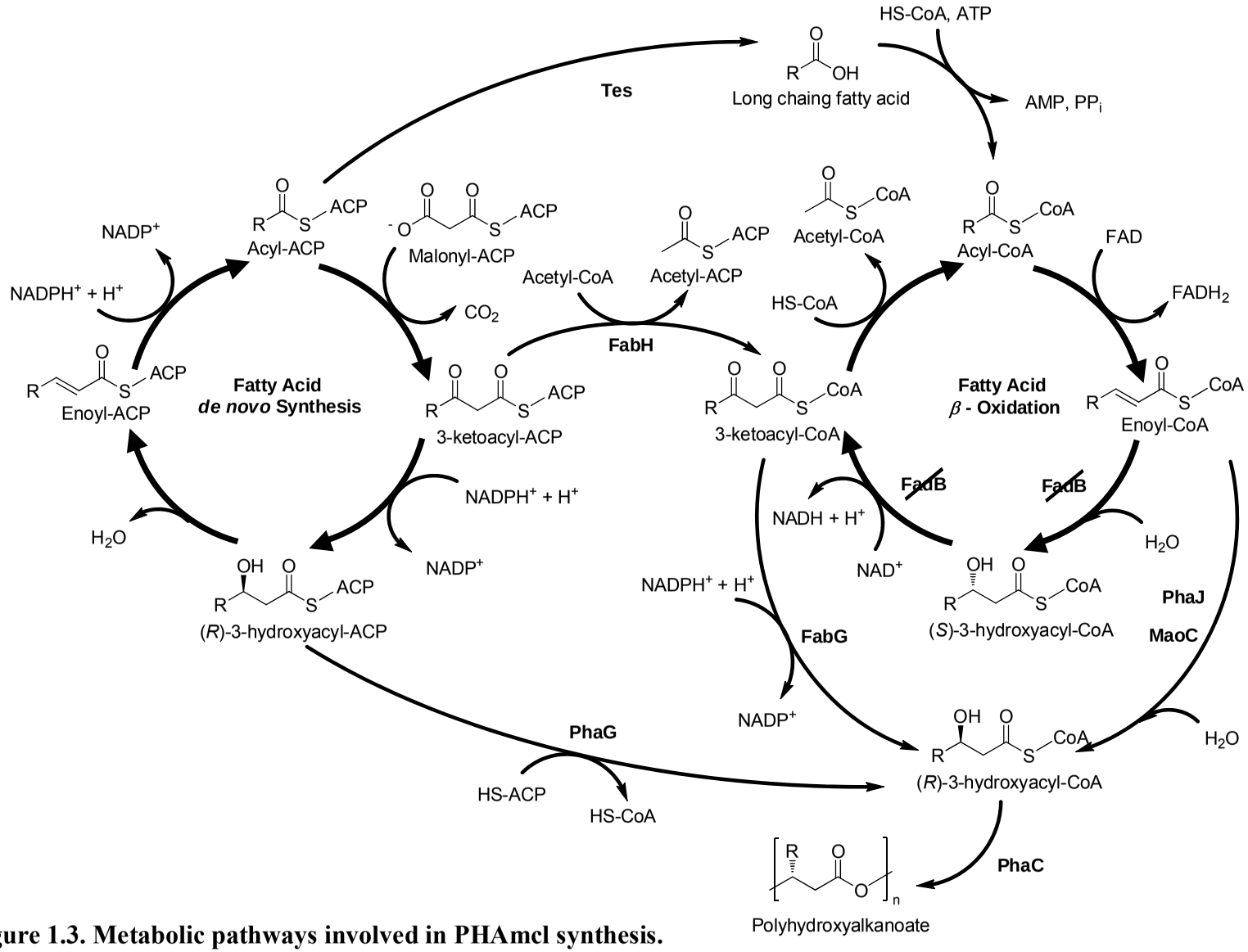

Figure 1.3. Metabolic pathways involved in PHAmcl synthesis.

Figure 1.3 Metabolic pathways involved in PHAmcl synthesis
(see previous page)Pathways included are those in native PHA producing organisms and recombinant *E. coli*. FadB, enoyl-CoA hydratase, 3-hydroxyacyl-CoA dehydrogenase, FabH, 3-ketoacyl-ACP synthase III, FabG, 3-ketoacyl-ACP reductase, MaoC, *R*-specific enoyl-CoA hydratase, (*E. coli*); PhaJ, *R*-specific enoyl-CoA hydratase, (*P. aeruginosa*) ; PhaG, (*R*)-3-hydroxyacyl-ACP to (*R*)-3-hydroxyacyl-CoA transacylase, (*P. putida*); Tes, acyl-ACP thioesterase, (*U. californica*); FabG, 3-ketoacyl-ACP reductase, PhaC, type II polymer synthase, (*P. sp.* 61-3).

Production of PHA_{scl} -co-PHA_{mcl}

As discussed previously, copolymers comprised of both PHA_{scl} and PHA_{mcl} have distinct advantages over conventional homopolymers. To generate such compounds requires synthase enzymes with broad substrate specificity for both scl and mcl type monomers as well as metabolic pathways for producing each monomer. Synthesis of both scl and mcl precursors may be obtained from the same fatty acid starting material through a truncated β-oxidation cycle as described earlier. As β-oxidation progresses mcl enoyl-CoA molecules are reduced by two carbons every time a cycle is completed, eventually creating scl enoyl-CoA molecules. Then the action of an (R)-specific enoyl-CoA hydratase (PhaJ) catalyzes the formation of (R)-3-hydroxyacyl-CoA monomers from the enoyl-CoA precursors. In one case a single PhaJ may have specificity for both scl and mcl enoyl-CoA molecules[62-63]. In other case multiple PhaJ*s* may act uniquely on enoyl-CoA molecules of different length[59]. Utilization of fatty acids with an even number of carbons produces (R)-3-hydroxyacyl-CoA monomers with an even number of carbons; while, utilization of fatty acids with an odd number of carbons produces odd numbered PHA monomers. Due to the cyclic nature of β-oxidation and fatty acid synthesis which produces successively smaller or larger substrates, respectively, the copolymers produced often contain a broad range of monomer types[6, 64]. See **Figure 1.4**. In 2004 Nomura et al. demonstrated that coexpression of a mutated 3-Ketoacyl-ACP Synthase III (*fabH*) with expanded substrate specificity along with a polyhydroxyalkanoate synthase, *phaC1*, gene of *Pseudomonas* 61-3 resulted in the production of PHA_{scl}-PHA_{mcl} copolymers utilizing glucose as a substrate [65]. Continuing with their investigation they then showed that the additional overexpression of 3-ketoacyl-ACP reductase (*fabG*) from either *E. coli* or *Pseudomonas sp.* 61-3 could be used to control the composition of PHA_{mcl} within the

copolymer [66-67]. In an alternate approach to copolymer synthesis Park and Lee combined the *phaAB* genes of *Ralstonia eutropha* along with the PHA synthase gene of *P. sp.* 61-3 in mutant *E. coli* strains deficient in the β-oxidation pathway. When the cells were cultured on a mixture of gluconate and decanoate expression of the *phaAB* genes allowed the cells to more effectively produce 3-hydroxyutyrate monomers from gluconate while deficiency in the β-oxidation pathway enhanced production of mcl monomers from decanoate [68]. See **Figure 1.2** for a description of known metabolic pathways for PHA synthesis.

β-Oxidation Cycle #	β-Oxidation intermediate	(*R*)-3-hydroyacyl-CoA monomer
1	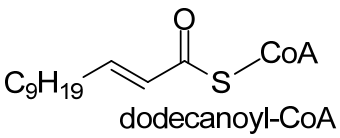 dodecanoyl-CoA	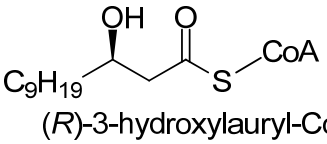 (*R*)-3-hydroxylauryl-CoA
2	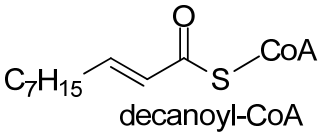 decanoyl-CoA	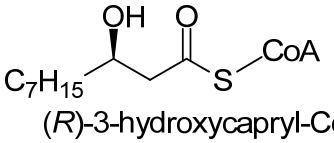 (*R*)-3-hydroxycapryl-CoA
3	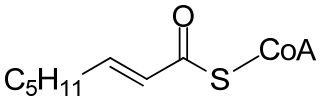 octanoyl-CoA	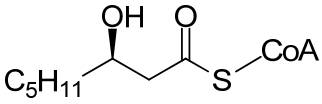 (*R*)-3-hydroxycaprylyl-CoA
4	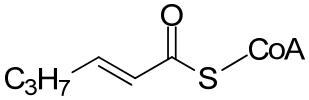 hexanoyl-CoA	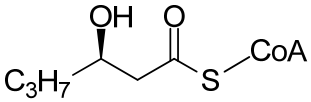 (*R*)-3-hydroxyhexanoyl-CoA
5	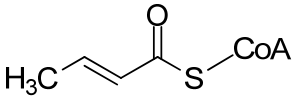 butanoyl-CoA	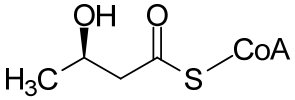 (*R*)-3-hydroxybutyryl-CoA

Figure 1.4 Polyhydroxyalkanoate monomers produced from β-oxidation.
Monomers are produced from successive rounds of fatty acid β-oxidation beginning with dodecanoic acid as the starting material. In addition each round of β-oxidation also produces one molecule of acetyl-CoA which is a precursor for the formation of PHB.

PHA Production in Eukaryotic Cells

Saccharomyces cerevisiae , also known as common yeast, is another organism that has been investigated for recombinant expression of PHAs, because yeast are already widely used in industry for the production of ethanol as biofuel. Additionally, producing both renewable fuels and plastics in the same organism is in line with the recent interest in biorefining technologies i.e. the production of multiple value added products from a single complex feed stock. Yeast are also an interesting host for PHA production because production of specialty plastics from a eukaryotic organism may offer enhanced biocompatibility for biomedical applications in eukaryotic human cells. In 1996 Leaf et al. demonstrated PHB production in *S. cerevisiae* was possible by expressing the PHB synthase gene of the bacterium, *Raslstonia eutropha* [69]. The production of PHB using only the synthase gene without additional synthesis enzymes indicated that *S. cerevisiae* already contained the necessary metabolic routes for PHB monomer synthesis. In 2006 Carlson and Srienc showed that by recombinantly expressing the *phaAB* genes of *Ralstonia eutropha* they could boost PHA production by 45x when compared to cells expressing only the *phaC* synthase gene [70]. Furthermore they also demonstrated that the yeast were capable of simultaneously producing PHA and ethanol under anaerobic conditions. In the same year Zhang et al. showed that PHA_{mcl} could be expressed in the yeast cytosol using a recombinant, cytosolically expressed *P. oleovorans* synthase in a *pex5* mutant [71]. β-oxidation enzymes utilized for the production of PHA_{mcl} precursors are typically expressed in yeast peroxisomes. The small size of these cellular compartments limits the available volume for polymer production. Cells deficient in the Pex5p receptor (*pex5*) are unable to target these β-oxidation enzymes to their native peroxisomal location and instead accumulate them in the cytosol, thereby creating a cytosolic PHA_{mcl} production pathway.

Another alternative for the economical production of polyhydroxyalkanoates is using transgenic plants. Researchers first achieved this feat in 1992 by the transformation of *phbB* and *phbC* genes from *Ralstonia eutropha* into *Arabadopsis thaliana*, a model organism. Cloning of the *phbA* gene was not included as the organism already produced its own β-ketothiolase within the cytoplasm. Production of PHB was

low, about 0.1% dry weight [72] Later, researchers boosted this level to 40% dry weight by transforming all three *Ralstonia eutropha* genes , *phbABC*, into *A. thaliana* and targeting them for expression in the chloroplasts via plastidial targeting sequences[73]. With an interest in the potential for biorefining, researchers have also turned their attention to plants already in use or being considered for food or energy production. Plants investigated include maize, sugar cane, rapeseed, and switchgrass [74-77]. In these efforts targeting polymer production to plastids or peroxisomes is a common approach. Mooney provides a comprehensive review on this topic [78].

Raw Material Sources for PHA Production

Currently the vast majority of plastics throughout the world are synthesized from petroleum based feedstocks, a source which is not sustainable and will likely be depleted within the current century. Furthermore the production of petroleum derived plastics also results in the net increase of atmospheric carbon dioxide, a significant contributor to global warming. With these concerns in mind, PHA based plastics offer an attractive alternative because of their capacity to be synthesized from renewable feedstocks. Common feedstocks are purified sugars, molasses, and propionate. However such feedstocks are more costly and less abundant than petroleum which in part contributes to the significantly higher price of PHAs when compared to conventional plastics [79]. In 2008 the price of Mirel brand polyhydroxyalkanoate plastic was ~ $5/kg, three times higher than the price of polypropylene [80]. While the use of renewable feedstocks may lessen the amount of associated greenhouse gas emissions, energy, often from fossil fuel sources, is still required for polymer production. Nevertheless a life-cycle analysis in 2008 by Kim and Dale suggested that PHB production provided significant environmental advantages to conventional petroleum derived plastics. The authors estimated that PHB production from corn grain required 2.5 MJ/kg PHB of nonrenewable energy compared to 69-100 MJ/kg plastic for petroleum-derived plastics. Much of the energy savings was accrued by burning leftover corn stover for electricity and steam generation. With respect to their impact on global warming, they estimated that PHB

provided greenhouse gas credits of -2.3 kg CO_2 equivalents / kg of polymer versus a greenhouse gas debit of 1.9-5.4 kg CO_2 equivalents / kg for petroleum-derived plastics [81].

Recently much research has been focused on the testing of other renewable feedstocks for which supplies may be greater, less costly and require less refining before conversion to PHA. The most ideal of these are waste streams from other industrial or bioprocesses. Carbon sources explored include: beet molasses, sugarcane liquor, hydrolysates from wheat, bagasse hydrolysates, corn stover hydrolysates, dairy whey, glycerol (a byproduct of biodiesel production), plant oils including: corn, palm, and soybean, CO_2 emissions from fossil fuel consumption or ethanol production, sewer sludge, waste solvent streams, and solid waste products that remain after oil extraction from biomass [82].

Process utilizing CO_2 are particularly exciting as they directly sequester greenhouse gasses. In addition to CO_2 these process require the feeding of H_2 and O_2 as a source of energy for carbon fixation. Interestingly, the native PHB producer, *Ralstonia eutropha*, is a natural chemolitoautotroph and is adept at survival on these gaseous substrates. Attempts at PHB production utilizing *Ralstonia eutropha* and CO_2 have been successful compared to conventional cultivation with organic carbon sources [82]; however, such efforts have been encumbered by the risk of hydrogen explosion. i.e. the need to keep oxygen below the flammability limit reduces the capacity of the bioreactor for effective oxygen mass transfer [83].

PHA Production using Mixed Microbial Cultures

Two particularly relevant features of renewable feedstocks are that they often contain a broad variety of nutrients and they may experience significant variations in quality depending on seasonal environmental factors. Isolation of a single nutrient source from a renewable mixture e.g. glucose from corn grain, requires additional energy for pretreatment and separation processes. If a monoculture is used for conversion of a mixed feed source it is likely that considerable work would be needed to optimize the strain for production and still this organism might be selective for just one specific nutrient within the mixture e.g. *E. coli's* preferential consumption of glucose over xylose

in cellulosic biomass. Thus, a complete conversion of all the available biomass may not be achieved. One potential solution to this problem is through the use of a mixed microbial culture such as the ones used for treatment of industrial and municipal waste streams. By process of natural selection those organisms which are better at utilizing the substrates available within the waste stream will become enriched within the population. If multiple carbon sources are present in the waste stream, a unique community of organism will evolve to consume the waste. If an upset in nutrient composition occurs, natural selection will again produce an optimized population for the new conditions.

Because of the competitive advantage that PHA production confers to microorganisms for survival during times of nutrient scarcity, this trait has been readily adopted by numerous organisms,[84] When mixed populations of microorganisms are subjected to repeated cycles of nutrient excess (feast) followed by nutrient limitation (famine) those organisms that can survive the feast and famine regimen by utilizing their stores of accumulated PHA become enriched within the population. Such conditions of feast and famine occur routinely in waste treatment processes, and in fact the production of polyhydroxyalkanoates by activated sludge has been well documented [85-87]. In this way mixed microbial populations can be optimized for both multiple substrate utilization as well as PHA productivity. PHA content in mixed microbial communities has been observed as high as 50-85% of cell dry-weight [88-91] and specific productivity (g of PHA/g of substrate/hr) of these cultures is approximately ten fold higher than for PHA producing *E. coli* cultures. [89] The highest levels of polymer accumulation are obtained by deliberate feast / famine cycling to enrich the culture in high PHA producing species. Furthermore, mixed microbial communities offer the advantage of not requiring sterilization, a significant energy requirement, and may be conducted in simple concrete basins as opposed to the expensive steel tanks required for monoculture fermentations requiring a significant capital investment.

Despite the advantages to mixed microbial cultures, volumetric productivity (g of PHA/ L/hr) remains below that of pure cultures because of low cell densities which are approximately 10 fold lower than for pure cultures [89]. This low volumetric productivity leads to additional costs for purification and recovery. Furthermore the polymer material produced from mixed microbial cultivation is likely to have a higher variability in

monomer composition and may be less pure than polymer produced from conventional monoculture processes thus targeting it towards applications with lower product quality requirements.

Recovery and Purification of PHAs from Microbial Culture

Another important factor impacting PHA production is polymer recovery and purification, which affects both the cost of the product as well as its value as an environmentally-friendly substitute to petroleum derived plastids. One common extraction technique is with the use of organic solvents which serve to both permeate the cell membrane and dissolve the polymer [92]. Solvents investigated include chloroform, 1,2-dichloroethane, and methylene chloride [93], ethylene carbonate and propylene carbonate [94-95], 1,2-propandiol, glycerol, diethyl succinate, and butyrolactone [96]. Of these solvents propylene carbonate has most recently experience renewed interest for its advantageous environmental properties e.g. extraction at atmospheric pressure, low volatility, and low toxicity [95]. Dissolved PHA is precipitated by the addition of a non-solvent e.g. methanol or water [97-98] Drawbacks of this type of purification include the large quantities of solvent required, the environmental hazard of such solvents, and the cost of solvent recovery operations. Benefits of organic solvent extraction are high product purity (>99%) and minimal reduction in polymer molecular weight [99].

Other methods of cell digestion include treatment with surfactants e.g. palmitoyl carnitine [100] and sodium dodecyl sulfate [101] which are less harmful to the environment but still require treatment of process wastewater due to the large amounts of surfactant used. Another additive which is very effective at cell lysis is sodium hypochlorite and purities as high as 99% have been obtained using this method; however, hypochlorite can in some cases cause a significant reduction in polymer molecular weight by ~50% [102] Researchers have also investigated the use of lytic enzymes for cellular digestion [103-106] These methods are desirable because they are much more environmentally friendly and produce good recovery yields; however, they are hampered by the high cost of enzymes [99] In addition various mechanical methods have been investigated for the recovery of PHA including bead mill disruption, high pressure homogenization, and ultrasonication

[107-109] Finally, researchers have investigated the potential for self-lysing cells producing PHAs. Such a functionality is engineered usually by the recombinant expression lytic enzymes cloned from viruses [110].

In vitro Synthesis of PHAs

In addition to synthesis from fermentation, polyhydroxyalkanoates have also been synthesized *in vitro*. While such synthesis routes may be less direct than *in vivo* synthesis, in theory they offer the advantage of allowing greater control over monomer compositions and product purity. Such qualities may be particularly important for biomedical applications where quality requirements are more stringent. In 1995 Gerngross and Martin reported the successful synthesis of PHB *in vitro* by combining purified polymer synthase from *Ralstonia eutropha* along with synthetically produced (R)-3-hydroxybutyryl CoA in a suitable buffer. By varying the initial concentration of polymer synthase they could control the molecular weight of the polymer molecules[111]. Beyond this early success, researchers realized that any large scale application of *in vitro* PHA synthesis would require the ability to recycle the costly CoA cofactor. In 2005 Satoh et al. devised a solution to this problem by incorporating into their reaction mixture an acyl-CoA synthetase cloned from *Pseudomonas oleovorans* along with CoA cofactor in addition to purified polymer synthase from *Ralstonia eutropha* and either the 3-hydroxybutyrate or 4-hydroxybutyrate substrates in a suitable buffer. This mixture allowed for the continuous regeneration of the HB-CoA complex. Additionally they showed that the monomer composition of P(3HB-co-4HB) copolymer could be controlled strictly by varying the ratios of the monomers in the reaction mixture [112].

Another *in vitro* route for the synthesis of PHB is through ring-opening polymerization of β-butyrolactone [113]. This substrate can be synthesized from 3-hydroxybutyric acid, a product which is easily obtained from microbial fermentation [114]. This route is similar to the way in which polylacticacid is obtained through the ring opening polymerization of lactide. While conventional ring-opening catalysts may be employed these are often toxic and may compromise the biocompatibility of the polymer. A greener alternative is the use of purified lipase enzymes [115] Such reactions must be

performed under anhydrous conditions as lipases also catalyze lactone hydrolysis in the presence of water. Thus neat organic solvents must be used to dissolve the monomers and associated polymer.

One alternative to the use of organic solvents is the use of ionic liquids with low temperature melting points. A significant advantage of these solvents is their non-volatility which eliminates a significant pathway for environmental release. While some ionic liquids can be toxic others have limited toxicity. In 2007 Gorke et al. tested several ionic liquid and lipase combinations for the synthesis of polyhydroxyalkanoates from various lactone precursors. Using lipase B from *Candida Antarctica* dissolved in the ionic liquid, 1-butyl-3-methylimidazolium bis(trifluoromethane)-sulfonimide, they synthesized polymers from β-propiolactone, δ-valerolactone, and ε-caprolactone with degrees of polymerization as high as 170, 25, and 85 respectively. Activity of the lipase towards β-butyrolactone and γ-butyrolactone was not as high, producing only 5-length oligomers [116]

Polylactic Acid

Within the field of renewable polymers another significant product is polylactic acid (PLA) or polylactide. Production of this polymer is considered renewable because the main feedstock, lactic acid, is produced by the fermentation of sugars, often corn-derived dextrose. Polylactide degrades naturally to carbon dioxide and water first by hydrolysis into lower molecular weight fragments and then via enzymatic degradation by microbes [117]. The lactic acid molecule has one chiral center allowing for the existence of two stereoisomers L-lactic acid and D-lactic acid. The chirality of the lactic acid produced depends on the type of microorganisms used for fermentation with different organisms producing pure D or L or a mixture of the two [118]. After the lactic acid has been purified from the microbial culture it is then catalytically converted to polylatctic acid; however, the polymerization also releases water which thermodynamically drives the reaction in the reverse direction. This prevents the formation of long chains. To bypass this limitation the mixture of low molecular weight oligomers is then subjected to a catalytic degradation reaction to produce lactide, the cyclic dimer of two lactic acid

molecules [119]. By vacuum distillation this product is then purified to remove the water. Depending on the starting quantities of L-lactic acid and D-lactic acid from the fermentation, the purified product contains L-lactide (two L-lactic acid molecules), D-lactide (two D-lactic acid molecules), and DL-lactide (a molecule of both L-lactide and D-lactide)[120]. The lactide is then converted to long chain PLA by either a ring opening polymerization typically using an anionic initiator (e.g. alkalai metal oxides) or a coordinated insertion polymerization using metal carboxylates as catalysts (e.g. stannous octanoate). See **Figure 1.5**. Isotactic PLA composed of only L-lactide (PLLA) is straight and regular; however, the inclusion of occasional D-lactide or DL-lactide impurities creates kinks in the chain which reduce the degree of crystallization in the polymer. Tacticity affects polymer crystalinity (i.e. amorphous versus semicrystalline structure), melting temperature, and degradation rate [121]. Control of tacticity may be achieved by varying the ratio of stereoisomers in the mixture or by the use of catalysts with a high degree of selectivity for one stereoisomer [122]. Using these selective catalysts research has demonstrated the synthesis of "stereo-block" copolymers from racemic lactide [123]. In a phenomenon known as stereocomplexation polymer chains with opposing tacticity display a higher affinity for one another than they do for chains of the same tacticity. For polylactide stereocomplexation of PLLA with PDLA produces a material with a melting temperature of 220-230 °C, significantly higher than for PLLA alone, 170-190°C [124]. In another route to the creation of renewable block copolymers utilizing PLA, researchers are investigating the addition of polymenthide (PM) derived from menthol found in mint plants. The menthol is first converted to menthone which is subsequently converted to menthide [125]. The menthide is then used as monomer for the synthesis of polymenthide by ring-opening polymerization. Polymenthide is then joined to polylactide to form a triblock copolymer, PLA-b-PM-b-PLA , with enhanced elongation and elasticity over PLA homopolymer [126].

Unlike the production of PHA which can be accomplished entirely through biosynthesis in a single organism, the commercial production of PLA is a multistep process requiring: (i) microbial fermentation to produce lactic acid, (ii) purification of lactic acid , (iii) chemical synthesis of the lactide dimer, (iv) purification of lactide, and (v) *in vitro* ring-opening polymerization to create PLA. Recognizing the benefit of a

more direct synthesis route, Taguchi et al. recently engineered recombinant *Escherichia coli* to produce copolymers of PLA and PHA enzymatically. [127] Noting that the chemical structure of lactic acid (2-hydroxypropanoic acid) is similar to the structure of 3-hydroxybutyric acid, they tested seven unique polymerase enzymes for their ability to incorporate the LA-CoA monomer. Only one of these enzymes was successful, a mutant of the *Pseudomonas* 61-3 polymerase with two amino acid substitution. However, the enzyme would incorporate the LA-CoA only in the presence of HB-CoA monomers. To generate an ample supply of LA-CoA monomers they inserted a *pct* gene from *Megasphaera elsdenii* coding for a propionyl-CoA transferase which had also been shown to have transferase activity toward lactic acid. For the production of HB-CoA monomers they included *phbAB* genes from *Ralstonia eutropha*. The recombinant *E. coli* produced polymer to 19 wt. % of cell dry weight with a lactate fraction of 6 mol%. Since then similar investigations have increased both polymer content and lactate fraction by means of improved polymerases, improved propionate CoA transferase enzymes, and mutant *E. coli* strains with enhanced lactate production pathways [128-130]. The most successful attempt boasts 46 wt. % polymer production with 70 mol% lactate synthesized from glucose alone. This area of research is particularly exciting as PLA is already widely used and production by complete biosynthesis could result in a significant cost savings.

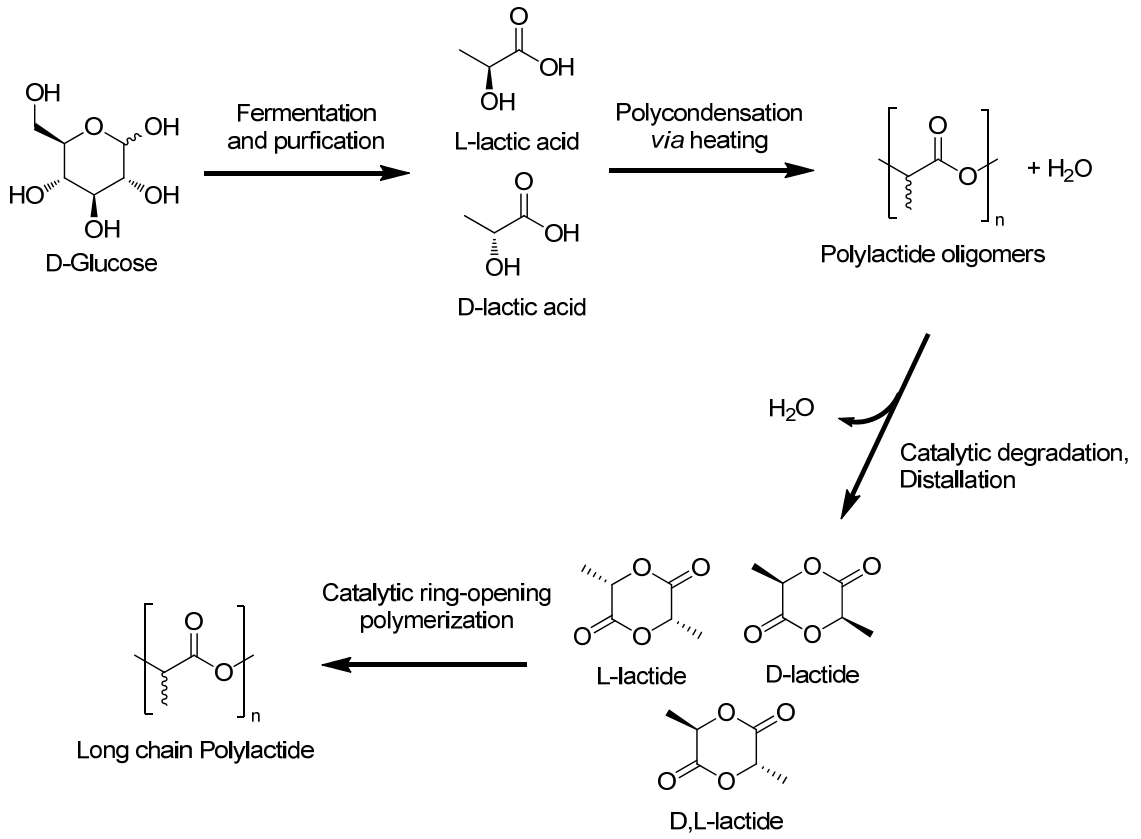

Figure 1.5 Biosynthesis and downstream organic synthesis steps to polylactide.

Applications of PHAs and PLA

Over the years PHA and PLA have been available as commercial products from several manufacturers. Trade names have include NatureWorks, Ingeo (PLA) Biopol, Biomer, Nodax, Biogreen, and Mirel (all PHA) [82] Bulk applications include biodegradable plastic bags, drinking cups, plastic cutlery, fibers for clothing, packaging materials for dairy and vegetables, film overwraps, and blister packages [82, 131] The application of PHA particles as an aqueous dispersion has been investigated for the creation of polymer coatings on paper and cardboard, biodegradable cheese rinds, and paints [16] Because PHA polymers are synthesized from only the R stereoisomer of hydroxyalkanoic acids, they have also been considered as a source of enantiomerically pure precursors for other fine chemical and pharmaceuticals [79, 114] PHA monomers have been produced by *in vitro* chemical digestion of PHA [132] as well as by *in vivo* enzymatic digestion using depolymerase enzymes [133-134] Interest has also been centered on the use of

PHAs for biomedical purposes because of their biodegradability and biocompatibility. Applications that have been investigated include: tissue patches, orthopedic implants, tissue scaffolding, sutures, drug release medium, nerve regeneration, and wound healing [135]

More recently PHA granules, the native cellular bodies that contain the polymer, have also attracted attention. When PHA is produced within the cell it forms small, spherical, water-insoluble inclusions. These granules are surrounded by a phospholipid monolayer [2, 136-137]. Embedded within this layer are several proteins including PHA synthase, PHA depolymerase, and PHA phasins. Depolymerase enzymes are responsible for degrading the polymer during times of nutrient scarcity while phasins interfere with granule coalescence which affects granule size [138] Using these "granule associated proteins" experimentalists have been able to attach various non-native proteins to the surface of the granules creating functionalized "biobeads". One application of these PHA biobeads is for protein purification. This is done my making a fusion protein in which the protein of interest is linked to the C terminal of a PhaP phasin protein. The phasin acts as an affinity tag by which the protein of interest becomes linked to the PHA granule. The PHA granules may be produced within the same cell as the protein of interest [139-140] or may be produced in separate cells and added *in vitro* to cell lysates containing the phasin fusion proteins [141] Centrifugation is used to separate the insoluble biobeads along with the protein of interest attached to the surface. Within the protein linker segment connecting the phasin to the protein of interest a protease cleavage site is used to release the protein from the biobead. Additionally fusion proteins have also been constructed using the PhaC polymerase. The synthesis of bifunctional biobeads containing both a GFP fusion protein and a mouse antigen demonstrated that the technology could also be useful as cell markers for flow cytometry [142] Recently Yao et al. demonstrated that PHA biobeads loaded with the dye molecule rhodamine B isothiocyanate and modified with cell specific ligands could be used to target delivery of the model drug to two unique tissue types in *in vivo* mouse experiments [143]

Summary

Petroleum derived plastics have become ubiquitous in human society; however, their production from nonrenewable sources, contribution to greenhouse gas emissions, and permanent presence in the environment after discard demand an alternative solution which is both environmentally friendly and sustainable. Both polyhydroxyalkanoates and polylactide show significant potential for meeting this demand. These materials are advantageous for their biodegradability and production from renewable feedstocks, and both are already available commercially. Applications of these materials include packaging, fibers for textiles, biomedical materials, and protein functionalized biobeads.

While the homopolymer forms of these materials may lack toughness, polymer blending and block copolymer synthesis have been successful at improving material properties. Furthermore, the large diversity of monomer units available for polyhydroxyalkanoates results in a spectrum of material properties ranging from stiff and strong to elastomeric. The ability to combine different monomers into copolymers has improved with the creation of mutant polymer synthase proteins with expanded monomer specificity.

Despite their environmental benefits the most significant obstacle to the proliferation of polyhydroxyalkanoates and polylactide is their cost which is approximately 3-5 higher than the cost of petroleum derived plastics. Much of this price disparity should decrease in the future as the cost of oil will surely rise with diminishing supplies. Other factors affecting the price of these bioplastics are raw materials cost and energy needed for sterilization of feedstocks. Typical fermentations to produce these plastics require the use of refined i.e expensive feedstocks such as glucose. To address this issue researchers are investigating the use of less refined feed sources, e.g. biomass and waste streams from other processes. Ideally polyhydroxyalkanoates could be produced as part of a larger biorefining operation, e.g. producing PHAs using glycerol waste from biodiesel production or CO_2 from ethanol production, thereby offsetting the overhead costs of utilities and infrastructure.

Furthermore, research to optimize the metabolic pathways of microorganisms will allow higher conversion of feedstocks. In some instances, mixed microbial cultures may be used to produce plastics without the need for feedstock sterilization.

Another way to reduce costs may be through process simplification. Researchers have already demonstrated that polylactide can be synthesized using an *in vivo* polymerase in the same way that polyhydroxyalkanoates are created, thereby eliminating several purification and chemical synthesis steps. Eventually plant-base technologies may allow direct production of plastics from carbon dioxide and sunlight in the same way that natural rubber is produced. See **Figure 1.6**

Lastly, for bioplastics to retain their image as environmentally friendly alternatives that are truly superior to petroleum derived plastics, processes should be designed which eliminate the need for toxic solvents in product recovery and purification.

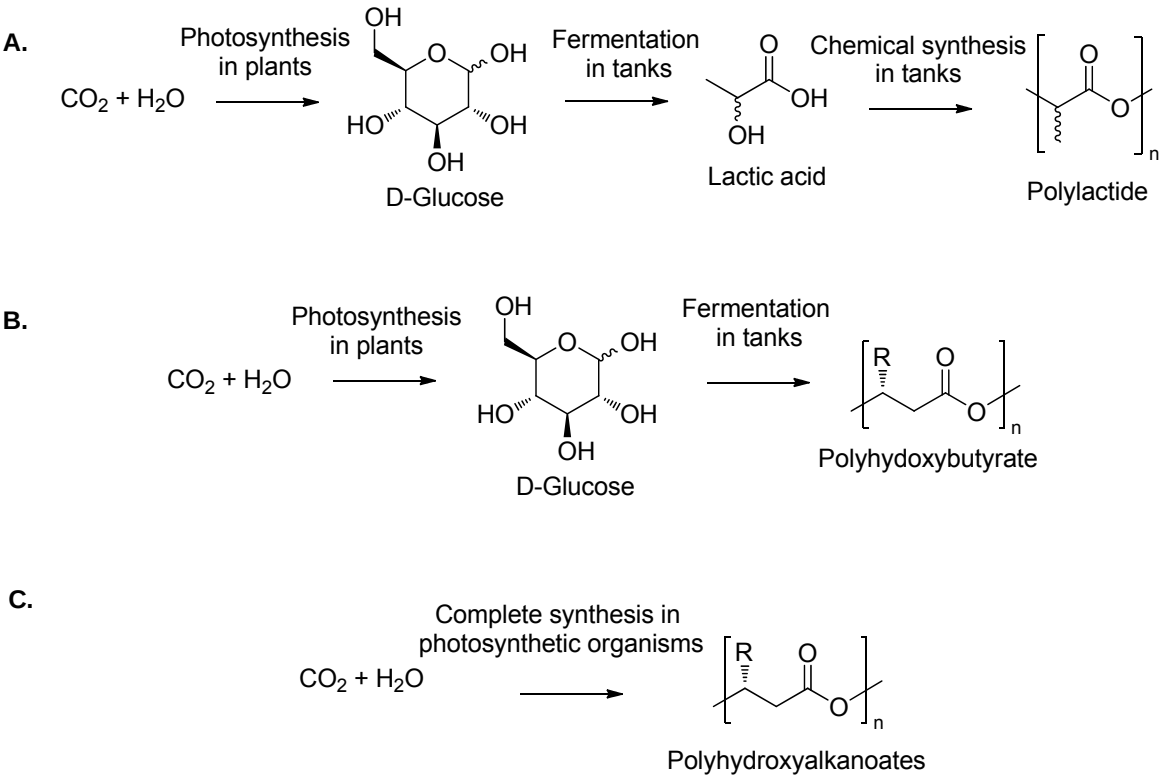

Figure 1.6 Different synthesis routes to biopolastics.
a. Current process for polylactide production. **b.** Current process for polyhydroxybutyrate production. Researchers have also demonstrated the ability to synthesize polylactide via this same process. **c**. Synthesis of bioplastics in plants or other photosysnthetic organisms could further reduce production costs. This technology has already been demonstrated in the laboratory.

Chapter 2. Polhydroxyalkanaote Block-Copolymers

Information in this chapter has been reproduced in part with permission from the following sources:

Figure 2.3
Matsen, M. W., Polydispersity-induced macrophase separation in diblock copolymer melts. *Physical Review Letters* 2007**,** *99* (14), 148304.
Copyright 2007, American Physical Socieity

and

Lynd, N. A.; Meuler, A. J.; Hillmyer, M. A., Polydispersity and block copolymer self-assembly. *Progress in Polymer Science* 2008**,** *33* (9), 875-893
Copyright 2008, Esevier

Figure 2.4.a
Kelley, A. S.; Srienc, F., Production of two phase polyhydroxyalkanoic acid granules in Ralstonia eutropha. *International Journal of Biological Macromolecules* 1999**,** *25* (1–3), 61-67.
Copyright 1999, Elsevier

Figure 2.4.b
Kelley, A. S.; Mantzaris, N. V.; Daoutidis, P.; Srienc, F., Controlled Synthesis of Polyhydroxyalkanoic (PHA) Nanostructures in R. eutropha. *Nano Letters* 2001**,** *1* (9), 481-485.
Copyright 2001, American Chemical Society

Figure 2.4.c
Pederson, E. N.; Srienc, F., Mass Spectrometry Feedback Control for Synthesis of Polyhydroxyalkanoate Granule Microstructures in Ralstonia eutropha. *Macromolecular Bioscience* 2004, *4* (3), 243-254.
Copyright 2004, John Wiley & Sons

Figure 2.6
Mantzaris, N. V.; Kelley, A. S.; Daoutidis, P.; Srienc, F., A population balance model describing the dynamics of molecular weight distributions and the structure of PHA copolymer chains. *Chemical Engineering Science* 2002**,** *57* (21), 4643-4663.
Copyright 2002, Elseveir

Figure 2.7
Pederson, E. N.; McChalicher, C. W. J.; Srienc, F., Bacterial Synthesis of PHA Block Copolymers. *Biomacromolecules* **2006,** *7* (6), 1904-1911.
Copyright 2006, American Chemical Society

Introduction

Poly(3-(*R*)-hydroxyalaknoate)s (PHAs) and their related poly(oxoester)s , e.g. poly(lactide) (PLA) and poly(caprolactone) (PCL), are an important class of polymers that have recently gained popularity for their environmentally friendly attributes. The distinction of these materials as "biopolymers" is typically attributed to their having at least one of three traits, including 1.) the capacity for rapid biodegradation and / or composting, 2.) synthesis from renewable feedstocks, or 3.) the utilization of some form of biosynthesis step during production. Highly crystalline forms of these poly(oxoester)s such as poly(hydroxybutyrate) (PHB) and PLA are strong but become embrittled over time as their crystallinity increases. Alternatively, PHAs containing medium-chain-length monomers (PHA_{mcl}), e.g. poly(hydroxyoctanoate) (PHO), and copolymers in which the secondary monomer fraction is near 50%, e.g. PHB-co-PHV(50%) or PHB-co-P4HB(50%), are much more amorphous materials. Because these materials have reduced crystallinity their strength is diminished but their elasticity is significantly enhanced. As with petroleum polymers, the application of block-copolymer technology to PHAs has been shown to be an effective tool for combining the unique properties from two disparate polymers, e.g. in producing materials which possess both strength and elasticity. The use of block-copolymer architectures is especially important when simple blends of polymers are thermodynamically unstable and result in macrophase separation. Biopolymers containing block structures have been produced via a number of routes, including complete organic synthesis, partial biosynthesis, and total biosynthesis. Furthermore, biosynthesis has been achieved by both *in vivo* and *in vitro* methods. In this review, we give a detailed report on the variety of syntheses that have been used to create block-copolymer molecules from different biopolymer constituents. In addition, we provide an extensive tabulation of the physical and mechanical properties observed for these materials. Because *in vivo* block-copolymers synthesis is a relatively new technique, we give additional focus to this area. Specifically we report the latest scientific findings regarding the molecular mechanism that control enzymatic polymer synthesis *in vivo*, and how factors of polymer synthase levels and the mechanism of chain termination can affect the molecular weight and product distributions of the resulting

block-coplymers. Because "living polymerization" is not typically observed for *in vivo* syntheses, repeated substrate switches are required if a significant quantity of block-copolymer molecules is to be produced. Consequently, the block-copolymer products formed *via* periodic substrate switching are often polydisperse in their segmental compostion and may also contain considerable fractions of homopolymers and random copolymers as well. Given the complexity that can arise in such mixtures, we highlight the need for careful analytical characterization in order for meaningful conclusiosn to be made regarding the correlation of structure and function in this valuable class of materials.

General Polymer Architectures

In polymeric materials, the chemical, physical, and mechanical properties observed in bulk samples are a direct result of both the monomer types and the physical configurations that make up the molecular structure of the material. See **Figure 2.1.** The most basic polymers, referred to as "homopolymers", are comprised of monomer units repeatedly linked together to form long chains. "Copolymers" are comprised of two or more monomer types, e.g. a combination of the monomers A and B. For "statistical" or "random" copolymers the monomer sequence is observed to be statistically random. In "alternating polymers", A and B alternate continuously at every postion, while in "periodic polymers", the alternation between monomer types can occur for any specific sequence repeated at any specific period. "Branched polymers" are composed of a linear chain along which additional chains are attached. When the monomer composition of the branches is different from the monomer composition of the central polymer chain, such architectures are referred to as "graft copolymers". "Star polymers" are formed by the attachment of three or more polymer chains connected to a central core structure.

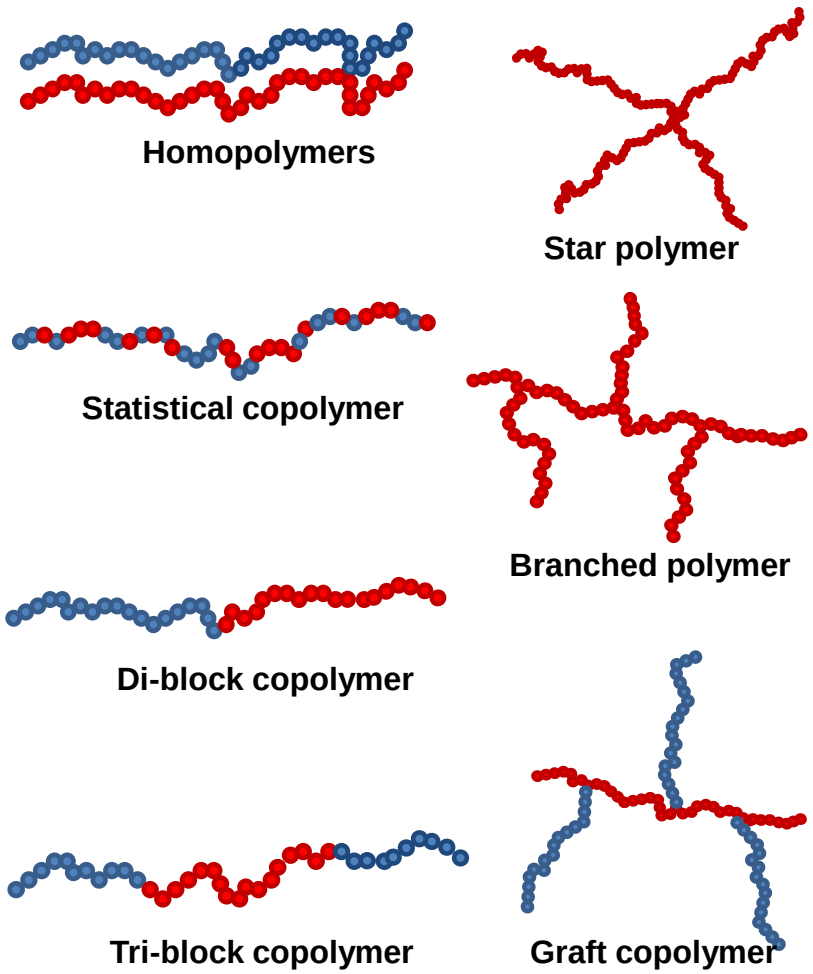

Figure 2.1 Various polymer architectures.

An alternate variation of the random copolymer is the "block-copolymer", in which two or more polymer chains made of different monomers are covalently joined to form a single polymer molecule with distinct "block" domains. Distinct blocks may be comprised of either homopolymers or copolymer. Depending on the number of distinct molecular domains, such "linear" block-copolymers are further classified as di-block (2), tri-block (3), or mulit-block (n).[144] Furthermore, graft-copolymers and star copolymers that contain more more than one homodomain are examples of "non-linear" block-copolymers.[145]

Polymer Phase Behavior

When the chemical interaction between different monomer types are significantly repulsive, block-copolymers are observed to form secondary, meso-structures of homogenous regions which can persist over small length scales[144]. Due to the covalent bonds that join the two polymer segents, the resulting micro-domains are forced to exist in intimate contact. As a result of their molecular constraint, the polymer domains adopt unique morphological configurations which allow them to minimize the Gibbs free energy (ΔG) within them as well as at their interface. These meso-structures are a reflection of the minimum Gibbs free energy ($\Delta G = \Delta H - T\Delta S$) that the polymer molecule forms at equilibrium. Formation of such meso-structures can be seen as balance between enthalpic and entropic forces arising from the polymer structure and any non-ideal intermolecular interactions between different monomer types. See **Figure 2.2**. As the polymer chains rearrange to assume their long-time conformation, repulsive forces existing between the different monomer types drive phase separation of polymer domains in order to minimize the system enthalpy (ΔH) . At the same time, the chain also experiences a natural tendency to become more disordered, which results in a maximization of system entropy (ΔS). This morphological optimization must be done to minimize not only the free energy between the domains of the single polymer molecule but also to minimize the free energy of the molecule as it relates to the domains of other block-copolymers surrounding it. Together these effects combine to produce a variety of unique meso-structures depending on the volume fraction of each polymer block and the degree of repulsion experienced between them.

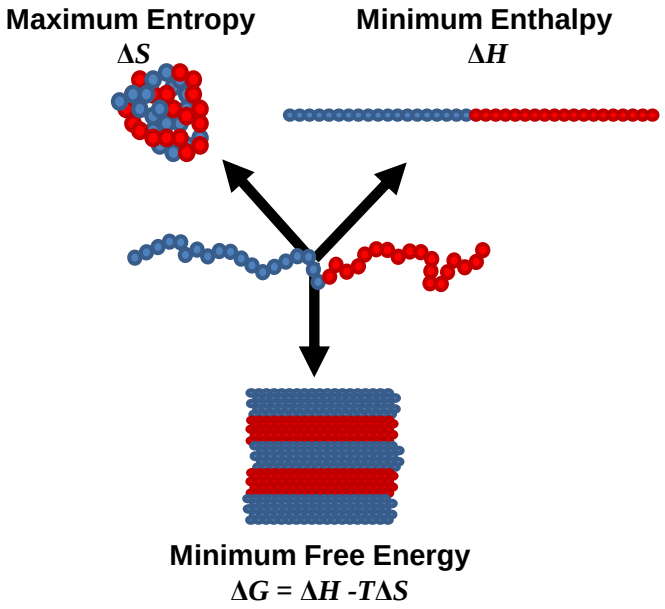

Figure 2.2 The effect of thermodynamic factors on block-copolymer self-assembly. The formation of meso-structures from block-copolymer molecules arises due to a balancing of enthalpic forces that promote order and entropic forces that promote disorder.

The phase space of an AB block-copolymer can be described by three parameters: N is the length of the polymer, f_A is the volumetric fraction of polymer A in the bulk material, and χ_{AB} is the enthalpic interaction parameter which incre. A mathematical interpretation of χ_{AB} can be taken from the Flory-Huggins model of mixing between a dilute polymer solute A and a solvent B[146]. The free energy of mixing (ΔG_m) between A and B is given by: $\Delta G_m = NRT[\, x_A \ln(f_A) + x_B \ln(f_B) + x_A f_B \chi_{AB}]$ where x denotes the mole fraction and f denotes the volume fraction. Essentially, χ_{AB} accounts for the added enthalpic effects between the solute and the solvent. These effects result from either attractive or repulsive forces between A and B. Recall, that for an ideal solution, intermolecular forces and hence enthalpic effects do not occur, i.e. $\chi_{AB} = 0$. A positive value of χ_{AB} indicates repulsive interactions between the two monomers and a driving force for phase separation. Furthermore, the driving force for separation increases as the number of monomer units, N, increases; thus, the product $\chi_{AB}N$ is an overall indicator of the repulsive forces between segments. **Figure 2.3**. shows a theoretical phase diagram for an AB block-copolymer, showing unique phases which depend on both the relative

volume of the individual blocks, i.e. f_A , and the force of the repulsive interactions, i.e. $\chi_{AB}N$, between the two polymer segments. Above a minimum value of $\chi_{AB}N$ the two polymeric domains are thermodynamically insoluble and thus segregate to minimize their free energy.[34], with the resulting microphase separation, manifesting as a variety of unique meso-structures.[144]

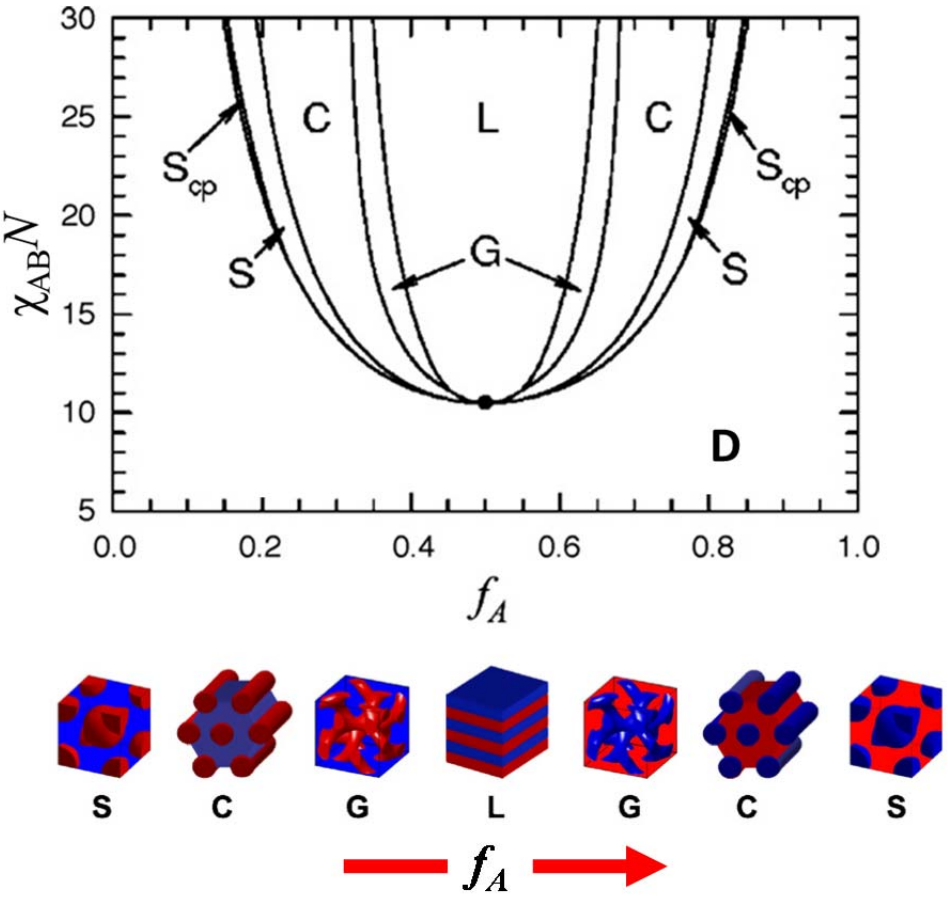

Figure 2.3 Phase diagram of AB block-copolymer with equal block lengths.
(f_A) Volume fraction of polymer A. (χ_{AB}) Enthalpic interaction parameter between A and B. (N) Polymer chain length. (S) Spheres on a body-centered cubic lattice. (S_{cp}) Close-packed spheres. (C) Hexagonally arrayed cylinders. (G) Bi-continuous gyroid. (L) Lamellar sheets. (D) Disordered mixture. Phase diagram adapted from Matsen et al.[147] Morphology illustrations adapted from Lynd et al.[148]

Form and Function

Due to their unique characteristics, block-copolymer molecules have been employed in a diversity of applications. The usefulness of these materials can be

attributed to two unique molecular properties, 1.) their amphiphilic nature, and 2.) their ability to undergo self-assembly and form heterogenous meso-structures . When the chemical properties of two different polymers are sufficiently different, their combination by simple mixture is not possible, and instead leads to macrophase separation. However, in block-copolymers, the presence of a strong covalent bond between the two polymer domains prevents macrophase separation, thereby allowing the chemical, physical, and mechanical properties from chemically distinct polymers to be intimately combined. Because of their amphiphilic nature, block-copolymers can be used to impart thermodynamic stability at molecular interfaces where there are strong repulsive forces between the two phases. This makes them ideal candidates for use as sufactants, lubricants, and as stabilizers in tertiary mixtures that contain large fractions of the constitutive homopolymers[149]. In plastics, for example, this trait can be very useful for imparting mechanical toughness, by combining a highly crystalline polymer, which is strong and stiff, with an amorphous polymer that is much more elastic[150]. While a simple mixture of these polymers might undergo phase separation, the use of block-copolymers can impart added thermodynamic stability.

The second important characteristic of block-copolymers, is their ability to undergo self-assembly. As a result, block-copolymers are observed to assume a variety of unique meso-structures depending on both the volume of the individual domains and the degree of their dissimilarity[144]. Illustrations of some commonly observed meso-structures are show in **Figure 2.3**. Two important characteristics for comparing the different block-copolymer morphologies are in terms of the continuity (i.e. percolation) and dimensionality of each polymer phase. For continuous phases the molecular domains of individual polymer molecules are interconnected in an extensive network that spans the entire sample across at least 1 dimension. Independent of their continuity, the periodic structures of a particular phase may be repeated in either 1-D, 2-D, or 3-D. For example, in the lamellar morphology, both phases percolate in 2-D and are aligned parallel to each other; however, neither phase shows continuity in the third dimension. In the body-centered cubic morphology, one phase demonstrates 3-D percolation: the second phase also shows 3-D periodicity; however, the spherical domains that form the larger phase do not form a continuous network . For the hexagonally arrayed cylinder

morphology, the surrounding phase percolates in 3-D while the cylinder phase percolates in only 1-D. Alternatively, in the bi-continuous gyroid morphology 3-D percolation occurs in both phases. Thus, by viewing block-copolymer morphologies in terms of their phase continuity and dimensionality, it is apparent how these materials are uniquely suited for simultaneously separating and directing the transport of mass, energy, and momentum for multiple species.

Apart from their behavior in bulk form block-copolymers may exhibit additional structure when placed in dilute solutions with differ solvents. For example, block-copolymers in dilute solution can organize into micelles forming core-shell particles as well as liposomes with internal cavities.[151] As such, these structures are commonly used to contain drug molecules for targeted delivery or other chemicals for transport and controlled release. [149] Alternatively, solid, core-shell particles can be used for dispersed coatings[152-154], as nanoparticles for mechanical reinforcement[155] or to improve dispersion of other nanofillers[156-157]. The lamellar morphology lends itself for application as lubricants[158-161] Such an effect may arise due to low shear slippage between layers, analogous to the way graphite acts as a lubricant, or by formation of a low viscosity coating for surfaces with otherwise strong surface energy. Furthermore, the meso-structures produced by block-copolymer can also be used as templates to aid in the creation of other nanostructured materials. One method for this is by selectively degrading one of the polymer phases, thereby creating a porous structure in which alternate materials may be deposited. Owing to the extremely small geometries of the block copolymers domains, the porous structures that are formed contain large amounts of surface area and as such are ideal for applications as selective membranes and catalyst supports with tunable size dimensions and surface modifications.[149].

By the opposite approach, block-copolymers themselves can be guided to self-assembly by the use of extra-polymeric templates[149]. When the thickness of a block-copolymer thin film is made similar to the dimensions of the hetero-domains in the bulk phase, the meso-structures formed within the film are often distinct from the morphologies seen in the bulk material. This is due to an increase in the per-volume magnitude of surface forces, which can arise at both the polmer- substrate interface and polymer-atmosphere interface. As a consequence, 2-D patterned surfaces have been

shown to increase long-range order in block copolymer thin films including either cylinder arrays or lamellar structures. It is envisioned that such techniques could be useful for the fabrication of polymer nanostructures with applications in photovoltaics and electronic circuitry. Another application for block-copolymers is in photonic crystals, which contain repeated domains of materials with different refractive indices[149]. Depending on both the size and spacing of the hetero-domains within the material, only certain wavelengths of light are permitted to pass. Correspondingly, block-copolymers exhibiting the body-centered cubic morphology as well as lamellar sheets are ideal candidates for use as photonic crystals.[149] Moreover, because the size of hetero-domains can vary with changes in the chemical and physical environment, block-copolymers materials have been explored for their potential as dynamically tunable devices, and stimuli-responsive materials. [149]

Due to the existence of 3-D percolation in both phases, the bi-continuous gyroid morphology is especially suited for mechanical applications, and more so than other morphologies such as lamellae and hexagonally arrayed cylinders.[34], Because the bi-continuous gyroid morphology allows stress to be carried by both phases and transmitted in all three dimensions, the intensity of an applied stress is more readily dissipated. Another explanation of the superior mechanical properties of this morphoogy was offered by Meuller et al. who prepared tri-block copolymers that consisted of a tough polymeric core flanked by more brittle end domains. They noted that within a bi-continuous network, a crack which originated in a brittle domain would be required to propagate across a tough domain at every single unit cell it traversed.[162] Such a mechanism is analogous to “rip-stop” nylon fabrics, in which a sparse mesh of high-tensile fibers acts to prevent tear propagation across the main fabric of lower-tensile fibers. By contrast, in block-copolymer morphologies which are not bi-continuous, crack propogation across a single phase can occur without every traversing the second phase.

Another important application of block-copolymer materials is in construction of nanostructured bulk heterojunctions for low-cost photovoltaics[163]. In such applications the effieincy of the solar cells is increased due to two factors: 1.) large interfacial surface areas for charge separation and 2.) strong network connectivity within the material for rapid transport of charge carriers to their respective electrodes[164]. As such, the ability of

block copolymers to intimately combine disparate polymeric materials in high surface area morphologies with strong connectivity makes them ideal candidates for study. Among the different morphologies, the bi-continuous gyroid is especially suited for this application owing to its capacity for 3-D percolation in both phases and its large interfacial area. [34, 165]

Organic Synthesis of Block-Copolymers

The synthesis of a basic AB block-copolymers can be achieved by one of three general methods.[145] The first method involves a continuous polymerization in which monomer A is added first via some chain-growth mechanism, followed by the similar polymerization of monomer B. Implicit in this this approach is the requirement that chain termination must not occur between the end of A addition and the start of B addition, such that the first molecule of B must be covalently bound to the last molecule of A. As a consequence, control of the uniformity of block-size for both A and B (i.e. degree of polymerization), across an ensemble of individual polymer chains, is most easily achieved when the chain-growth process behaves as a "living polymerization" . The essential requirement for a living polymerization is that the rate of the chain propagation must be much greater than either the rates of chain termination or chain transfer. Furthermore, when the rate of chain propagation is much greater than the rate of chain initiation, the polydispersity of the resulting molecules (PDI = M_w/M_n) takes on a value of $1+1/N_n$ where N_n is the sum total of all polymerized monomers[146]. In an ideal living polymerization, all initiation reactions for polymer A occur simultaneously $t = 0$, and propagation occurs uninterrupted and equally across all polymer chains, until the entire supply of monomer is consumed. Thus, the resulting product is an ensemble of A homopolymers in which the degree of polymerization is identical for all chains. If monomers for the second polymer B are then added to the reaction with initiation occurring at the last A molecule, then the product formed will consist of an ensemble of AB block copolymers all with identical compostion. In organic syntheses, living polymerization is most commonly achieved through anionic polymerization or by some method of controlled radical polymerization.

The second approach to block-copolymer synthesis is to fully synthesize each copolymer separately and then join them together by means of a unique functional group on their terminal ends, which can react to form a covalent bond between the individual chains. In the third approach, which is a combination of the first two, polymer A is completely synthesized and then terminated by a special functional group. Using this terminal group, polymer A is then converted to a macroinitiator species to start the propagation of polymer B, via an alternate polymerization reaction.

Biosynthesis of Block-Copolymers

Most polymers are synthesized *via* organic reactions contained within large, inert, vessels; however, some polymers can be produced *in vivo* by living cells. In these instances, polymerization occurs via enzymatic catalysis that occurs inside the cell with extracellular feedstocks being converted to the necessary monomers by a chain of additional enzymatic reactions *in vivo*. Examples of polymers produced *in vivo* include DNA, RNA, polyphosphate (polyP), and polyhydroxyalkanoates (PHA). In the case of DNA and RNA, often referred to instead as macromolecules, each is a copolymer of 4 distinct monomers and is used by the cell to store and translate genetic information needed to control cellular processes. Unlike most organic polymerizations which are kinetically controlled, the syntheses of DNA and RNA are template-controlled according to the sequence of the parent molecule from which they are copied. Thus, creation of a DNA block-copolymer would require a preexisting DNA molecule with a block-copolymer sequence. Such large DNA block-copolymers do not naturally occur in nature; however, with the advent of modern *in vitro* polymerization techniques, it is now possible to create DNA block-copolymers, which can be used as templates to create other block-copolymer molecules using either *in vivo* replication or the *in vitro* polymerase chain reaction (PCR). Similar to conventional block copolymer molecules, DNA molecules with specially designed sequences are also capabl of self-assembly to form unique structures such as "DNA-origami"[166]

Alternatively, polyP, and PHA are polymers used by cells to store surplus phosphate, carbon, and energy during times of nutrient excess. Later, when nutrient

supplies are limited, the polymer can be depolymerized to release the stored nutrients and energy. Given the broad substrate specificity of some PHA synthase enzymes, PHA is often found as a copolymer which can include up to 14 common monomer types, depending on the monomer supply pathways of the host cell. Examples of PHA that can be incorporated into copolymers by *in vivo* methods include polyhydroxybutyrate (PHB, C_4), polyhydroxyvalerate (PHV, C_5), polyhydroxyoctanoate (PHO, C_8), and polyhydroxytetradecaonate (PHTd, C_{14}), and even polylactide. While block-copolymers of PHA are not found naturally in cells, novel biosynthesis processes have now been developed to produce PHA block-copolymers at high yield.

Compared to conventional organic synthesis methods, biosynthesis of polymeric materials do present certain advantages. One advantage is the ability of biosynthesis to transform relatively unrelated feedstocks such as sugars, plant oils, volatile organic acids, industrial and municipal waste streams, and even CO_2 into complex polymeric molecules without the need for organic solvents and toxic catalysts. Furthermore, biosynthesis of block-copolymers allows for gains in process simplicity by avoiding multiple extractions and purification steps. With respect to control of polymerization, the molecular weight of PHB produced by enzymatic synthesis has been reported as high as $2x10^7$ Da compared to molecular weights of $1x10^5$ Da for many conventional polymers. In addition, polymer synthase enzymes are highly steroselective allowing for the synthesis of atactic polymers with enhanced crystallinity an therefore greater stiffness.

A primary distinguishing characteristic of block-copolymers is their ability to undergo self-assembly into micron and sub-micron geometries. Similarly, PHA granules in their native intracellular state are also sub-micron in size, and when these granules contain components from two distinct PHA types, micro-phase separation can occur within individual granules. Moreover, this heterogeneity, which can be observed via TEM with various staining techniques, became the source of much scientific speculation about the molecular mechanism of polymer and copolymer formation *in vivo,* and the implications this had for controlling the micro-structure of PHA granules as well as the molecular structure of single PHA molecules.

Early observations of heterogenous microstructures in microbially produced PHAs was reported by Horowitz and Sanders[167] in 1994, who noted that a mixture of

PHO and PHB polymers underwent phase separation in sub-micron particles emulsified using surfactants. Then in 1996, Curley et al[168] produced heterogenous, PHA, core-shell granules in the cells of *Pseudomonas oleovorans* by sequentially feeding 5-phenylvaleric acid followed by a mixture of 5-phenylvaleric acid with nonanoic acid. The intracellular inclusions that formed were shown to have a core of poly-3-hydroxy-5-phenylvalerate and a shell of poly-3-hydroxynonate.

The first report of PHA block-copolymers synthesized *in vivo* were made in 1995 by Shi, Gross and Rutherford[169]. Using *R. eutropha* the authors produced block-copolymers of (PHB-co-P4HB-co-PHV)-*b*-PEG by supplying 4-hydroxybutyric acid as a source for 3HB, 4HB, and 3HV monomers simultaneously with oligomeric fragments of polyethylene glycol (PEG, n = 4-5, M_n = 200 g/mol,). Based on the data, it was concluded that the PEG fragments acted as termination agents to the PHA synthase, resulting in the formation of covalent linkage between the PHA and PEG fragments. However, when a similar study was completed, in which fragements of PHB homopolymer were produced in *R. eutropha* using fructose as the carbon source, the addition of PEG fragments did result in chain termination, but covalent bonding was not observed with the PHB segments[170]. Thus, they concluded that formation of a covalent bond was somehow dependent on the terminal structure of the PHA chain, i.e. 3HB, 4HB, or 3HV. Alternatively, when the same group used the related species *Alcaligines latus* DSM 1122 and cultivated it on glucose, covalent bonds were formed between PHB and PEG segments[171]. This suggested that the ability of an elongating PHB chain to undergo chain termination is likely affected by the structure of the polymerase enzyme. Covalent linkages were observed with PEG fragments ranging from 100-1000 g/mol; however, neither chain termination nor di-block formation was observed for PEG fragments > 1000 g/mol. Furthermore, they concluded that the propensity of PEG fragments to act as transfer and/or termination agents decreased as the size of PEG fragments increased.

In essence, the approach by Shi and Ashby involved the joining of two pre-polymers, PHB-S-CoA with PEG-diol to form PHB-*b*-PEG. Alternatively, Kim et al. chose to conduct their synthesis as one continual propagation with a transient switch from one monomer to another[172]. The polymerization was performed *in vivo* using

Pseudomonas oleovornas. Initially segments of poly(3-hydroxynonanoate) (PHN) were synthesized by growing the culture on nonanoic acid, after which had been consumed, the second monomer substrate,10-undecenoic acid, was added to produce poly(3-hydroxyundecenoate) (PHU) . While homopolymers of PHN and PHU were the major products of the synthesis, a hexane fractionation of the batch to separate the two compounds, revealed that a disproportionately high mass of PHU was extracted with the PHN, when compared to a control sample prepared by simply mixing PHN and PHU homopolymers. I.e. the presence of additional PHU in the PHN fraction was presumed to be from segments of PHU covalently joined to PHN. This result along with a supporting test that diminished the likelihood of forming a random copolymer of PHN and PHU, pointed to the conclusion that a small fraction of block-copolymers had been formed during the biosynthesis.

At the same time Kelly et al. were exploring the feasibility of a an *in vivo* process to produce block copolymers that combined poly(hydroxybutyrate) (PHB) with poly(hydroxyvalerate) (PHV)[173]. As motivation for their study, they noted that the ability to control the formation of block regions within a polymer molecule depends on knowledge of the precise time when substrate exhaustion occurs and the ability to rapidly switch between two substrates with minimal overlap in their supply. As a solution, they proposed a process for block-copolymer synthesis whereby a gaseous substrate could be used to control intracellular monomer fluxes. Because of the low solubility of gasses, their residence time in a continually aerated vessel is minimal. Thus, after the supply is switched off, any residual gas is rapidly consumed by the culture or stripped from the media by the flow of an inert gas. To implement such a process they focused on the chemolithoautotrophic bacterium *Ralstonia eutropha*, which can derive energy from hydrogen gas to fix CO_2 while simultaneously utilizing various other sugars and organic acids. In their experiments they tested the effects of periodic hydrogen supplementation while maintaining a continuous supply of different substrates, including valeric acid, propionic acid, and fructose. Under an air atmosphere, the consumption of valeric acid resulted in the synthesis of monomers for both PHV and PHB, resulting in the accumulation a PHB-co-PHV random copolymer. However, when the gas supply was switched to hydrogen, the selectivity of polymer synthesis toward PHV (rate of PHV

synthesis / rate of PHB synthesis) increased dramatically compared to growth under an air atmosphere. Moreover, when the atmosphere was cycled from hydrogen, to air, and back to hydrogen, polymer synthesis continued, and PHV selectivity again increased. Based on these results they reasoned that repeated cycling between air and hydrogen could be used to create two distinct polymer domains with different PHV compositions.

Shortly afterward, Madden et al. reported in 1998 on an alternate process in *R. eutropha* designed to synthesize block-copolymers of PHB and PHV *in vivo*, using propionate as source of PHV monomers, with the addition of glucose for PHB monomers[174]. To test the effects on copolymer composition they tested various periods of propionate addition (20, 10, 8, or 5 h) with alternating periods of glucose supply. During glucose feeding, they observed the formation of PHB homopolymer, while during propionate addition they observed the formation of PHV-co-PHB random copolymer. To probe for the presence of block copolymers, the authors fractionated the polymers using a mixture of chloroform and heptane and tested the individual fractions using DSC and NMR. While the data they collected did not completely confirm the presence of block-copolymers, the data were not inconsistent with such a hypothesis either. In addition to compositional testing, the authors performed mechanical testing on the different polymer samples but observed that modulus and resistance to embrittlement were no better than simple blends. Ultimately, the authors concluded that they had not formed block-copolymers of PHB and PHV; however, in light of findings reported in later studies[40, 153], it is likely that Madden et al. had indeed produced a small fraction of these molecules but simply failed to identify them. Part of their justification for rejecting the presence of block-copolymers was based on their estimate of the chain propagation rate at 6.7 monomers/polymerase/second. The authors noted that this was significantly faster than a previous estimate of 2 monomers/polymerase/second [175-176], which assumed ~18,000 polymerases per cell[175]. Based on the value of 6.7 and assuming a polymer chain of 700,000 g/mol, Madden et al. estimated that the average time to synthesize a chain was 18 minutes, which is similar to the estimate of Kelley et al. of 12-24 minutes[173]. With such a short life-span for active chain propagation, Madden et al. rationalized that a switching period of 5 h was too infrequent to produce block-copolymers.

In that same year, Kelley and Srienc produced two-phase, core-shell "nanoparticles" in *R. eutropha*[177]. See **Figure 2.4**. The biosynthesis employed a two-step feeding strategy in which fructose and valeric were fed for the first 12 h of the culture, followed by only fructose for the remaining 12 h. The PHA granules produced inside the cells were observed to have a core of PHB-co-PHV copolymer surrounded by pure PHB homopolymer. In addition, they observed that such biphasic granules constituted only 30-40% of all the granules formed, while other granules appeared homogenous in composition. These results were consistent with the idea presented by Madden et al. that the processes of chain initiation and termination occurred throughout the polymer accumulation phase. Furthermore, the Kelley and Srienc speculated about the possibility for block-copolymer synthesis, if the time-span of valeric acid uptake was made shorter than the period of chain propagation.

A year later Su et al. published results from a study investigating the *in vitro* polymerization of PHB and PHV copolymers from monomers of (*R*)-3-hydroxybutyryl-CoA (3HB) and (*R*)-3-hydroxyvaleryl-CoA (3HV), respectively.[179] A key finding of their research was that the rate of polymerization of 3HB *in vitro* (40 molecules of 3HB-CoA / polymerase / s) was approximately 20x higher than the rate estimated for *in vivo* polymer synthesis using *R. eutropha.*[175-176] Furthermore, the *in vitro* rate of PHB synthesis was 2x higher than the *in vitro* rate they measured for PHV synthesis. This was different than the earlier results of Kelley and Srienc who observed that for *in vivo* polymerization the rates of PHB and PHV synthesis were practically identical[177] , and that the individual rates of polymerization were additive when monomers for PHB and PHV were supplied simultaneously.

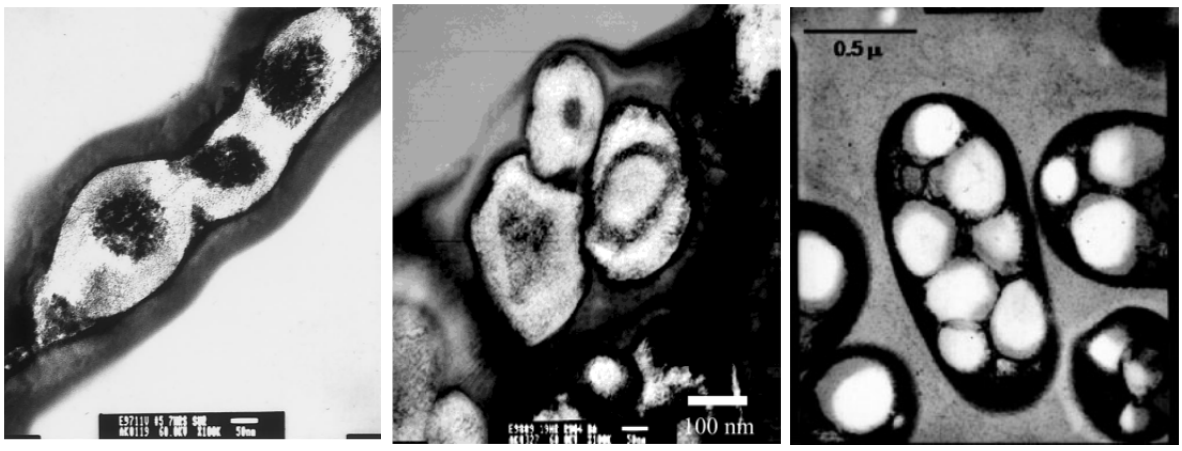

Figure 2.4 TEM images of PHB / PHB-co-PHV granules from R. eutropha
Granules are stained with RuO_4: PHB domains are white, while PHB-co-PHV domains stain darker. a.) Granules with a PHB-co-PHV core surrounded by a PHB shell. [177] b.) A multi-layered granule with PHB-co-PHV as the middle layer.[178] c.) Granules *in vivo* with a PHB core surrounded by PHB-co-PHV shell.[153] Photos adapted from their respective manuscripts.

Su et al. attributed their own results to the fact that for the *in vitro* studies they had used monomer concentrations that were 50x higher than the estimated K_m of the polymerase enzyme. Another key finding by Su et al. was that when the PHA synthase enzyme is operated in a purified *in vitro* system, the process is capable of behaving as a "living polymerization", for at least 72 minutes, indicating a negligible occurrence of termination or chain-transfer events. When Su et al. polymerized 3HB-CoA first, followed by a second addition of 3HV-CoA, they produced a copolymer material of PHB and PHV. Based on the increase in molecular weight seen after the second monomer was added, in addition to NMR results, they concluded that the polymer was most likely a block-copolymer

Factors Affecting Living Polymerization in vivo

As mentioned previously, the most ideal circumstances for block copolymer synthesis occur under conditions of a "living polymerization", whereby molecular weight steadily increases throughout the entire synthesis. As such, exploration of the physical mechanism behind initiation, propagation, and termination, and how the relative kinetics of these process affect the molecular weight and polydispersity of polymer chains has been a focus of numerous studies.

For the PhaC$_{R.e.}$ synthase of *R. eutropha* it is known that dimerization of the molecule results in faster initiation and propagation[180-182] but with the dimer producing only one elongating chain[180]. However, even for dimeric species of PhaC$_{R.e.}$ a lag phase is still observed[111, 182]. For *in vitro* polymerizations across numerous species it has been observed that the rate of polymer propagation is significantly faster than the rate of initiation[64, 182-187], resulting in the presence of a short lag-phase prior to rapid propagation. Elimination of the lag phase *in vivo* has been achieved by the addition of surfactants[111, 188] and with the use of oligomeric PHB fragments as primers[181, 189-190]. Moreover, in studies where the *phaC$_{R.e.}$* was purified from recombinant *E. coli,* a clear lag-phase existed[182-183], but when Cho et al. purified the enzyme from its native host strain—along with several other proteins bound to the synthase—the lag-phase was eliminated[191-192]. In the most recent findings, Pfeiffer et al have attributed much of this affect to PhaM, a recently discovered protein associated with PHA granules with the capacity for DNA-binding. Addition of the purified molecule to PhaC (without need for DNA), significantly reduced the lag time of the *in vitro* polymerization from ~3 minutes to <0.5 minutes. Increasing levels of PhaM further reducing the lag-time. In addition, Cho et al. showed that another granule associated protein, PhaP, can solubilize individual PHB chains bound to PhaC, thereby suggesting that binding by PhaP may play an important role in the development of nascent PHB chains before their fusion into larger, insoluble granules. The transient role of the PhaP1 proteins was supported by the observation that the ratio of PhaP1 to PHB molecules was 4-9:1 for the soluble PHB fraction but <0.6:1 for insoluble PHB granules which grow larger with time. Furthermore, the soluble PHB fraction did not

contain other granule-associated proteins (e.g. PhaR, PhaZ) which are typical of mature granules.

For PHAs produced *in vivo*, the weight average molecular weight (M_w) typically ranges between 0.2-3x10^6 g/mol [193]. For example, in *R. eutropha* the M_w of PHB ranges between 0.6-1.1x10^6 Da[175] while various *Pseudomonas* species produce copolymers of PHA_{mcl} in the range of 0.09-0.33x10^6 Da depending on the substrate used[44, 194-195]. However, in recombinant *E. coli*[14, 196-197] and for some *in vitro* polymerization[111, 179] exceptionally high values for M_w have been reported for PHB in the range of 4-20x10^6 Da. Possible explanations for this may be that some termination / transfer agents present in the wild-type systems are not produced in recombinant system, or perhaps that other proteins in the wild-type systems help to regulate molecular weight. In the case of *in vitro* systems, the use of purified reagents likely eliminates many possible termination agents. An additional factor that has been shown to affect polymer molecular weight is the initial concentration of polymer synthase enzymes. This was verified by Sim et al. in recombinant *E. coli*[14], and by Gerngross and Martin[111] in an *in vitro* system, who both demonstrated that fewer synthase enzymes result in higher molecular weights.

Initially, Kawaguchi and Doi[175] proposed that *in vivo* cessation of polymer propagation occurs as the result of termination / transfer agents that compete for the active site thioester, thus causing the release of the completed PHB chain. Indeed, subsequent studies have identified numerous substrates whose addition during polymer synthesis resulted in a significant reduction to molecular weight when compared to cultivation on sugars alone. The common characteristic of most of these compounds is the presence of one or more hydroxyl groups. Termination agents identified include alcohols, e.g. methanol, ethanol, isopropanol, and butanol, as well as polyols e.g. glycerol, ethylene glycol, polyethylene glycol (PEG), 1,2-propanediol, 1,3-propanediol, and 1,4-butanediol[198-200]. By comparison, 3-hydoxybutyric acid and 4-hydroxybutyric acid (i.e. PHA monomers sans CoA) as well as lactic acid and acetic acid showed little or no reduction in molecular weight[200]. However, for butyric acid, an opposite result was observed by Shimizu et al. who noted a positive correlation between increased levels of butyric acid in the media and reduced molecular weight[201]. High levels of glucose and succinic acid have also been reported to cause a reduction in molecular weight[202].

Furthermore, Gengross and Martin found that polymerase enzymes present in the insoluble fraction of an *in vitro* reaction product (i.e. synthases bound to large PHB granules) synthesized polymer more than 10x faster than soluble (i.e. presumably unassociated enzymes), although after the initial monomer was consumed and more monomer was added, both soluble and insoluble synthases remained primed and showed no lag-phase. Because surplus reactant (S/E = 1.2 $x10^6$ mol 3HB-CoA / Enzyme) could not be converted after the M_w increased above $12x10^6$ they concluded that the PHA synthase of *R. eutropha* was not capable of chain termination under the specific *in vivo* conditions tested[111]. Thus, if association with the PHB granule can increase the rate of chain propagation during early periods of polymer synthesis, it is conceivable that a similar effect might also slow and eventually stop the propagation process when the granule becomes too large.

Alternatively, Tian et al. observed that for the heterodimeric, Class III synthase complex (PhaEPha$C_{A.v.}$) of *Allochromatium vinosum* the Pha$C_{A.v.}$ unit was able to dissociate from a growing polymer chain after reaching a molecular weight of ~1.8 MDa. Other data in the study indicated that the PhaEPha$C_{A.v.}$ complex is capable of some form of chain-transfer or hydrolysis mechanism that allows cleavage of polymer from the enzyme. Following cleavage, a shorter fragment of polymer remained in the synthase which acted as a primer for rapid initiation of the next polymer molecule. The authors presented further evidence that suggested that a similar chain termination mechanism might also exist for Pha$C_{R.e}$. Interestingly, this result contradicts that of Gengross and Martin who concluded that chain termination for Pha$C_{R.e.}$ did not occur in *in vitro*. Here it is notable that the S/E ratio used by Gerngross and Martin was $1.2x10^6$ while that used by Tian et al. was < 300. In their study Tian et al noted that for the Type III synthase, very short oligomers (<20) were cleaved more readily than longer ones, and that the rate of cleavage was much shorter than the rate of propagation. Thus, with the enzymes in the study by Gerngross and Martin being attached to very long polymer chains their expected rate of cleavage would be small, and depending on how long the reactions were run before quenching, sufficient time may not have been available to observe any cleavage / chain termination effects.

An alternative perspective on the issue was presented by Tian et al. whose *in vitro* polymerization study indicated that final molecular weight could also be a determining factor in termination[189]. For the Type III synthase of *Allocromatium vinosum*, they observed that the rate of termination increased rapidly as the polymer molecular weight approached 1.8 MDa. This result suggested that the propensity for termination may be an inherent trait of the synthase. Consistent with this hypothesis, studies in which protein mutagenesis was applied to PHA synthase enzymes have reported significant alterations in polymer molecular weight depending on the substitution of certain residues at key catalytic locations[203-206]. In addition , both pH and temperature have be cited as factors affecting molecular weight[196-197, 201, 207].

This apparent living polymerization observed by Tripathia et al. is in distinct contrast to other reports of PHA production in wild type *R. eutropha*[175, 201] and *Pseudomonas putida*[208] that show the average molecular weight of polymer chains reaches its maximum value very early in the biosynthesis (<5 h). This rapid plateau in M_w indicates that frequent termination and or chain transfer become limiting, thereby precluding the existence of a living polymerization . However, for *in vitro* polymerizations of PHB, Gerngross and Martin concluded that chain transfer / termination does not occur[111], and Su et al. reported continual propagation for > 72 h without interruption.[179]. Such results support the hypothesis that certain "termination agents" may aid in disrupting the propagation process. Alternatively, it may be that by a using non-native host with only the polymer synthase gene of ($phbC_{R.e.}$) Tripathi avoided some unknown regulatory mechanism designed to limit molecular weight in the native *R. eutropha* host. However, this theory is challenged by another report of recombinant PHB production in *E. coli* in which a continual increase in molecular weight was not observed[14]. In this study the researchers expressed the entire *phbABC* operon of *R.eutropha* and used glucose as the monomer precursor. By adjusting the level of *phbC* expression inside the cell *via* an IPTG-inducible promoter, the investigators were able to control the final M_w of the polymer, but the early plateau was always present. Moreover, the observation of a living polymerization made by Tripathia et al. is especially perplexing given that the substrates they employed, 1,3-propanediol and 1,4-butanediol, have been shown also be especially effective agents for inducing chain termination[200].

In contrast to observations by Su et al. which showed that *in vitro* polymerization can continue for longer than 72 minutes[179], prior studies of *in vivo* polymerization[173-174] suggested that the average life-span of an elongating chain could be much shorter (12-24 min) inside a living cell. This disparity was attributed to a higher frequency of either termination or transfer events within the cell, possibly due to competition for the enzyme by foreign species, thereby interrupting the propagation process. While Shu et al. demonstrated the potential of the PhaC synthase to produce block-copolymers in a carefully controlled reaction *in vitro*, the short life-times estimated for chain propagation inside living cells made the prospect of obtaining significant quantities of block-copolymer via microbial biosynthesis more uncertain. The early studies by Kelly et al.[173, 177] and by Madden et al.[174] reflected their understanding that the synthesis of block-copolymers *in vivo* likely required the execution of multiple substrate switches, and that the period of these switches was dependent on chain life-span. Madden's study probed this hypothesis by testing the effect of different feeding periods, but in the end, they were unsuccessful at detecting PHA block-copolymers.

Mathematical Modeling of in vivo Block-Copolymer Synthesis

To gain a better insight into the dynamics of the polymerization process *in vivo*, Mantzaris et al. created a mathematical model for the synthesis of PHB-*b*-(PHV-co-PHB) block-copolymers in *Ralstonia eutropha*[40]. In the hypothetical biosynthesis, fructose was supplied continuously during the polymerization phase, while small doses of valerate were added periodically. Output of the model provided estimates for the size and number of block domains in each molecule as well as the distribution of molecular weights for all species.

Kinetic parameters for the model were based on physiological measurements of polymer synthesis in *R. eutropha* while utilizing a mixture of fructose and valeric acid[177]. The basis of the model was a population balance over all polymer molecules that divided them into groups of either active or inactive chains, with only active chains allowed to form block-copolymers at the time of a substrate switch. Given that the life-span for an actively elongating chain (< 0.5 h) was much shorter than the time of the polymer

accumulation phase (> 24 h), Mantzatis et al. recognized that a substrate switch, implemented midway through the polymer accumulation phase, would affect only the small fraction of chains that were actively elongating when the switch was made. As a result, the majority of polymer produced over the 24 h polymer accumulation phase would be either PHB homopolymer that was synthesized before the switch, or a random copolymer of PHB-co-PHV that was synthesized after the addition of valeric acid, with only a small fraction of block-copolymer synthesized shortly after the time of the switch. To increase the content of block-copolymer molecules within the cells, Mantzaris provided the mathematical rigor to support Kelley and Madden's earlier idea that continual switching events would be needed throughout the entire polymer accumulation phase. **Figure 2.5** illustrates the result of different feeding strategies on the composition of PHA polymers produced *in vivo*.

Previously, Kelley et al. had observed that when both fructose and valeric acid were present in the media, the total rate of PHA synthesis was 2x greater than the rate of PHB synthesis that occurred when only fructose was supplied, and that the polymer formed was PHV-co-PHB with ~50 mol% PHV[177]. To add to this information, Mantzaris et al. conducted a second copolymer synthesis experiment and collected data for the overall molecular weight distribution as a function of time. By fitting the model to this data, they were able to estimate the rates of reaction for polymer initiation, propagation and termination. As a basis for the model, Mantzaris et al. chose to consider the production of 50:50 PHB-b-(PHV-co-PHB) block-copolymers i.e., the number of monomers in the PHB block are equal to the number of monomers in the PHV-co-PHB block.). Calculations based on the experimental data indicated that to achieve a 50:50 molecular structure, the time period for valerate addition should be ½ of the time period without valerate addition (i.e. fructose only.) .

Using this model, the authors were able to predict the correlation between the number of "substrate switches" and the fraction of block-copolymer molecules produced. See **Figure 2.6**. According to the model, a "substrate switch" is defined so that the start and stop of one substrate addition are counted as 2 switches. The maximum fraction of di-block molecules (50% of the total polymer mass) was obtained when the number of substrate switches was $N = 39$. This corresponded to a 30-min period for PHV-co-PHB

synthesis during valerate addition followed by 60-min period for PHB synthesis using only fructose. The model predicted that below this number, more mono-block molecules (i.e. homopolymer) would be produced, and above this number, more tri-block molecules would be produced, with additional switching events leading to successively higher order multi-block copolymers. For tri-block molecules, a maximum fraction (29% wt.) was obtained when the number of substrate switches was N = 90, corresponding to a 12.5-min synthesis period for PHV-co-PHB followed by a 25-min period for PHB. For N =39, the model predicted the sum total of all different block-copolymer molecules to be 69% of the total polymer mass, with this fraction increasing to 92% wt. % for N = 90. . This implies that with the addition of valeric acid at N = 0, N = 39 specifies 20 periods of PHB-co-PHV synthesis, alternating with 20 periods of PHB synthesis. In a second paper, Mantzaris et al. extended their analysis to allow for transient variations in the frequency and duration of the substrate additions[209]. This was in contrast to the first model, which assumed a constant period of substrate switching throughout the entire polymer synthesis phase. Results of the optimization, revealed that for the synthesis of 50:50 block-copolymers, N = 39 was in fact a global optimum resulting in a maximum di-block molecule fraction of 50.6 wt.%.

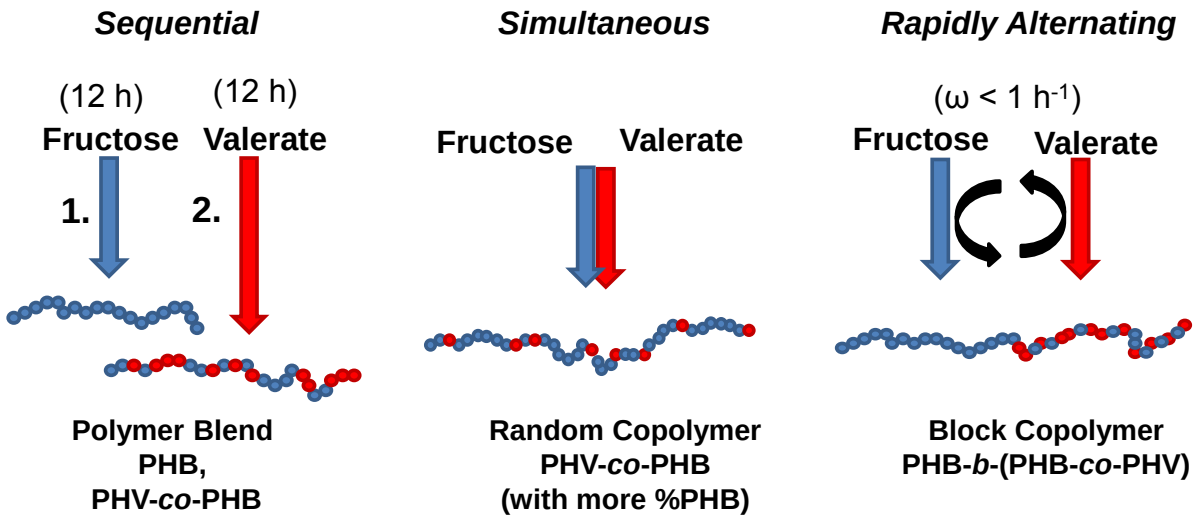

Figure 2.5 Substrate feeding methods for in vivo polymerization and the polymer products they produce.
In wild-type *Ralstonia eutropha,* feeding of fructose results in the production of PHB, while valerate produces a random copolymer of PHV-co-PHB (~45% PHV). When the two substrates are fed simultaneously, the random copolymer that is produced contains a higher fraction of PHB. To maximize the production of block-copolymers, the substrates must be cycled rapidly at a frequency faster than the average life-time of an elongating chain. As the average life-time of a polymer chain increases, the required period of substrate switching decreases.

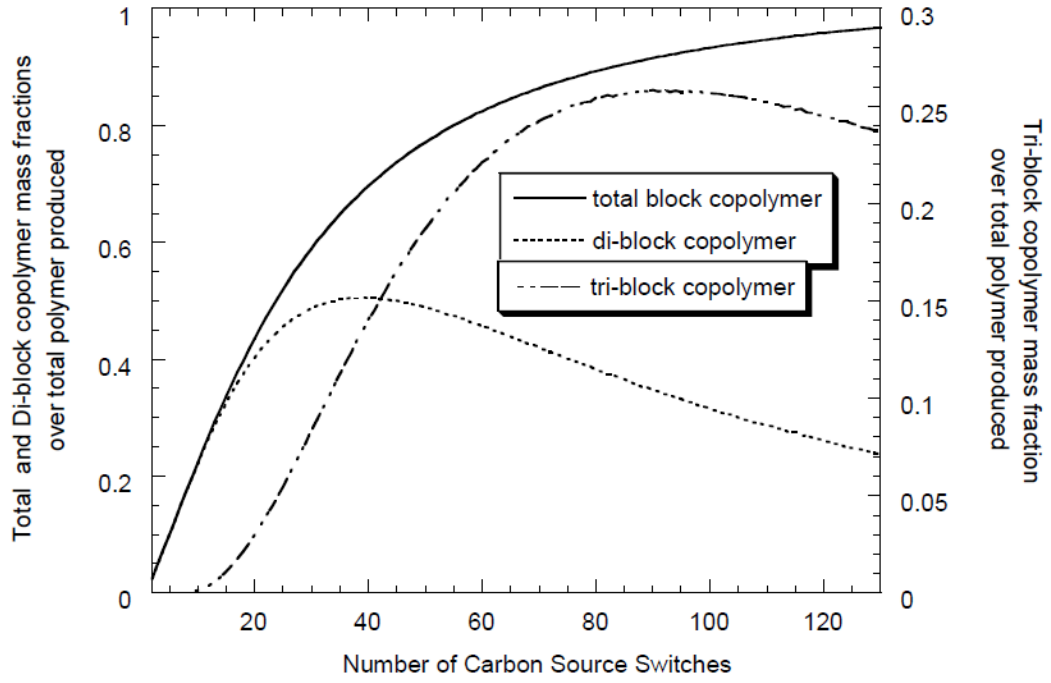

Figure 2.6 The effect of the number of substrate switching events on block-copolymer synthesis in vivo.
The figure shows the mass fraction of di-block, tri-block, and total PHB-*b*-(PHB-co-PHV) block-copolymers produced during *in vivo* synthesis as a function of the number of carbon source switches performed during a finite synthesis window. Calculations are based on a population balance model of polymer synthesis. The maximum di-block fraction occurs at at $N = 30$ switches, and the maximum tri-block fraction occurs at $N = 90$ switches. Figure adapted from Mantzaris et al.[40]

Process Control of in vivo Block-copolymer Synthesis

The first experimental study to test the findings of Mantzeris et al. was performed by Kelley et al., who carried out *in vivo* polymer production in *R. eutropha*[178]. The biosynthesis they employed, just as Mantzaris had modeled, involved a continuous supply of fructose, while making periodic additions of valerate. In their first experiment, valerate was added twice during a 20 h synthesis period, with each addition lasting ~4-5 h. TEM images of the PHA granules produced during the synthesis revealed the presence of a variety of microstructures. In addition to homogenous granules, they observed the presence of core-shell particles consisting of a PHV-co-PHB core surrounded by a PHB shell. Also, they noted the formation of unique multilayered granules in which a PHB core was surrounded by a concentric ring of PHV-co-PHB and then an outer ring of PHB.

See **Figure 2.4**. Despite the appearance of bi-phasic granules, the presence of actual block-copolymer molecules in the granules was expected to be small.

In their second set of experiments, which was designed specifically for block-copolymer synthesis, they reduced the period of valerate addition to 16 times in 15 h, with each valerate shot lasting ~36 min before its depletion. Recognizing the need to confirm the depletion of valerate before initiating the PHB synthesis phase, the authors relied on measurements of dissolved oxygen (DO) in the culture medium to serve as a proxy for valerate addition. With this analysis method, DO was observed to make a sharp drop, corresponding precisely to the addition of valerate, followed by a rapid rise to its initial level upon depletion of the valerate. After the polymer was extracted and purified, repeated fractionations produced a material which was apparently homogenous and displayed two distinct melting endotherms, one at 85˚C and the other at 160˚C, thus suggesting the presence of block-copolymer molecules. A TEM image of the isolated block-copolymer showed the presence of two, intercalated, phases with homogenous domains of 200-1000 nm.[178]

The next attempt at *in vivo* synthesis of PHB-*b*-(PHV-co-PHB) block-copolymers was performed by Pederson et al. who prepared multiple batches in which they systematically decreased the substrate switching time[210]. This was done in order to vary the relative composition of di-block and tri-block molecules within the final polymer composition. The switching times they tested (i.e. periods of valerate addition) included 32, 14, 10, and 8 minutes. In all cases, the duration of fructose-only feeding was made for 2x the duration of valerate feeding. According to the model predictions made by Mantzaris et al.[40], the relative ratio of tri-block to di-block molecules was expected to increase as the switching time decreased below 30 minutes. For comparison, the researchers also prepared batches of PHB-co-PHV random copolymer with PHV fractions similar to those of the block-copolymers.

A significant achievement of Pederson's study was the use of biosynthesis off-gas analysis, *via* online mass-spectroscopy measurements, to monitor and control the time periods of valerate addition. See **Figure 2.7**. Similar to how Kelly et al. had first employed DO measurements as a proxy for valerate consumption[178], Pederson et al. observed that the culture's oxygen uptake-rate (OUR, mmol/L/h) made a rapid rise at the

time of valerate addition, followed by a sharp decline in OUR with depletion of the substrate. At the same time, the carbon dioxide evolution rate (CER, mmol/L/h) showed a similar pattern. Moreover, these changes in the metabolic state of the culture were detected almost instantly. By comparison, offline methods to quantify the concentration of valerate in the media (e.g. HPLC or GC) can take between 0.5-1 h to complete only a single sample. Another benefit of the off-gas monitoring was the ability it provided to control the timing and size of valerate addition when metabolic rate / polymer synthesis began to decline. Previously, Pederson and Srienc had employed the same off-gas analysis technique in order to control the dimensions of core-shell granules composed of PHB and PHV-co-PHB polymers[153]. See **Figure 2.4**. While DO measurements do show a response to valerate addition, the use of off-gas analysis to monitor the size of molecular domains is preferable. This is because DO is often an important process variable for regulating the metabolic state of a culture, with the use of agitation as a control variable to maintain the DO set-point. Thus, a correction in the DO value by agitation adjustment may give a premature indication of valerate exhaustion.

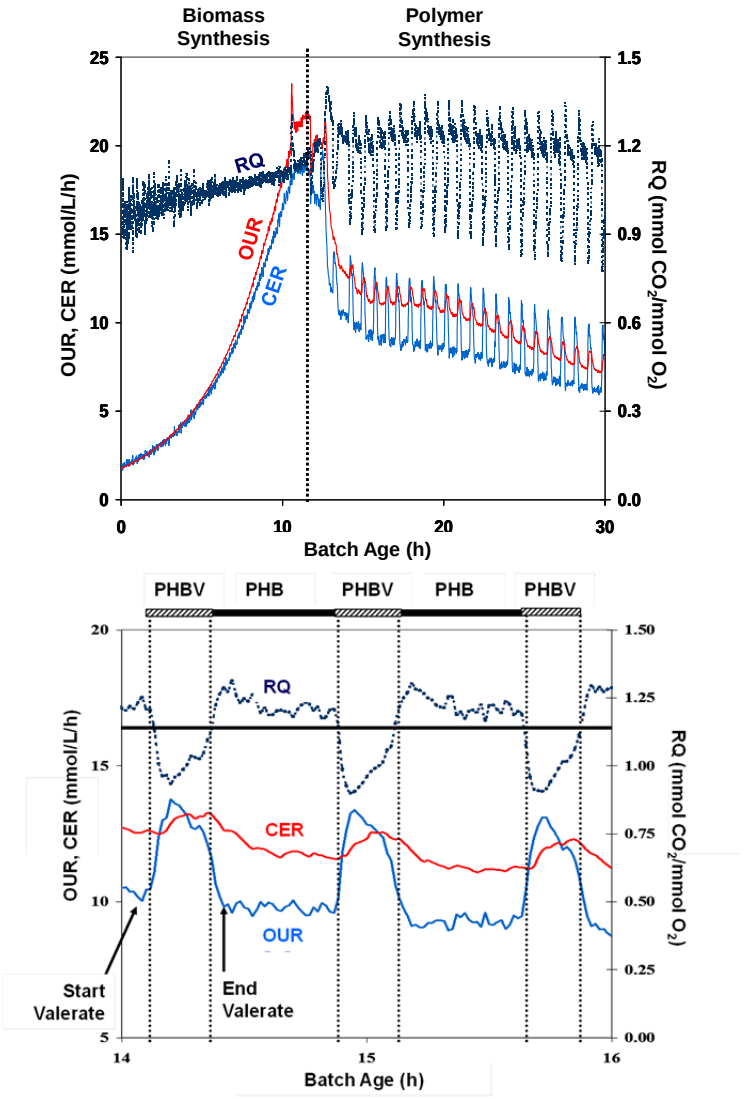

Figure 2.7 Off-gas monitoring off block-copolymer synthesis in vivo
Data is collected from mass-spectroscopy analysis of biosynthesis off-gas. **a.)** Metabolic profile during block-copolymer synthesis. OUR (oxygen uptake rate, mmol O_2/L/h), CER (carbon dioxide evoluation rate, mmol CO_2 /L/h) and RQ (respiratory quotient, CER/OUR, mmol CO_2/mmol O_2) Biomass production occurs until either nitrogen or oxygen become limiting. After which time rapid polymer accumulations begins, with the periodic addition of valeric acid used for block-copolymer synthesis. **b.)** Detailed view of off-gas profile during block-copolymer synthesis. The addition of valerate to the culture media results in a rapid rise in the OUR. During this period the cells produce a random copolymer of PHB-co-PHV. After the valerate is consumed OUR returns to its baseline level. At this time, only fructose is available in the media , which results in the production of PHB homopolymer. Block-copolymer molecules are formed specifically by those polymerases which are active at either the start or end of valerate addition. **7.b** is adapted from Pederson et al.[210] **7.a**. is previously unpublished data from the same report.

By performing extensive characterization of both block and random copolymer samples using differential scanning calorimetery (DSC), rheology, dynamic mechanical analysis, and strain-to-break testing, in addition to DSC and NMR analysis of fractionated block-copolymer samples, the authors were able to provide strong evidence for the synthesis of block-copolymer molecules. While block-copolymer samples did show improved toughness compared to random copolymer samples, the results were not sufficient to establish a correlation between material properties and the relative proportions of di-bock and tri-block molecules.

One important question raised by Pederson's initial study was, how do the properties of PHA block-copolymers change upon aging? For PHB homopolymer, as with many polymeric materials, it is known that crystallinity increases with aging, which can enhance strength but also leads to embrittlement. This issue was addressed in a study by McChalicher and Srienc, which examined the time-depndent variation in mechanical properties of PHB-*b*-(PHV-co-PHB) block-copolymers versus random copolymers[20]. The polymers tested were taken from the same polymer batches synthesized earlier by Pederson et al. The results of the study by McChalicher and Srienc showed that after 1 day of aging, a random copolymer of PHV-co-PHB (29% PHV) had a significantly higher elongation at break, >500%, compared to 15% for PHV-co-PHB (8% PHV) However, after only 1 month of aging, the elongation at break of both polymer had decreased to <15%. By contrast, two different PHB-*b*-(PHV-co-PHB) block-copolymers, one with 15% PHV and the other with 23% PHV, showed values for elongation at break of 100% and 160%, respectively, even after 3 months. With respect to modulus and strength, the block-copolymers showed similar performance to random copolymers, when also considering the effect of PHV content.

Subsequent Developments in Block-copolymer Synthesis in vivo

Encouraged by the positive findings of McChalicher et al., more recent studies of *in vivo* polymer synthesis have focused on creating new block-copolymers combining a range of PHA types, as well as utilizing alternate microbial hosts and even artificial genetic circuits for synthesizing the polymers. In 2006 and 2007 Iadevaia and Mantzaris completed two modeling studies which explored the feasibility of using synthetic genetic circuits to control the formation of PHA copolymer molecules[42-43]. Contrary to previous biosyntheses which had relied on switching of external substrates to affect individual block formation, Iadevaia and Mantzaris proposed to regulate monomer fluxes, instead, by the switching of critical enzymes in each monomer supply pathway. In their first model, based on a novel gene network first constructed by Gardner et al.[211], Mantzaris et al. employed a bistable, genetic network that could be toggled between distinct states of 3HB and 3HV synthesis[42] by either the addition of the exogenous inducer molecule IPTG or a transient temperature shift from 37˚C to 42˚C. With the combined capacity to control monomer fluxes by manipulating both substrate and enzyme levels, they suggested that they could more tightly regulate the composition and discreteness of polymer domains. In their follow-up study Iadevaia and Mantzaris demonstrated the potential of a synthetic genetic oscillator to automatically regulate the period of substrate switching[43]. Inspiration of the design was taken from Elowitz and Leibler's famous, "repressilator" gene circuit[212].

In 2008 Pereira et al. attempted to synthesize PHB-*b*-(PHV-*co*-PHB) block-copolymers from fructose and propionic acid *via R. eutropha* using an alternating feeding schedule[39]; however, details of the feeding scheme were vague. Using a combination of DSC, NMR, and crystallization kinetic studies, they concluded that the polymer produced was not a statistically random copolymer and that the possibility of some block-copolymer molecules could not be excluded. Mechanical properties of the material were not reported.

More recently, the laboratory of G.Q. Chen has been a prolific source for studies on PHA block-copolymers[213-218]. In 2011, Li et al.[215] became to the first to report on the *in vivo* synthesis of block-copolymers that contained both PHB and PHA_{mcl} , specifically

PHHp (poly(3-hydroxyheptanoate), in the form of PHB-*b*-(PHHp-co-PHV). To achieve this, they combined a mutant *Pseudomonas putida* strain, deficient in fatty acid *β*-oxidation (Δ*fadA* ΔfadB) as well as its native polymer synthase (Δ*phaC*), with a recombinant plasmid expressing the PHA synthesis operon of *Aermonas caviae* (*phaPCJ-*$_{A.e.}$) The expanded substrate specificity of the *A. caviae* synthesis genes allowed the mutant strain to incorporate the monomers of both PHA_{scl} as well as PHA_{mcl}; otherwise, *P. putida* is capable of producing only PHA_{mcl}. The researchers fed butyrate first to produce segments of PHB followed by a period of heptanoate in order to produced segments of PHV-co-PHH. Whether the authors used a 2-step sequential feed or multiple substrate alternations was not clear. The modulus of the purported block-copolymer was reduced compared to that of PHB homopolymer, but the elongation at break was significantly enhanced. See **Table 2.1** While it seems likely that the process did produce some block-copolymer molecules, the analysis did not address the possibility that the block-copolymer sample could have also contained significant amounts of PHB homopolymer and PHHp-co-PHV random copolymer.

Later that year members of Chen's group published another study, detailing their synthesis of block-copolymers containing PHB (poly(3-hydroxybutyrate)) and P4HB(poly(4-hydroxybutyrate)). The biosynthesis used by Hu et al.[213] employed an enhanced *P. putida* mutant (Δ(*fadA fadB fadAx fadB2x phaC phaG*) along with recombinant expression of the polymer synthase of *Ralstonia eutropha* (*phbC*$_{R.e.}$) and the 4-hydoxybutyryl-CoA transferase gene of *Clostridium kluyveri* (*orfZ*$_{C.k.}$). After 12 h of biomass accumulation on rich media, γ-butyrolactone was fed for a period of 24-48 h to synthesize P4HB, after which, butyrate was fed for another 48 h to synthesize PHB. During the synthesis glucose was supplied to further sustain growth. The purported block-copolymer did showed greater strength than a similar random copolymer, but the elongation at break was reduced. See **Table 2**.**1** Given that only one substrate switch was performed during the biosynthesis, it is unlikely that a significant fraction of block-copolymer molecules was produced. The reported D value from NMR analysis (356) clearly indicates that the polymer was not a random copolymer, which is signified by a D value close to 1; however, such a result is not conclusive to distinguish between block-copolymers or a simple blend of polymers.

A 2012 report from Chen's group reported on the production of block-copolymers of PHB and PHHx. For this study Tripathi et al.(2012)[217] employed the same *P. putida* strain and recombinant PHA_{scl} pathway (*phaPCJ*$_{A.e.}$) used by Li et al. (2011), along with a similar sequential feeding strategy used by Hu et al. (2011). A PHB homopolymer was produced when the culture was fed butyrate, and a copolymer of PHHx-*co*-PHB was produced when hexanoate was fed. Thus, any block-copolymer formed was expected to be PHB-*b*-(PHHx-*co*-PHB). As with the sequential, 2-period, feeding strategy used by Hu et al., it is likely that the polymer contained some fraction of PHB-*b*-(PHHx-*co*-PHB), but significant amounts of PHB homopolymer and PHHx-*co*-PHB random copolymer would also be expected. To account for this possibility, the authors fractionated the purported block-copolymer mixture using a mixture of chloroform and heptane, before performing NMR on the individual fractions. The analysis revealed that one fraction contained mostly PHB homopolymer, with a second fraction giving a spectrum indicative of a block-copolymer. NMR spectra for fractions with higher heptane solubility, which would have contained random copolymer molecules of PHHx-*co*-PHB, were not included. Compared to a polymer blend of similar composition, the block-copolymer was distinctly more elastic but with a noticeably reduced modulus. See **Table 2.1**

Subsequently, in 2013, Tripathi synthesized block-copolymers of P4HB and P3HP (poly(3-hydroxypropionate))[218]. This time, *Escherichia coli* was selected as the microbial host and was transformed with a 5-gene heterologous pathway, including *phbC*$_{R.e.}$ of *R. eutropha* as the polymer synthase. 1,3-propanediol and 1,4-butanediol were used for the production of homopolymers P3HP and P4HB, respectively, while a random copolymer of P3HP-co-P4HB was formed when both substrates were fed simultaneously. To create the block-copolymer molecules, Tripathi et al. employed a sequential, 2-period, feeding strategy, similar to the one used in their earlier study. More than any other previous study by Chen's group, this report provided the strongest evidence for the production of significant amounts of block-copolymer material. This result was supported by four key findings. 1.) The block-copolymer showed significantly different mechanical properties compared to both a random copolymer and a polymer blend of similar composition. 2.) NMR data showed clear and logical distinctions between the block-copolymer and the polymer blend. 3.) Fractionation of the purported

block-copolymer resulted in only one fraction, which showed the same NMR spectrum as the unfractionated material. i.e. The unfractionated material did not appear to contain significant amounts of homopolymers of P3HP or P4HP nor any copolymer of the two. 4.) Time-course data collected for the polymer molecular weight showed a constant increase throughout the entire biosynthesis. At the end of 24 h of cultivation on 1,4-butanediol the molecular weight was $3.3x10^5$ Da; following this, 1,3-propanediol was supplied for another 24 h, resulting in a final molecular weight to $5.5x10^5$ Da.

Monomer switching can also be controlled using genetic circuits *via* external signaling molecules, as was originally demonstrated in the *in silico* polymerization model of Iadevaia and Mantzaris[42]. Recently, such an idea was actually demonstrated *in vivo* by Wang et al.[219]. In their system, addition of the extracellular inducer IPTG was used to activate a P_{T7} promoter upstream of genes for converting glycerol to 3HP monomers, while the addition of arabinose was used to activate a P_{BAD}-Ara promoter upstream of genes required for production of 3HB from fructose. Furthermore, when glycerol was supplied to the culture, glucose was added simultaneously in order to stimulate the catabolite repression system of *E. coli,* thereby shutting down activation of the P_{BAD}-Ara promoter. The authors demonstrated that by adjusting the relative amounts of IPTG and arabinose, they could closely control the final composition of the polymer. Similar to the block-copolymer syntheses of G.-Q. Chen, Wang et al. used only one substrate switch during their biosynthesis. While DSC and NMR results were not inconsistent with the hypothesis of block-copolymers, the quantity of these molecules in the purified material was questionable. Measurements of mechanical properties of the materials were not included in the report.

In the most recent report from Chen's group, Li et. al. detailed their synthesis of PHDd-*b*-PHDe random and block-copolymers (poly(3-hydroxydodecanoate), poly(3-hydroxydecenoate)) using dodecanoate and 9-decenol as substrates[214]. The organism they used, *Pesudomonas entomophila,* is a native PHA producer and was selected for its ability to consume alcohols and transform them into fatty acids which are the precursors to PHA monomers. In order to avoid the production of PHA molecules containing fewer carbons than the full length substrates, the researchers deleted several β-oxidation genes in the organism, thereby hindering its ability to degrade fatty acids. The

incorporation of unsaturated monomers of 3-hydroxydecenoate from 9-decenol was chosen to enable the formation of a gel-network *via* ultra-violet initiated cross-linking. Production of various, random copolymers was achieved through simultaneous supply of both substrates in varying proportions, while a purported block-copolymer was synthesized by providing dodecanoic acid for the first 12 of the cultivation followed by 9-decenol for the final 36 h. The material was then fractionated before performing NMR. Results showed that the fractioned specimen was distinct from a random copolymer, and similar to a blend of homopolymer, with some minor differences suggesting the possibility of block-copolymer molecules. Compared to similar random copolymers, the material suspected to contain some fraction of block-copolymers exhibited a modulus that was more than 2x greater than the random copolymers while maintaining a similar elongation at break.

Verification of Block-copolymer Synthesis

For block-copolymer synthesis *in vivo*, the typical method employed for synthesizing distinct polymer domains is to feed one substrate for some period, immediately followed by a second substrate with the assumption that chain propagation be uninterrupted over the entire period. In most of the recent reports of block-copolymer synthesis *in vivo* [213-215, 217-219] the typical practice has been to perform only one substrate switch, usually at some time in the middle of the polymer synthesis phase, which often lasts between 12-36 h. Attempting to synthesize block-copolymers in this way, makes the implicit assumption of a "living polymerization". Mechanistically, such a living polymerization requires that the rate of chain propagation be far greater than the rates of chain termination or transfer. To produce substantial quantities of block-copolymers in this way, propagation of a single polymer molecule must occur continuously for at least several hours and ideally for the entire period of polymer synthesis. As an indication of this type of action, the average molecular weight of the polymer molecules must be seen to continually increase throughout the entire biosynthesis. However, it has been shown for PHA polymerization across multiple host species[14, 175, 208] that polymer molecular weight usually reaches its maximum value very early in the biosynthesis and plateaus or

even decreases for the remainder of the polymer accumulation phase. The appearance of such a molecular weight profile indicates that chain termination events are occurring continuously throughout the biosynthesis and may even increase in frequency as the batch proceeds. It is also know that in native PHA producers, chain degradation often occurs simultaneously with propagation. However, only for the second report by Tripathi et. al did the authors observe a molecular weight profile that continually increased for the entire batch, thereby giving evidence for a living polymerization[218].

If conditions for a living polymerization are not present, then biosyntheses that implement only one substrate switch over the entire batch will likely not produce a significant fraction of block-copolymer molecules in the polymer mixture. This is because many elongating chains will terminate before the switch and many more will start only after the switch. Rather the mixture produced would be essentially a blend, containing large fractions of homopolymers formed either before or after the switch. Only the population of chains that are active at the precise time of the switch will become block-copolymers.

The effects of chain termination on block-copolymer quantity and composition were clearly described in the mathematical model proposed by Mantzaris et al.[40]. To account for the effect of frequent chain termination, the authors calculated that substrate switching must occur repeatedly throughout the polymerization period, arriving at an optimal value of 39 switches to maximize the production of di-block molecules in *R. eutropha.* Based on these recommendations, the first *in vivo* biosyntheses of PHA block-copolymers made by Kelley et al.[178] and Pederson et al.[153] made numerous substrate additions, utilizing either dissolved oxygen levels or changes in the oxygen uptake of the culture as a proxy to signify the alternating periods of polymer synthesis.

Since the report by Pederson et al. most attempts at block-copolymer synthesis *in vivo* have made no acknowledgement of the possibility of frequent chain termination and the impact that this can have on the final product. In a few instances the resulting materials produced from these single-switch processes have exhibited significantly different mechanical properties when compared to random copolymers or blends. Such results do suggest the presence of block-copolymer molecules; however, it is well known that even small additions of block-copolymers can create noticeable changes to polymer

blends by acting as compatiblizers between otherwise immiscible phases. To substantiate their claims of block-copolymer synthesis, these reports have frequently referred to DSC and NMR results, which often show unique patterns depending on the presence of a random copolymer, block-copolymer, or simple blend. The problem is that for such comparisons, the magnitude of the important distinction are sometimes small and can be degenerate for other polymer mixtures. For example, in NMR, the application of Bernoullian statistics can be used to determine if a copolymer sequence is statistically random by calculation of the D-statistic[220]. This metric, calculated as a quotient of the mole fraction of specific monomer diads ($D = F_{AA}F_{BB}/F_{AB}F_{BA}$) takes on a value of 1 for a statistically random copolymer while values $>\sim1.5$ or $<\sim0.6$ indicate either a non-random distribution or a regularly alternating sequence, respectively[221]. In many of the recent reports of block-copolymer synthesis *in vivo*, the calculation of a large D-value has been cited as strong evidence for the presence of block-copolymers. However, as Kamiya et al. pointed out the same result can also be obtained when the Bernoullian model is applied to a mixture of two different random copolymers or a mixture of homopolymer and random copolymer. In special cases such as block-copolymers or blends, Kamiya et al. demonstrated that a first-order Markovian model or a sum of two Bernoullian models may be more appropriate[221]. For example, the NMR spectrum produced by an A-B block-copolymer is almost identical to the one produced by an equivalent blend of A and B homopoymers in the same proportion. The only difference is seen in the presence of a small fraction of AB diads, which ensure a finite value for the D-statistic, i.e. the D-value for a homopolymer blend is undefined. For a block-copolymer chain composed of 500 A monomers joined to 500 B monomers, the single AB diad at the center of the chain represents only 0.1 % of the entire mole fraction of diads. Given that 0.1% is usually beyond the resolution of NMR, the spectrum of an AB block copolymer could easily be confused with a tertiary mixture comprising a blend of A and B homopolymers with a small amount of random copolymer. In the absence of a living polymerization, such a tertiary mixture would be expected from a polymer biosynthesis in which only one substrate switch was made, with a small amount of random or block copolymer formed immediately following the switch.

To account for this possibility a prudent practice is to perform a solubility fractionation of the polymer mixture prior to NMR in order to remove any homopolymer or random copolymers. While this can help to purify any block-copolymers present, the fractions collected are not expected to be completely homogenous. This is due to the dependence of solubility on molecular weight, e.g. small chains of a low solubility polymer may co-fractionate with longer chains of a high solubility polymer. Moreover, when the homopolymer segments that comprise a block-copolymer are structurally very similar, differences in their solubility may not be large enough be to obtain a good fractionation. While some studies of PHA block-copolymers did perform fractionation prior to NMR, the details of these procedures were under reported. A thorough analysis must include data for the solvent composition and mass of polymer collected for each fraction.

Provided that the specificity of the PHA synthase accepts both types of monomers, it is most probable that a single substrate switch performed during the polymer accumulation phase will result in the formation of some block-copolymer molecules. However, the quantity of block-copolymer molecules produced is highly depended on both the average life-time of an elongating polymer chain and the number of switches made[40]. The ideal scenario in which the entire population of polymer chains are converted to block-copolymers using a single substrate switch is achieved only when termination events occur so infrequently that a living polymerization is possible. While the use of purified reagents for *in vitro* polymerizations can be used to limit termination events[111, 179], studies have reported that for *in vivo* polymerization numerous molecular species can act as chain termination agents, including the monomer feedstocks themselves[198-202].

In the case of living polymerizations, which are commonly employed in organic synthesis of block-copolymers, the demonstration of additive molecular weights before and after the addition of the second monomer provides the strongest evidence for block-copolymer formation. However, when block-copolymer synthesis is carried out under non-living polymerization, which is apparent in the observation of a constant molecular weight profile in time, then the burden of proving block-copolymer synthesis becomes higher. Rheological mesurements of polymer melts[210], dynamic mechanical analysis,

DSC, NMR[221], as can all be used to infer the existence of block copolymer molecules[210], especially when the components are separated by careful fractionation. Furthermore, these arguments can be made even stronger if a primary fraction showing block-copolymer characteristics is then subjected to a second round of fractionation[178]. In addition matrix-assisted laser desorption with time-of-flight mass spectroscopy (MALDI-TOF) has also been used for the determination of PHA block-copolymers[222-223] and provides results which are more conclusive than those of NMR.

While it is likely that all of the *in vivo* studies referenced in this review did produce some block-copolymer molecules, the fraction of these molecules present in the purified polymer is highly questionable, and in some cases may only constitute a small amount. In the biosynthesis reported by Pederson et al.[210], calculations provided by the mathematical modeling of Mantzaris et al. predicted that the polymer should contain almost 70% of block-copolymer molecules; however, even Pederson's investigation did not include a rigorous experimental validation of this prediction. Thus, it is unclear if the properties that have been observed with PHA block copolymers are primarily a characteristic of the block-copolymer molecules or rather the properties stemming from thermodynamically stabilized blends. In order to begin to thoroughly understand these materials, a quantitative correlation must be established to relate the fraction and molecular structure of block-copolymer molecules with the changes in physical and mechanical properties they produce. To achieve this goal and advance the field of study, greater attention to the specifics of *in vivo* polymerization (e.g. by careful manipulation of the concentration, duration, and frequency of substrate additions) will be necessary, combined with more thorough analytical investigations to measure the complex compositions of PHA products produced.

Organic Synthesis of PHA Block-Copolymers

Parallel to investigations pursuing *in vivo* synthesis of PHA block-copolymes, alternate studies have focused on the synthesis of these molecules via conventional organic synthesis routes. An early attempt to synthesize PHA block-copolymers was made by Abe et al. in 1994[224]. Using ring-opening polymerization they synthesized segments of atactic P(*R,S*)HB from racemic β-butyrolactone followed by the addition of ε-caprolactone to synthesize segments of isotactic P6HHx. Verification of block-copolymer molecules was made on the basis of additive molecular weights observed before and after the addition of the ε-caprolactone. When P(*R,S*)HB-*b*-P6HHx was used as a compatibllizer to blends of the substituent homopolyers, the modulus of the blends decreased but their elasticity improved. See **Table 2.2**.

In 2002 Andrade et al. prepared block copolymers comprising hard segments of scl PHB joined to soft segments of mcl PHO-co-PHHx[225]. The multi-block copolymers with a M_w of ~34,000 g/mol contained on average 2 segments of PHB and 2 segments of PHO-co-PHH joined together by urethane linkages. To assemble the block-copolymers the researches first took microbially synthesized PHB and PHO-co-PHHx and hydroxylated their carbonyl end-groups to form telechelic PHA-diols. Next, the PHB-diol and the PHO-co-PHHx-diol were combined with L-lysine methyl ester diisocyanate to create urethane linkages. The formation of a multi-block copolymer was verified by additive molecular weights and NMR. The modulus of the material was 213 MPa with an elongation at break of 37%.

Polyethylene glycol (PEG) is another biodegradable polymer that is particularly useful for its solubility in water. This is in contrast to most PHAs which are hydrophobic. In biomedical applications for tissue engineering, drug delivery, and degradable implants, pure PHB is a poor material choice because of its brittleness, hydrophobicity, and high crystallinity which are resistant to hydrolytic degradation and cell attachment. Thus, to create novel materials with improved properties for biomedical application, researchers have sought to temper the brittleness of PHB and enhance hydophilicty by linking it to segments of PEG. Joining of the two molecules has been achieved in numerous forms including : multi-block polyurethanes [216, 226-231], tri-block

molecules using PEG as a macroinitiator for ring-opening polymerization of (*R,S*)-β-butyrolactone [228], di-block molecules by transesterficaiton[232], and di-block molecules using PEG fragments as termination agents to *in vivo* PHB synthesis[171].

Initial reports of polyurethane synthesis were made by Zhao et al. in 2004 and 2005[229-230]. To prepare the polymers, they took microbially synthesized PHB and converted it to telechilic PHB-diols (M_N = 2.7 kDa) by transesterification with 1,4-butanediol. These fragments were then combined with low molecular weight PEG (M_N = 1.0 kDa) *via* the addition of hexamethylene diisocyanate (HDI) to join the fragments with urethane linkages. By adjusting the feed ratio of PHB-diols to PEG, the researchers produced block-copolymers with different PEG contents. The molecular weights (M_n) of the PHB-*b*-PEG-*co*-Ur molecules ranged from 33-60 kDa. GPC results gave the strongest evidence for block-copolymer formation: the final product had a high molecular weight and a unimodal distrbution, i.e. a multimodal distribution containing low M_n peaks would indicate unreacted pre-polymers. NMR and FTIR results also supported the hypothesis of block-copolymers. In general, the presence of more PEG within the polyurethanes resulted in a a reduction in modulus and ultimate strength but an improvement in the elongation at break. See **Table 2.2**.

Later, Li et al.[226] and Liu et al.[227] performed a more in-depth analysis of the same PHB-*b*-PEG-*co*-Ur molecules by varying not only proportions but also the relative sizes of PHB (M_N = 1.1-3.2 kDa) and PEG (M_N = 2.0-8.0 kDa) fragments. The synthesis procedure was essentially identical to that used by Zhao et al., with the exception that the PHB-diols were prepared using 1,3-propanediol instead. Final M_n of the polymers ranged from 23-40 kDa. Verification of block-copolymer formation was made by comparing the GPC distribution of the high M_n block-copolymer with those of the low M_n pre-polymers, with additional support from NMR and FTIR. In contrast to the observations by Zhao et al., Li et al. found that when the fraction of PEG in the polyurethane was increased—by the incorporation of larger PEG fragments rather than the addition of numerous small fragments—the modulus of the material actually increased, and so did the elongation at break. Thus, increasing the content of PEG can improve crystallinity (and modulus) but only if the added monomers are contiguous to existing homo-domains. However, the same enhancement effect was not seen for PHB.

Results from both Li et al. and Liu et al. showed that when the size of PEG fragments were held constant while PHB fraction was increased by either 1.) increasing the size of PHB fragments or 2.) by increasing the number of PHB fragments, elasticity of the material always decreased, often dramatically, although modulus still increased.

Additionally, both studies showed a clear correlation between the amount of PEG in the block-copolymer and the amount of water adsorbed by the material. Pure PHB had an equilibrium water content of 5% wt. while the block-copolymer containing 50 mol% PHB absorbed > 35 wt.% water. Under conditions of water saturation, the block-copolymers retained >75% of their ultimate strength while increasing their elongation at break.

In addition to their synthesis of PHA block-copolymers *in vivo*, the laboratory of G.Q. Chen has also been active in the area of organic polymerizations to produce biodegradable polyurethanes. Specifically they have explored combinations of PEG with PHB[231], PHB-co-P4HB[231], and PHB-co-PHHx[216]. For the synthesis of PEG-*b*-(PHB-co-PHHx)-co-PU they used PEG with PHB-co-PHHX-diols and HDI, using either solution polymerization in 1,2-dichloroethane (75˚ C) or by melt polymerization (120˚ C). Results showed that the M_n of the melt polymerization products were higher by 14-24%, but also with higher poly dispersity by 47%. Both modulus and the elongation at break were significantly higher with the melt polymerized materials, 71% and 390% respectively; however, values for the ultimate strength were not significantly different. The authors attributed this difference in material properties to the higher molecular weight of the melt polymerized product and to the existence of some branch chains stemming from the urethane linkages due to the higher concentration of HDI in the melt. With respect to the effect of the of PHB-co-PHHx / PEG ratio, similar values of modulus (E ~ 200 MPa) were found for the 90/10 and for the 30/70 compositions, while strain at break improved dramatically for the 50/50 composition (ε = 875%) versus (ε < 17%) for either of the former compositons. See **Table 2.2**.

Another "soft segment" that has been used to improve the toughness in PHA block-copolymers is poly(ε-caprolactone) (PCL) or poly(6-hydrxoyhexanoate) (P6HHx). While the polymer is not degradable by enzymes that degrade PHB it is degradable by lipase enzymes.[233] PCL is most commonly used as a soft segment in polyurethanes

containing petroleum derived polymers. Given its popularity as such, it has also received much attention as component in many PHA-based block-copolyers. Various block-copolymers and synthesis routes have been employed to combine PHA with PCL including: di-block copolymers using PHB-O-Al(ethyl)$_2$ pre-polymer as a macroinitiator for ring-opening polymerization of ε-caprolactone[234], di-block copolymers *via* transesterification of PHB and PCL[235-237], polyurethanes by combining telechelic hydroxylated PHB-diols and PCL-diols with diisocynate as a coupling agent, and tri-block copolymers using either PHB-diol or PHB-co-PHV-diol as a macroinitiator for ring opening polymerization of ε-caprolactone with either a lipase[238] or dibutylin dilaurate[239] as the catalyst.

In the polyurethanes synthesized by by Hirt et al.[240] the authors combined low molecular weight PHB-co-PHV-diols (4 mol% PHV) (M_n = 2.3 kDa) with low molecular weight PCL-diols (M_n= 1.2 and 2.0 kDa) and coupled them using methyl (S)-2,6-diisocyanatohexanoate (LDI). The compositions of the block-copolymers were adjusted by changing the relative amounts of reactants used, with final M_w of the polymers ranging between 35-152 kDa. GPC analysis of the final reaction products revealed that no reactants were present, and final molecular weight values were consistent with the amounts of reactants charged, thus confirming the formation of block copolymers. The general trend observed in mechanical properties was that increasing the fraction of PHB-co-PHV hard segments resulted in higher values of modulus and ultimate strength but with reduced elongation at break.

An alternate type of biopolyester poly(2-hydroxypropionate), more commonly known as polylactide (PLA), has received considerable attention due to its stiffness, strength, and optical clarity. PLA and PHA are similar in that the both are produced from renewable substrates (e.g. sugars) and can be rapidly degraded. While PHA is readily digested by environmental microorganism, the degradation of PLA requires composting at elevated temperatures to first hydrolyze the polymer into smaller fragments. Like PHB, materials formed from pure PLA are somewhat brittle, so considerable effort has been focused on toughening of PLA[241]. Given that both PLA and PHA are renewable and easily degradable, several studies have focused on the preparation of block-copolymer molecules combining these two materials. Compositions and methods

include: di-block copolymers by use of PHB-O-Al(ethyl)$_2$ and PHB-co-PHHx-O-Al(ethyl)$_2$ pre-polymer as macroinitiators for ring-opening polymerization (ROP)of *L*-lactide[29, 234, 242], tri-block copolymers synthesized by using telechelic P(*R,S*)HB-diol as a macroinitiator for ROP of *L*-lactide[243], and tri-block copolymers formed by sequential addition of 1.) *L*-lactide, 2.) (*R,S*)-β-butyrolactone, and 3.) *L*-lactide *via* living polymerization[244].

Unlike, the enzymatic synthesis of PHA which produce only isotactic, poly(*R*-3-hydroxyalkanoate) polymers, organic syntheses from β-butyrolactone allow the incorporation of both *R* and *S* monomer types. The resulting atactic and often syndiotactic copolymers produce a low crystallinity material with significantly enhanced elasticity when compared to isotactic PHB. Thus, segments of P(*R,*S)HB can be combined with segments of more crystalline and stronger polymers to improve mechanical toughness. In 2000 Hiki et al. reported on the advantageous properties of PLLA-b-P(*R,S*)HB-b-PLLA block-copolymers[243]. The first step of the synthesis involved formation of a telechelic diol of P(*R,*S)HB by ROP of racemic β-butyrolactone using 1,4-butanediol as a microinitiator. In the next step, the P(*R,S*)-diol was used a macroinitiator for the ROP of *L*-lactide. The M_n of the P(*R,S*)HB pre-polymer was 10.1 kDa, and the M_n of the subsequent tri-block copolymers ranged between 16 and 30 kDa. Verification of the intended synthesis was made by comparison of GPC traces of the pre-polymer and block-copolymer as well as NMR. As the mole fraction of PLLA increased from 0 to 1 the modulus of the material monotonically increased from 24-800 MPa while the elongation at break monotonically decreased from 610-7.2 %.

Simple blending of PLA and PHA can be used to create new materials with enhanced mechanical properties; however, immisciblity between the two compounds results in thermodynamic lability. As a solution to this Shreck and Hillmyer investigated the potential of PLA-*b*-(PHB-co-PHHx) block-copolymers to act as blend stabilizers[29]. To prepare the block-copolymers, microbially synthesized Nodax^{TM} (PHB-co-PHHx, 7% PHHx) with a M_w of 450,000 g/mol was degradaded *via* acid-catalyzed methanollysis to various M_w between 7,700 and 74,000 g/mol. This oligomeric product was then used as a macroinitator for the ring-opening polymerization of L-lactide. Tertiary blends were prepared using PLA-*b*-(PHB-co-PHHx) (50% wt. PHA) as a compatibilizer between the

Nodax and PLA phases. While the tertiary blends did show better dispersion, as indicated by a reduction in PHA particle size from 0.97 μm to 0.59 μm, addition of the block-copolymers produced no significant improvement in the toughness (*via* Izod Notched Impact) over binary mixtures. The authors reasoned that chain scission during melt processing at 190˚C led to a reduction in the molecular weight of the PHA segments. As a result, the shortened PHA chains were unable to effectively entangle with the surrounding PLA, thereby limiting interfacial adhesion and stress transmission between the PLA matrix and the dispersed PHA particles.

Alternatively, Aluthge et al. employed a living polymerization to achieve PLA / PHA tri-block copolymers[244]. To do this, they conducted a conventional ROP using lactone monomers, but instead selected a dinuclear indium catalyst $[(NNO)InCl]_2$ (μ-OEt)(μ-Cl) that was noted to have a very minimal rate of chain transfer / termination events. PLLA-*b*-P(*R,S*)HB-*b*-PLLA tri-block molecules were synthesized by sequential charges of 1.) *L*-lactide, 2.) racemic β-butyrolactone, and 3.) *L*-lactide. In addition, the authors synthesized other tri-block combinations by interchanging PLLA segments with PDLA and/or P(*R,S*)HB blocks with atactic PLDLA. Confirmation of the target molecules was made by GPC and NMR. Hiki et al. produced molecules in which the M_n of the center P(*R,S*)HB block was held constant at 10.1 kDa, while varying the total M_n between 16-30 kDa; whereas, Aluthge et al. studied molecules where the molecular weight was held constant (115-130 kDa) while the size of the center P(*R,S*)HB block was adjusted to include lengths of either 32,13, or 7 kDa. Results demonstrated that increasing the size of the PHB segment increased the elongation at break from 9-21% while decreasing the modulus from 847-338 MPa. Related tri-block molecules in which the P(*R,S*)HB center block was substituted with PLDLA had changes in the elongation at break and modulus that were much smaller and of little practical significance.

Organic Synthesis of PHA Graft-copolymers

Typically the designation of block-copolymers is in reference to "linear" molecules, e.g. di-block, tri-block, and multi-block copolymer; however, the classification of block-copolymers can also include various "non-linear" block-copolymers. Like linear block-copolymers, these also arise from the combination of distinct regions of monomer homogeneity, but instead the block domains are connected in non-linear architectures such as star-polymers and graft-copolymer. One early study exploring the properties of PHA graft-copolymers was made by Hazer[245] in 1995 who grafted polystyrene chains (PS) onto a PHN (polyhydroxynonate) backbone. To prepare the material Hazer polymerized polystyrene using oligo azo or oligo peroxides as initiators. Next, these "activated" polystyrene pre-polymers were added to the microbially derived PHN (M_n = 73 kDa). To iniatate the grafting process, heat was applied to break the peroxide and azo bonds thereby transforming the styrene chains into free-radicals for subsequent attack along the PHN backbone. Polymers were preapred using activated PS of two different M_n 10,000, and 35,000 g/mol. The addition of up to 18 wt.% PS in PHN-g-PS resulted in dramatic improvements in both the ultimate strength and elongation to break; however, the type and magnitude of the effects varied sporadically with PS content, possibly due to the M_n of the PS chain used. In contrast, a graft-copolymer containing 30 wt% styrene showed no improvement in mechanical properties.

In the same study, Hazer also prepared PHN-g-PMMA by instead grafting segments of PMMA (poly(methyl metacrylate)) (M_n = 63 kDa) onto the PHN backbones. Final M_n ranged from 160-180 kDa. Data showed that the maximum strength of the composites occurred at 5 wt% PHN; however, further increases in the PHN fraction up to 18% caused significant decreases in modulus, ultimate strength, and elongation at break. In a follow-up report from Hazer's lab[246], Eroglu et al. synthesized PHN-g-PMMA, but this time employing a one-pot synthesis in which γ-irradiation was used to polymerize methyl metracrylate (MMA) monomers from PHN backbones (M_n = 73 kDa). The final M_n of the polymer ranged from 370-473 kDa. In contrast to the PHN-g-PMMA polymers prepared by Hazer, those prepared by Eroglu et al. retained more of the strength of

PMMA homopolymer. In the latter case, the higher ultimate strength was likely due to the higher M_n. The results show some inconsistencies, but the general trends indicates that elongation at break increases as the fraction of PHN increases up to ~15%.

In a report by Ceccorulli et al. in 2002, the authors demonstrated that the addition of only 5% graft copolymer containing atactic P(*R,S*)HB grafted onto chains of polymethymethacrylate (PMMA) significantly improved the ductility of PMMA / PHB blends[247]. However, blending of the P(*R,S*)-g-PHB with PHB and PMMA was effective only for blends containing < 50% PHB. Beyond, this level the crystallinity of PHB could not be reduced. The graft copolymers were synthesized first by converting PMMA to an anionic macroinitiator by the addition of 18-crown-6 potassium hydroxide. To the activated [PMMA-O^-]K^+18C6 was then added monomers of butyrolactone, polymerized by anionic, ring opening polymerization to form chains of P(*R,S*)HB grafted to the PMMA backbone.

In 2011, the commercial PHA producer Metabolix published a patent under the name "Methods for Branching PHA Using Thermolysis", which claimed processes for the synthesis of branched PHA polymers, including graft-copolymers, as well as block-copolymers[248]. According to their method, microbially produced PHA was subjected to controlled thermolysis at temperatures for ranging from 190-250˚C for a period of 0.1-1.6 minutes, thereby causing a reduction in the molecular weight by >40%, and leaving unsaturated end-groups at the point of chain scission. Following this a peroxide catalysts was added to the degraded polymer to act as a free-radical initiator, thereby creating new free radicals along the polymer backbone. These radicals may then recombine with themselves or with radicals on other chains . A branched copolymer is formed when the unsaturated end-group of one polymer chain reacts with a free radical site along another polymer chain. When recombination occurs between two end-groups, a linear polymer is formed. At a catalyst loading of 0.15% wt., branching of the thermolysed polymer resulted in an increase in M_w by ~1.3x. With such a minimal increase in molecular weight, it is likely that most chains would have no grafts while those that did would likely have only one graft. In addition to branched PHA homopolymers, claims were also made for branched molecules formed from PHA copolymers as well PHA blends. In the case when branching is performed on a blend of two distinct PHA polymers, the products

formed would be considered non-linear graft-copolymers. While claims for linear block-copolymers were not made specifically, it is expected that such molecules would form when recombination occurs between polymer end-groups

Presumably, this first patent then became the basis a second patent by Metabolix published in December, 2013 under the title, "Biobased rubber modified biodegradable polymer blends"[249]. In this patent claims are made for branched copolymers comprised of PLA joined to a PHA copolymer. In one embodiment, branching is performed by reactive blending in which PHA pellets containing a peroxide catalyst are melt-blended with PLA, thereby producing linkages between PHA chains as well as between both PLA and PHA chains. This results in the formation of PLA-*g*-PHA graft-copolymes and PLA-*b*-PHA block-copolymers that can act as compatiblizers between the bulk PLA and PHA domains. The patent filing included mechanical data for specific compositions of PHB-co-P4HB rubbers reactively blended in PLA using the branching / cross-linking catalyst tert-amylperoxy 2-ethylhexyl carbonate (TRIGONOX 131^{TM}) (0.2%) with additional lubricants, plasticizers, and mineral fillers (<11%). For comparison,the researchers tested the toughening of four different PHA compositions containing different amounts of the P4HB comonomer between 16-41%. For binary blends of PLA and PHA (i.e. normal blending) little improvement in mechanical properties was seen; however, for tertiary blends including graft and block-copolymers (i.e. reactive blending) the elongation to break of the composite materials was dramatically increased with only a small drop in tensile strength. Furthermore, PHB-co-P4HB copolymers with higher P4HB content and displaying greater elasticity (25-88% 4HB) enhanced toughness more than did copolymers with less P4HB. This result is in contrast to the result of Shreck and Hillmyer who found no improvement in the toughness of PLA / PHB-co-PHHx blends when they added PLA-*b*-(PHB-co-PHHx) compatiblizers. Two possible reasons may exist for this. 1.) The PHB-co-PHHx material used contained only 7 mol% PHHx, i.e. with such a low comonomer content, the copolymer would be expected to exhibit very minimal elasticity, a key property for toughening. 2.) Shreck and Hillmyer added only 5 wt.% of the block-copolymer molecules, compared to the preparations of Metabolix in which branching was performed on blends containing 20-30% PHA.

Most recently, Metabolix announced news of the release of a new line of PHA-based additives designed to enhance the mechanical toughness of both PLA and PVC (poly(vinyl chloride)). The method they report is based on the blending of a small fraction of "amorphous" PHB (a-PHB) shown to have an elastomeric quality. The presence of small domains of a-PHA within the more rigid PLA and PVC helps to reduce the crystallinity of the matrix and absorb additional stress. The results show that the a-PHB additive produces a significant improvement in toughness. This is similar to conventional methods using dispersed styrene-butadiene rubber to toughen certain thermoplastics. Metabolix has indicated that the a-PHB is a copolymer formed by the addition of another comonomer (unspecified) that results in the reduction of the copolymer's crystallinity, which assumes a minimum value near 50%. Observations of low crystallinity in PHB copolymers have been made for a variety of comonomers including, PHV, PHP, PHHx, and P4HB, the latter three comonomers resulting in a completerly amorphous material, as inferred by a complete elimination of the crystallization enthalpy. Furthermore, Metabolix reported that improvements in toughness were especially pronounced in tertiary blends containing an additional "compatiblizer" that is activated during reactive blending.

Analysis of Block-Copolymer Metadata

Figure 2.8 shows a log-log plot of the Young's modulus (*E*) versus the elongation at break (ε_b) of the individual samples in each polymer system. What is immediately apparent is the strong inverse correlation seen between ε_b and *E*. For reference, the four dashed lines represent nulclines of constant ultimate strength, with each one corresponding to a hypothetical set of polymers, all having different moduli but the same ultimate strength (U) . Assuming perfect elastomers, all polymers on a given line are described by the same relation: $E^*\varepsilon_b = U$ with U a constant. The diagonal lines in **Figure 2.8** correspond to U = 1, 10, 100 and 1000 MPa. Note, however, that U nulclines do not indicate the actual ultimate strength of each polymer, but instead what the ultimate strength of the polymer would be based on extrapolation of the same modulous at $\varepsilon = 0$ all the way to $\varepsilon = \varepsilon_b$. A mechanistic interpretation a U nulclines can be made as a set of

polymer networks with internal rubber bands, being analogous to polymer chains. Inside the matrix, some rubber bands are connected in series while others are connected parallel. A matrix of many parallel connections would produce a high modulus polymer with a low elongation at break, while many rubber bands connected in series would create a low modulus material with a high elongation at break. But, in either case the ultimate strength of the network remains the same. An example of this occurs when the addition of molecular cross-links, nanoparticles, or polymer crystals (acting as junctions for molecular cross-linking) cause densification of a polymer network by linking multiple chains together. Effectively, cross-linking takes long springs, i.e. series connections, and doubles them back to create multiple, shorter springs connected in parallel. Increased entanglement may also occur when polymer cross-sections become smaller due to smaller functional groups along the polymer backbone, e.g. strands of polylactide more easily entangle than do strands of polyhydroxydecanoate. With a larger bend radius, polymer chains are less likely to become entangled.

While some polymer systems are show variation that is parallel to U nulcines, other systems have slopes that are more horizontal. In one extreme, completely horizontal lines represent nulclines of constant modulus, e.g. a set of elastomers with $E^*\varepsilon_b = U$ where E is constant. Increases in strength with minimal changes in modulus can result from an increase in the length of polymer chains, which requires that they must reptate further before breaking their initial entanglements. As a result the polymer material can be stretched to higher strains and consequently higher stresses before breaking . While horizontal nulclines moving in the direction of increasing ε_b may cross a number of U nulclines, an increase in the ultimate strength may not necessarily occur in the real polymer system. This is because the nulclines are defined under the assumption of a perfectly elastic polymer material; however, for viscoelastic solids beyond the yield point elongation may continue to occur with little or no increase in the modulus.

In the opposite extreme, vertical nulclines indicate increases in both modulus and strength with no change in the elongation of the material, e.g. a set of elastomers with $E^*\varepsilon_b = U$ where ε_b is constant. Such changes can arise from alterations to the intermolecular forces within polymer crystals. e.g. from hydrogen bonding between chains, or by the introduction of comonomers which reduce crystalline perfection.

By using the three different types of nulclines as a basis set, it is possible to make inferences about the origins of mechanical enhancements in the different block-copolymer systems. While a thorough analysis of each polymer system is left to the reader, we highlight a few noteworthy trends. Systems which display data roughly falling along U nulclines include PHN-g-PS, PHB-*b*-(PHB-co-PHHx), and PLA-*b*-P(*R,S*)HB-*b*-PLA. Polymers sets with more horizontal character showing minimal change in modulus include PLA-*b*-P(*D,L*)LA-*b*-PLA, PHB-g-PMMA, and (PHB-co-PHV)-co-PCL-co-Ur. Alternatively, one polymer system with a distinctly vertical character is PHP-*b*-P4HB which shows a sharp drop in modulus with the addition of P4HB monomers. This implies that much of the effect of the additional P4HB is simply in disturbing the crystallinity of the PHP with little improvement in the modulus of the material. PHB-*b*-PEG-co-Ur also shows more vertical character, but instead the modulus actually increases with increasing elasticity. In this case the trend is caused by the addition of increasingly larger segment of PEG within the polyurethane.

A particularly good example of the impact of block-copolymer architecture on mechanical properties can be seen for the PHB-*b*-(PHB-co-PHV). The two random copolymer in the data set fall along a U nulcline that originates from PHB homopolymer; however, for the two block-copolymer the slope of the line decreases as it shifts in the direction of higher elongation. Such a horizontal shift implies a reduction in the entanglement density of the material, which is consistent with the author's reports of reduced crystallinity in the block copolymers. While moving from the random copolymers to the block-copolymers does traverse U nulclines of increasing strength, U only increases for one of the block-copolymers but decreases for the other. This is because much of the increase in elongation of the polymer occurs after the polymer has yielded.

Figure 2.9 is a graph of U/ε_b versus ε_b. The quantity U/ε_b has the same units as E, [GPa], and represents the average modulus of a material over its entire elongation range. This is in contrast to E plotted in **Figure 2.8**, which is the strain-independent modulus of the material at $\varepsilon = 0$. In **Figure 2.8** data is spread across 3 decades of U nulclines, but in **Figure 2.9** the data is largely condensed to < 2 decades. Thus, there is much less difference in the ultimate strength of the different polymer systems than what is predicted

from the modulus values at $\varepsilon = 0$. Note, in **Figure 2.9** U nulclines can be used to gauge ultimate strength values of individual polymers. Because high levels of strain result in the disentanglement of polymer chains, the elastic properties of the materials become more dependent on the strength of elongated polymer chains rather than their ability to form tight networks or strong crystalline strucutres. In accord with this, it is logical that the ultimate strength of all the polymers in a given system should be more similar under elongated conditions because of the commonality of a polyoxoester bonds within each polymer backbone. Those polymer showing the largest difference between E and U/ε_b are ones with high values of ε_b, thus permitting polymer chains to undergo maximum reptation to disengage their initial entanglements. On the other hand, polymers with low values of ε_b are not able to significantly alter their entanglement structure before breaking, and therefore show little difference between E and U/ε_b. Moreover, because the changes from E to U/ε_b occur along vertical nulclines, it is apparent that crystallinity plays an important role in the enhancement of modulus in block-copolymer materials.

Table 2.1 Properties of Biopolymers Prepared using Biosynthesis *in vivo*

Sample Composition[a]		t_{age} (days)	T_g (˚C)	T_m (˚C)	M_n (10^5 Da)	PDI –	E (GPa)	Y (MPa)	U (MPa)	ε_b (%)	Ref. (#)
PHB-co-PHV	[92/8]	3	17	151	1.1	2.0	0.270	–	17	12	[20]
PHB-*b*-(PHB-co-PHV)	[85/15]	3	-9, 8	164	1.0	2.0	0.190	–	20	110	
PHB-co-PHV	[71/29]	3	-10	101	1.0	2.0	0.145	–	19.5	65	
PHB-*b*-(PHB-co-PHV)	[77/23]	3	-1	161	1.0	2.1	0.115	–	11.5	545	
PHB-co-PHV	[92/8]	90	–	–	–	–	0.264	–	20.6	12	
PHB-*b*-(PHB-co-PHV)	[85/15]	90	–	–	–	–	0.225	–	28.1	99	
PHB-co-PHV	[71/29]	90	–	–	–	–	0.223	–	19.7	15	
PHB-*b*-(PHB-co-PHV)	[77/23]	90	–	–	–	–	0.156	–	16.7	178	
PHB		14	3.1	171.8	–	–	1.470	–	18.0	3.0	[215]
PHV		14	-15.7	106.2	–	–	0.389	–	6.6	3.5	
PHHp		14	-32.1	no	–	–	–	–	–	–	
PHV-*co*-PHHp	[51/49]	14	-26.4	no	–	–	–	–	–	–	
PHB-*co*-PHV-*co*-PHHp	[72.9/13.1/14]	14	-7.3	no	1.27	2.9	0.127	–	7.0	462	
PHB-*b*-(PHV-*co*-PHHp)	[71.5/12.7/15.8]	14	-23.6, 3.5	170.6	0.52	8.7	0.366	–	7.5	63.4	
PHB + PHV + PHHp	[71.5/12.7/15.8]	14	-20.0, 4.4	166.5	0.81	4.4	0.257	–	5.3	24.0	
PHB		–	0.7	171.6	–	–	–	–	–	–	[213]
P4HB		–	-45.7	50.1	–	–	–	–	–	–	
PHB-*co*-P4HB	[30/70]	–	-22.4	50.1	–	–	–	7.3	9.9	729	
PHB-*b*-P4HB	[20/80]	–	-47.3	54.2, 161.4	0.5	3.1	–	13.3	19.9	438	
PHB + P4HB	[20/80]	–	-48.6	56.0, 171.2	–	–	–	10.9	16.5	357	
PHHx		~7	-28.2		–	–	–	–	–	–	[217]
PHB-*co*-PHHx	[79/21]	~7	-18.1	55.4	–	–	0.024	–	1.8	75.3	
PHB-*b*-(PHB-*co*-PHHx)	[58/42]	~7	-16.1, 2.7	172.1	0.81	2.5	0.0076	–	1.4	207	
PHB + PHHx	[58/42]	~7	-27.3, -8.2	173.8	–	–	0.080	–	4.3	10.1	
PHP		14	-17.9	78.1	1.10	1.5	2.889	33.8	21.5	498	[218]
P4HB		14	-47	61	3.32	1.2	0.181	13.8	34.7	697	
PHP-*co*-P4HB	[75/25]	14	-31.2	62.7	1.96	1.3	0.015	1.7	6.4	963	
PHP-*co*-P4HB	[62/38]	14	-36.1	63.5	2.15	1.3	0.004	0.9	0.5	1611	
PHP-*b*-P4HB {226/322-k}	[71/29]	14	-46.2, -20.2	55.0, 67.6	2.17	2.5	0.177	20.0	44.7	877	
PHP-*b*-P4HB	[63/37]	14	-45.2, -21.6	53.4, 66.8	2.09	2.6	0.113	7.4	25.3	1031	
PHP + P4HB	[75/25]	14	-47.0, -16.2	57.1, 78.1	1.72	2.8	0.190	10.8	13.8	95	

[a] (monomer wt.%), [monomer mol%], {M_n of constitutive block dominas, kDa} Compositions are given in the order that they appear in the sample name. Symbols: t_{age} (sample age time), T_g (glass transition temperature), T_m (melting temperature), M_n (number average molecular weight), PDI (polydispersity index = M_w/M_n), E (Young's modulus), Y (yield strength), U (ultimate strength), ε_b (elongation at break), Ref. (reference citation)

Table 2.1 Properties of Biopolymers Prepared *via* Biosynthesis *in vivo* (continued)

Sample Composition[a]		t_{age} (days)	T_g (˚C)	T_m (˚C)	M_n (10^5 Da)	PDI –	E (GPa)	Y (MPa)	U (MPa)	ε_b (%)	Ref. (#)
PHB		–	4	176	3.27	1.8	–	–	–	–	[219]
PHP		–	-22	76	1.14	1.6	–	–	–	–	
PHB-*co*-PHP	[22/78]	–	-20	72	1.58	2.1	–	–	–	–	
PHB-*b*-PHP	[25/75]	–	-20, -1	73, 164	2.78	3.2	–	–	–	–	
PHB + PHP	[25/75]	–	-21, 3	76, 173	2.56	2.5	–	–	–	–	
PHDd		14	-49.3	82.4	0.52	1.5	0.061	5.5	5.5	60	[214]
PHDd-*co*-PHDe	[90/10]	14	-48.4	68.6	0.58	1.6	0.051	2.1	4.0	221	
PHDd-*co*-PHDe	[60/40]	14	-53.7	52.0	0.55	1.6	0.020	1.4	3.5	206	
PHDd-*co*-PHDe	[48/52]	14	-55.3	45.1	0.63	1.7	0.003	2.2	2.3	124	
PHDd-*co*-PHDe	[23/77]	14	-55.3	43.2	0.66	1.5	0.003	1.2	3.6	173	
PHDd-*co*-PHDe	[19/81]	14	-55.8	43.3	0.62	1.5	0.005	1.0	3.7	105	
PHDd-*b*-PHDe	[30/70]	14	-55.2	46.1	0.71	1.8	0.008	3.0	3.0	138	

[a] (monomer wt.%), [monomer mol%], {M_n of polymer segments in kDa}, Compositions are given in the order that they appear in the sample name. Abbreviations: t_{age} (sample age time), T_g (glass transition temperature), T_m (melting temperature), M_n (number average molecular weight), PDI (polydispersity index = M_w/M_n), E (Young's modulus), Y (yield strength), U (ultimate strength), ε_b (elongation at break), Ref. (reference citation)

Table 2.2 Properties of Biopolymers Prepared *via* (Partial or Total) Organic Synthesis

Sample Composition[a]		t_{age} (days)	T_g (˚C)	T_m (˚C)	M_n (M_w) (10^5 Da)	PDI –	E (GPa)	Y (MPa)	U (MPa)	ε_b (%)	Ref. (#)
PHB		21	4	178	6.50	1.8	1.560	–	38	5	224
P(*R,S*)HB		21	3	no	0.20	1.1	–	–	–	–	
P6HHx		21	-70	57	0.59	1.5	–	–	–	–	
P(*R,S*)HB-*b*-P6HHx[50%] (BCP)		21	3	61	0.43	1.4	–	–	–	–	
PHB+P6HHX	(75/25/0)	21	4	57, 178	–	–	0.740	–	22	10	
PHB+P6HHX+ BCP	(81/14/5)	21	4	57, 178	–	–	0.530	–	22	38	
PHB+P6HHX+ BCP	(71/24/5)	21	5	57, 178	–	–	0.340	–	17	62	
PHB+P6HHX+ BCP	(68/23/9)	21	3	57, 178	–	–	0.320	–	15	68	
PHB-co-PHV[4%] (PHBV)		–	–	–	–	–	1.7	–	–	5	240
PHB-co-PHV[4%]-diol {2.3-k}		–	-14	140	0.023	–	–	–	–	–	
PCL-diol {1.2-k}		–	-70	45	0.012	–	–	–	–	–	
PCL-diol {2.0-k}		–	-70	45	0.02	–	–	–	–	–	
PCL-co-Ur {1.2-k}	(85/15)	–	-45	38	(1.1)	–	0.046	–	–	–	
PHBV-*b*-PCL-co-Ur {2.3/1.2-k}	(29/58/13)	–	-45	116	(1.5)	–	0.063	–	7.4	830	
PHBV-*b*-PCL-co-Ur {2.3/1.2-k}	(44/44/12)	–	-45	122	(0.66)	–	0.200	–	9.9	610	
PHBV-*b*-PCL-co-Ur {2.3/2.0-k}	(44/43/13)	–	–	–	(0.55)	–	0.260	–	9.3	240	
PHBV-*b*-PCL-co-Ur {2.3/1.2-k}	(69/21/10)	–	-15	134	(0.51)	–	0.500	–	15.9	21	
PHBV-co-Ur {2.3-k}	(92/8)	–	8	131	(0.35)	–	1.26	–	15.0	2.3	
PHB		14	–	–	–	–	1.47	–	27.0	3.4	
PHB-*b*-PEG-co-Ur {2.7/1.0-k}	(44.3/44.3/11.4)	14	-47.1	12.1, 138.7	0.33	2.9	0.055	–	7.5	76	230
PHB-*b*-PEG-co-Ur {2.7/1.0-k}	(29.1/58.1/12.8)	14	-47.8	17.9, 133.9	0.53	2.5	0.021	–	4.6	133	
PHB-*b*-PEG-co-Ur {2.7/1.0-k}	(17.2/68.9/13.9)	14	-44.7	21.7, 133.3	0.60	2.4	0.0046	–	2.7	119	
PHB {87-k}		2	–	–	0.87	2.6	1.14	–	25.7	2.3	250
PEG {8.0-k}		2	–	61.6	0.080	1.0	–	–	–	–	226
PHB-diol {1.7-k}		2	–	135.0	0.0174	–	–	–	–	–	
PHB-*b*-PEG-co-Ur {1.7/8.0-k}	(16.0/74.8/9.2)	2	–	55.7, no	0.371	1.2	0.120	10.2	10.7	1912	
PHB-*b*-PEG-co-Ur {1.1/3.3-k}	(18.0/53.2/28.8)	2	–	40.9, 82.2	0.259	1.5	0.041	5.9	6.5	1112	
PHB-*b*-PEG-co-Ur {1.7/4.2-k}	(26.0/63.5/10.5)	2	–	45.8, 123.8	0.375	1.4	0.065	7.3	11.0	1408	
PHB-*b*-PEG-co-Ur {1.7/3.3-k}	(30.9/59.1/10.0)	2	–	42.7, 125.6	0.344	1.5	0.037	5.5	8.9	943	
PHB-*b*-PEG-co-Ur {1.7/2.0-k}	(40.7/46.9/12.3)	2	–	31.4, 126.0	0.304	1.6	0.021	3.0	5.1	227	
PHB-*b*-PEG-co-Ur {3.2/3.3-k}	(48.8/49.6/1.6)	2	–	40.6, 148.5	0.338	1.5	0.078	–	8.9	11	

[a] (monomer wt.%), [monomer mol%], {M_n of constitutive block domains in kDa}, Compositions are given in the order that they appear in the sample name. Abbreviations: t_{age} (sample age time), T_g (glass transition temperature), T_m (melting temperature), M_n (number average molecular weight), PDI (polydispersity index = M_w/ M_n), E (Young's modulus), Y (yield strength), U (ultimate strength), ε_b (elongation at break), Ref. (reference citation)

Table 2.2 Properties of Biopolymers Prepared *via* (Partial or Total) Organic Synthesis (continued)

Sample Composition[α]		t_{age} (days)	T_g (˚C)	T_m (˚C)	M_n (10^5 Da)	PDI –	E (GPa)	Y (MPa)	U (MPa)	ε_b (%)	Ref. (#)
PHB-diol {1.8-k}		2	–	144.8	0.018	1.2	–	–	–	–	227
PHB-*b*-PEG-co-Ur {1.2/2.0-k}	(55.7/36.2/8.1)	2	–	114.6	0.227	1.7	0.178	7.9	9.1	1090	
PHB-*b*-PEG-co-Ur {1.8/2.0-k}	(55.9/31./12.9)	2	–	128.1	0.239	1.6	0.285	–	11.1	20	
PHB-*b*-PEG-co-Ur {1.2/2.0-k}	(67.2/21.8/11.8)	2	–	137.7	0.400	1.7	0.429	12.8	11.3	100	
PHB-*b*-PEG-co-Ur {1.8/2.0-k}	(69.6/19.4/11.0)	2	–	130.0	0.243	1.7	0.616	–	18.0	12	
PHO-co-PHHx[91/9]		3	-41.9	53.7	0.23	3.1	0.005	–	6.4	425	251
PHO-co-PHHx[88/12] (PHOH)			-30	61	0.236	2.8					252, 225
PHOH-diol {2.4-k}			-56	no	0.024	–					252, 253
PHB		21	4	178	0.650	1.8	1.560	–	38	5	,
PHB-*b*-PHOH-co-Ur {2.6/2.4-k}	[22/22/56]	–	-6	146	0.106	2.7	0.213	–	7.0	37	225
							Notched Izod Impact Resist. (J/m)				
PHB-co-PHHx[93/7] (PHBH)			–	–	1.5	3.0					
PLA		3	55	172	0.56	–		22			29
PLA-b-PHBH {17.1/17.5-k}	(55/45)	3	1,55	–	0.346	1.4		–			
PLA + PHBH	(85/15)	3	55	172	–	–		44			
PLA + PHBH + PLA-*b*-PHBH	(81/14/5)	3	–	–	–	–		44			
PHB-co-PHHx[88/12] (PHBH)		2			2.2	1.6	0.353		8.1	14	216
PHBH-diol {5.5-k},{2.4-k}		2	-5.6	106.5	–	–	–	–	–	–	
PEG {3.4-k}, {2.2-k}		2	–	59.2	0.035	1.2	–	–	–	–	
PHBH-*b*-PEG-co-Ur {5.5/3.4-k}	(87/11/2)	2	-12.7	101.3	0.92	1.8	0.187	–	6.4	17	
PHBH-*b*-PEG-co-Ur {5.5/3.4-k}	(67/28/5)	2	-29.8	27.3, 98.0	0.72	2.0	0.063	–	3.7	20	
PHBH-*b*-PEG-co-Ur {2.4/2.0-k}	(65/28/7)	2	-27.1	94.1	0.97	2.2	0.071	–	3.9	30	
PHBH-*b*-PEG-co-Ur {5.5/3.4-k}	(44/46/10)	2	-40.8	31.1, 65.1	0.91	2.5	0.035	–	7.7	875	
PHBH-*b*-PEG-co-Ur {5.5/3.4-k}	(25/64/11)	2	-24	42.8, 93.9	0.64	2.4	0.204	–	5.4	4.5	
P(*R,S*)HB {10-k}		–	-2	52,80	0.10	1.2	–	–	–	–	243
P(*R,S*)HB {95-k}		–	–	–	0.95	1.7	0.024	–	15	610	
P(*L*)LA-*b*-P(*R,S*)HB-*b*-P(*L*)LA {3/10/3-k}	[22/56/22]	–	0.7	50, 71, 124	0.16	1.2	0.030	–	10	200	
P(*L*)LA-*b*-P(*R,S*)HB-*b*-P(*L*)LA {5/10/5-k}	[26/47/26]	–	4.1	138	0.2	1.2	0.130	–	14	150	
P(*L*)LA-*b*-P(*R,S*)HB-*b*-P(*D*)LA{10/10/10}	[35/31/35]	–	4.8	152	0.3	1.2	0.160	–	15	86	
P(*D*)LA {99-k}		–	–	173	0.99	1.9	0.800	–	39	7.2	

[a] (monomer wt.%), [monomer mol%], {M_n of constitutive block domains in kDa}, Compositions are given in the order that they appear in the sample name. Abbreviations: t_{age} (sample age time), T_g (glass transition temperature), T_m (melting temperature), M_n (number average molecular weight), PDI (polydispersity index = M_w/ M_n), E (Young's modulus), Y (yield strength), U (ultimate strength), ε_b (elongation at break), Ref. (reference citation)

Table 2.2 Properties of Biopolymers Prepared *via* (Partial or Total) Organic Synthesis (continued)

Sample Composition[a]		t_{age} (days)	T_g (˚C)	T_m (˚C)	M_n (10^5 Da)	PDI −	E (GPa)	Y (MPa)	U (MPa)	ε_b (%)	Ref. (#)
P(*L*)LA-*b*-P(*D,L*)LA-*b*-P(*L*)LA {61/47/61-k}	(36/28/36)	−	53.3	168.9	1.7	1.1	2.548	−	56	4.8	244
P(*L*)LA-*b*-P(*D,L*)LA-*b*-P(*L*)LA {51/87/51-k}	(27/46/27)	−	57.3	no	1.9	1.2	2.674	−	40	4.6	
P(*L*)LA -*b*-P(*D,L*)LA-*b*-P(*D*)LA {55/43/55-k}	(36/28/36)	−	62.8	212.8	1.5	1.2	2.637	−	58	3.5	
P(*L*)LA -*b*-P(*D,L*)LA-*b*-P(*D*)LA {41/70/41-k}	(27/46/27)	−	62.8	208.4	1.5	1.2	2.654	−	45	2.8	
P(*L*)LA-*b*-P(*R,S*)HB-*b*-P(*L*)LA {61/7/61-k}	(47/5/47)	−	53.2	171.3	1.3	1.3	0.847	−	34	9.7	244
P(*L*)LA-*b*-P(*R,S*)HB-*b*-P(*L*)LA {57/13/57-k}	(45/10/45)	−	48.6	171.0	1.3	1.2	0.729	−	40	14.2	
P(*L*)LA-*b*-P(*R,S*)HB-*b*-P(*L*)LA {41/32/41-k}	(36/28/36)	−	38.7	166.7	1.2	1.3	0.338	−	20	21.0	
P(*L*)LA-*b*-P(*R,S*)HB-*b*-P(*D*)LA {65/7/65-k}	(47/5/47)	−	4.5	207.6	1.4	1.2	0.548	−	33	10.6	
P(*L*)LA-*b*-P(*R,S*)HB-*b*-P(*D*)LA {41/32/41-k}	(36/28/36)	−	4.8	208.9	1.1	1.3	0.431	−	15	7.3	
PS-perox {10-k}		−	−	−	0.1	2.6	−	−	−	−	245
PS-azo {35-k}		−	−	−	0.35	1.9	−	−	−	−	
PS {11-k}		−	−	−	0.11	2.7	−	−	−	−	
PHN {73-k}		−	-47	55	0.73	1.9	0.00137	−	1.4	277	
PHN-g-PS {73/10-k}	(3% PS)	−	−	−	−	−	0.00164	−	3.5	575	
PHN-g-PS({73/35-k}	(6% PS)	−	−	−	0.78	1.9	0.00079	−	4.8	1430	
PHN + PS {73/11-k}	(94/6)	−	−	−	−	−	0.00020	−	1.6	4000	
PHN-g-PS {73/35-k}	(16% PS)	−	-40	52, 100	0.94	1.9	0.00062	−	1.5	786	
PHN-g-PS{73/10-k}	(18% PS)	−	−	−	1.1	1.7	0.00299	−	7.5	600	
PHN-g-PS{73/35-k}	(30% PS)	−	−	−	0.49	3.0	0.00362	−	1.5	167	
PMMA-azo {63-k}		−	−	−	0.63	2.5	0.039	−	23	14	245
PHN-g-PMMA {73/63-k}	(5% PHN)	−	−	−	1.60	1.7	0.082	−	15.8	23	
PHN-g-PMMA {73/63-k}	(10% PHN)	−	-40	51, 110	1.74	1.3	0.022	−	9.3	11	
PHN-g-PMMA {73/63-k}	(18% PHN)	−	−	−	1.76	1.7	0.012	−	3.65	21	
PMMA		−	−	−	−	−	−	−	68.5	5.4	246
PHN {73-k}		−	−	−	0.73	1.9	−	−	1.4	277	
PHN-g-PMMA {73/− k}	(5% PHN)	−	−	−	3.7	4.5	−	−	52.1	5.8	
PHN-g-PMMA {73/− k}	(10% PHN)	−	−	−	4.3	3.6	−	−	38.7	10.3	
PHN-g-PMMA {73/− k}	(15% PHN)	−	−	−	4.2	3.5	−	−	42.4	12.8	
PHN-g-PMMA {73/− k}	(15% PHN)	−	−	−	4.7	3.9	−	−	38.7	5.9	
PHN-g-PMMA {73/− k}	(20% PHN)	−	−	−	3.3	4.0	−	−	37.3	9.5	

[a] (monomer wt.%), [monomer mol%], {M_n of constitutive block domains in kDa}, Compositions are given in the order as they appear in the sample name. Abbreviations: t_{age} (sample age time), T_g (glass transition temperature), T_m (melting temperature), M_n (number average molecular weight), PDI (polydispersity index = M_w/ M_n), E (Young's modulus), Y (yield strength), U (ultimate strength), ε_b (elongation at break), Ref. (reference citation)

2.2 Properties of Biopolymers Prepared *via* (Partial or Total) Organic Synthesis (continued)

Sample Composition[a]		t_{age} (days)	T_g (˚C)	T_m (˚C)	M_n (M_w) (10^5 Da)	PDI –	E (GPa)	Y (MPa)	U (MPa)	ε_b (%)	Ref. (#)
PMMA-g-PHB (GCP) {40,1.7-k}	[67% PHB]	21	13	no	1.1	–	–	–	–	–	247
PMMA		21	110	no	1.69	2.1	1.6	–	49	10	
PMMA + GCP	(95.2/0/4.8)	21	–	no	–	–	1.4	–	42	18	
PHB + PMMA	(30/70/0)	21	–	166	–	–	1.2	–	30	17	
PHB + PMMA + GCP	(28.6/66.6/4.8)	21	–	158	–	–	0.8	–	20	36	
PHB + PMMA	(40/60/0)	21	–	166	–	–	1.1	–	23	30	
PHB + PMMA + GCP	(38.1/57.1/4.8)	21	–	156	–	–	0.6	–	11	100	
PHB + PMMA	(50/50/0)	21	–	169	–	–	1.0	–	16	3	
PHB + PMMA + GCP	(47.6/47.6/4.8)	21	–	160	–	–	0.6	–	10	74	
PHB		21	0	173	3.5	3.3	1.6	–	25	3	
PLAα {high M_n} + (GCP)[b] + add.[d]	(PLA/GCP/add.)										249
(no GCP)	(89/0/11)	–	–	–	–	–	–	–	36.6	9	
(PLA-*g*-(PHB-co-P4HB(16.8%)[c])	(59/30/11)	–	–	–	(6.5)	–	–	–	37.7	5	
(PLA-*g*-(PHB-co-P4HB(16.8%)[c])	(59/30/11)	–	–	–	(6.5)	–	–	–	25.5	116	
(PLA-*g*-(PHB-co-P4HB(25.5%))	(59/30/11)	–	–	–	(1.6)	–	–	–	29.4	193	
PLAβ {low M_n} + (GCP)[b] + add.[d]	(PLA/GCP/add.)										249
(PLA-*g*-(PHB-co-P4HB(6.8% 4HB)[c])	(59/30/11)	–	–	–	(6.5)	–	–	–	30.0	11	
(PLA-*g*-(PHB-co-P4HB(27.7% 4HB))	(59/30/11)	–	–	–	(9.6)	–	–	–	44.2	181	
(PLA-*g*-(PHB-co-P4HB(40.3% 4HB))	(69/20/11)	–	–	–	(11.4)	–	–	–	44.8	195	
(PLA-*g*-(PHB-co-P4HB(40.3% 4HB))	(59/30/11)	–	–	–	(11.4)	–	–	–	34.1	210	

[a] (monomer wt.%), [monomer mol%], {M_n of constitutive block domains in kDa}, Compositions are given in the order as they appear in the sample name. Abbreviations: t_{age} (sample age time), T_g (glass transition temperature), T_m (melting temperature), M_n (number average molecular weight), PDI (polydispersity index = M_w/ M_n), E (Young's modulus), Y (yield strength), U (ultimate strength), ε_b (elongation at break), Ref. (reference citation)

[b] Graft copolymers (GCP) were synthesized by reactive blending of PHA copolymers with PLA. The given values of M_w are for the molecular weight of the PHA copolymer used to form the GCP

[c] The PHA used for GCP synthesis was a blend consisting of of 10-14% PHB homopolymer, 46-50% PHB-co-P4HB (8-14 wt.% 4HB) , and 38-42% PHB-co -P4HB (25-33 wt.% 4HB)"rubber phase" copolymer;. Mixture contained 16.8 wt.% 4HB, total. M_w = 652,889 g/mol)

[d] Additives (add.) included various combinations of catalyst, plasticizes, wax, inorganic nucleating agent, and toughener.

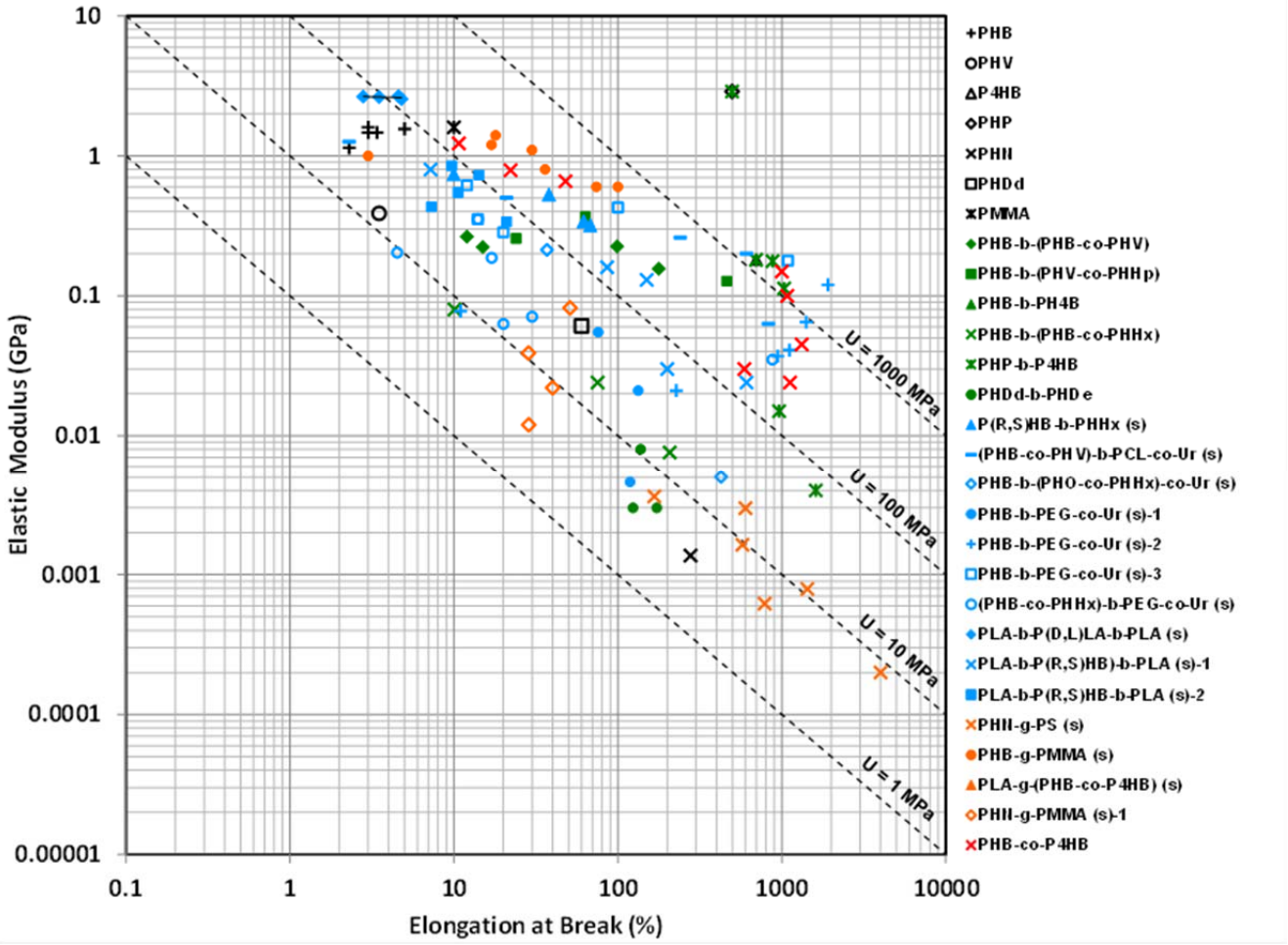

Figure 2.8 Elastic modulus (E) and elongation at break (εb) for different PHA and PLA polymers.
Each data set corresponds to a specific study and contains data for block-copolymers, as well as other random copolymers and blends prepared from the same materials. See **Tables 2.1** and **2.2** for exact material compositions. Symbol colors are assigned as follows: black; homopolymers, green; block-copolymers synthesized *in vivo,* blue; block-copolymers derived via chemical synthesis, orange; graft-copolymers derived *via* chemical synthesis. Diagonal lines correspond to the ultimate strength of a hypothetical, perfect elastomer, i.e. for any given ordered pair, [254], $U = E^{*}\varepsilon_b$.

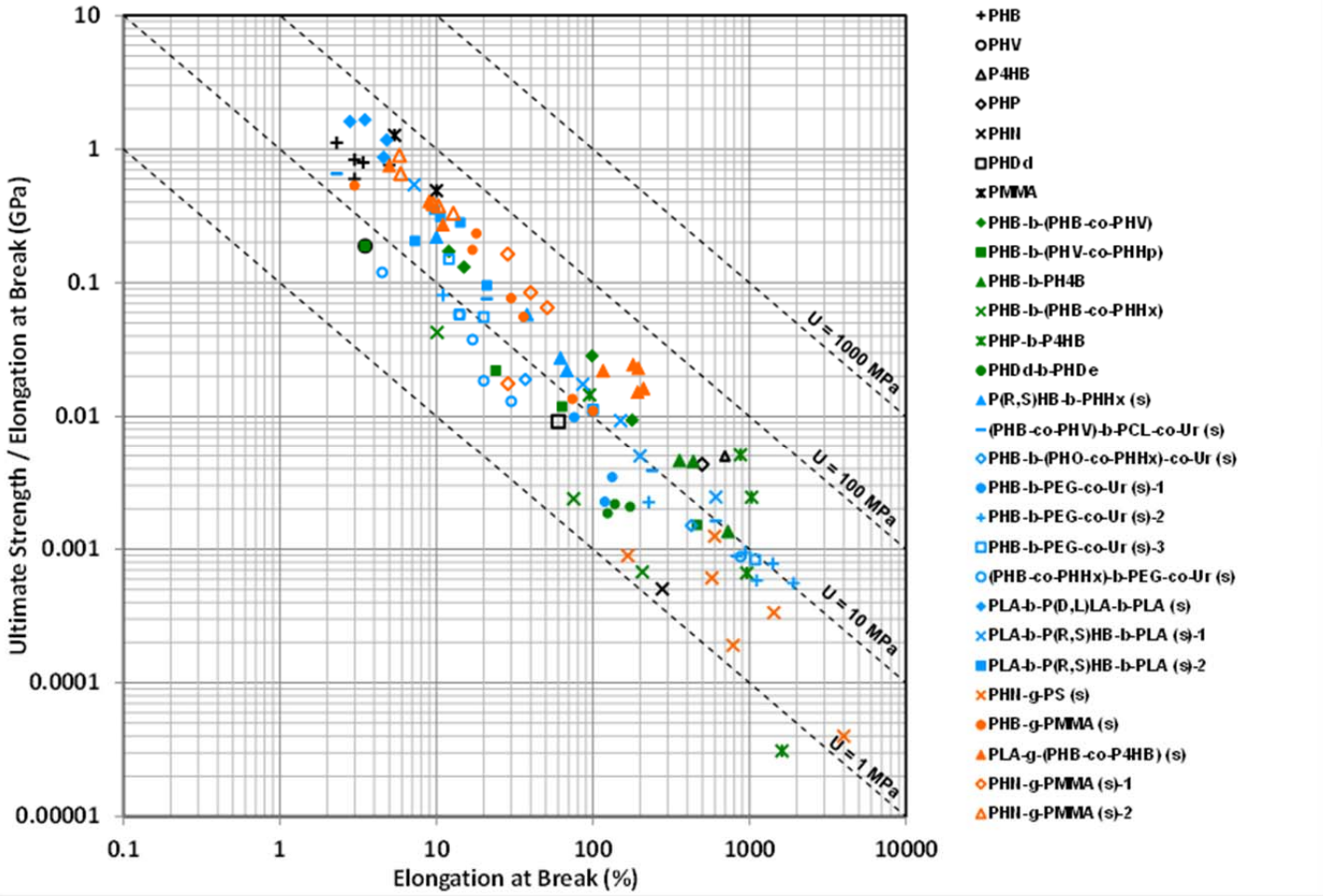

Figure 2.9 Ultimate strength (U) and elongation at break (ε_b) for different PHA and PLA polymers.

U values are normalized as U/ε_b. Each data set corresponds to a specific study and contains data for block-copolymers, as well as other random copolymers and blends prepared from the same constituent materials. See **Tables 2.1** and **2.2** for exact material compositions. Symbol colors are assigned as follows: black; homopolymers, green; block-copolymers synthesized *in vivo,* blue; block-copolymers derived via chemical synthesis, orange; graft-copolymers derived *via* chemical synthesis. Diagonal lines correspond to the ultimate strength of a perfect elastomer, i.e. for any given ordered pair, [254], $U = E^*\varepsilon_b$.

Summary

Biopolymers including poly(hydroxalkanoate)s, polylactide, and polylactones are an important class of materials valued for their attributes of rapid biodegradation, synthesis from renewable feedstocks, and / or use of bioprocesses in their production. Similar to petroleum polymers, the application of block-copolymer architectures to these biopolymers can create new materials with notable improvements in mechanical properties. Block-copolymers containing biopolymer constituents have been synthesized by a variety of methods resulting in the creation of structures including linear, di-block, tri-block, and multi-block copolymers, as well as non-linear graft copolymers. For block-copolymers derived via organic synthesis, the methods and characterization techniques employed have already been widely demonstrated for petroleum polymers. Often, purified PHAs syntheseized *in vivo* are used as prepolymers for the addition of other monomers by organic synthesis.

Alternatively, for block-copolymer synthesis completely *in vivo,* methods are still relatively new. Because, these biosyntheses frequently do not behave as a living polymerization, repeated substrate switching must be performed in order to maximize the fraction of block-copolymers in the product material. As a result, specific values for polymer synthesis rate, chain termination rate, and time-dependent behavior of polymer molecular weight must be obtained. Knowledge of these parameters is necessary in order to predict how the duration and frequency of substrate switches will affect the final polymer composition. Because, *in vivo* biosynthesis often produces multiplex mixtures of di-block and tri-block molecules as well as random copolymers and homopolymers, proper analytical techniques to confirm the polymer composition are critical. Without this information, it will be difficult for this nascent synthesis method to advance to the next technological level in which block-copolymer composition and structure are carefully tuned to achieve the mechanical properties desired in bulk materials. Ultimately, it is likely that recombinant platforms for PHA biosynthesis will be developed that more closely approach the conditions of living polymerization, thus allowing greater uniformity in the molecular structure of block-copolymer molecules. Futhermore, recent studies into

the effectiveness of various chain termination agents suggest that that end-group modification during biosynthesis, e.g. to produce esters and diols, may be an effective strategy to prepare new pre-polymers, eliminating the need to perform capping reactions on purified polymers. Given the broad variety of substrate incorporation possible via biosynthesis and the additional capabilities afforded by synthetic catalysis, we envision that the continued merging of bio- and organo- synthetic techniques will give way to a much-welcomed proliferation of new biopolymers with unique properties to meet the demands of the high-performance plastics market.

Chapter 3. Materials and Methods

Acknowledgement of Research Contributors

Most of the work described in this thesis was performed by the author with the help of various undergraduate research assistants. When applicable, contributions by more autonomous collaborators are mentioned at the end of the corresponding method.

PHA Biosynthesis in Recombinant Escherichia coli

Microorganisms and Media

All multi-knock-out mutants were made in the putative wt. *E. coli* MG1655. Viral lysates containing the gene deletions were prepared from various single-gene mutants of *E. coli* BW25113. Plasmid construction was done in the *E. coli* cloning strain DH5α. Site-directed mutagenesis was performed in the *E. coli* cloning strain Top10®. The gene $phaJ_{P.o.}$ was cloned from *Pseuodomonas oleovorans.*

Agar plates for cloning consisted of LB media (10 g/L tryptone, 5 g/L yeast extract powder, 5 g/L NaCl). When appropriate the following antibiotic concentrations were used: kanamycin 50 ug/mL, ampicillin 100 ug/mL, and streptomycin 50 ug/mL. Double-plasmid strains were maintained in antibiotic media containing both kanamycin and streptomycin at a concentration of 50 ug/mL. Basic media for polymer synthesis studies consisted of 10 g/L tryptone, 5 g/L yeast extract powder, 0. 5 g/L NaCl, and 100 mM sodium phosphate buffer (pH 7.1). Depending on the requirements of the experiment, supplemental carbon was added in the form of 3 g/L of dodecanoic acid, 20 g/L glucose, or 20 g/L glycerol. Undefined media components, phosphate salts, and dodecanoic acid were autoclaved together, while glucose and glycerol were sterile filtered and added post-autoclave. The use of the phosphate buffer was critical to extending the active growth period of shake flask due to their excretion of various organic acids which lowered the pH of the media to inhibitory levels.

Genome Deletions

Strains for PHA biosynthesis were constructed from the putative wt. *E. coli.* MG1655. Gene deletions in the chromosome were made by the method of P1 phage transduction using single-deletion mutants as donor strains[254]. Briefly, viral lysates were prepared from single-gene mutants in *E. coli* BW25113 obtained from the Keio collection[255]. Deleted regions in the strains are replaced by kanamycin resistance markers for selection. Viral lysates derived from the BW25113 mutants then were used to transfect the recipient strain MG1655. Transfectants were selected using kanamycin plates. A second group of lysates was prepared from the MG1655, single-gene knockouts before final trasnfection into the multiple-knockout strain. For JSBS01 (*ΔfadR, ΔfadB, ΔptsG*) genes were deleted in the order, *ΔfadR, ΔfadB, ΔptsG*, as *fadB* expression, and hence *kanR* expression, is repressed by constitutive expression of *fadR*. After each subsequent deletion, the kanamycin resistance marker was excised from the mutant using a temperature inducible, helper plasmid pFT-A expressing the Red Recombinase enzyme and an ampillicin resistance marker[256]. Proper knockouts were confirmed by PCR amplification of genomic DNA surrounding the gene deletions. Strain TCS010 (*Δzwf Δndh ΔsfcA ΔmaeB ΔldhA ΔfrdA ΔpoxB Δpta Δmdh ΔadhE*) was derived from strain TCS099[257] by the additional deletion of *adhE* using P1 phage transduction.

Plasmids

Plasmid pPT500 contains the *Ralstonia eutropha* PHB synthesis operon, *phbA, phbB, and phbC,* under control of their native *R. eutropha* promoter. pPT500 was synthesized by ligating to operon excised from pAeT41[48] and cloning into the pCR-Blunt vector (Invitrogen) (ColE1 ori, $kanR^+$, $zeroR^+$). Plasmid pPT700 was derived from pPT500 by replacing the *phbC* polymer synthase gene of *R. eutropha* with the *phaC1* polymer synthase gene of *Pseduomonas oleovorans.* A detailed cloning procedure for pPT500 and pPT700 may be found elsewhere[258]. Plasmid pPT700_ST_QK was derived from pPT700 by incorporating amino acid substitutions, S325T and Q481K, in the *phaC1* sequence. Plasmid pCDFBB_*phaJ* contains the *R*-specific enoyl-CoA hydratase gene

(*phaJ*$_{P.o.}$), from *Pseudomonoas oleovoran*[57]*s*, and was synthesized from the parent vector pCDFBB-eGFP[259] (CloDF13 ori, *strp*$^{R+}$) The *phaJ* gene was amplified from *P. oleovorans* genomic DNA using GoTaq polymerase (Promega) and primers with ~20 bp of *phaJ* homology and ~40 bp of vector homology: forward 5'-TGTGTGGAATTGTGAGCGTCTAGTAGAAGGAGGAGATCTatgtcccaggtcaccaacacg-3', reverse 5'-AGAATCAGTGATGGTGATGGTGATGCTCGAGGCGGCCGC-ttagctcgccacaaagttcgg-3' The pCDFBB vector was digested with BglII and NotI to remove the 753 bp eGFP fragment . The amplified insert and the digested vector were purified via gel extraction using crystal violet dye. Vector and insert were assembled by the method of homologous recombination[260] using chemically competent *E. coli* DH5α cells with a transformation efficiency of ~1x10^{9} cfu/μg DNA prepared via the method of Inoue[261]. Similar to the report by Bubeck et al,[260] we also experienced difficulty using electroporation for this cloning technique. For the homologous recombination 120 ng of insert (546 bp) was combined with 13 ng of vector (2203 bp). Positive transformants were selected on streptomycin plates, identified visually by their lack of green coloration, then by colony PCR, and verified by DNA sequencing. For strain and plasmid characterization studies, transformations were done by electroporation. For JSBS01, pPT700_ST_QK was transformed first, followed by preparation of new electrocompentet cells on kanamycin media, and then transformation of of the cells with pCDFBB_*phaJ*. Double transformants were selected on plates containing 25 ug/mL of kanamycin and 25 ug/mL of streptomycin.

Polymerase Mutations

Single amino acid mutations to the *P. oleovorans phaC1* polymer synthase were performed via site directed mutagenesis, using non-overlapping, 5' phosphorylated primers, with the mutated codon carried on a single primer. The full-length plasmid, pPT700, was amplified via polymerase chain reaction (PCR) using Phusion High Fideity Polymerase (New England Biolabs). The PCR product was gel purified and visualized using crystal violet in the loading dye and agarose which allowed the gel fragment to be

excised under ambient lighting. Visualization of DNA using crystal violet dye, which avoids the mutagenic effects of ethedium bromide and uv-light, greatly increases cloning efficiency[262]. The purified, blunt-end, plasmid with phosphorylated 5' ends was ligated using T4 DNA ligase (Invitrogen), and the circularized plasmid was transformed into high-efficiency Top 10® chemically competent cells (LifeTechnologies) Proper clones were confirmed by DNA sequencing. For the substation of lysine (K) at the glutamine (Q) 481 residue the primers were: forward 5'-P- GCGGCCACATCAAGAGCATCCTCAACCC-3' and reverse 5'-P- TGTTGGACAGCACGAACTCGATCTTGCC-3'. Following verification of the Q481K mutation, the mutant plasmid was then subjected to a second round of site directed mutagenesis. For the substitution of threonine (T) at the serine (S) 325 position the primers were: forward 5'-P- CCCTGCTGGTCACCGTGCTGGACACC-3' and reverse 5'-P-TCAGGGCATTGACCTTGTTTTCGCCG-3'.

Shake-Flask Studies

Characterization studies of strain and plasmid combinations were performed in 250-mL Erlenmeyer shake-flasks with 50-mL of buffered LB media containing different carbons sources depending on the study. Flasks were incubated at 30 °C for a period of 72 hrs in a shaker with a 2.5 cm throw-diameter rotating at 250 RPM. To prepare the inoculums for the flasks an agar plate was streaked from a glycerol stock at -80 °C and incubated at for 24-48 hrs. Solid culture from the plate was used to inoculate a 50-mL liquid culture of buffered LB media at a starting optical density of ~0.1 OD_{600}. The culture was shaken in a 250-mL flask at 250 RPM for ~ 12-18 hr . The OD_{600} of each seed culture was measured before inoculating all flasks at a starting density of ~0.1 OD_{600} For all seed stages the temperature was maintained at 30 °C,

Bioreactor Experiments

Controlled bioreactor experiments were conducted in a 10-L, *d* = 19 cm, Biostat-B reactor vessels (Sartorius-Stadiem) with automatic control units for pH, agitation, dissolved oxygen, and substrate feeding. Agitation was provided via two, 7-cm, Rushton turbines, spaced 8.3 cm apart, with additional turbulence created from two, 2.7-cm mixing baffles. Reactors were charged with 4.5 L of buffered LB media (pH = 6.9) and 3 g/L of dodecanoic acid. The initial media charge was concentrated by 1.11x to account for the addition 500 mL of inoculums Following autoclaving sterile filtered glucose (400 g/L) was used to add 100 g of glucose for a post-inoc concentration of ~20 g/L. pH control was maintained using 6 M NaOH. To minimize foaming due to the dodecanoic acid, pH was controlled below 6.9, and ~3-5 mL of Antifoam-A (Sigma-Aldrich) was added as needed. The temperature of the biosynthesis was maintained at 30 °C via a water-cooled jacket. Air was supplied by sparging at flow rate of 1.3 lpm to give a normalized flow of ~0.25 vvm. The dissolved oxygen sensor was calibrated to 100% in air-saturated media at 30 °C and atmospheric pressure. For the 0% calibration the sensor was momentarily disconnected from the meter to provide an electronic zero-point. Control of dissolved oxygen was maintained automatically via manipulation of agitator speed. At the time of inoculation dissolved oxygen was initially at 100% saturation with the impeller speed set to 300 RPM. Dissolved oxygen was allowed to fall until it reached the target set point, at which time feedback control by agitation was initiated.

To prepare the inoculum for the bioreactor, an agar plate was streaked from a glycerol stock at -80 °C and incubated at for 24-48 hrs. Solid culture from the plate was used to inoculate a 50-mL liquid culture of buffered LB media at a starting density of ~0.1 OD_{600}. The culture was shaken in a 250-mL flask at 250 RPM for 12-18 hr . Then the entire culture was transferred to a 500-mL culture of buffered LB media with 5 g/L of glucose and shaken in a 2-L flask at 250-RPM for 4-6 hrs before transfer of the entire volume of media into the 5-L production stage. For all seed stages the temperature was maintained at 30 °C.

In Batch 1the initial media contained 20 g/L of glucose and 3 g/L of dodecanoic acid. Over the course of the biosynthesis, an additional 20 g/L of glucose (100 g) was supplied to the batch using a sterile solution (400 g/L) and substrate feeding pump. The concentration of glucose in the batch was periodically monitored via a glucose analyzer, and the rate of glucose feeding was manipulated to control the glucose concentration at ~10 g/L until the feed was exhausted. In Batch 2 the initial media contained 10 g/L glucose and no dodecanoic acid. An additional 30 g/L of glucose (150 g) was added over time in order to maintain the glucose concentration at ~10 g/L until the feed was exhausted. During the batch a total of 1 g/L of dodecanoic acid was added over 30 injections. Shots were administered using a controlled timer and a substrate pump to deliver 500 uL of dodecanoic acid solution in ethanol (333 g/L) at 1-hr intervals.

Quantification of Cell Growth

Cell density in liquid media was estimated from optical density measurements made at 600 nm (OD_{600}) using a UV-Vis spectrophotometer (Agilent 8453). A conversion factor of ~$1x10^9$ cells/mL/OD_{600} was assumed. For estimation of cell dry weight (CDW) a sample of 5-10 mL of cell broth was centrifuged at 2000 rcf for 15 min, washed in 1 volume of DI water and centrifuged again. After decanting the supernantnat, the cell pellet was transferred to a pre-weighed glass tube and dried at 100 °C until a constant mass was obtained, ~24 hrs.

Determination of Glucose

The concentration of glucose in bioreactor samples was determined by using a glucose analyzer (Yellow Springs Instruments). Before measurement, samples were centrifuged and supernatant was diluted in distilled water to bring the glucose concentration < 2 g/L.

PHA Composition

The composition of PHA contained in cell pellets as well as purified polymer samples was determined via gas chromatography. In order to increase their volatility, polyhydroxyalkanoic acids were derivatized to their corresponding propyl esters by the method of propanolysis[263]. Identities and retention times of the different 3-(*R*)-hydroxyalkanoic (3HA) propyl esters were determined using a GCxGC TOF Mass-Spectrometer (Vendor) to analyze dried cell mass known to contain a multi-component PHA. The instrument was equipped with a DB-WAX column ID 0.32 mm and 0.5 μm film thickness (Agilent Technologies) followed by a cryogenic trap and another kind of column. **Figure 3.1** shows the 2-D distribution of peaks obtained from the method. The x-axis displays the separation produced by the non-polar column, and the y-axis displays the separation produced by the polar column. The total mass intensity of each peak is indicated by color with blue representing zero response and red representing maximum response. **Figure 3.1.a** shows all compounds detected within the cell mass, including several peaks of fatty acid propyl esters in addition to the target, 3-hydroxyalkanoic propyl esters. Peaks of 3-hydroxyalkanoic propyl esters were identified by the presence of 131 m/z mass fragment that was common among all species. See **Figure 3.1.b**.

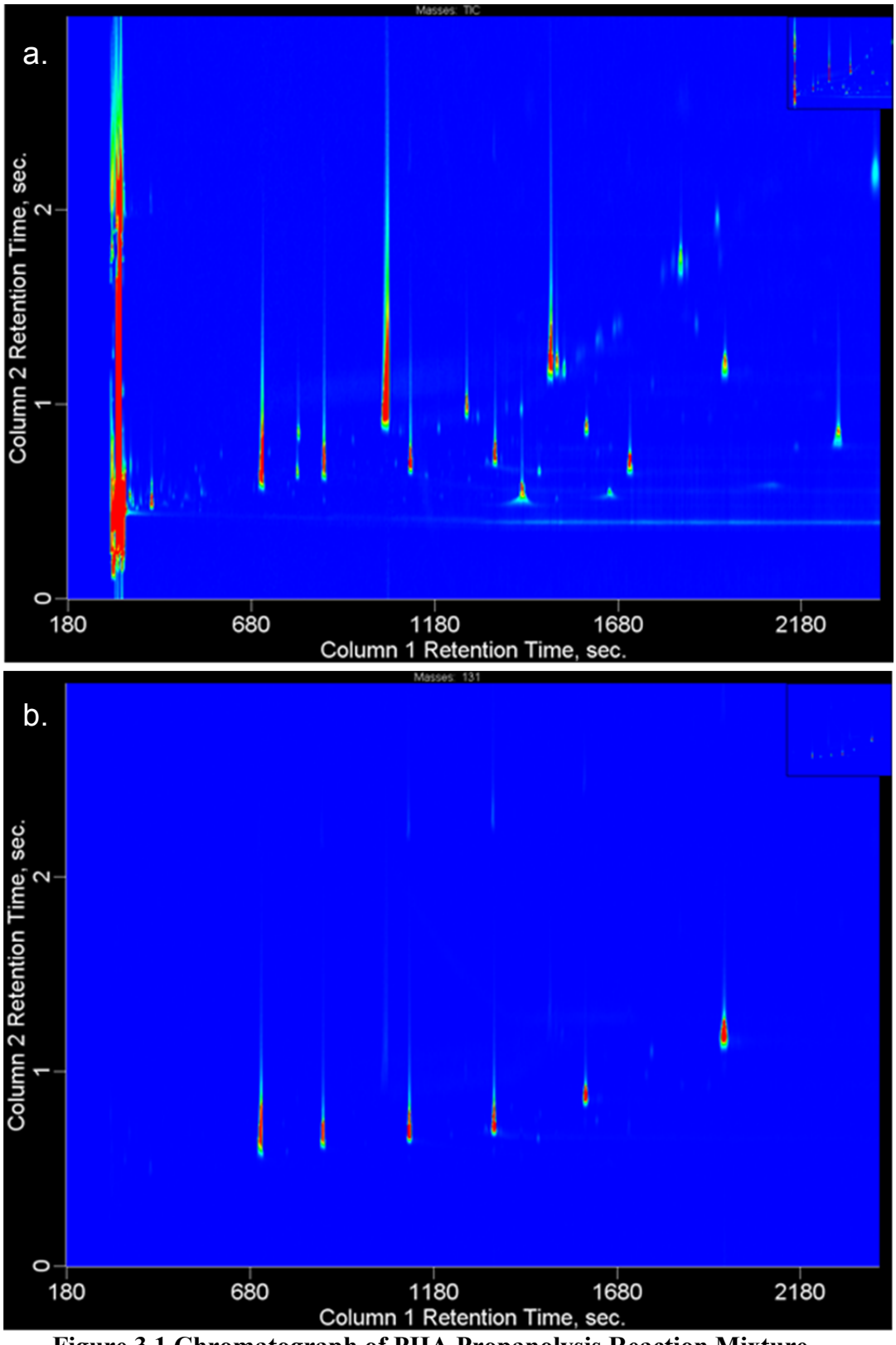

Figure 3.1 Chromatograph of PHA Propanolysis Reaction Mixture

Figure 3.1 Chromatograph of PHA Propanolysis Reaction Mixture
(see previous page) Data was collected from a GCxGC Time of Flight Mass Spectrophotometer. The x-axis displays the separation produced by the non-polar column, and the y-axis displays the separation produced by the polar column. The total mass intensity of each peak is indicated by color with blue representing zero response and red representing maximum response. The sample analyzed contained a PHA copolymer consisting of both short-chain monomers and medium-chain monomers as well as residual biomass from the recombinant *E. coli* cells used to produce the polymer. Cells were cultured on rich media including glucose and dodecanoic acid as additional carbon sources. **a.**) Chromatogram showing all compounds within the reaction mixture. **b.**) The same chromatogram as in **a**, but showing only those peaks containing the characteristic 131 mass fragment, common among 3-hydroxyalkanoic propyl esters. From left to right the peaks are 1.) *R*-3-hydroxybutyric acid propyl ester 2.) *R*-3-hydroxyhexanoic acid propyl ester 3.) *R*-3-hydroxyoctanoic acid propyl ester 4.) *R*-3-hydroxydecanoic acid propyl ester 5.) *R*-3-hydroxydodecanoic acid propyl ester and 5.) *R*-3-hydroxytetradecanoic acid propyl ester

Routine quantitative analysis of polymer composition was performed via gas chromatography with a flame ionization detector (GC-17A with FID, Shimadzu) using the DB-WAX column specified previously. The response factor (peak area / g of sample) for each 3HA propyl ester was determined by preparing calibration curves from a combination of purified copolymers and single component 3-hydroxyalkanoic acids (Sigma-Aldrich). The relative response factors, which are dimensionless and calculated with respect to the 3HB propyl ester, are shown in **Figure 3.2**. The relative response factors show a linear correlation with the number of carbons in the 3-hydroxyalkanoic acid. Response factors are subject to experimental variability associated with the preparation of standards, the concentration of the internal standard (benzyl alcohol), and the performance of the flame ionization detector; however, we assume that correlation between relative response factor and the number of carbons in each 3-hydroxyalkanoic acid remains constant. Similar correlations have also been observed for fatty acids and ω-hydroxy fatty acids[264].

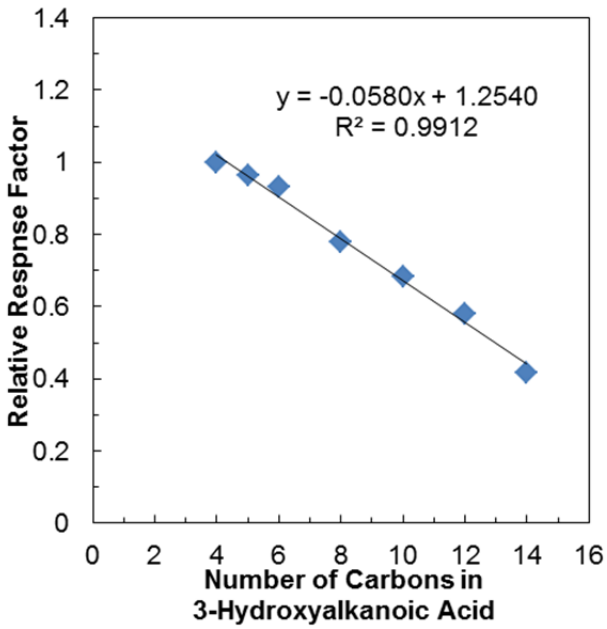

Figure 3.2 Relative response factors for 3-hydroxyalkanoic propyl esters
Response factors [peak area / g of polymer] for different 3-hydroxyalkanoic propyl esters were determined using GC-FID. Calibration curves for each analyte were prepared from propanolyis reactions using either purified copolymers or single component 3-hydroxyalkanoic acids. Relative response factors, which are dimensionless, were normalized with respect to the response factor for PHB (C_4). Response factors are subject to experimental variability associated with the preparation of standards, the concentration of the internal standard (benzyl alcohol), and the performance of the flame ionization detector; however, we assume that correlation between relative response factor and the number of carbons in each 3-hydroxyalkanoic acid remains constant.

PHA-Graphene Nanocomposites

PHA Biosynthesis

Synthesis of the various PHA_{mcl} copolymers was performed by a method similar to that used by Lageveen et al.[6]. Briefly, the polymers were produced by fed-batch biosynthesis using the wild-type organism *Pseudomonas oleovorans* in minimal media with specific alkanes as the sole carbon source. Octane, decane, and octene were used to synthesize polyhydroxyoctanoate (PHO) polyhydroxydecanoate (PHD) and polyhydroxyoctenoate (PHOe) respectively. More specifically, the PHOe copolymer was synthesized via repeated cycles between octane and 1-octene. Previous studies on the synthesis of PHA copolymers suggested that repeated cycling between different carbon sources produces a mixture of the two corresponding polymer types with some fraction of the polymer chains expected to be di- and tri-block-copolymers[21, 40] .

Initially, one fresh colony of *Pseudomonas oleovorans* was selected and inoculated into a test tube containing 5-mL of LB medium (Tryptone 10 g, Yeast Extract Powder 5 g, and NaCl 5 g in 1L of water) and grown overnight at 30°C. The culture was then transferred into a 2-L baffled flask with 500-mL of LB medium + 1% (v/v) alkane for an additional 16 hours at 30°C with shaking at 250 RPM. This 500-mL culture was used to inoculate a 10-L bioreactor containing 5-L of E medium + 2% (v/v) alkane. E medium was based on a formulation used by Lageveen et al.[6] and was composed of $(NH_4)_2HPO_4$ 1.1 g, K_2HPO_4 5.8 g, $KHPO_4$ 3.7 g, $MgSO_4 \cdot 7H_2O$ 0.25 g, and 1 mL of trace metals in 1 L of water. Trace metals consisted of $FeSO_4 \cdot 7H_2O$ 2.78 g, $MnCl_2 \cdot 4H_2O$ 1.98 g, $CoSO_4 \cdot 7H_2O$ 2.81 g, $CuCl_2 \cdot 2H_2O$ 0.17 g, $ZnSO_4 \cdot 7H_2O$ 0.29 g, $CaCl_2 \cdot 2H_2O$ 1.67 g, in 1 L of 1-mM HCL. Airflow and agitation were adjusted to maintain dissolved oxygen in the culture above 40%. During biosynthesis carbon dioxide evolution rate (CER) of the culture was monitored via mass spectroscopy. A sharp decline in CER indicated depletion of the carbon source, at which time more alkane was added to maintain growth. Batches were harvested at 50 hrs.

Synthesis of the PHOe copolymer was achieved by a similar fed-batch procedure utilizing both octane and 1-octene. In the first phase of the 5-L production culture, 225 mL of octane was used as the sole carbon source for biomass accumulation. After a decline in CER signaled the depletion of the octane, copolymer synthesis was initiated with a 10-mL addition of 1-octene, which produced a large rise in CER. After depletion of the 1-octene, CER again declined, and 50-mL of octane was added to the batch. Periodic switching of carbon sources continued every time the CER indicated carbon source depletion. Cycling was continued for 7 periods until the batch age reached 30 h. Biosynthesis of PHA_{mcl} polymers was performed by Mr. Dan Rouse of the University of Minnesota.

PHA Extraction and Purification

Following polymer biosynthesis cells were harvested via centrifugation at 10,000 RPM for 20 min. The resulting cell pellet was flash frozen in liquid nitrogen and lyophilized overnight to remove residual moisture. Polymer material was extracted from the dried cells into 1-L of boiling chloroform for 16 hr using a Soxhlet apparatus. The extract was concentrated by evaporation to 100 mL before precipitation in excess methanol, 8:1 (vol/vol). The purified polymer was dried in air to remove excess solvent. The initial extraction and purification of PHA materials was performed by Mr. Dan Rouse of the University of Minnesota. A second round of purification was performed by John Barrett.

Polymer Composition

Purified PHAs were analyzed via gas chromatography fitted with a flame ionization detector (GC-17A, Shimadzu) using a DB-WAX column (ID 0.32 mm, 0.5 μm film thickness) (Agilent Technologies). Prior to analysis, polyhydroxyalkanoic acids were converted to 3-hydroxyalkanoic propyl esters by the method of propanolysis[263]. Quantitative determination of different PHAs was made by comparison to standards synthesized from purified 3-hydroxyalkanoic acids (Sigma).

Polymer Molecular Weight

Polymer molecular weights were determined by gel permeation chromatography (PL GPC 220 high temperature chromatograph, Polymer Labs) using 3, PL-gel 10 μm mixed B columns in series. TCB (1,2,4-triclorobenzene) was used as the mobile phase, and the column was operated at 160 °C. Calibration of the instrument was performed using polystyrene standards, and molecular weights are reported in polystyrene equivalents. Operation of the GPC was performed by Dr. David Giles of the University of Minnesota, CEMS Polymer Rheology Laboratory.

Graphene Synthesis

Thermally reduced graphene (TRG) was produced following the thermal exfoliation method[265-266]. In this method, graphite was first oxidized using Staudenmaier method[267] as follows: 5 g graphite was placed in an ice-chilled flask containing a mixture of 90 mL of H_2SO_4 and 45 mL of HNO_3. Potassium chlorate, 55 g, was slowly added to the cold reaction mixture. After 96 hr the reaction was quenched by combining the mixture with 4 L of water. The resulting graphite oxide (GO) was washed once in 5% HCl followed by additional water washes to remove the residual acid before drying overnight in a vacuum oven. TRG was produced by exfoliating the GO via rapid heating in a tube furnace (Barnstead Thermolyne) at 1000 ^{o}C under flow of nitrogen for 30 s. TRG was prepared at the Petroleum Institute in Abu Dhabi, UAE under the direction of Professor Ahmed Abdala.

Verification of Reduction and Exfoliation of Graphene Oxide

X-Ray diffraction (XRD) (X'Pert PRO MPD diffractometer, PANalytical) was used to test the oxidation of graphite and the complete exfoliation of graphite oxide. XRD scan between 5-35° was conducted at a scan rate of 0.02 °/sec with instrument parameters of 40 kV voltage, 20 A intensity, and 1.5406 Å CuKα radiation. Transmission electron microscopy (TEM) (FEI Tecnai G20 TEM) images of TRG were obtained with point-to-

point resolution of 0.11 nm. Samples for TEM were prepared by dispersing approximately 0.5 mg of TRG in 25 mL of dimethylformamide by sonication at room temperature in a sonicating bath for 10 minutes. Two drops of the suspension were deposited on a 400 mesh copper grid covered with thin lacey carbon film. XRD and TEM of TRG was performed at the Petroleum Institute under the direction of Professor Ahmed Abdala.

Preparation of PHA-Graphene Nanocomposites

First, 1 g of polymer was mixed with 20 mL of chloroform in a sealed tube and agitated using a vortex mixer. Periodic incubation of the mixture in an 80° water bath was used to promote dissolution. Second, graphene was dispersed in chloroform at a concentration of 0.5 mg/mL. To promote the dispersion of single graphene sheets, the mixture was sonicated for 6 min using a probe type sonicator (Misonix 3000) at a power density of 1.5 - 3 W/mL. The sonicator program consisted of 28 cycles of 15 s sonication followed by 45 s rest period to dissipate heat. The graphene dispersion was then added to the polymer solution and stirred for 1 hr. The nanocomposite solution was solvent-cast by transferring it into a petri dish placed over a 55 °C hotplate with light stirring for ~1 hr. Films were dried overnight to remove excess chloroform.

Thermal Stability

The nonoxidative thermal stability of the pure and composite samples was assessed using a simultaneous thermal analyzer (STG) (Netzsch STA 449 F1 Jupiter), which performs both thermal gravimetric analysis (TGA) and differential scanning calorimetery (DSC). The polymer nanocomposite sample (~10 mg) was placed in a ceramic crucible and heated from 25 – 600° C at a heating rate of 20° C / min under nitrogen flow.

Thermodynamic Transitions

The glass transition temperature (T_g), melting temperature (T_m), and heat of melting (ΔH_m) of the pure and composite samples were measured using differential

scanning calorimetry (Netzsch 204 F1 Phoenix). The polymer nanocomposite sample (6-10 mg) was placed in crimped but unsealed aluminum pans and heated from -60 °C to 250° C at a heating rate of 5° / min under nitrogen flow. All samples were aged for 72 hours prior to testing.

Preparation of Polymer Thin Films

Specimens for mechanical, rheological, and surface resistance measurements were prepared using a hot-press (Tetrahedron, MTP-10) at 100 °C and 1.0 MPa for 5 minutes to form a thin film (0.4 – 0.5 mm). Samples were aged at room temperature for > 72 hrs prior to testing.

Resistivity

Surface resistance measurements were obtained using 11-point probe (Prostat Corp., PRF-914B probe with PRS-801 meter). For each sample, four readings were collected, two from each side of the film.

Rheology

Rheological properties of the pure and composite samples were determined via dynamic oscillatory measurement (TA Instruments, AR2000ex) using an 8-mm parallel plate geometry. Strain and frequency sweeps were performed on 8 x 0.5 mm circular disks at 70 °C.

Mechanical Properties

Mechanical testing of the pure and composite samples was performed using a dynamic mechanical analyzer (DMA) (TA Instruments, RSAIII). 50 x 5 x 0.5 mm specimens were tested at a strain rate of 5 mm/min. Mechanical testing was performed at the Petroleum Institute in Abu Dhabi, UAE under the direction of Professor Ahmed Abdala.

Scanning Electron Microscopy

The fracture surface of the pure and composite samples were examined using SEM (Philips FEI Quanta 200 SEM) operated at a high-vacuum mode. SEM was performed at the Petroleum Institute in Abu Dhabi, UAE under the direction of Professor Ahmed Abdala.

Transmission Electron Microscopy

Dispersion of graphene within the polymer matrix was analyzed with transmission electron microscopy (TEM) (JEOL, 1200 EXII). Thin sections of composite samples, 70-100 nm, for TEM characterization were prepared without resin embedding using an ultramicrotome (Leica EM UC6) at -80 ºC. Samples were mounted on 200-mesh copper grids with carbon type-B coating (Ted Pella) Thin-film sections were prepared at the University of Minnesota. Some TEM images were collected at the University of Minnesota, and some were collected at the Petroleum Institute in Abu Dhabi, UAE under the direction of Professor Ahmed Abdala.

PHA Biosynthesis in Ralstonia eutropha

Microorganism and Media

Ralstonia eutropha H16 was the organism used in the study. All cell cultivations were made using mineral salts medium (MSM) for autotrophic growth. The formula used was based on one given by Ramsay et al.[268] and contained the following per liter: $Na_2HPO_4 \cdot 7H_2O$ (6.7 g), KH_2PO_4 (1.5 g), $(NH_4)_2SO_4$ (4 g, 160 g/L stock), $MgSO_4 \cdot 7H_2O$ (200 mg, 20 g/L stock), ferric ammonium citrate (6 mg, 60 g/L stock), $CaCl_2 \cdot 2H_2O$ (10 mg, 100 g/L stock), trace elements (1 mL, 1000x stock). Trace elements (1000x stock) contained the following per liter: H_3BO_4 (300 mg), $CoCl_2 \cdot 6H_2O$ (200 mg), $CuSO_4 \cdot 5H_2O$ (10 mg), $MnCl_2 \cdot 4H_2O$ (30 mg), $NiCl_2 \cdot 6H_2O$ (20 mg), $NaMo_4 \cdot 2H_2O$ (30 mg), $ZnSO_4 \cdot 7H_2O$ (100 mg). To prepare the media, phosphate salts were dissolved in 960 mL of deionized water and autoclaved. The remaining components, prepared as stock solutions, were combined separately and sterilized through an 0.22 μm filter before addition to the autoclaved salts. After a few days, a light precipitate would often appear in the media, so for production batches media was prepared fresh. Agar plates for autotrophic growth contained the same MSM along with 15 g/L agar. As a production batch progressed, we often observed the occurrence of lemon-lime tinge in the batch supernatant, which has been previously attributed to iron depletion[269]. Increasing the concentration of ferric ammonium citrate to 60 mg/L reduced the supernatant coloration and resulted in greater production of residual biomass; however, effects on the final PHA titer were less obvious. At the start of the *R. eutropha* project, much time was spent on the identification of the proper media and environmental conditions necessary for reliable cultivation of *R. eutropha* under autotrophic conditions. In this area, Dr. Luz Perez, was a an essential collaborator.

Apparatus for Autotrophic Cultivation

Safety

For autotrophic cultivation systems, the explosion hazard associated with hydrogen and oxygen mixtures is of primary concern. For combinations of these two gasses at atmospheric pressure the lower explosion limit is is 4.8 mol% O_2, and the upper explosion limit is 4 mol% H_2. While the gas mixture we most frequently used, H_2:O_2:CO_2 = 80:10:10, lies above the lower explosion limit, the ultimate size of such an explosion can still be limited by minimizing the volume in the reactor head-space, the gas pressure, and the fraction of the stoichiometrically limiting reactant, i.e. O_2. To reduce the hazard of the operation, we avoided preparing large volumes of feed mixtures, choosing instead to prepare the mixtures continuously from compressed gas cylinders. Gasses were piped using 1/8" copper tubing to avoid additional fire hazard associated with plastic tubing. Moreover, the use of metal plumbing allowed the entire system to be electrically grounded in order to prevent static discharge. For additional safety, both check valves and flame arresters were installed immediately downstream of the gas cylinders. Off-gas from the vessel (<= 1 L/min) was routed for disposal in a fume hood. To prevent over-pressurization, in the event of an explosion, leading to catastrophic destruction of the vessel, we used a loosely inserted rubber stopper in the reactor head-plate to act as a safety relief valve. In addition, a sealed electrical motor was used to power the agitator. See **Figure 3.3** for a schematic of the apparatus and associated controls.

Seed-Stage

Seed for the bioreactor was cultivated in a 2-L, side-arm flask, containing a rubber stopper with a glass tube inserted to a position ~1" off the bottom of the flask. For sample collection and seed transfers, a long plastic tube, ~45cm x 1mm, was inserted through the rubber stopper and fitted with small syringe. Gas was filled through the glass insert and vented through the side-arm, each port being sealed with rubber tubing and tube clamps. For testing of various seed conditions, similarly constructed, 500-mL flasks were prepared. Gas plates were incubated in a 3-L, plastic, gas chamber

Production-Stage

The production reactor was, 2-L jar fermentor (Sartorius, Biostat B) fitted with a single, 4.5 cm diameter, Rushton turbine. To promote turbulence, the reactor was fitted with two, 1" mixing baffles.

Gas Composition

Control of gas composition was achieved using mass-flow controllers (Datametrics, Model 825) to adjust individual flow rates prior to inline mixing and feeding. For gas-uptake calculations, the exact composition of the feed-gas and off-gas was verified using online mass-spectroscopy connected to the production-stage vessel.

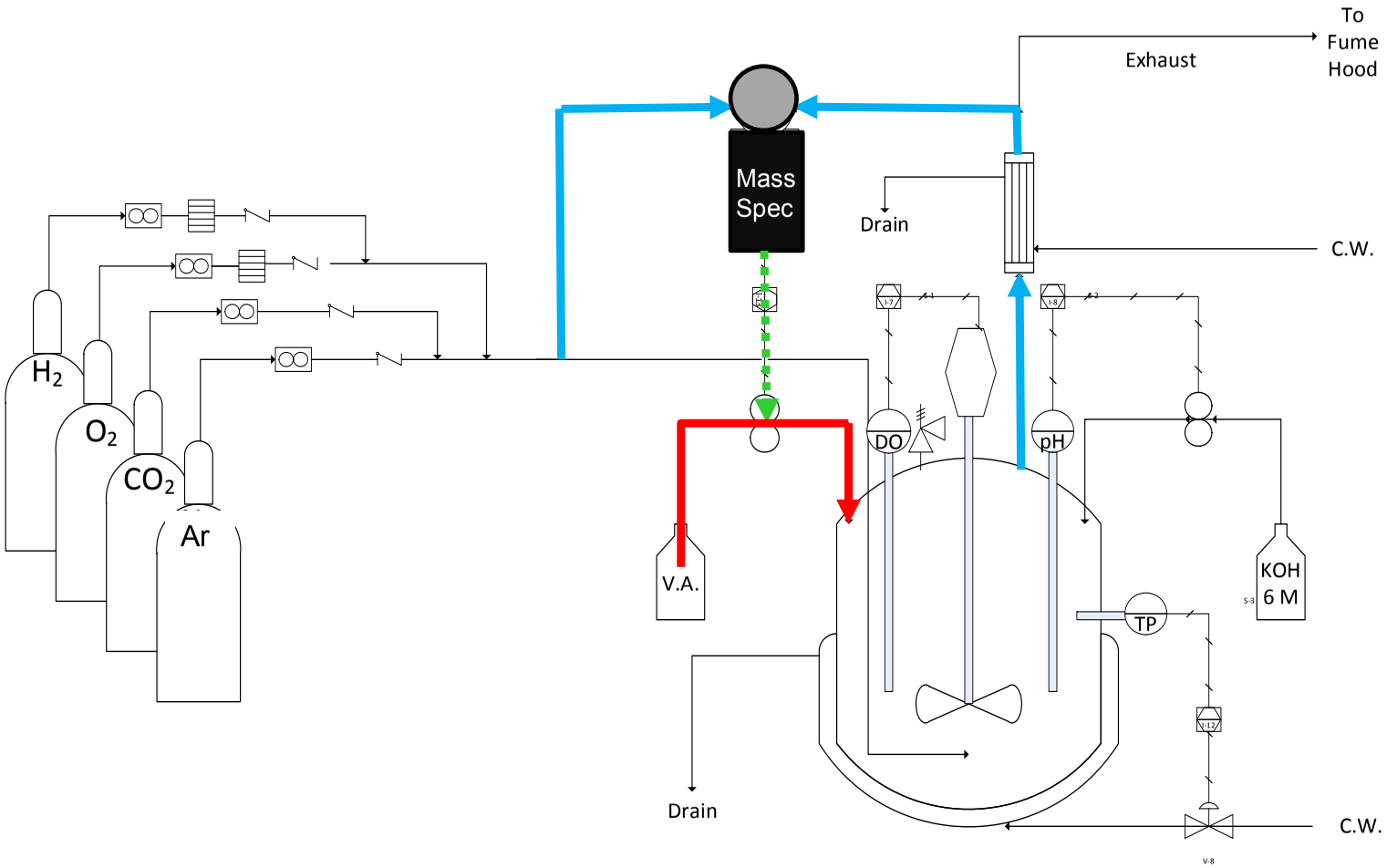

Figure 3.3 Apparatus for Autotrophic Cultivation

H_2 O_2, and CO_2 were supplied as substrate gasses while Ar was fed as a reference gas. Mass-spec analysis of the inlet and outlet gas streams allowed for the determination of gas uptake during transient does of valeric acid. For safety, check valves were installed downstream of all gas cylinders, and flame arresters were installed downstream of the O_2 and H_2 cylinders. A sealed electric motor was used for the agitator and a rubber stopper in the head plate was used for a pressure relief device.

Inoculum Development

For long-term storage periods, *Ralstonia eutropha* was preserved in a glycerol stock at -80°C. For routine growth experiments, *R. eutropha* colonies, recently cultivated under autotrophic conditions, were temporarily stored on agar plates at 4°C. To begin a seed train, several colonies from a refrigerated plate were streaked on a fresh plate and cultivated under autotrophic conditions for 2-3 days. Autotrophic gas-plates were maintained at 30°C under an atmosphere of hydrogen, oxygen, and carbon dioxide in the proportion H_2:O_2:CO_2 =70:20:10. After sufficient biomass had formed on the plates, cells were transferred to liquid media for continued growth. Shake flasks filled with liquid MSM were purged with the autotrophic gas mixture and allowed to equilibrate for approximately 1 h before inoculation. Inoculum for the liquid culture was prepared by streaking cells from the gas-plate to create a dense, cell suspension of ~ 15-20 OD_{600} in MSM, which was used to inoculate the flask at the target OD_{600}.

For bioreactor experiments, the liquid culture was grown in a 2-L shake flask containing 50 mL of MSM and substrate gas with a composition of H_2:O_2:CO_2 = 80:10:10. The culture was inoculated at a density of ~ 0.3 OD_{600} and incubated at 30°C with shaking at 250 RPM. The seed was harvested just after the cells entered stationary phase, typically 18-24 h, at which time a syringe was used to remove the cells and inject them into the production stage vessel.

Shake-flask Trials

Optimal conditions for seed growth were studies in 500-mL, autotrophic, shake-flasks filled with 25 mL of MSM and various gas mixtures. Prior to inoculation, a dense inoculum in MSM was prepared from a freshly cultivated gas plate. Trials were used to study the effect of both inoculum density and gas substrate composition on cell growth. Flasks were incubated at 30°C with shaking at 250 RPM.

Bioreactor Operation

PHA production was carried out in a 2-L, controlled bioreactor filled with 1 L of MSM. Calibration of the dissolved oxygen probe was performed under conditions of air-saturated MSM, at 30°C, and 1 atm, corresponding to a dissolved oxygen (DO) value of 100%. For the zero-point calibration, the probe was temporarily unplugged to eliminate all electrical current. Feed-gas was supplied to the reactor at a rate of 1 L/min with an initial composition of H_2:O_2:CO_2:Ar = 80:5:10:5, controlled by adjusting the flow rates of individual gases. Argon, which is not consumed by the cells, was used as a reference gas for mass-spectroscopy measurements. Immediately upon inoculation. DO was set to 25%, with agitation controlled at 250 RPM. As the oxygen demand of the culture increased and DO declined, we manually adjusted the O_2 composition in the feed-gas up to 10 mol% to maintain the 25% DO set point. After reaching 10 mol% O_2, dissolved oxygen was controlled automatically via closed-loop control of the agitator set-point which was allowed to increase up to 1200 RPM. The initial pH of the media was 6.9, but after inoculation pH was allowed to drop to a value of 6.0 before active control was initiated using 6M NaOH. To control foaming during the batch, a sterile solution of Antifoam A (Sigma) in water (50% v/v) was added in doses of 100 μL (max total 300 μL). For autotrophic cultivations especially, the addition of antifoam must be judicious, particularly near the limits of maximum gas flow and agitation, as it is known that antifoaming agents can reduce the gas-liquid $K_l a$. Indeed, we observed that immediately following the addition of antifoam, the batch responded with a sudden drop in DO followed by a sustained increase in agitator speed to restore the DO set-point. Foaming was also attenuated in batches in which the concentration of ferric ammonium citrate was increased from 6 mg/L to 60 mg/L. This is in agreement with another report of iron deficiency leading to increased batch foaming[269].

PHV-co-PHB Copolymer Synthesis

For the synthesis of various PHB-co-PHV copolymers, CO_2 was used as the precursor to 3HB monomers, and valeric acid (VA) was used as the precursor to 3HV monomers. At the start of VA addition, it is important that the media still contain some residual nitrogen so that the cells can upregulate the enzymes for VA metabolism. For the biosyntheses we conducted, VA addition was initiated shortly after the end of exponential growth, ~24 h batch age. Random copolymers were synthesized by supplying a continuous feed of VA (100-900 μL/h) over the polymer synthesis period. Block-copolymers were synthesized by making discrete doses (100 μL/ min for < 1 min) delivered every hour, over the polymer synthesis period. Mathematical simulations of block-copolymer synthesis in *R. eutropha* have predicted the fraction of di-block copolymer molecules produced during the biosynthesis is maximized when substrate additions are made at a period equal to the average life-span of an actively elongating chain (<1 h). Substrate additions were made using a syringe pump (Harvard Apparatus) controlled by a programmable on-off timer.

Off-gas Monitoring with Mass-Spectroscopy

During biosynthesis, real-time, mass-spectroscopy measurements (Prima Instruments, δB) were used to measure the composition of both the feed-gas and off-gas streams. Argon mixed with the feed-gas to a concentration of 5 mol% served as an inert reference gas by which the difference in total molar flow rate between the feed-gas and off-gas streams was determined. This data was in turn used to calculated the uptake rates of the different gases, which acted as proxies for indicating VA utilization.

Cell Growth Measurements

Growth of *R. eutropha* cells was measured by optical density (OD) by UV-Vis spectroscopy (Agilent, 8453) at a fixed wavelength of 600 nm. To determine the cell dry weight (CDW) batch samples (2-5 mL) were centrifuged at 6000 RCF and 4°C for 15 min, washed in 1 volume of DI water, and centrifuged again. The resulting pellet was transferred to a glass vial and dried at 100°C until constant mass (~24 h).

Polymer Composition

For determination of PHA composition, PHA contained in the dried cells was derivatized to its 3-hydroxyalknyl propyl-esters via the method of propanolysis[263]. Reaction extracts were analyzed using gas chromatography with a flame ionization detector (Shimadzu, GC17-A, DB-wax column 30m x ??) Relative response factors were determined from purified polymer standards of known composition.

Polymer Isolation and Purification

Batch whole-broth was centrifuged at 2000 RCF and 4°C for 15 min then washed in 1 volume of DI water and centrifuged again. The cell pellet was frozen overnight at -20°C. Subsequently the pellet was chilled in liquid nitrogen and chipped into small pieces. Residual water was removed from the frozen pellet by lyophylization (Virtis) for 36 hours. Next, polymer from 10 g of dried cell pellet was extracted in 250-mL chloroform and agitated for 18 h at room temperature. The resulting slurry was vacuum filtered using cellulose filters (Watman #1) to remove residual cell debris. The polymer filtrate was then concentrated under vacuum to a volume of ~ 35 mL. The extracted polymer was then purified by precipitation in excess methanol (7 v/v) while stirring. After resting overnight at 4°C, excess solvent was removed from the polymer slurry by vacuum filtration through a glass microfiber filter (Watman GFA). The filtrate was then further dried in a fume hood, overnight, at room temperature.

Polymer Molecular Weight

Polymer molecular weight was determined via gel permeation chromatography (GPC) with an RI-detector (Polymer Labs PL High-Temperature GPC). Samples were run at 160 °C using a series of 3, PL-gel 10-μm mixed-B columns with TCB (1,2,4-triclorobenzene) (1mg/ml) as the mobile phase. The instrument was calibrated using polystyrene standards (PS). Molecular weights are reported as PS equivalent values. Operation of the GPC was performed by Dr. David Giles of the University of Minnesota, CEMS Polymer Rheology Laboratory.

Preparation of Polymer Thin-films

Prior to processing, purified polymer prills were processed in a grinder to ensure sample homogeneity. To prepare films, 1 g of polymer was dissolved in 20 ml of chloroform and heated in a sealed, glass tube up to 80°C to promote dissolution. The solution was poured into a 5-cm, glass petri dish and allowed to evaporate in a fume hood, overnight, at room temperature. Subsequently films were dried in a vacuum at 60 ˚C for 24 h to remove residual solvent. During experimentation we observed that films which contained a high fraction of PHB often became distorted and wrinkled upon drying, presumably because crystallization was occurring at the same rate (or faster) than solvent evaporation. Thus, in order to remove the physical defects and promote uniform crystallinity within the test specimens, the final polymer films were prepared using a hot-press (Tetrahedron, MTP-10). In order to prepare films for mechanical and rheological analysis, sample was loaded into the press at 170°C inside of a custom Teflon mold. Samples were then compressed at a rate of 1 lb/min to 500 lb and held for 2 minutes. The sample was then ramped to 5000 lb and held for 3 minutes. Finally the sample was rapidly cooled to 49°C under 5000 lb and held for 3 minutes. Films were then removed from the mold and trimmed using a die and press. Film thickness was ~ 0.5 mm. Polymer films were prepared by Mr. Malcolm Davidson at the Petroleum Institute in Abu Dhabi, UAE.

Thermodynamic Transitions

The glass transition temperature (T_g), and melting temperature (T_m), crystallization temperature (T_c), and corresponding normalized enthalpies of polymer samples were measured using differential scanning calorimetry (DSC) (Netzsch 204 F1 Phoenix). Samples (5-15 mg) were placed in a crimped but unsealed TA-Zero aluminum pan and purged with a constant nitrogen flow and then exposed to a typical heat-cool-heat (HCH) experiment. In the first step, samples were heated to 200° C to remove any thermal history. In the second step, the sample was cooled to -50 °C before being heated to 200° C at a rate of 10°C / min. Additional work was performed on a TA Discovery DSC equipped with auto sampler and RCS 90 ballistic cooling unit. Measurements were made by Mr. Malcom Davidson at the Petroleum Institute in Abu Dhabi, UAE.

Mechanical Properties

Measurements of the modulus of elasticity, ultimate strength, and elongation at break were made using thin strips (50 x 5 mm) cut from the polymer films. Controlled elongation of tests strips was conducted at room temperature using a dynamic mechanical analyzer (DMA) (TA Instruments, RSAIII) at a strain rate of 0.12 mm/min with an initial gap of 5 mm. Particularly ductile samples were subjected to a 0.12 mm/min initial strain rate in order to observe the elastic region and then ramped to 5 mm/min to observe the break conditions. Testing was performed by Mr. Malcom Davidson at the Petroleum Institute in Abu Dhabi, UAE.

Elementary Mode Analysis

E. coli Metabolic Network

The mathematical model used for elementary mode analysis was based on the *E. coli* network described by Trinh *et al*. (2009) with reactions for the pyruvate decarboxylase , acetaldehyde dehydrogenase, and alcohol dehydrogenase of pLOI297 removed from the model. For PHB production, reactions were added for a β-ketothiolase, acetoacetyl-CoA reductase, and PHB synthase. Strain TCS010 A detailed description of the model is given in **Figure 4.13**. Elementary mode and flux balance analyses were performed using the CellNetAnalyzer program (available for free download online) developed by Steffen Klamt and Axel von Kamp.

R. eutropha Metabolic Network

The mathematical model used for elementary mode analysis was based on network of *R. eutropha* metabolism under strictly autotrophic condtions. The model was first developed for the Srience lab by Gilsinia Lopez and further refined by Dr. Luz Perrez (results unpublished). For conditions of mixotrophic metabolism studied in this thesis, the basic autotrophic model was augmented with extra reactions for the metabolism of valeric acid and the synthesis of PHV, but no other reactions associated with heterotrophich substrates (e.g. catabolic or anabolic pathways specific for fructose metabolism) were added. A detailed description of the model is given in **Figure 6.12**. Elementary mode and flux balance analyses were performed using the CellNetAnalyzer program (available for free download online) developed by Steffen Klamt and Axel von Kamp.

Chapter 4. Engineering Monomer Fluxes to Control the Synthesis of PHB-co-PHAmcl Polymers Using a Mutant P. oleovorans PhaC1 Synthase

Overview

Polyhydroxyalkanoate plastics display a range of mechanical properties from stiff to elastomeric, which depend primarily on the molecular structure of their constituent monomers. Furthermore, the creation of copolymers can be used to combine the functionality of different monomers types for the creation of novel properties. Controlling the monomer composition in a homopolymer or copolymer, is achieved through two ways: 1.) by adjusting the substrate specificity of the PHA synthase and 2.) by regulating the level of different monomer fluxes within the cell. In this study we construct a mutated version of the PhaC1$_{P.o.}$ synthase of *Pseudomonas oleovorans*. We characterize the specificity of the PhaC1$_{mut}$ synthase towards both PHB (C_4) and PHA$_{mcl}$ (C_6-C_{14}) monomers using two different *E. coli* strains. The first strain, designed using elementary mode analysis, produces significant enhancements in the rate of PHB synthesis as well as the substrate to product yield. The second strain is designed for simultaneous delivery of monomers for both PHB and PHA$_{mcl}$. Furthermore we explore how adjusting the ratio of glucose and dodecanoic acid feedstocks may affects the relative compositions of PHB and PHA$_{mcl}$. Transient profiles of polymer synthesis during fed-batch biosyntheses reveal that formation of PHB occurs throughout the entire batch, while formation of PHA$_{mcl}$ is upregulated during biomass synthesis and diminishes when biomass synthesis ceases. Moreover, by calculating metabolic rate data from mass spectroscopy measurements of biosynthesis off-gas, we are able to monitor the transient consumption of small doses of dodecanoic acid, a process control function that is critical for the synthesis of PHB-b-PHA$_{mcl}$ block copolymers.

Background

Earlier in the Introduction (of the thesis), we discussed how variation in the physical and mechanical properties of PHAs arises from the type and size of the appendages that stem from the 3' carbon of each monomer. PHAs with aliphatic appendages at the 3' position include PHA_{scl} (short-chain-length, C_3-C_5) and PHA_{mcl} (medium-chain-length, C_6-C_{14}). Due to the steroselectivity of the PHA synthase enzyme, the resulting polymer is isotactic which promotes crystallization. PHB (polyhydroxybutyrate, C_4), the most common PHA_{scl}, has a high level of crystallinity (~80%), with gives the polymer its strength but also its brittleness. Alternatively, PHA copolymers containing PHB with small amounts of randomly distributed PHA_{mcl} have reduced crystallinity, which reduces the polymer's strength but also imparts it with greater elasticity[270]. Block-copolymers, in which co-monomers are segregated into large homogenous domains, result in the formation of highly ordered secondary structures that can impart a range of useful mechanical properties[34]. Recently Pederson et al. reported on the synthesis of block-copolymer molecules of PHB and PHV (polyhydroxyvalerate, $C_{5)}$ via a carefully controlled biosynthesis process[21]. These materials demonstrated dramatically improved mechanical toughness and resisted embrittlement over time compared to random copolymers of the same compositon[20]. In Pederson's study the block-copolymers were composed of two, structurally similar, PHA_{scl} monomers. Alternatively, we are interested in studying the material properties that emerge when such block-copolymer molecules are created by combining PHB with a more dissimilar PHA_{mcl} monomer, e.g. C_8 or C_{10}.

The biosynthesis of PHA_{scl}–co-PHA_{mcl} copolymers, in either a random and block configurations, has two main requirements: 1.) a polymer synthase enzyme with specificity for both scl and mcl monomers and 2.) the capacity to transiently regulate both monomer fluxes within the cell. In this study we investigated how the composition of PHA copolymers is affected by enzyme specificity, strains selection, and the transient control of substrate concentrations during fed-batch biosynthesis.

Using the technique of site-directed mutagenesis, we constructed a mutant PHA synthase (*phaC1*$_{mut}$) with broad, scl-mcl specificity, based on the wild-type, PHA_{mcl}

synthase of *Pseudomonas oleovorans* (*phaC1*$_{P.o.}$). To enable synthesis of PHB monomers, the *phaC1*$_{mut}$ enzyme was then cloned into a plasmid containing the *phbA* (β-ketothiolase) and *phbB* (acetoacetal-CoA reductase) genes of *Ralstonia eutropha.* For synthesis of PHA$_{mcl}$ monomers, *phaJ*$_{P.o.}$ (*R*-specific enoyl-CoA hydratase) from *Pseudomonas oleovorans* was recombinantly expressed on a separate plasmid. For characterization of PHB production we evaluated the mutant synthases in a strain designed to maximize the flux of acetyl-CoA (TCS010), while for PHA$_{mcl}$ production we used a mutant strain with an interrupted β-oxidation cycle (JSBS01).

E. coli TCS010 is a 10-gene knockout strain designed using elementary mode analysis (EMA) to increase the flux of 3HB-CoA monomers and maximize the product yield when glycerol is used as the substrate. Moreover, the production of PHAs from glycerol is especially appealing, because of glycerol's current low-price, which is due to the generation of glycerol as a waste product from biodiesel production.

The second strain, JSBS01, is a 3-gene knockout mutant designed to simultaneous deliver both 3HB-CoA and 3HA-CoA (3-(*R*)-hydroxyalkanoyl-CoA, mcl) monomers for production of PHB-co-PHA$_{mcl.}$ In addition, we incorporate the catalytic activity of a recombinant, *R*-specific enoyl-CoA hydratase, PhaJ$_{P.o.}$ (*phaJ*$_{P.o.}$) from *P. oleovorans* to further boost 3HA-CoA production in JSBS01. Using this recombinant platform we characterize how the ratio of glucose and dodecanoic acid feedstocks affects the final copolymer composition.

Lastly, we present a time-course evaluation of PHB and PHA$_{mcl}$ synthesis kinetics during fed-batch biosyntheses using JSBS01 / *phaJ*$_{P.o.}$ / *phaC1*$_{mut}$. We conduct the trials in a controlled, 10-L, bioreactor with simultaneous feeding of glucose and dodecanoic acid. Results are presented for two different polymer synthesis techniques, one in which dodecanoic acid is charged in a single bolus, and the other in which dodeconic acid is added hourly in small doses. In both batches we observe that the synthesis of PHA$_{mcl}$ occurs only during periods of biomass synthesis, while PHB synthesis occurs throughout the entire batch. By computing values of the oxygen uptake rate (OUR) and carbon dioxide evolution (CER) from mass-spec monitoring of biosynthesis off-gas data, we are able to quantify the transient consumption of dodecoanic acid during the batch. Such

information is essential for controlling the size of homopolymer domains in PHA_{scl}-b-PHA_{mcl} block copolymers.

Results and Discussion

Mutation of the P. oleovorans PHA synthase for enhanced 3HB-CoA specificity

Table 4.1 Strains and plasmids used for PHA biosynthesis.

	a.k.a.	Parent	Genotype
Strains (*E. coli*)			
MG1655		K12	*F⁻ λ⁻ ilvG- rfb-50 rph-1*
TCS010		MG1655	*Δ(zwf ndh sfcA maeB ldhA frdA poxB pta mdh adhE)*
JSBS01		MG1655	*Δ(fadB fadR ptsG)*
Plasmids			
pPT500	$phbC_{R.e.}$	pCR-Blunt	$phbCAB_{R.e.}$ kan^R zeo^R *ColE1 ori*
pPT700	$phaC1_{P.o.}$	pPT500	$\Delta phbC_{R.e.}$ $phaC1_{P.o.}$
pPT700_STQK	$phaC1_{mut}$	pPT700	$phaC1_{P.o.}$* (S325T Q481K)
pCDFBB_*phaJ*	$phaJ_{P.o.}$	pCDFBB-eGFP	*ΔeGFP* $phaJ_{P.o.}$ $strp^R$ *CloDF13 ori*

PHA synthases are categorized by their substrate specificity. Type I polymerases, e.g. PhbC ($phbC_{R.e.}$) of *Ralstonia eutropha*, are enzymes with substrate specificity for short-chain-length (scl) monomers containing 3-5 carbons. Type II polymerases, e.g. PhaC1 ($phaC1_{P.o.}$) of *Pseudomonas oleovorans* , are enzymes with substrate specificity primarily for medium-chain-length (mcl) monomers containing 6-14 carbons[3]. However, the synthesis of PHA copolymers that contain both short-chain-length (scl) monomers and medium-chain-length (mcl) monomers requires the use a polymer synthase enzyme with a broad substrate specificity to accept both types of monomers. $PhaC1_{P.S.}$ ($phaC1_{P.s.}$) of *Pseudomonas sp. 61-3* is a Type II synthase that has a low specificity for 3HB-CoA

monomers[9]. Attempting to improve the 3HB-CoA specificity of this enzyme, Takase et al. created a mutant library[12]. Results of their study revealed that amino acid sustitutions at the serine-325 and glutamine-481 positions of *phaC1*$_{P.s.}$ had a significant effect on the specificity of the enzyme toward 3HB-CoA monomers and in the overall activity of the enzyme for PHA synthesis[271]. For the mutant with substitutions of threonine at the 325 position and lysine at the 481 position (S325T Q481K), both the specificity toward 3HB-CoA and the overall activity of the enzyme for PHA synthesis were approximately 2x greater than wild-type . Moreover, substitutions at these same residues within *Pseudomonas* species orthologs[11, 129, 272] have generated similar improvements in substrate specificity and activity. However, due to an inability to crystallize the proteins, a structural model for neither the type-I or type-II synthase has been determined. Thus, the mechanism by which these mutations control catalytic activity remains vague.

A protein sequence alignment between the PhaC1$_{P.s.}$ synthase of *P. sp* 61-3 and the PhaC1$_{P.o.}$ synthase of *P. oleovorans* shows that the two enzymes share 84% and 92% sequence identity and similarity, respectively. Given the high sequence homology, we wanted to explore what effect mutations at these positions might have on the specificity and rate of the *P. oleovorans* enzyme. Using site directed mutagenesis we made a library of 11 mutants by modifying the amino acid at one or both of these locations. Substitutions of cysteine or threonine were made at the serine-325 position, and lysine, arginine, or methionine were substituted at the glutamine-481 position. Similar to the results of Takase et al., S325T Q481K showed a very strong improvement over the wild-type, and so we selected it for further evaluation in our engineered strains. To gauge the performance of the mutant polymerase for both mcl and scl monomers we compared it against both the *P. oleovorans* wild-type *phaC1*$_{P.o.}$ and the *R. eutropha* wild-type *phbC*$_{R.e.}$ in different *E. coli* strains designed for either PHB production, TCS010, or PHA$_{mcl}$ production, JSBS01. The polymerases *phaC1*$_{P.o.}$, *phaC1*$_{mut}$ **,** and *phbC*$_{R.e.}$ are carried on plasmids pPT700, pPT700_ST_QK, and pPT500 respectively. See **Table 4.1** Data for polymerase testing experiments are presented in subsequent sections.

Metabolic engineering for increased PHB Productivity

In recombinant *E. coli* the conversion of the central carbon metabolite acetyl-CoA to PHB is easily achieved via the introduction of the three-gene, biosynthesis pathway from *Ralstonia eutropha*[48], which includes a β-ketothiolase ($phbA_{R.e.}$), an acetoacetyl-CoA reductase ($phbB_{R.e.}$), and a PHA synthase gene ($phbC_{R.e}$). In our study we expressed this pathway along with its native promoter on plasmid pPT500. Plasmids pPT700 and pPT700_ST_QK contain the same promoter and $phbAB_{R.e.}$ genes with the exception of a different polymerase gene.

We performed PHB production studies using glycerol as the primary carbon feedstock. Glycerol is an ideal substrate for PHB production because of the additional reducing equivalent that is generated from its catabolism which is utilized during the NADPH dependent conversion of 3-ketobutyryl-CoA to 3HB-CoA. Moreover, glycerol is beginning to receive more attention as a renewable carbon feedstock because of its low price and market surplus due to its generation as a waste stream from biodiesel production[273]. As a caveat, some studies have reported lower PHB molecular weights from glycerol utilization, suggesting that glycerol may act as a chain termination agent to polymer elongation.

In order to maximize the production of 3HB-CoA from glycerol we used an *E. coli* knockout mutant TCS010 Δ(*zwf, ndh, mdh, sfcA, maeB, ldhA, frdA, poxB, pta, adhE*.), designed to eliminate the production of unwanted metabolites including carbon dioxide, lactate, acetate, ethanol, and excess biomass. Gene deletions were chosen by elementary mode analysis (EMA), a computational technique which identifies gene deletions by systematically evaluating the production efficiency of all possible reaction pathways (i.e. elementary modes) within the cell. The metabolic model used for our study was originally developed by Trinh et al.[274], who used the model as a guide for the construction of a 9-gene deletion strain TCS099, which was shown to maximize ethanol production from glycerol when an enthanologenic plasmid pLOI297 was added. Using TCS099 as the parental strain, we deleted *adhE* (aldehyde-alcohol dehydrogenase) to eliminate ethanol synthesis by the strain. A schematic of these deletions is presented in the supporting

information. After adding the necessary reactions to enable PHB synthesis, EMA calculations from our model show that when glycerol is used as the primary carbon substrate, the wild-type metabolism consists of 10113 elementary modes with 90% of these producing biomass and 16% producing PHB. Incorporation of the 10 gene deletions reduces the number of elementary modes to 16, with 25% of these producing biomass and 100% producing PHB. In the wild-type strain the least efficient mode has a product yield of 0 (mol PHB / mol glycerol) and the most efficient mode has a yield of 0.5. In the 10-gene knockout strain all 16 modes have a product yield of 0.5. Additional details of the EMA calculations are given as supporting information.

Comparison of PHB productivity by different PHA synthases

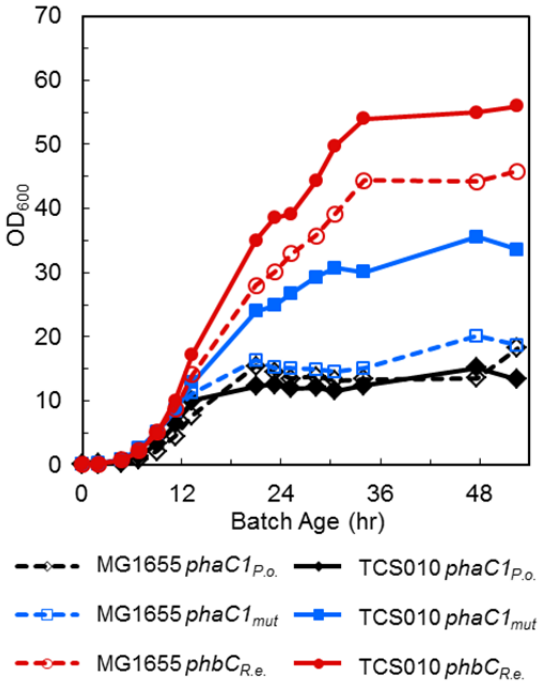

Figure 4.1. Recombinant PHB production in E. coli TCS010: optical density.
The figure shows optical density profiles of MG1655 and TCS010 cultures containing either pPT700 (*phaC1*$_{P.o.}$), pPT700_ST_QK (*phaC1*$_{mut}$) , or pPT500 (*phbC*$_{R.e.}$). Media consisted of LB broth in 100 mM phosphate buffer with 20 g/L glycerol.

Optical density profiles (OD_{600}) for the production of PHB in TCS010 versus the wild-type MG1655 are presented in **Figure 4.1** For the experiment we tested three

different polymer synthase enzymes, $phaC1_{P.o.}$, $phaC1_{mut}$, and $phbC_{R.e.}$. The growth profiles were obtained from shake flask cultures of rich media supplemented with 20 g/L glycerol. Growth was exponential for approximately the first 12 hours, and before 9 hours all cultures had very similar growth rates of 0.44 h^{-1} with the exception of *phaC1P.o.* in TCS010 which had a growth rate of 0.38 h^{-1} Cultures with low PHB productivity quickly transitioned to stationary phase; whereas, high PHB producing cultures entered into an extended period of linear growth until stationary phase at ~36 hrs. Values for PHB production are given in **Figure 4.2.a**. In the wild-type MG1655, the native scl polymerase from *R. eutropha* $phbC_{R.e.}$ produces 6.89 g/L PHB at 48 h while the native mcl polymerase from P.oleovorans, $phaC1_{P.o.,}$ produces no PHB. However the hybrid mcl-scl polymerase, $phaC1_{mut}$ produces 0.98 g/L PHB. In the optimized TCS010 strain, $phbC_{R.e.}$ and $phaC1_{mut}$ show dramatic improvements in PHB production to 9.3 g/L and 4.1 g/L, respectively, while $phaC1_{P.o}$ is still incapable of PHB production. These results show that efficient PHB polymerization is affected by both the activity of the polymerase enzyme as well as the supply of monomers from the host strain. In the optimized TCS010 strain it is likely that the elimination of competing side reactions that produce acetate, lactate, ethanol, biomass, and CO_2 leads to the buildup of acetyl-CoA which drives the formation of the 3-(*R*)-hydroxybutyryl-CoA monomers.

Data for residual biomass (cell dry weight (g/L) – PHB (g/L)) and culture pH are given in **Figure 4.2.b**. We observe that strains carrying either the $phaC1_{P.o}$ or the $phaC1_{mut}$ polymerase produce approximately 3.5 g/L of residual biomass at 48 hr, while strains that carry the $phbC_{R.e.}$ polymerase produce approximately 2.0 g/L. This suggest that the rate of polymerization by $phbC_{R.e.}$ is sufficiently strong to divert carbon flux away from biomass synthesis. With respect to the culture pH, we observed that strains with low PHB productivity finished with low pH, <6, and strains with high PHB productivity finished with high pH, >6.5. This result indicates that the presence of a strong PHB expression pathway minimizes the production of organic acids in the cell which is in agreement with the observations of Carlson et al. for anaerobic production of PHB[275].

Using the data presented in **Figures 3.2.a,b** along with the time course OD_{600} data in **Figure 4.1** as an indicator of CDW accumulation, we can make an estimate of the

average specific productivity for residual biomass (mg/g/h) and for PHB (mg PHB / g residual biomass / hr) between 0-25 hr. See **Table 4.2**. For $phbC_{R.e}$, in MG1655 and TCS010, values for specific productivity of PHB are practically identical. However, the specific productivity of biomass is noticeably greater for TCS010 than for MG1655. Thus, $phbC_{R.e.}$ in TCS010 produces more PHB because more of the carbon flux is efficiently diverted to biomass which in turn can produce more PHB. In a related study (data not shown) we observed that $phbC_{R.e.}$ in MG1655 excreted a large amount of acetic acid early in the biosynthesis but later consumed the acetic acid after the primary carbon source had been depleted, while the same polymerase in TCS010 produced very minimal acetic acid for the entire course of the biosynthesis. For $phaC1_{mut}$ the specific productivity of biomass is similar between both strains; however, the specific productivity of PHB in TCS010 is greater than in MG1655 by a factor of ~2.8. Thus we see how the apparent rate of the mutant $phaC1_{mut}$ polymerase is dramatically enhanced when the pool of available monomers is increased by eliminating competing side reactions. For $phbC_{R.e.}$ which already has a very high PHB synthesis rate, the impact of the modified metabolism of TCS010 offers little enhancement in the specific rate of PHB synthesis; however, the more efficient metabolism of TCS010 allow a greater conversion of glycerol to both biomass and PHB. For full conversion of glycerol to PHB via glycolysis, the maximum theoretical conversion is 0.5 (mol PHB / mol glycerol) or 0.467 (g PHB / g glycerol). If we attribute all biomass synthesis to the carbon derived from rich media components (10 g/L tryptone and 5 g/L YEP) and assume that only glycerol (20 g/L) is used for the production of PHB we can calculate the % of maximum conversion of glycerol for each strain and plasmid combination. See **Table 4.2**. In MG1655 the % of maximum conversion for $phaC1_{mut}$ is 10%, and for $phbC_{R.e.}$it is 74%. When the biosynthesis is carried out in TCS010 the % of maximum conversion for $phaC1_{mut}$ is 44%, and for $phbC_{R.e.}$ it is 99%. The reduced pH observed for the $phaC1_{mut}$ cultures indicates that the remaining glycerol is converted to some type of organic acid. It is likely that unpolymerized 3HB-CoA is converted to 3-hydroxybutyric acid for excretion from the cell: formic or succinic acids may also be byproducts as well. Thus the optimized TCS010 provides a significant improvement in efficiency for the conversion of glycerol to PHB.

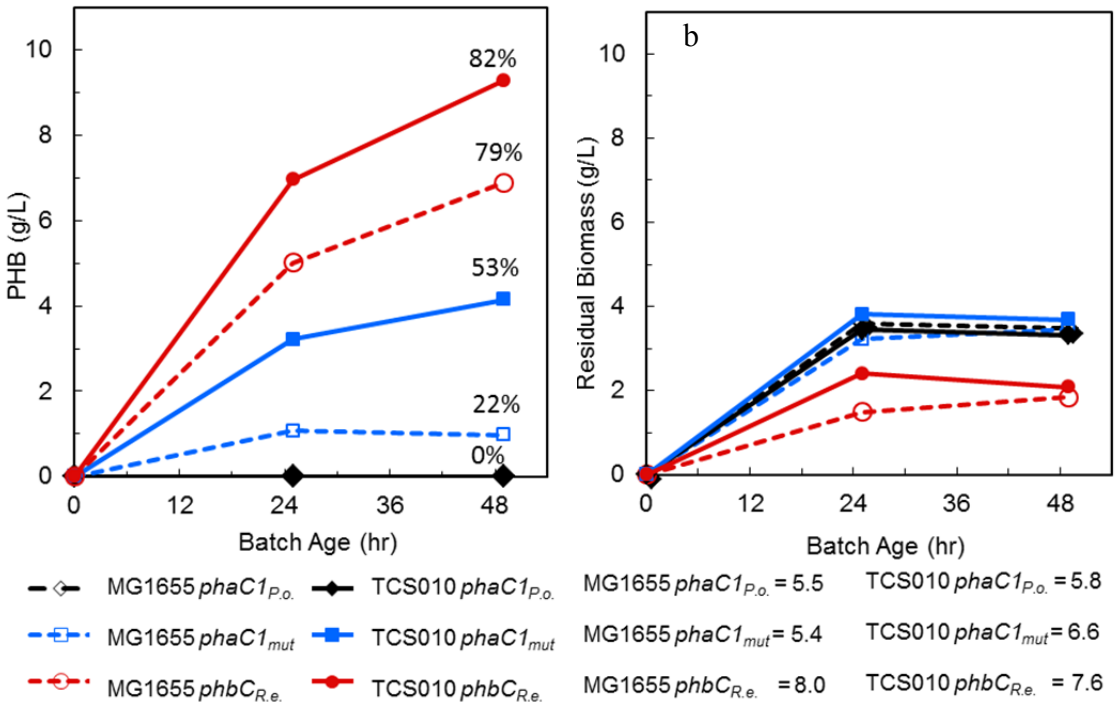

Figure 4.2 Recombinant PHB production in E. coli TCS010: PHB and residual biomass.
Data is shown for MG1655 and TCS010 cultures containing pPT700, pPT700_ST_QK, and pPT500. **a.**) PHB production. The percentages displayed are the PHB/CDW (%) measured at 48 h. **b.**) Residual biomass production. Numerical value are for the media pH measured after 40 hr of growth. Media consisted of LB broth in 100 mM phosphate buffer with 20 g/L glycerol.

Table 4.2 Specific Productivity and Substrate Conversion of MG1655 versus TCS010 for various Polymerase enzymes.

			Specific Productivity			
		Age	PHB		Residual Biomass	[a]Conversion
Strain	Polymeras	(h)	(mg/g/h)	(mmol/g/hr)	(mg/g/h)	(%)
MG165	$phaC1_{P,o,}$	0-25	0	0	176	0
MG165	$phaC1_{mut}$		19	0.22	174	10
MG165	$phbC_{R.e.}$		160	1.85	153	74
TCS010	$phaC1_{P,o,}$		0	0	179	0
TCS010	$phaC1_{mut}$		53	0.61	179	44
TCS010	$phbC_{R.e.}$		159	1.85	170	99

[a]Conversion is given with respect to the theoretical, stoiciometric maximum PHB obtainable from 20 g/L glycerol.

Testing of PHB productivity in minimal media

For the accurate determination of substrate conversion efficiencies the use of a defined media with a single carbon source is a more desirable test. Therefore, we attempted to cultivate the different strain and plasmid combinations on a defined media using either glucose or glycerol as the sole carbon source. In addition to MG1655 and TCS010, we also tested TCS099 used by Trinh et al., thereby allowing us to probe the effect of deleting the *adhE* gene from TCS099. Because TCS010 was designed to couple biomass accumulation with PHB production we anticipated that cell growth might be greatly reduced in the absence of a PHB production pathway. Furthermore, because of the advantageous effects of the PHB production pathway, we speculated that plasmid maintenance might occur naturally without the need for antibiotic-mediated selection. To probe these hypotheses we also tested the case in which strains did not contain a PHB production pathway, as well as conditions in which no antibiotic was added to the growth media. Results of growth studies on agar plates are presented in **Table 4.3**. Plates were cultivated at 30 °C for 72 hr followed by an additional incubation period at 37 °C for 68 hrs.

For TCS099 some growth was observed for all plasmids and substrate combinations. Growth was stronger with glucose than with glycerol, and the additional incubation period at 37 °C further increased growth. When Trinh et al. cultivated TCS099 with the ethanol producing plasmid pLOI297 in minimal media containing glycerol at 37 °C they reported a specific growth rate of 0.33 h^{-1} versus 0.27 h^{-1} for pLOI297 in MG1655. For the cultivation of TCS099 with $phbC_{R.e.}$ (pPT500) in minimal media containing glycerol at 30°C, we have observed a growth rate of 0.14 h^{-1}. (Data not shown.) In TCS099, targeted deletions created a strain in which the conversion of pyruvate to ethanol, via the plasmid-expressed $adhB_{Z.m.}$ (on pLOI297) or the chromosomally expressed *adhE*, was the only mechanism available for the regeneration of NAD+. As a result, EMA calculations predicted that cell growth should be directly coupled to ethanol synthesis, i.e. cell growth in minimal media could only occur if the cell was simultaneously producing ethanol.

In TCS010 our goal was to couple cell growth to PHB synthesis. To do this we removed the pLOI297 plasmid from TCS099, and deleted *adhE* from the chromosome, thereby removing ethanol production as a fermentative product of *E. coli*. Thus, we anticipated that the growth of TCS010 in minimal media should be severely inhibited without the reintroduction of some metabolic pathway capable of reducing either NAD+ or NADP+. (Note: in *E. coli,* NADP+ and NADH are interchangeable to NADPH and NAD+ via SthA). By introduction of the PHB production pathway, which produces 1 molecule of NADP+ for every monomer synthesized, we expected that the capacity for biomass synthesis would be restored. For TCS010 growth on glycerol was very poor at 30 °C, even when the strain contained no plasmid and the media contained no antibiotics. For $phbC_{R.e.}$ in TCS010 no growth was observed under any conditions. Increasing the incubation temperature to 37°C did not improve growth. When TCS010 cultures were grown on glucose, no growth was observed under any conditions.

One reason for the minimal growth in TCS010 may be that the PHB pathway does not have the same net consumption of NADH that the ethanol pathway does. Starting with two pyruvate, the production of two ethanol molecules consumes two NADH, while the synthesis of one monomer of PHB from two pyruvate consumes only one NADPH but

produces two NADH. Furthermore, some studies have reported that *adhE* may function to prevent oxidative damage by reducing highly oxidizing species within the cell.

Table 4.3 Growth of *E. coli* knockout strains in Minimal Media.

Strain	Plasmid	30 °C (72 h)[a]				37 °C (68 h)			
MG1655	none	++++	++	++++	++	++++	+++	++++	++
	$phaC1_{mut}$	++++	++++	+++	+++	++++	++++	++++	++++
	$phbC_{R.e.}$	++++	++++	+++	+++	++++	++++	++++	++++
TCS099	none	+++	+++	+	+	+++	+++	++	++
	$phaC1_{mut}$	+++	+++	+	++	+++	+++	+++	+++
	$phbC_{R.e.}$	+++	+++	+	++	+++	+++	++	++
TCS010	none	–	–	+	++	–	–	+	++
	$phaC1_{mut}$	–	–	+	++	–	–	+	++
	$phbC_{R.e.}$	–	–	–	–	–	–	–	–
	Antibiotic	none	Kan	none	Ka	none	Kan	none	Kan
	Substrate	glucose		glycerol		glucose		glycerol	

[a] Equal measures of inoculum were deposited onto agar plates containing different test medias. The plates were incubated at 30˚C for 72 hr followed by an additional 68 h at 37˚C. Growth estimates are semi-quantitiave and represent the relative coverge of the plates by colonies. No growth (−) max growth (++++)

Study of buffer composition and concentration on PHB productivity

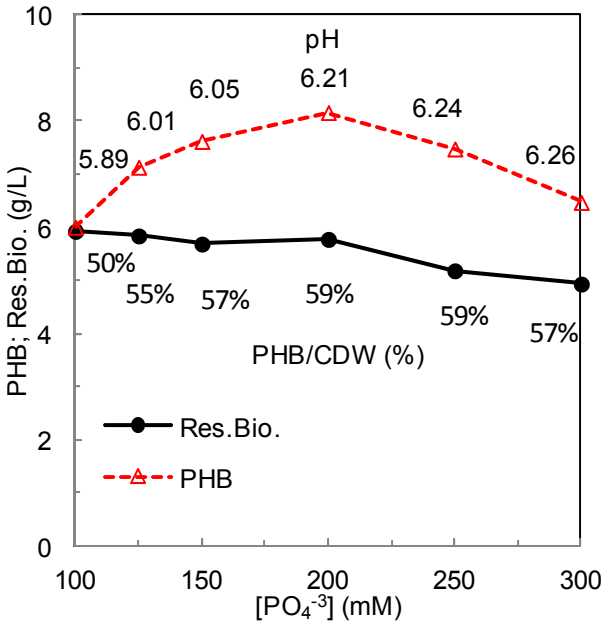

Figure 4.3 Effect of buffer concentration on PHB and residual biomass. Data is shown for strain TCS010 containing pPT700_ST_QK. Numbers above the PHB curve are the final pH of the flasks. Percentages below the residual biomass curve are PHB/CDW (%). At inoculation media contained 20 g/L of glycerol: an additional 20 g/L was added after 24 hr. Cultures were harvested after 94 hr.

As was seen in **Figure 4.2,** decreasing PHB production is strongly correlated with decreasing culture pH. We attribute this effect to the excretion of organic acids which are produced in the absence of a strong PHB polymerase to rapidly consume high levels of glycolytic flux. Given that all plasmids contain the same $phbAB_{R.e.}$ genes, the secretion of 3-(*R*)-hydroxybutyric acid would be expected in the absence of a polymerase with a high rate of PHB polymerization. Furthermore, in the wild-type MG1655 the production of lactic acid and acetic acid is also likely. While it clear to see how slow PHB synthesis can cause low culture pH we wanted to investigate the alternative effect that low pH might have on PHB synthesis. To do this we set cultures of Δ10 with $phaC1_{mut}$ in media containing increasing amounts of phosphate buffer from 100-300 mM in order to extend the time period for which pH was above 6.5. Results of the experiment are presented in **Figure 4.3.** As the concentration of phosphate buffer is increased from 100-200 mM the

final pH of the culture increases from 5.89 to 6.21. Correspondingly, PHB production also increases by 36%, from 6.0 g/L to 8.2 g/L. As the phosphate concentration is further increased from 200-300 mM, pH continues to remain relatively constant; however, PHB synthesis decreases from 8.2 to 6.5, likely due to stress caused by high osmolality of the media.

It is known that exponentially growing *E. coli* attempt to regulate their intracellular Na^+ and K^+ concentrations to target levels independent of extracellular concentrations. Maintenance of these ion concentrations against opposing gradients requires the expenditure of additional ATP. Thus it may be necessary for cells to increase flux through the TCA cycle, and oxidative phosphorylation to meet ATP demands. As a result of an upregulated TCA cycle the flux through acetyl-CoA and the production of NADH would increase, both of which are a boon for 3HB-CoA production. To explore this effect we evaluated cultures of TCS010 with $phaC1_{mut}$ in phosphate buffered media (100 mM) in which the ratio of Na^+ to K^+ ions was varied by the use of either sodium or potassium phosphate salts and the addition of small amounts either KCl or NaCl. Cultures contained 20 g/L glycerol and were analyzed after 24 h growth. See **Figure 4.4**. The data shows a clear trend, albeit nonlinear, in which increasing the mole fraction of Na^+ ions causes an increase in PHB from 1.6 g/L to 2.9 g/L and a decrease in residual biomass from 3.2 g/L to 2.4 g/L. The effect is most dramatic when considering the increase in the estimated, specific productivity of PHB which more than doubles from 40 to 100 mg PHB/ h/ g residual biomass. The increase in carbon flux to PHB is consistent with our original hypothesis, and a reduction in the rate of biomass synthesis indicates that the high sodium levels placed a significant burden on cell metabolism.

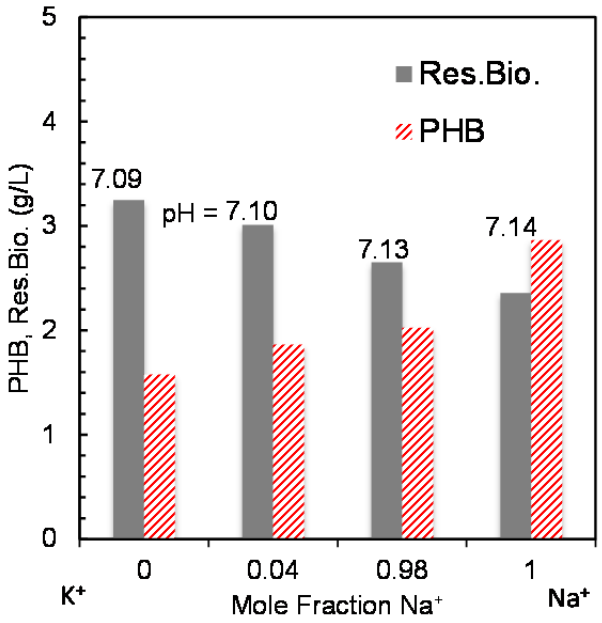

Figure 4.4 Effects of Na+ and K+ ions on PHB and residual biomass productivity. Data is shown for strain TCS010 containing pPT700_ST_QK. Numbers shown in the figure are the final pH values of the flasks. At inoculation the media contained 20 g/L of glycerol. Samples were collected at 24 h.

Metabolic engineering for PHAscl-co-PHAmcl copolymer synthesis

In order to allow the simultaneous production of monomers of $3HA_{mcl}$-CoA and 3HB-CoA we constructed an *E. coli* knockout mutant JSBS01 Δ(*fadB, fadR, ptsG*). In *E. coli* deletion of the *β*-oxidation gene *fadB* (FadB), which codes for an *S*-specific enoyl-CoA hydratase, results in PHA_{mcl} synthesis from fatty acids[54, 276]. FadR (*fadR*), is a transcriptional repressor that controls the expression of 5 different genes required for fatty acid uptake and catabolism[277]. In addition to the relief of FadR repression, genes responsible for the uptake of fatty acid require activation by the c-AMP receptor protein (CRP)[277] which mediates the catabolite repression effect seen in the presence of glucose. It is known that deletion of the glucose-specific transporter PtsG (*ptsG*) disrupts catabolite repression and permits simultaneous uptake of glucose with other carbon sources[278-279] including fatty acids[280-281] Deletion of *fadR* and *ptsG* was made to eliminate the time delays associated with genetic regulation which could hinder rapid switching

between different monomer production pathways, a critical factor for controlling the size and composition of block-copolymer domains. Furthermore, to boost the production PHA_{mcl} we recombinantly expressed *phaJ*$_{P.o.}$ (PhaJ$_{P.o.}$) of *P. oleovorans* which is responsible for the *R*-specific enoyl-CoA hydratase activity that is necessary to convert *β*-oxidation intermediates to $3HA_{mcl}$-CoA monomers[57].

Figure 4.5. shows a comparison between JSBS01 and the wild-type MG1655, with and without the presence of *phaJ*$_{P.o.}$ The polymerase used for PHA synthesis was *phaC1*$_{mut}$. Strains were grown in LB media with 3 g/L of dodecanoic acid. The gene deletions in JSBS01 dramatically increase the composition of PHA_{mcl} to 87% versus 5% for MG1655. Furthermore the addition of PhaJ$_{P.o.}$ to JSBS01 results in a >5x increase in total polymer production compared to the wild-type. While *fadB* is a known participant in β-oxidation, a secondary pathway of β-oxidation genes that is differentially expressed under anaerobic conditions is thought to be the source of various $3HA_{mcl}$ monomers observed in the copolymer [282-283].

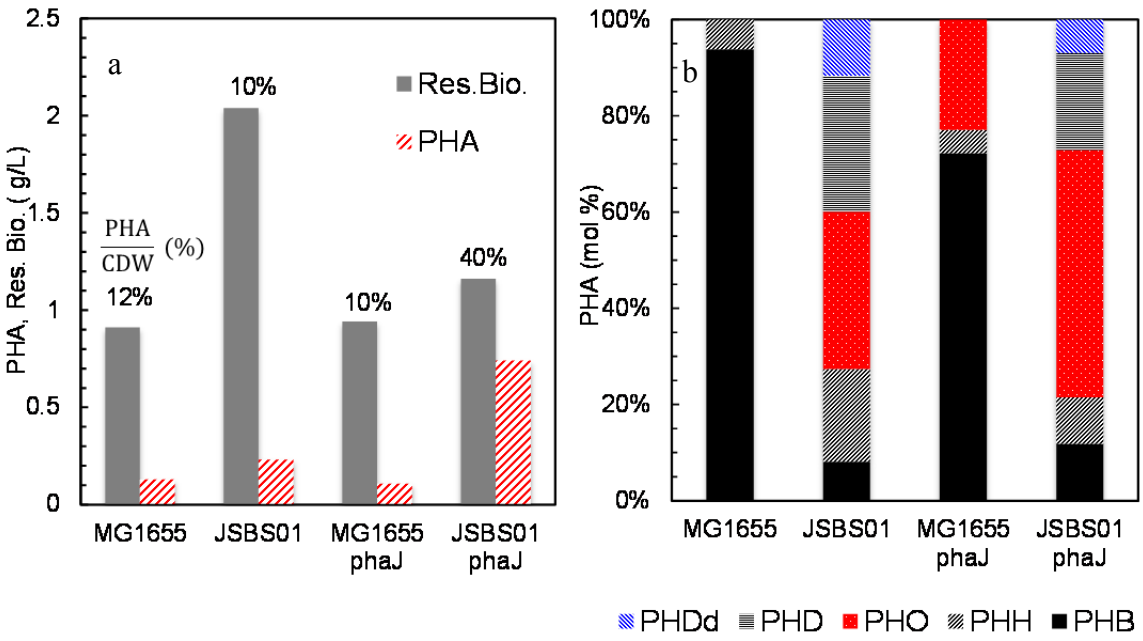

Figure 4.5 PHB-co-PHAmcl production in E. coli JSBS01 with PhaJ$_{P.o.}$.
Data is shown for MG1655 versus JSBS01 containing pPT700_ST_QK with and without the presence of pCDFBB_*phaJ*. **a.)** PHA and residual biomass production. Percentages at the bottom of the graph are the %PHA of CDW. **b.)** PHA composition. Media contains 3 g/L dodecaonic acid.

Control of Polymer Composition by Varying Glucose and Fatty Acid Concentrations

In order to increase the fraction of PHB as well as boost total polymer production, we tested the effects of supplementing dodecanoic acid with varying amounts of glucose. See **Figure 4.6**. While glycerol was used to test PHB production in TCS010, we found that the use of glycerol in conjunction with dodecanoic acid resulted in unexpectedly low growth. We speculate this may be due to an excess of reducing equivalents within the cell caused by two highly reduced feedstocks. (data not shown). Alternatively, the combination of glucose with dodecanoic acid gave improved growth, presumably due to a better balance in the redox potential between the two substrates. In **Figure 4.6.a** the data show that the addition of up to 20 g/L of glucose increases total PHA from 0.5 g/L to 3.1 g/L and residual biomass from 1.1 g/L to 4.8 g/L. The nature of this effect is approximately linear with increasing glucose concentration. Moreover, we observe in **Figure 4.6.b** that the addition of glucose dramatically changes the fraction of PHB in the polymer from 24% with no glucose supplementation to 86% with 20 g/L glucose.

Figure 4.6.c. is a plot of specific PHB and specific PHA_{mcl} in which the polymer mass is normalized by the residual biomass (g PHA / g residual biomass). With increasing glucose the specific PHB increases by a factor of 8. For specific PHA_{mcl} an opposite trend is observed in which the value decreases by a factor of 0.35. This result suggests that increased flux rates through glycolysis may reduce the cell's uptake of fatty acid, possibly by the accumulation of acetyl-CoA or by raising the intracellular redox potential. Alternatively it may be that 3HB-CoA monomers hider the polymerization of $3HA_{mcl}$-CoA monomers by competitive inhibition or through more complicated allosteric changes to the polymerase, possibly due to the presence of a polymerized 3HB monomer immediately adjacent to the active site of polymer synthesis.

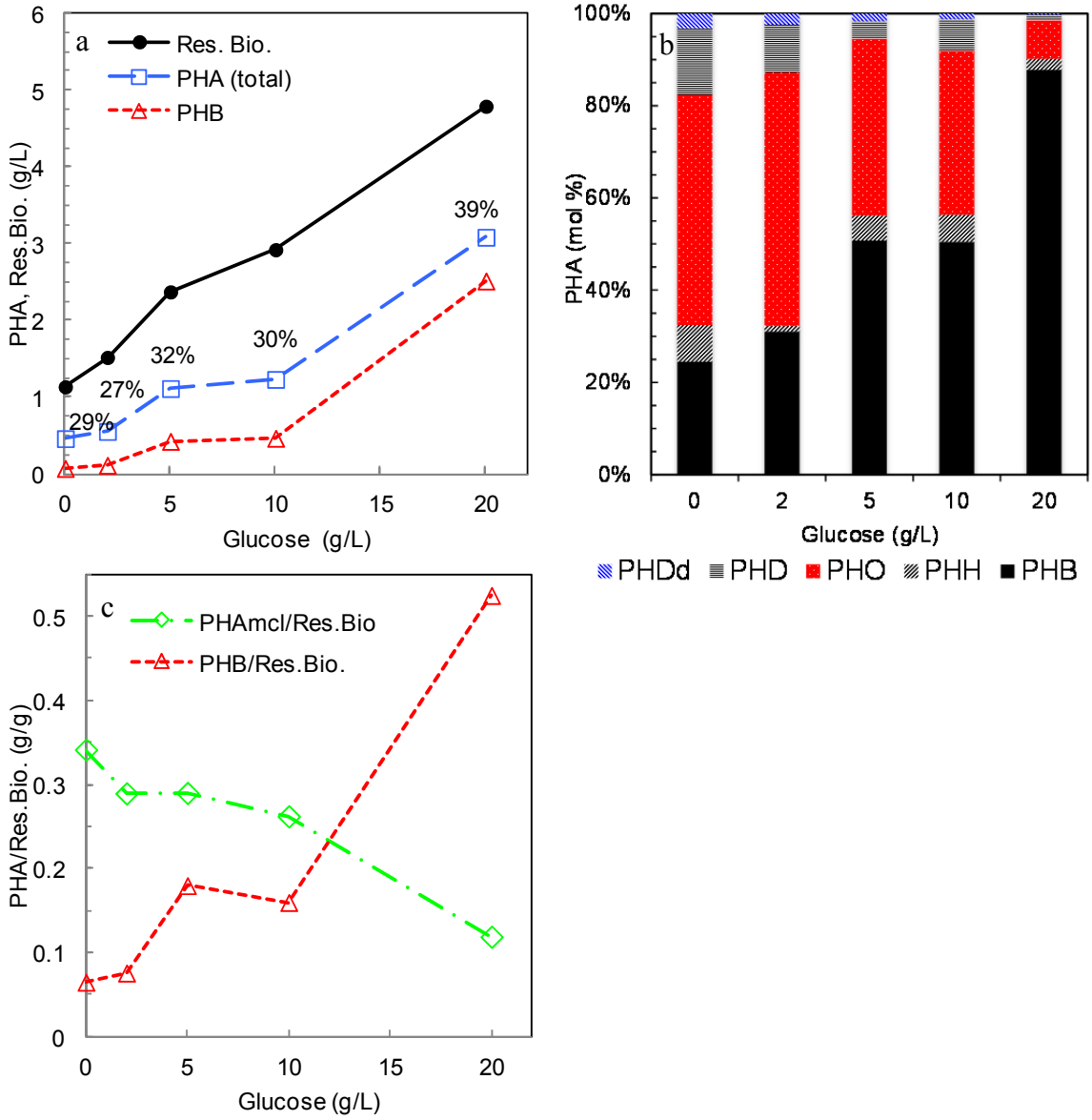

Figure 4.6 Test of glucose concentration on PHB-co-PHAmcl productivity. Data is shown for strain JSBS01 containing pPT700_ST_QK and pCDFBB_*phaJ*. **a.**) PHA and residual biomass production. Percentages are for PHA / Res.Bio. (%). **b.**) PHA composition (mol. %). **c.**) PHB and PHAmcl production normalized to residual biomass production. Media contained 3 g/L dodecanoic acid with varying amounts of glucose.

Figure 4.7.a shows data when glucose is held constant at 20 g/L and dodecanoic acid is varied. The addition of dodecanoic acid, up to 2 g/L, results in a dramatic increase in total PHA from 0.2 g/L to 3.4 g/L; however, beyond 2 g/L the effect becomes saturated. A similar profile is seen for residual biomass, which increases from 3.3 g/L to 5.5 g/L, with the maximum value occurring at 1 g/L. **Figure 4.7.b** shows the details of polymer composition. As expected increasing dodecanoic acid also increase the fraction of PHA_{mcl} in the polymer from 5% mcl at 0 g/L to 20% mcl at 1 g/L.

Figure 4.7.c shows data for specific PHB and specific PHA_{mcl}. With the addition of 2 g/L dodecanoic acid specific PHB is increased by a factor of 8 and specific PHA_{mcl} is increased by a factor of 37. While it is intuitive that adding dodecanoic acid to the media would increase the amount of PHA_{mcl} produced per biomass, it is peculiar that it would also result in a significant increase in the amount of PHB produced per biomass. Final pH values presented in **Figure 4.7.a** give insight. In the absence of dodecanoic acid the culture is distinctly acidic, pH = 5.09, but the addition of only 1 g/L is sufficient to raise the final pH to 6.97. Typically, low pH under aerobic conditions is an indication of acetate excretion due to glycolytic overflow. Because of supplementation with fatty acid, fewer NADPH are required for fatty acid biosynthesis, 2 for every acetyl-ACP not consumed. Additionally, the first step of β-oxidation, which is required for synthesis of $3HA_{mcl}$-CoA, generates reducing equivalents in the form of $FADH_2$. These factors combine to create an overall increase in redox potential of the cell which causes downregulation of the TCA cycle via the ArcAB global regulator[284-286]. Cessation of the TCA cycle in turn causes a buildup of acetyl-CoA, which along with high levels of NADH / NADPH create favorable conditions for PHB synthesis[287]. However, these are also conditions which stimulate acetate overflow[284]. Further insight is gained from a recent report by Valgepea et al. which proposes that the initiation of acetate overflow is triggered by the carbon-catabolite repression system[288], a hypothesis that is supported by other reports that the deletion of *ptsG* reduces acetate excretion[289-290] Thus, disruption of the acetate overflow system of JSBS01 via *ptsG* deletion and the use of highly reduced substrates, i.e. fatty acids, may contribute to enhanced PHB expression. A similar effect was noted by Lee et al. in which PHB production from glucose in recombinant *E. coli* was

increased by ~3x using oleic acid supplementation[291] Given that only 0.69 g/L of PHAmcl is synthesized from 2 g/L of dodecanoic acid, we speculate that a significant portion of the fatty acid must be routed into fatty acid biosynthesis. This hypothesis is supported by GC data from propanolysis reactions of cell pellets that show significant dodecanoic acid peaks, even after the cell pellets were washed with ethanol to remove residual dodecanoic acid. (data not shown)

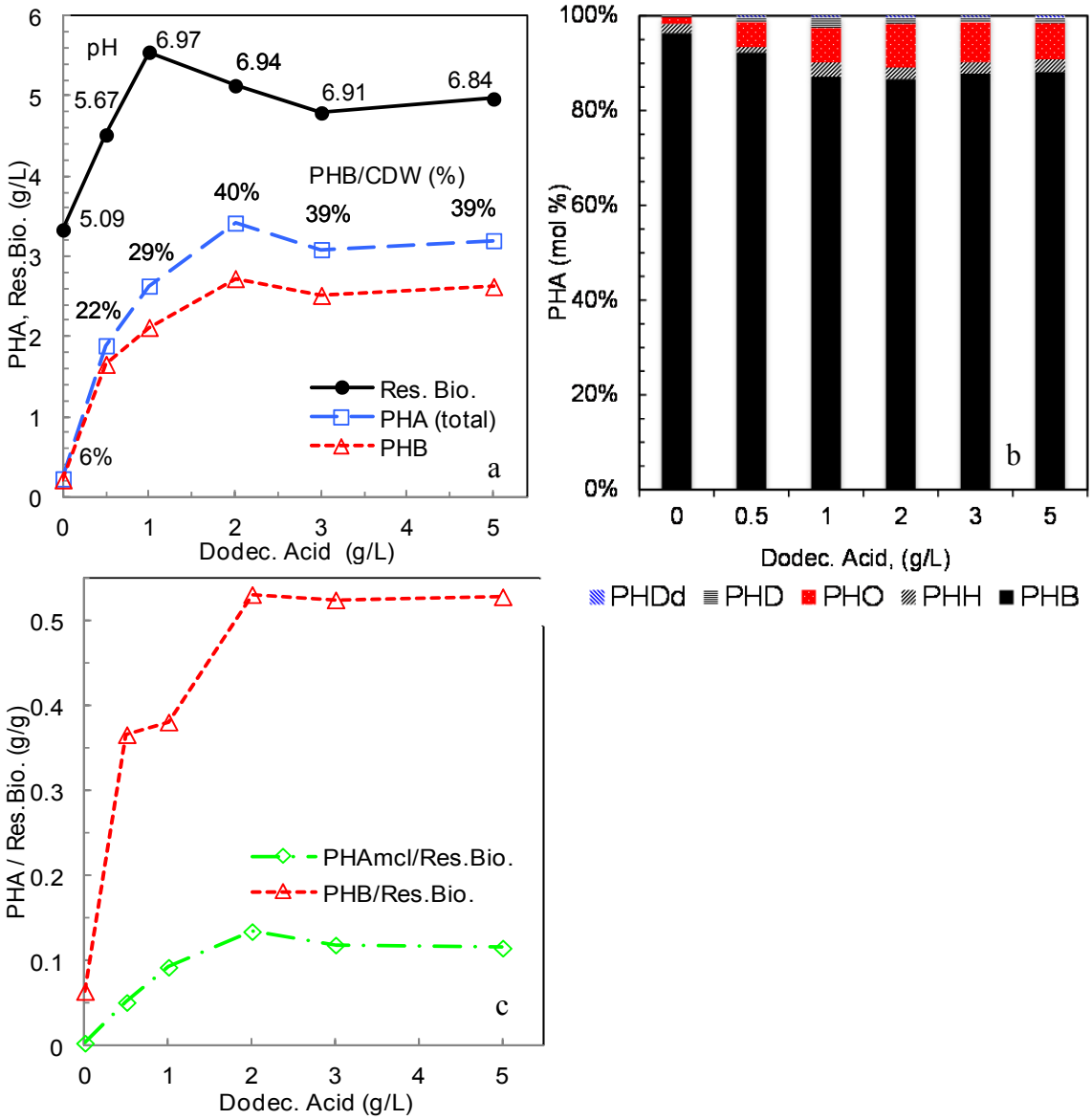

Figure 4.7 Test of lauric acid concentration on PHB-co-PHAmcl productivity. Data is shown for strain JSBS01 containing plasmids pPT700_ST_QK and pCDFBB_*phaJ*. **a.**) PHB, total PHA, and residual biomass production. Percentages are for PHB/CDW (%). Numbers above the residual biomass curve are final pH values **b.**) PHA composition. **c.**) PHB and PHAmcl production normalized to residual biomass production.

Comparison of PHB-co-PHA$_{mcl}$ productivity by different PHA synthases

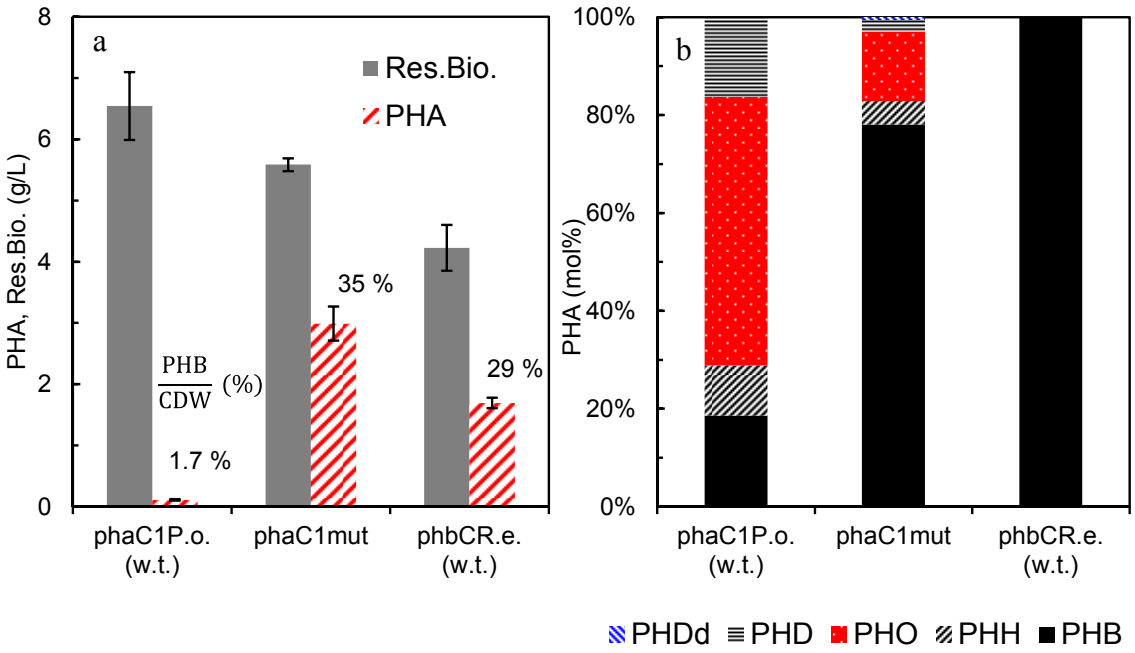

Figure 4.8 Comparison of PHB-co-PHA$_{mcl}$ productivity by different polymerases. Data is for strain JSBS01 with *phaJ$_{P.o.}$* Each strain contains a different PHA synthase plasmid . **a.**) PHA and residual biomass production. Numbers at the top of the graph are the final pH values of flask cultures. Percentages at the bottom of the graph are the % PHA content (g PHA / g CDW). **b.**) PHA composition in mol %. Media contained 20 g/L of glucose and 3 g/L dodecanoic acid.

Based on the results of our media optimization studies we selected 20 g/L glucose and 3 g/L of dodecanoic acid as an appropriate balance for achieving a copolymer with a high PHB fraction, ~80% (wt.) and substantial PHA accumulation of ~40% (g PHA/ g CDW). Using this media formulation we compared the polymer synthesis capabilities of the three different polymer synthase genes *phaC1$_{P.o.}$* ,*phaC1$_{mut}$* , and *phbC$_{R.e.}$* in strain JSBS01 / *phaJ$_{P.o}$* . In **Figure 4.8.a**. results show that total PHA production is greatest for *phaC1$_{mut}$* followed by *phbC$_{R.e,}$*, and smallest for *phaC1$_{P.o,}$*. PHA composition is shown in **Figure 4.8.b**. As expected *phbC$_{R.e.}$* shows the highest fraction of PHB while *phaC1$_{P.o.}$* shows the lowest fraction of PHB. For *phaC1$_{mut}$*, the amino acid mutations increase both the PHB fraction and the total PHA accumulation significantly when compared to *phaC1$_{P.o.}$*.

What is interesting is the significant fraction of PHB in the polymer produced by *phaC1*$_{P.o.}$, ~18 mol% PHB. When the wild-type *phaC1*$_{P.o.}$ was cultivated in TCS010 with glycerol no PHA was produced ; however, when the same enzyme was cultivated with with *phaJ*$_{P.o.}$ in JSBS01 with glucose and dodecanoic acid as nutrient sources, both PHA$_{mcl}$ and PHB were produced. This indicates that *phaC1*$_{P.o.}$is capable of accepting 3HB-CoA monomers, but only if 3HA$_{mcl}$-CoA monomers are also present for polymerization. A similar result was seen for the wild-type *phaC1*$_{P.61\text{-}3}$ of *Pseudomonas* -61-3[12, 271]. The data in **Figure 4.8** shows that when monomers are supplied for both PHB and PHA$_{mcl}$ using JSBS01 / *phaJ*$_{P.o}$, the mutations in *phaC1*$_{mut}$ create an increase in the relative specificity for 3HB-CoA by 4.2x however, for total polymer productivity the increase is 27.1x

It is interesting that while the *phbC*$_{R.e.}$ polymerase produced high levels of PHB in the wild-type MG1655 (> 6 g/L PHB from 20 g/L glycerol), polymer accumulation by the enzyme in JSBS01 was much smaller (< 2 g/L from 3 g/L DDA and 20 g/L glucose). A sign of the poor productivity by *phbC*$_{R.e.}$ in JSBS01/ *phaJ*$_{P.o.}$ can be seen in final pH value of the cultures (pH = 5.21), which is an indication of excess production of acidic metabolites, likely acetate and possibly lactate. We suspect that the onset of overflow metabolism may have been triggered by an excess of reducing equivalents ($FADH_2$) due to the inability of the *phbC*$_{R.e.}$ to consume any of the incoming fatty-acid flux.

Time-course evaluation of PHB-co-PHA$_{mcl}$ synthesis in a controlled bioreactor

While shake flask studies verified that the *phaC1*$_{mut}$ polymerase was capable of synthesizing both PHB and PHA$_{mcl}$, time-course data was needed to verify if PHA$_{mcl}$ synthesis was occurring sequentially or simultaneously with PHB synthesis. To investigate this we cultured strain JSBS01 / *phaJ*$_{P.o}$ with *phaC1*$_{mut}$ and in 10-L, controlled bioreactors supplemented with glucose and dodecanoic acid. For Batch 1, dodecanoic acid (3 g/L) and glucose (10 g/L) were charged at the start of the batch. Additional glucose was fed continuously to control the concentration at ~10 g/L. Productivity data

for Batch 1 is shown in **Figure 4.9.a**. From inoculation until 16.5 h culture growth is characterized by rapid biomass accumulation up to 3.1 g/L but with no PHA production. Then at 16.5 h biomass accumulation stops and a period of rapid PHA synthesis is initiated that shortly decreases after 21.5 h. Data for the specific productivity of residual biomass PHB, PHA_{mcl}, total PHA, are shown in **Table 4.4** During the initial phase of the batch, 7-26 h,the molar specific productivity (mmol PHA / hr / g residual biomass) is ~1.7x greater for PHB than for PHA_{mcl}. After 21.5 hr production of PHA_{mcl} rapidly diminishes and completely stops by 29 h. While PHB production is also diminished it does not stop completely and instead continues at a reduced rate from 25.5-46 h. Thus, the data confirms that the mutant *P. oleovornas* polymerase $phaC1_{mut}$ is capable of simultaneously synthesizing both PHB and PHA_{mcl} ; however, some metabolic effect within the cell causes production of PHA_{mcl} to stop while PHB production continues. Polymer composition is shown in **Figure 4.9.b**. Due to the discontinuation of PHA_{mcl} synthesis by 29 hr, we expect that the final polymer, with an overall composition of 19 mol% PHA_{mcl}, actually contains a blend: 61 wt% of PHB-co-PHA_{mcl} (37 mol% PHA_{mcl}) and 39 wt% of PHB homopolymer.

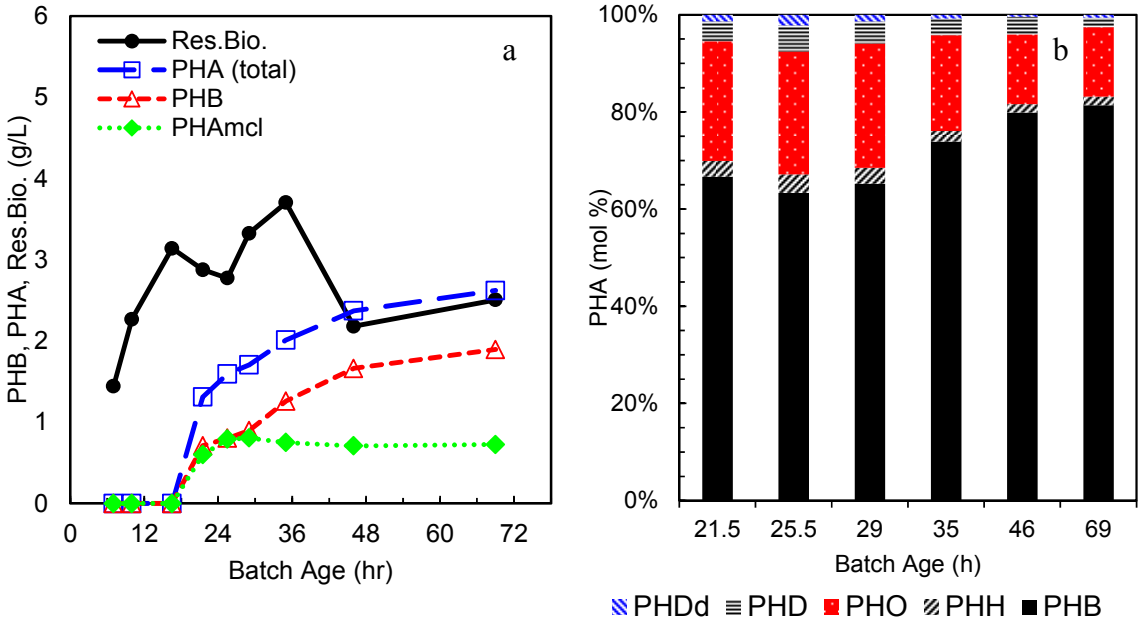

Figure 4.9 Production of PHB-co-PHAmcl synthesis with constant dodecaonic acid supply.
Data is for strain JSBS01 containing pPT700 and pCDFBB_*phaJ* cultivated in a 5-L stirred bioreactor. Dodecanoic acid was present in the media for the entire biosynthesis. **a.**) PHA and residual biomass production. **b.**) PHA composition. Media contained 20 g/L of glucose and 3 g/L of dodecanoic acid. An additional 20 g/L of glucose was fed over the course of the biosynthesis

In Batch 2 we attempted to replicate the dual substrate feeding strategy previously demonstrated by Pederson et al. for the synthesis of block copolymer of PHB and PHV in *Ralstonia eutropha*[21]. During the batch glucose was fed continuously to maintain a target concentration of 10 g/L. Dodecanoic acid dissolved in ethanol at a concentration of 333 g/L was administered hourly in 500 uL doses. A total of 1 g/L dodecanoic acid was added over the course of 30 shots beginning at 8 h. During the batch we monitored the consumption of dodecanoic acid additions via mass-spectroscopy data collected from the biosynthesis off-gas. Using gas composition data we calculated values for the CER (carbon dioxide evolution rate, mmol CO_2 / L/h), OUR (oxygen uptake rate, mmol

O_2/L/h), and RQ (respiratory quotient, CER / OUR). The repeated addition of dodecanoic acid shots is clearly seen in the off-gas data shown in **Figure 4.11.a** In **Figure 4.11.b** a close-up view of a two, repeated dodecanoic acid shos are shown. The addition of 0.033 g/L of dodecanoic acid produces a temporary increase in both the CER and OUR of the culture which reflects a higher level of metabolic flux within the cell. The redistribution of carbon flux from glycolysis to β-oxidation during dodecanoic acid consumption is indicated by the decrease in the RQ value (CER / OUR). This makes sense given that dodecanoic acid is a more a more highly reduced substrate than glucose and so requires the consumption of more oxygen to oxidize the extra $FADH_2$ and NADH produced during β-oxidation. The first shots of dodecanoic acid produce spikes in OUR that are sharp and last for a short duration, but after ~15 h when the rate of cell metabolism peaks, additional shots of dodecanoic acid are consumed more slowly resulting in peaks of shorter height and broader width. After 25 h subsequent shots are unrecognizable in the CER and OUR trends, indicating a likely cessation in the uptake of dodeconic acid. To probe the possibility that the RQ response of the cell might be caused by the consumption of ethanol contained with the dodecanoic acid solution, we administered a 333 uL of pure ethanol at ~20.4 h. Unlike previous shots, the addition of pure ethanol resulted in an immediate drop in OUR and CER and a sharp increase in RQ which lasted until a shot of dodecanoic acid was added an hour later. This indicates that that the observed decrease in RQ at the time of each shot is indeed due to the consumption of dodecanoic acid.

Trends which are seen in the off-gas data of Batch 2 are reflected in the productivity data presented in **Figure 4.10.a** and **Table 4.4**. The onset of PHA production occurs sometime before 8 h and increases linearly until ~44 hr. Between 8-27 hr the molar specific productivity of PHB is ~1.4x greater than that of PHA_{mcl}. The synthesis of residual biomass is at its greatest rate between 0-18.5 h which is reflected in the rapid rise in CER and OUR between 0-15 h. After 18.5 h the production of both residual biomass and PHA_{mcl} begin to diminish and reach their plateau by 26.75 hr. This corresponds to the cessation of dodecanoic acid uptake after 24 h that is observed in the off-gas data

presented in **Figure 4.11**. In the initial stage of the batch the molar specific producityv of PHB is 0.07 (mmol PHB / g residual biomass / h); however, after the cessation of PHA_{mcl} synthesis the molar specific productivity increases to 0.13 from 27-44 h .

Polymer composition values are presented in **Figure 4.10.b**. For the period between 8-26.75 h the polymer produced has a PHA_{mcl} fraction of 33 mol%, but after 26.75 hr the polymer produced contains only 6 mol% PHA_{mcl}. Thus, we expect that the final polymer, with an overall composition of 17 mol% PHA_{mcl}, is a blend of two block-copolymers, 42 wt% of PHB-b-PHA_{mcl} (33 mol% PHA_{mcl}) and 68 wt% of PHB-b-PHA_{mcl} (6 mol% PHA_{mcl}).

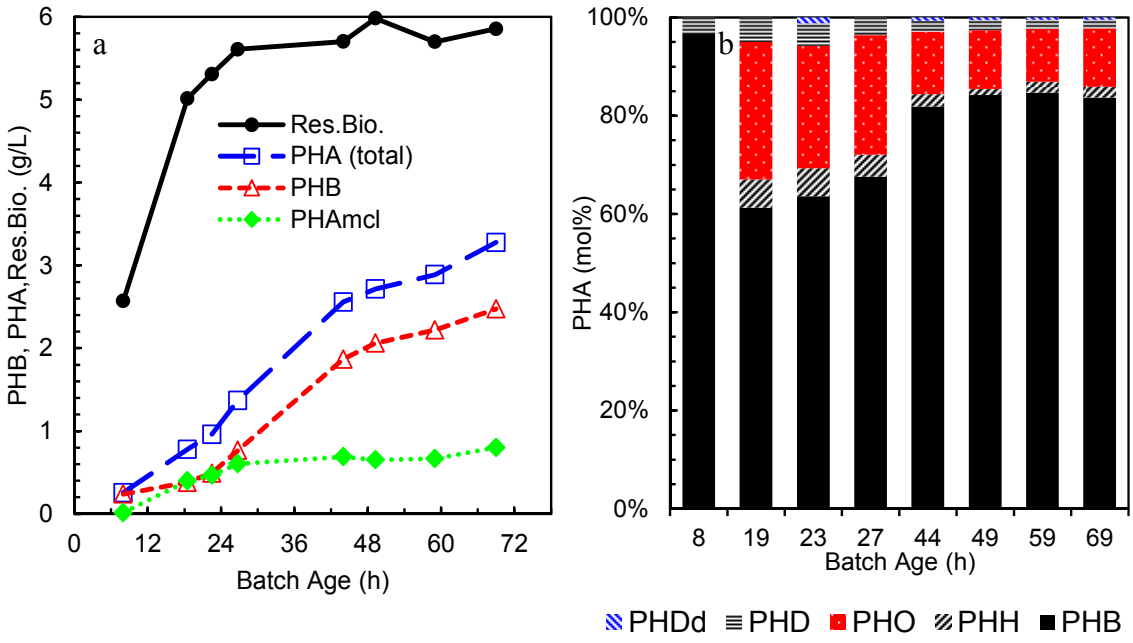

Figure 4.10 Production of PHB-co-PHAmcl synthesis with periodic dodecanoic acid additions.
Data is for strain JSBS01 containing pPT700 and pCDFBB_*phaJ* cultivated in a 5-L stirred bioreactor. Dodecanoic acid was added in periodic shots (33 mg/L after dilution in the batch). **a**) PHA and residual biomass production. **b**.) PHA composition. Media contained 20 g/L of glucose and 1 g/L of dodecanoic acid fed over the course of 30, hourly shots of 0.033 g/L. An additional 20 g/L of glucose was fed continuously over the course of the biosynthesis

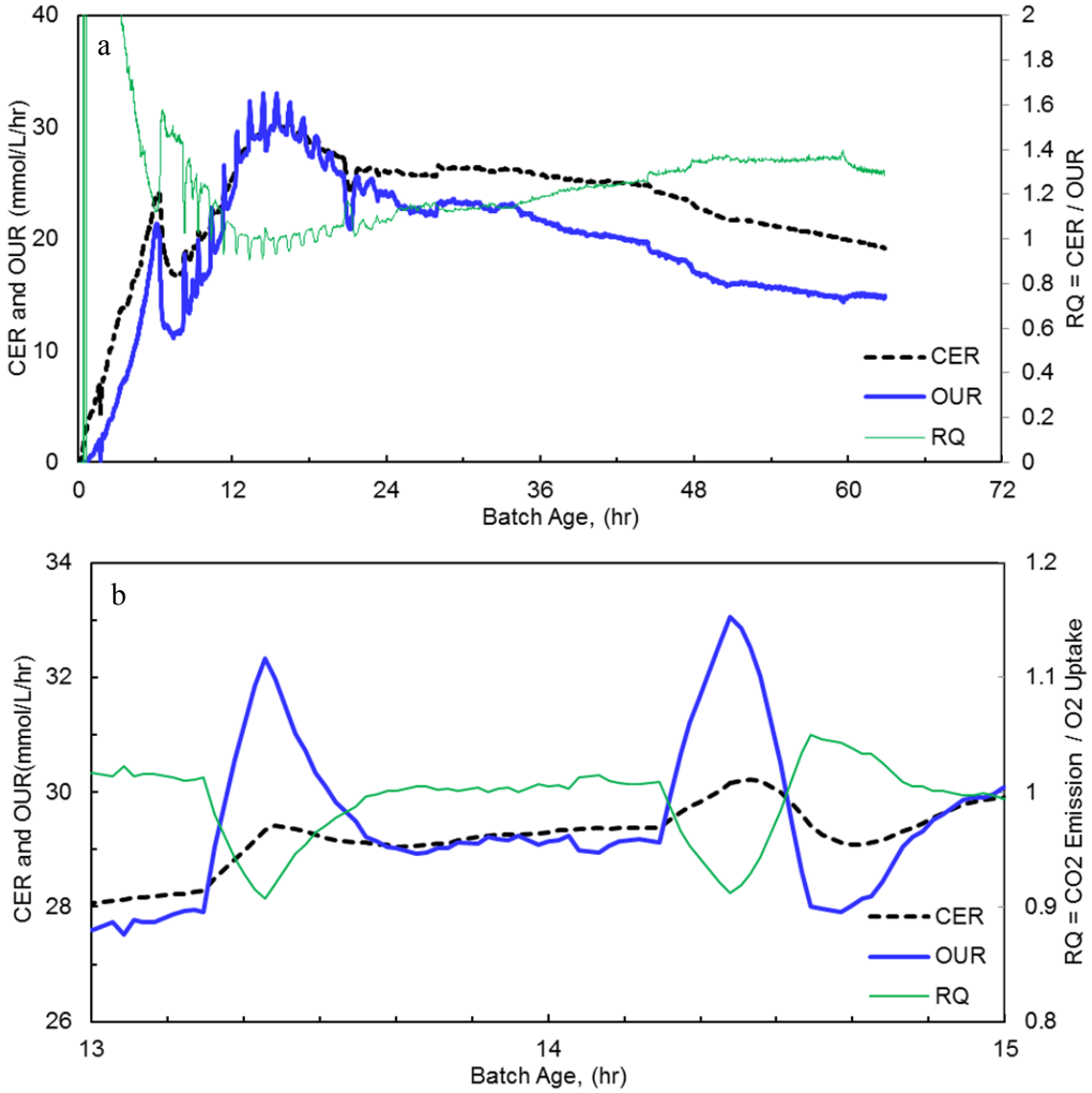

Figure 4.11 Metabolic rate data during periodic additions of dodecanoic acid. **a.)** CER and OUR data for Batch 2. **b.)** Close-up view of a single dodecanoic acid shot given at 16.2 h. Values were determined from the molar composition of the inlet and outlet streams determined *via* mass-spectroscopy .

Table 4.4 Specific Productivity of PHA Copolymer Batches

		Age	Specific Productivity		Age	Specific Productivity	
		(h)	(mg/g/h	(mmol/g/hr	(h)	(mg/g/h)	(mmol/g/hr
First Stage	PHB	7-26	15	0.17	8-27	6	0.07
	PHA_{mcl}		14	0.10		7	0.05
	PHA_{tot}		29	0.27		13	0.12
	Res.Bio.		35	--		40	--
Second Stage	PHB	26-47	13	0.15	27-44	11	0.13
	PHA_{mcl}		-1	-0.01		1	0.01
	PHA_{tot}		12	0.15		12	0.14
	Res.Bio.		-11	--		1	--
Maximum	PHB	16-22	47	0.55	0-8	30	0.35
	PHA_{mcl}	16-22	40	0.27	8-19	10	0.07
	PHA_{tot}	16-22	87	0.82	0-8	34	0.36
	Res.Bio.	0-7	250	--	0-8	291	--
			Batch 1			Batch 2	

Batch 1 received a single charge of 3 g/L of dodecanoic acid administered at the beginning of the batch. Batch 2 received a total of 1 g/L dodecanoic acid administered over 30 shots of 0.033 mg/L. While the elevated dodecanoic acid concentration in Batch 1 resulted in a higher specific productivity of total PHA, the specific productivity of residual biomass was higher in Batch 2. This is consistent with the productivity data observed in shake flask cultures. See **Figure 4.7.a**. Although values for specific productivity of PHA are higher in Batch 1, the total amounts of PHA and residual biomass produced over the entire biosynthesis were greater in Batch 2. This is likely due to reduced toxicity of dodecanoic acid in Batch 2.

Conclusions

The main goal of this study was to characterize the monomeric specificity of a mutant polymer synthase gene of *Pseudomonas oleovorans* (*phaC1*$_{mut}$). The double mutant *phaC1*$_{mut}$ (S325T, Q481K) expressed in recombinant *E. coli* showed enhanced selectivity toward short-chain-length PHB as well as an increase in the overall polymer synthesis rate by > 1200%. By employing elementary mode analysis to predict favorable gene deletions, we constructed a mutant *E. coli* strain, TCS010, to maximize the production of 3HB-CoA monomers from glycerol. Using this strain the specific productivity of PHB by *phaC1*$_{mut}$ was estimated to be 0.61 (mmol PHB / g residual biomass / h) versus a specificity productivity of 0.22 in the wild-type MG1655 strain. Production of PHB by the parental *P. oleovorans phaC1*$_{P.o.}$ was not observed in either strain. By comparison, the *phbC*$_{R.e.}$ of *Ralstonia eutropha* showed a specific productivity of 1.85 (mmol PHB / g residual biomass / h) in both TCS010 and MG1655. This demonstrates the significant effect that metabolic flux can have on *in vivo* estimates of synthase activity, especially for synthases with lower synthase activity.

In order to characterize the specificity of the mutant synthase toward the monomers of PHA$_{mcl}$ we constructed *E. coli* JSBS01 with an interrupted β-oxidation cycle and added the activity of an *R*-specific enoyl-CoA hydratase from *phaJ*$_{P.o.}$. Using this strain we tested the effect of various ratios of glucose and dodecanoic acid on the final polymer composition. In the presence of 3 g/L dodecanoic acid, increases in the glucose concentration up to 20 g/L increased the specific PHB (g PHB / g residual biomass) by a factor of 8 and decreased the specific PHA$_{mcl}$ (g PHA$_{mcl}$ / g residual biomass) by a factor of 0.35. It is unclear if this result is due to competitive inhibition among monomers at the polymerase or if it is due to reduced catabolism of the dodecanoic acid in the presence high glycolytic flux . Conversely, when glucose was held constant at 20 g/L, the addition of up to 2 g/L of dodecanoic acid increased specific PHB by a factor of 8 and increased specific PHA$_{mcl}$ by a factor of 37. We attribute the increase in specific PHB to the additional acetyl-CoA and reducing equivalents generated from fatty acid catabolism.

When we compared the activity of all three polymer synthase enzymes in JSBS01/*phaJ*$_{P.o.}$ we were surprised to find that the wild-type *phaC1*$_{P.o.}$was indeed capable

of synthesizing PHB as high as 82 mol%. Moreover, the mutant *phaC1*$_{mut}$ produced only a modest increase in PHB compostion to 92 mol%. The most significant improvement by the *phaC1*$_{mut}$ was in total polymer accumulation which increased by ~1200% over the wild-type *phaC1*$_{P.o.}$ The fact the *phaC1*$_{P.o.}$ was unable to synthesize any PHB when expressed in TCS010, i.e. in the presence of 3HB-CoA monomers only, indicates that the presence of medium-chain-length monomers may be required to initiate polymer synthesis for the wild-type synthase. Thus, the point mutations in *phaC1*$_{mut}$ appear to have the largest impact on the overall productivity of the enzyme and a lesser effect on its selectivity for 3HB-CoA.

A more detailed time course evaluation in controlled bioreactors verified that the JSBS01 / *phaJ*$_{P.o.}$/ *phaC1*$_{mut}$ recombinant strain does indeed synthesize both PHB and PHA_{mcl} simultaneously. Moreover, the elimination of catabolite repression by deletion of *ptsG* in JSBS01 is sufficient to permit simultaneous glucose and dodecanoic acid consumption. When the glucose concentration was controlled at 10 g/L and dodecanoic acid in the media was 3 g/L, the ratio of the rate of PHB synthesis to that of PHA_{mcl} synthesis was 1.7. When the concentration of dodecanoic acid was maintained at 0.033 g/L a similar ratio of 1.4 was observed. Had these production rates remained constant in time, the resulting polymer would have contained between 37-41 mol% PHA_{mcl}.

In both batches the synthesis of PHB occurred throughout the entire course of the biosynthesis, while the synthesis of PHA_{mcl} was greatly reduced after ~24 h growth. The correlation of PHA_{mcl} cessation with the end of biomass production suggests the possibility that genetic regulation of fatty acid uptake is closely tied to biomass synthesis. Moreover, OUR data also indicated that the uptake of fatty acid uptake ended at this time.

Because of the early termination of PHA_{mcl} synthesis, the resulting polymers contained a mixture of two distinct type of polymer. Production of a more homogenous polymer for physical characterization will require that PHA_{mcl} synthesis be active during the entire course of the batch. If fatty acid consumption occurs only during biomass production, it may be possible to prolong the period of PHAmcl synthesis by the addition of a small, continuous feed of nitrogenous media until the end of the batch. Otherwise, it may be necessary to make explore genetic modifications which would enable the

constitutive expression of fatty acid uptake and degradation genes.. This could be done by alteration of certain genetic regulatory elements within the host strain or through plasmid expression of required genes.

Additionally, we demonstrated that CER and OUR values obtained from the biosynthesis off-gas can be used to provide a clear indication of the consumption of dodecanoic acid shots in concentrations as low as 0.033 g/L. Such real-time process monitoring is essential for controlling the sizes of block copolymer domains.

Given the success of strain TCS010 for producing high levels of PHB, our future plans include incorporating deletions of *fadR, fadB,* and *ptsG* in TCS010 to enable higher yield and higher PHB fraction in PHB-co-PHA_{mcl} copolymers.

Supporting Information

Elementary Mode Calculations

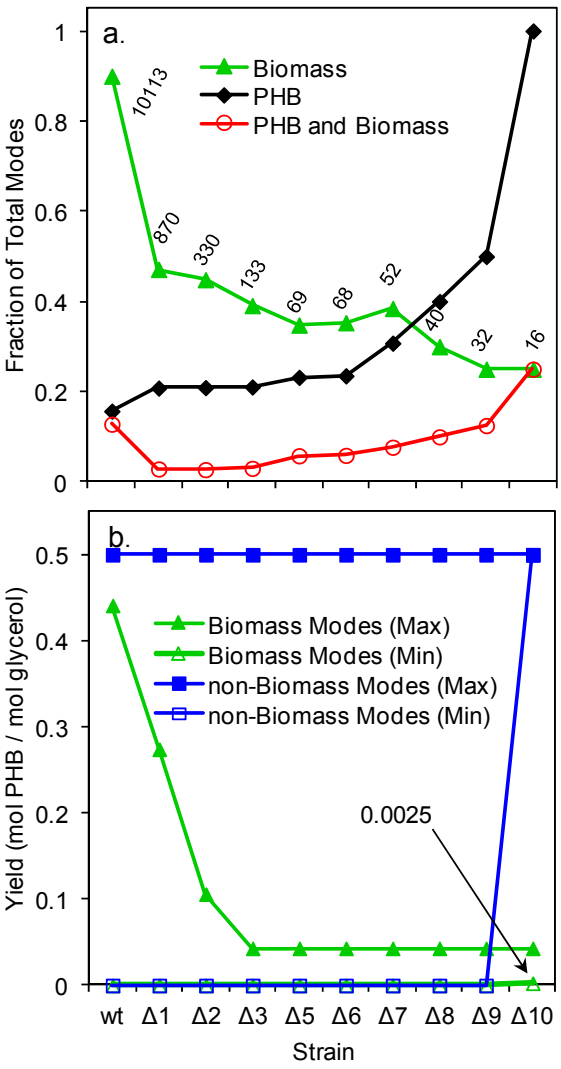

Figure 4.12 Elementary modes present in successive E. coli knockout mutants. **a.**) The fraction of total modes which produce PHB, Biomass, or both. The numbers given for each strain are the total number of modes calculated. **b.**) The maximum and minimum PHB yields (mol PHB / mol glycerol) of Biomass-producing and non-Biomass-producing modes. Genes were deleted in the following order: *zwf, ndh, mdh, (sfcA / maeB), ldhA, frdA, poxB, pta, mdh,* and *adhE*. *Δ1* contains the *zwf* deletion. *Δ2* contains the *zwf* and *ndh* deletions, *Δ3* contains *zwf, ndh,*and *mdh* etc. etc. *Δ10* contains all 10 deletions.

E. coli Metabolic Model

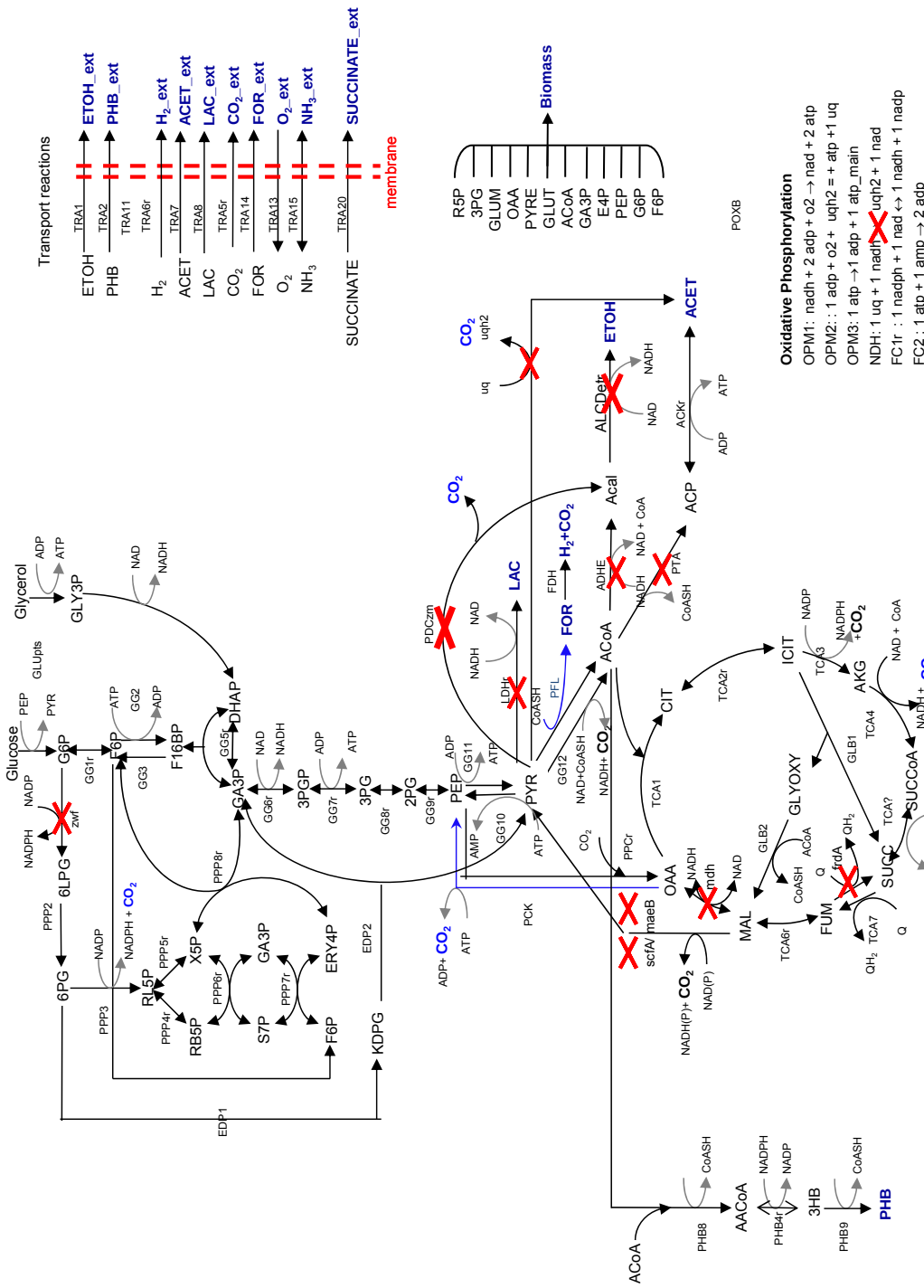

Figure 4.13 E. coli Metabolic Model used for Elementary Mode Analysis

Chapter 5. Polyhydroxyalkanoate Elastomers and their Graphene Nanocomposites

Information in this chapter has been reproduced in part with permission from the following sources:

Barrett, J. S. F., Abdala, A, and Srienc, F., "Poly(hydroxyalkanoate) Elastomers and their Graphene Nanocomposites", *Macromolecules*, 2014, 47, 3926-3941

and

Abdala, A, Barrett, J.S.F., and Srienc, F., "Synthesis of Poly-(R)-3-Hydroxyoctanoate (PHO) and Its Graphene Nanocomposites", ACS Symposium Series, 2013, 1144, 199-209

Overview

Medium-chain-length polyhydroxyalkanoates (PHA_{mcl}) are biopolymers with elastomeric qualities. While the modulus of these materials is ~ 3 orders of magnitude smaller compared to PHB homopolymer, their elongation at break is ~2 orders of magnitude greater. Thus, technologies which can be used to enhance the modulus of PHA_{mcl} polymers are of much practical utility. Herein we report on the preparation and characterization of composite materials using thermally reduced graphene (TRG) nanoparticles as filler with three, different PHA_{mcl} polymers. The matrices vary with respect to chain packing length, capacity for non-covalent bonding with the TRG surface, and the presence of covalent cross-linking. Results show that the addition of up to 2.5 vol.% TRG to PHA_{mcl} increases the melting temperature by 1-3° C, the modulus by 200-590%, and the electrical conductivity by > 7 orders of magnitude. Additionally, we use rheology and microscopy to characterize the composites. We discuss our results in light of polymer entanglement theory and the effects of polymer structure, filler loading volume, and the role of graphene-polymer interfacial forces. We extend our discussion by comparing the modulus enhancements of PHA_{mcl} composites to those reported in other studies in which layered carbon nanofillers are combined with structurally related bio-polyesters including: polylactide, polylactide-co-polyglycolide, polycaprolactone, and two other PHA copolymers.

Background

Polyhydroxybutyrate (PHB, C_4), the most common form of PHA, has a Young's modulus of 3.5-4 GPa, < 5% elongation at break, and a melting temperature of 175-180 °C[292]. Medium-chain-length polyhydroxyalkanoates (PHA_{mcl}, C_6-C_{14}), which are more elastomeric, have a Young's modulus of 0.003-0.07 GPa, up to 500% elongation at break, and a melting temperature of 45-60 °C[293-294]. Despite the useful characteristics of these basic forms of PHA, their continued proliferation into new applications requires the development of a more diverse range of physical and mechanical properties.

One commonly employed technique for enhancing the physical and mechanical properties of polymers is via the formation of composite materials by dispersion of fillers into the polymer matrix. Moreover, a growing trend has been in the use of nano-sized filler materials, i.e., nanocomposites. Because of their small size, nanofillers provide a large surface area for molecular contact with the polymer chains with only a minimal loading. A few composites with PHB have already been studied with nanofillers including: wood flour[295], clay[296], layered silicate[297], and carbon nanotubes[32, 298]. The addition of these nanofillers resulted in changes in the thermal, mechanical, and crystallization properties of PHB.

Among nanofiller materials, carbon allotropes, which include exfoliated graphite[299], carbon nanotubes[300], and graphene[301], have received additional attention because of their exceptional strength, low weight, and capacity for electrical conductivity. Graphene, the nanofiller used in this study, is an atomic-thick sheet of sp^2 –hybridized carbon atoms. With measured Young's modulus and ultimate strength of 1 TPa and 130 GPa, respectively, graphene is the stiffest and strongest material ever measured.[302]. The theoretical surface area of graphene[303] is estimated to be 2630 m^2/g. The addition of graphene to various polymers has been shown to enhance their resistance to thermal degradation, improve mechanical properties, increase electrical conductivity, and lower gas permeability[304]. Moreover, theoretical and experimental results indicate that the modulus enhancement with graphene addition is more pronounced with low-modulus, elastomeric polymers than with high-modulus, glassy polymers[304]. Therefore, the addition

of graphene has a significant potential for creating a range of useful functionalities in a class of polymers that is highly valued for its eco-friendly and biocompatible qualities.

Understanding the way by which a nanofiller affects the viscoelastic properties of dense polymer systems is based on the theory of polymer entanglements. These entanglements can form between neighboring polymer chains [146, 305-306] as well as between the polymer and the nanofiller[307-311]. Adding nanofiller to a polymer matrix alters its viscoelastic behavior due to the formation of additional entanglements between the particles and the polymer chains, thereby enhancing the stiffness of the polymer matrix. While attractive intermolecular forces between the matrix and filler do contribute to the viscoelastic behavior of nanocomposites, size, shape and aspect ratio of the nanofillers also have significant influence on reinforcing effects[309, 312-313], and the existence of molecular attraction between the matrix and filler is not required for reinforcement to occur[311, 314]. The prevalent theory of this phenomenon is that non-interacting nanoparticles block and confine the primitive paths of reptating chains, creating entanglements purely based on physical interactions[309-311].

When interfacial forces between graphene sheets and the polymer matrix are significantly attractive, additional entanglements can originate at the interface[308]. Transmission of stress between the matrix and the graphene surface can occur via π–π stacking, cation-π, or van der Waals interactions with available sp^2 networks[315]. Graphite oxide (GO), an alternate form of graphene, contains additional moieties such as epoxide, carbonyl, and hydroxyl groups on the surface that permit the formation of hydrogen bonds. GO can be reduced chemically or thermally to produce reduced graphene with much lower oxygen content than GO. In this study, we use thermally reduced graphene (TRG) which is synthesized by rapid heating of GO that leads to simultaneous reduction and exfoliation of the GO layers. The C:O ratio of TRG is 10:1 compared to 2:1 for GO[265] While hydrogen bonding can occur between TRG and the polymer matrix, it can also occur between multiple sheets of TRG, thereby leading to particle aggregation and poor dispersion. Modification of reduced graphene by incorporating other chemical moieties on its surface can also be used to promote interfacial attraction with a specific matrix[304].

Herein, we report on the preparation of composite materials by incorporating TRG into three, unique PHA_{mcl} copolymers: nominally, they are PHO (polhydroxyoctanoate, C_8), PHD (polhydroxydecanoate, C_{10}), and PHOe (polyhydroxyoctenoate, C_8). The copolymers vary in their composition of C_6, C_8, and C_{10} monomers. While all polymers contain a majority of C_8 monomers, PHD contains a significant fraction of C_{10} monomers and is predicted to have a greater packing length based on its cross-section which is wider than that of PHO. Thus, PHD should be less likely to participate in polymer entanglements. Moreover, the longer aliphatic appendages of PHD can shield non-covalent bonding with the polyester backbone. PHOe is very similar to PHO with the exception that PHOe contains a small fraction of C_8 monomers with an unsaturated carbon at the terminal position. Thus, PHOe is capable of forming a network structure via covalent cross-linking. We discuss the effectiveness of graphene reinforcement in each matrix in the theoretical context of polymer entanglements and the ability of each polymer to engage in non-covalent interactions with the oxygenated TRG surface. Finally, we compare our results to other studies in the literature that combine layered carbon nanofillers with similar biodegradable polyesters. **Figure 5.9** depicts the chemical structures of the different PHA_{mcl} matrices along with related polyoxoesters.

Results and Discussion

Properties of Purified PHA

Polyhydroxyalkanoate (PHA) polymers were produced in vivo using the microorganism *Pseudomonas oleovorans* with different hydrocarbons as substrates. The composition of different polymer samples can be controlled via the type of carbon substrate fed to the batch during biosynthesis e.g. the metabolism of octane produces the monomer 3-(*R*)-hydroxyoctanoyl-CoA, and decane produces 3-(*R*)-hydroxydecanoyl-CoA. However, due to the cyclical nature of the β-oxidation pathway, which degrades these molecules, the metabolism of a single substrate produces a random copolymer consisting of related monomers differing by -2n carbons, where n is number of β-oxidation cycles[292].

Figure 5.1 describes the metabolic pathway used by *P. oleovorans* for the production of PHAs. Inside the cell, alkane is converted to its corresponding fatty acid via a string of enzymatic reactions. The molecule is further activated via the attachment of a CoA moiety. From the fatty acyl-CoA intermediate the molecule is degraded via the β-oxidation cycle in which two carbons are removed to produce the corresponding n-2 fatty acyl-CoA and the central metabolite, acetyl-CoA.

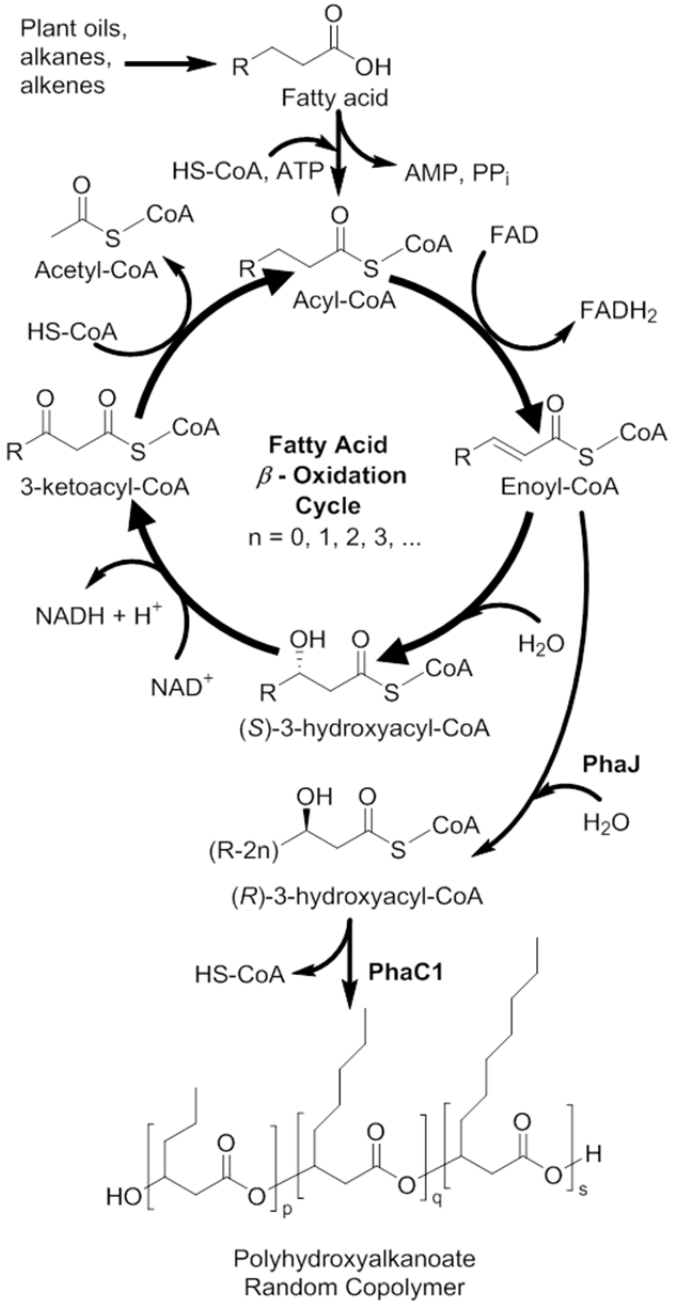

Figure 5.1 Metabolic pathway for PHA synthesis in *P. oleovorans*
The process of fatty-acid β-oxidation, coupled with the (*R*)-specific enoyl-CoA hydratase activity of the PhaJ enzyme, produces a range 3HA-CoA monomers that decrease in size by -2n carbons for every cycle completed.

Subsequent rounds of β-oxidation are required to completely degrade the fatty acyl molecule. While the process of β–oxidation does produce the (S)-3-hydoxyalkanoyl-CoA species, only the *R* enantiomer is recognized for polymerization by the PhaC1 synthase. In *P. oleovorans*, trans-2-enoyl-CoA is thought to be converted to the proper stereoisomer, (*R*)-3-hydoxyalkanoyl-CoA, via an *R*-specific, 3-enoyl-CoA hydratase, PhaJ. These monomers are then polymerized to PHA via the PhaC1 synthase enzyme. Due to the cyclical nature of β-oxidation a distribution of enoyl-CoA molecules of decreasing chain length is produced. This, combined with the broad substrate specificity of the PhaJ and PhaC1 enzymes, produces a random copolymer comprised of several monomer species.

Nominally, PHO (polyhydroxyoctanoate), PHOe (polyhydroxyoctenoate), and PHD (polyhydroxydecanoate) designate copolymer materials that contain full-length monomers as well as shorter monomers created by β–oxidation. PHO and PHD were synthesized from octane and decane, respectively. PHOe was synthesized from cyclical additions of octane and octene and so contains both saturated and unsaturated monomers along the polymer chain[316]. Given the cyclical nature in which octane and octene feeds were administered, we expect that the purified polymer may contain some block-copolymer molecules[21, 40] comprised of distinct domains enriched in polyhydroxyoctene. The presence of double bonds along the polymer backbone of PHOe permits the formation of chemical cross-links between chains. In a previous report, researchers produced similar polyhydroxyalkanoate polymers synthesized from octane and octene and subjected them to varying intensities of electron-beam radiation to promote cross-linking[316]. While PHOe used in this study was never subjected to concentrated radiation, its exposure to environmental, ultra-violet radiation over a 1-year period likely contributed to the formation of a small degree of cross-linking. **Table 5.1** provides the composition and molecular weight for the pure polymers.

Table 5.1 Chemical composition and molecular weight of purified polyhydroxyalkanoates.

	Molecular Weight[a]		Composition[b]					
	M_w	M_w/M_n	(% wt)					
	(10^3 g/mol)		3HB	3HH	$3HH_{6:1}$	3HO	$3HO_{8:1}$	3HD
PHO	71	3.1	0.4	7.0	---	91.4	---	1.2
PHO	54	2.3	---	4.2	< 0.1	89.5	6.1	< 0.1
PHD	57	2.6	0.4	6.4	---	61.5	---	31.7

[a] Weight average molecular weight (M_w), Number average molecular weight (M_n).
[b] 3HB (3-(*R*)-hydroxybutyrate), 3HH (3-(*R*)-hydroxyhexanoate), $3HH_{6:1}$ (3-(*R*)-hydroxyhexenoate), 3HO (3-(*R*)-hydroxyoctanoate), $3HO_{8:1}$ (3-(*R*)-hydroxyoctenoate), 3HD (3-(*R*)-hydroxydecanoate)

Properties of Thermally Reduced Graphene

The oxidation of graphite leads to the production of GO with C/O ratio of ~ 2/1. The rapid thermal heating of GO causes a simultaneous reduction and exfoliation of GO. As a result, the thermally reduced graphene (TRG) has a much higher C/O ratio and unlayered structure. The complete exfoliation of GO to TRG is confirmed by x-ray diffraction (XRD) analysis. **Figure 5.2.a** shows the XRD patterns for graphite, GO, and TRG. The diffraction pattern of graphite shows the strong 002 diffraction peak at $2\theta = 26.5°$ corresponding to d-spacing = 3.37 Å. Due to the presence of the polar oxygen-containing groups[315] on GO surface and the intercalation of adsorbed water, the 002 diffraction peak shifts to $2\theta = 11.4°$ indicating the expansion of the interlayer spacing to 7.8 Å. In contrast to graphite and GO diffraction patterns, which is characterized by the presence of ordered layered structure, the TRG diffraction pattern shows no noticeable diffraction peaks confirming the complete exfoliation of GO and the production of non-stacked, unlayered sheets.

The morphology of TRG was examined by transmission electron microscopy (TEM). As shown in **Figure 5.2.b,** the TEM image of TRG precipitated from its DMF suspension indicates that TRG is composed of thin and large wrinkled sheets. Translucent TRG sheets are clearly visible with edges appearing as dark fields.

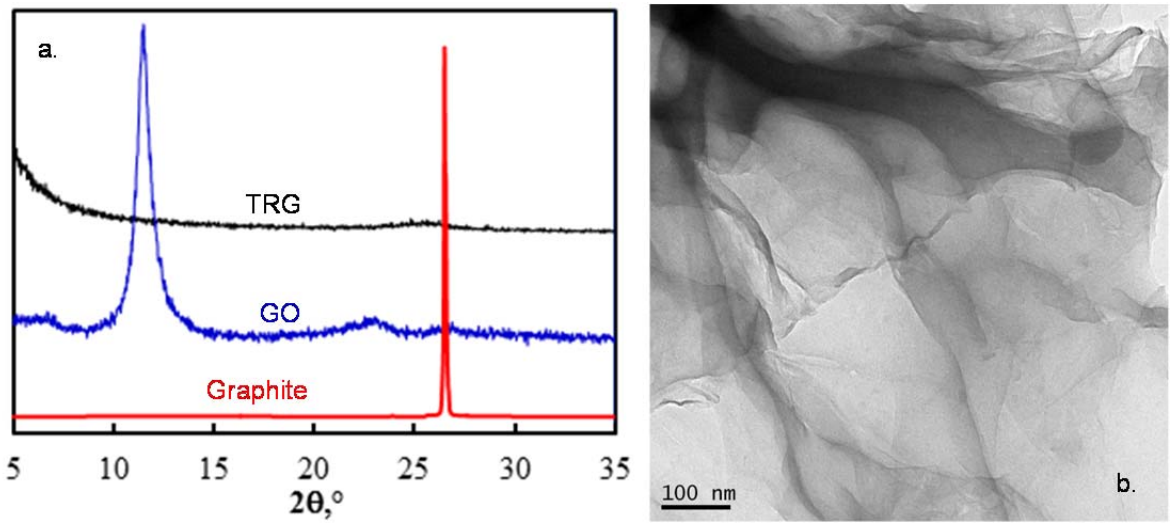

Figure 5.2 Characterization of the electronic reduction and exfoliation of TRG sheets.
a.) XRD diffraction patterns of graphite, GO, and TRG The XRD scale of the intensity (y) axis for graphite is 500 times the scale of the intensity (y) axis for GO and TRG. **b.**) TEM image showing the morphology of TRG.

Thermal Stability

The nonoxidative thermal degradation of pure PHA_{mcl} polymers and their graphene nanocomposites was measured between 50- 350 °C. Measurements were made under nitrogen flow using simultaneous thermal gravimetric analysis (TGA) and differential scanning calorimetry (DSC). **Figure 5.3** shows the effect of graphene loading on different thermal properties. $T_{50\%}$ is the temperature at which 50% of the composite mass remains (**Figure 5.3.a**). $E_{50\%}$ is the total endothermic heat-load incurred during heating from 270-$T_{50\%}$°C, and C_p is the specific heat capacity of the composite measured at 270 °C (**Figure 5.3.c**). For easy comparison with C_p values (J/g/°C) $E_{50\%}$ values (J/g) have been scaled by the corresponding increase in temperature between 270-$T_{50\%}$ °C and are presented in units of J/g/°C (**Figure 5.3.c**). Full thermograms are provided in the Supporting Information. In general, the addition of graphene increases the $T_{50\%}$ values of composites samples: at 2.5% loading $T_{50\%}$ increases by 4-6 °C. One exception to this trend is the PHD-0.5% composite, which shows a decrease in $T_{50\%}$ by -4.6 °C. While increases in $T_{50\%}$ indicate that the addition of graphene can improve the thermal stability of composites, $E_{50\%}$ values provide an alternative perspective. For PHD-1.0% and PHO-2.5% $E_{50\%}$ values increase by 23% and 60% respectively. This indicates improved thermal stability, because more heat is required for degradation to proceed. On the other hand, for PHOe-2.5% and PHD-2.5% $E_{50\%}$ values decrease by 16% and 30% respectively.

Some insight into this result can be gained by considering the specific heat capacity of the samples at 270 °C, just prior to the onset of thermal degradation. The C_p values show an obvious correlation with $E_{50\%}$ values. For PHO the addition of graphene causes a linear increase in the heat capacity of the composite samples. This could be due to an increase in the entanglement density of the composites thereby raising their capacity to store potential energy. Another storage mechanism for potential energy is the formation of hydrogen bonds between the ester groups of polymer chains and hydroxyl and carboxyl moieties on the TRG surface. As for why C_p of pure PHO is lower than that of pure PHOe and PHD, it is has been shown that C_p is inversely proportional to polymer molecular weight[317], and the M_w of PHO is ~25% greater than that of PHOe and PHD.

For PHOe the addition of graphene actually causes a small decrease in the heat capacity of the composites. We hypothesize that the intercalation of graphene particles within the gel network of PHOe may increase the internal strain of the matrix, thereby consuming some of its capacity to store potential energy. While the PHD-1% composite shows a large increase in heat capacity, the opposite is true for the PHD-2.5% composite. This suggests that under some conditions entanglements with graphene may form less easily for PHD than for PHO, and instead graphene may produce a solvating effect, which reduces the entanglement density of PHD.

The strong correlation between heat capacity and the total endothermic heat-flow indicates that changes to the entanglement density of the composite are a significant factor in controlling the thermal stability of the composites. However, the presence of graphene can provide protection against thermal decomposition by other mechanism as well. Given that graphene composites show a significant reduction in gas permeability[304] it is likely that their presence retards degradation by slowing the migration of volatile decomposition gases to the sample surface. Furthermore, it has been shown that the formation of a surface char layer on carbon nanocomposites can act as an additional barrier to gas evolution and may act as a protective heat shield, delaying the rise of sample temperature[318]. Ultimately, an increase in the heat capacity of the composite requires an increase in the average kinetic energy of the material, i.e. temperature, to disrupt the physical entanglements that prevent bond breakage necessary to initiate decomposition reactions. Additionally, temperature must increase for gas particles to overcome the graphene barriers that hinder their migration to the surface. For PHO and PHD the effect of graphene on $T_{50\%}$ appear to saturate by 1% loading, and $T_{50\%}$ values for all three matrices converge to within 0.7 °C by 2.5% loading. This suggests that beyond 1% loading, the kinetics of the decomposition process are governed primarily by the barrier properties of graphene despite the varied entanglement structure of the composites.

For PHD-0.5%, which is the only composite with a reduced $T_{50\%}$, we note that it is also the only composite with an increased $E_{50\%}$ while having a lowered C_p. Thus, the degradation reaction that initiates early in the decomposition of PHD-0.5% is distinctly more endothermic, suggesting that an alternate decomposition process may be at play.

Furthermore, we note that among all three polymer matrices the 0.5% composites show higher mass loss rates, d(mass)/dt (mass%/min) than the pure polymer matrices. Data are provided in the Supporting Information. Thus, it is a possibility that the oxygen-containing species on the TRG surface may cause an increase in the decomposition rate, especially if the filler loading is too sparse to hinder escaping gases. For PHOe-0.5%, which experiences an even greater drop in heat capacity but with a slight increase in $T_{50\%}$, it is possible that the restriction of polymer motion due to the gel network may provide an additional hindrance to gaseous diffusion, thereby raising the decomposition temperature.

Values for char formation are presented in **Figure 5.3.b**. Given that single layer graphene has been shown to be stable up to 2600 K[319], it is expected to be present as part of the residual char of the degraded composites. Thus, we have adjusted the final char values by subtracting the mass of graphene added to each composite. Note: 0.5, 1.0, and 2.5 %vol graphene ≈ 1.0, 2.5, and 5 %wt.. For pure PHO and PHD no residual char is observed; however, for pure PHOe ~13% char was observed. This difference is attributed to the presence of double bonds in the PHOe structure, which can act as a source of free-radicals for the initiation of cyclization reactions that lead to the formation of char instead of more volatile compounds[320]. For PHOe the addition of graphene results in an usual reduction in char formation. One possibility may be that oxygen-containing radicals liberated from TRG compete for the alkene groups of PHOe thereby reducing the rate of cyclization reactions. For PHO and PHD it is interesting that some composites produce char while others do not. Since char formation does not occur between polymer segments alone, it is most likely that additional carbon atoms are retained by bonding to the TRG surface. Presumably, such reactions are aided by the epoxide, alcohol, and carboxyl moieties on the TRG surface. At low graphene loadings polymer chains are the primary reactant at the graphene surface, but at higher loadings, especially in the case of poorly dispersed filler and weak polymer-filler attraction, oxygen-containing species on adjacent TRG sheets may compete with polymer chains for reaction, thereby reducing char formation.

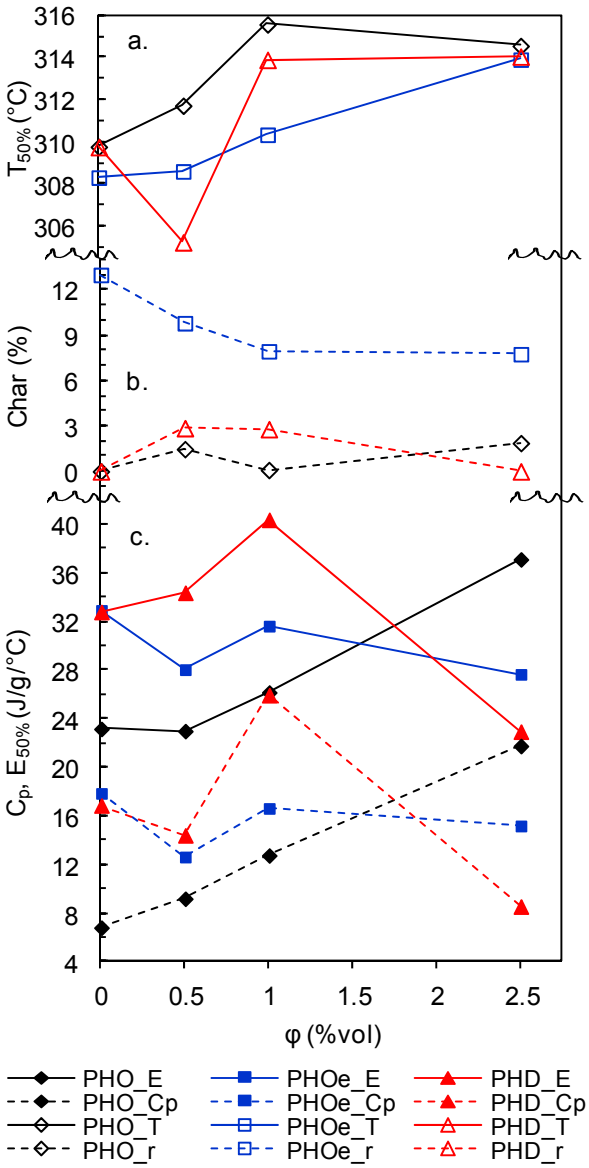

Figure 5.3 Thermal decomposition data for PHA-graphene composites. **a.** Temperature when 50% of the composite mass has been degraded ($T_{50\%}$) **b.** Residual char (Char, r) at 345°C minus wt. % of corresponding graphene loading, and **c.** Specific heat capacity at 270°C ($C_{p)}$ and total endotherm ($E_{50\%}$) when 50% of the composite mass has been degraded. $E_{50\%}$ values (J/g) are scaled by the corresponding temperature increase between 270-$T_{50\%}$ °C to give units equivalent to specific heat capacity (J/g/°C).

Thermodynamic Transitions

The physical transitions of pure and composite samples were measured using DSC. Values for the glass transition temperature (T_g), melting temperature (T_m), specific enthalpy of melting (ΔH_m), specific entropy of melting (ΔS_m), and relative crystallinity (x_c / x_p) are shown in **Table 5.2**. Among pure polymer samples, T_m of PHO is higher than that of both PHOe and PHD, which is consistent with previously reported results[293, 316]. We attribute this to the reduction in the crystal-forming ability of the PHOe and PHD polymers caused by disruption of the regularity of the PHO chain by $3HO_{8:1}$ (3-(*R*)-hydroxyoctenoate) and 3HD (3-(*R*)-hydroxydecanoate) monomers, similar to the finding of Noda et al[270]. Nonetheless, the higher T_m of PHO may also be attributed to its higher molecular weight[146]. The effect of graphene on the thermal transitions is demonstrated by a small increase in the T_m of PHO and PHD by ~ 0.5 - 3 °C depending on graphene loading. These results are consistent with a similar increase in T_m with graphene loading reported for other polyoxoester-graphene composites[321-322]. This increase in T_m along with the decrease in ΔH_m with graphene loading, implies that graphene addition leads to a significant reduction in entropy: recall $\Delta S_m = \Delta H_m / T_m$. This decrease in entropy is expected as a result of the hindrance of polymer chain rotation by graphene sheets and the confinement of chain movement within smaller spaces.

Contrary to PHO and PHD composites, PHOe composites showed a decrease in T_m by as much as 7.5 °C at only 0.5 vol.% graphene loading. This decrease in T_m is associated with a decrease in ΔH_m (maximum of 11%) and a smaller decrease in ΔS_m (maximum of 8%). To offer a possible explanation for this effect, we again consider the entropic and enthalpic contributions to T_m. We propose that the intercalation of graphene particles within the gel fraction of the polymer creates additional stain within the network, thereby raising the enthalpy of the solid phase. However, the corresponding increase in entropy is not as large, because the preexisting, covalent network prevents the polymer chains from fully mixing with the nanoparticles. Thus, the decreases in ΔH_m is greater than the decrease in ΔS_m, and T_m is lowered. While a solution of un-vulcanized polymer chains, i.e. PHO and PHD, can easily relax to accommodate the addition of nanoparticle

inclusions, a network of cross-linked polymer chains would be forced to expand to accommodate the nanofiller, similar to the phenomenon of solvent induced swelling in rubbers.

The T_g for pure PHD is significantly lower than that of PHO and PHOe, in agreement with an earlier report[293]. At 0.5 % graphene loading the PHO polymer displays a significant increase in T_g by 3.8 °C while PHD and PHOe show an insignificant decrease by less than 1 °C. As the second order T_g transition is known to be a kinetically controlled effect, this result suggests that the presence of graphene nanoparticles slow the motion of PHO chains by blocking reptation paths and creating entanglements. Further additions of graphene to PHO produce a minimal recovery of the T_g toward its pure polymer value. For the PHD polymer, the addition of graphene causes a sustained decrease in the glass transition temperature with a maximum change of -2.6 °C at 2.5% loading. This result suggests that in PHD, graphene particles provide a plasticization effect by increasing the free volume within the polymer matrix. We attribute this effect to a weaker interfacial attraction between the TRG surface and PHD than with PHO. Moreover, in studies utilizing molecular dynamics simulations, researchers observed that the presence of unattractive nanoparticles in a polymer solution resulted in accelerated molecular motion near the particle surface[314] and disentanglement of polymer chains with increasing nanoparticle loading[323]. Because of shielding of the polyester backbone by longer aliphatic appendages we expect the PHD polymer to have a lower molecular affinity for the TRG surface than the PHO polymer; thus, the movement of PHD chains should be less affected by TRG particles. For PHOe the change in T_g with graphene loading is less significant, ~1° C. This again supports our hypothesis that the presence of cross-linking in PHOe prevents the formation of additional entanglements with the graphene particles. Other experimental studies combining graphene based fillers with related polyoxoesters have reported both increases[321] and decreases[322] in T_g.

Table 5.2 Physical properties of PHA-graphene nanocomposites.

TRG Loading	Glass Transition Temperature			Melting Temperature			Enthalpy of Melting			Entropy of Melting			Relative Crystallinity		
ϕ (%vol)	T_g (°C)			T_m (°C)			ΔH_m (J/g)			ΔS_m (J/kg.K)			x_c / x_p		
	PHO	PHOe	PHD	PHO	PHOe	PHD	PHO	PHO	PHD	PHO	PHOe	PHD	PHO	PHOe	PHD
0	-41.9	-39.3	-48.1	53.7	50.7	45.2	15.5	20.9	22.5	47.4	64.5	70.8	1	1	1
0.5	-38.1	-39.8	-48.7	55.7	43.1	44.9	13.9	18.7	15.3	42.3	59.1	48.2	0.90	0.89	0.68
1.0	-38.6	-39.9	-48.8	55.5	46.8	48.1	9.0	20.6	11.1	27.4	64.4	34.5	0.58	0.99	0.49
2.5	-39	-38.6	-50.7	54.1	47.2	47.3	12.2	19.9	10.1	37.3	62.1	31.4	0.79	0.95	0.45
Max Change	+3.8°	+0.5°	-2.6°	+2.0°	-7.6°	+2.9°	-42%	-11%	-55%	-42%	-8%	-51%	-42%	-11%	-55%

Without reference data for the specific enthalpy of melting of pure PHA crystals (ΔH_m^0) the absolute crystallinity of a sample ($x = \Delta H_m / \Delta H_m^0$) cannot be determined from DSC endotherms. However, the specific enthalpy of melting (ΔH_m) data may still be used to infer changes in the relative crystallinity of the composite compared to the crystallinity of the pure polymer. If x_c is the fraction of crystals in the composite and x_p is the fraction of crystals in the pure polymer, then the relative crystallinity of a composite sample (x_c/x_p) may be estimated as $x_c/x_p = (\Delta H_m^c / \Delta H_m^0)/(\Delta H_m^p/\Delta H_m^0) = \Delta H_m^c/\Delta H_m^p$. Thus, the zaddition of graphene to PHO and PHD causes a decrease in the relative crystallinity of the composites to 0.79 and 0.45, respectively, at 2.5% graphene. For PHOe the reduction in crystallinity is minimal, 0.95. The significant increases in the amorphous fraction of PHO and PHD shows that the presence of graphene-polymer entanglements creates a significant hindrance to chain movement and crystal formation. For PHOe the minimal change in crystallinity compared to PHO suggests that the pure PHOe matrix is already more amorphous, thereby giving support to the hypothesis of a super-molecular network in PHOe. Moreover, the presence of covalently bonded polymer-polymer entanglements in PHOe likely precludes the formation of polymer-graphene entanglements.

Similar reductions in the enthalpy of melting and/or crystallization have been observed for various PHA composite systems including: PHB with exfoliated graphite nanoplatelets[324], PHB-co-PHV (13% PHV) with microwave expanded graphite[325], PHB

with organo-modified montmorillonite clay (organo-MMT)[326], and PHB-co-PHV (4% PHV) with organo-MMT[326].

Rheological Properties

In order to determine the elastic (G′) and viscous (G″) moduli of the composite materials in the melt phase, samples were investigated using oscillatory shear rheometry at 70° C. Frequency sweep profiles for the pure and composite samples are presented in **Figure 5.4** Data for the pure polymer samples indicates that PHOe has the highest G′ followed by PHO then PHD. The higher modulus of the PHO matrix compared to that of the PHD is attributed to a greater entanglement density of polymer chains in the PHO polymer due in part to its higher molecular weight. Moreover, the 3HD monomers in the PHD polymer increase the cross-sectional area of the polymer chain. The result of this is an increased packing length of the PHD chains, and so the propensity for PHD chains to form entanglements is reduced[146]. Thus, PHO chains with their smaller cross-section and longer length are expected to form more entanglements leading to a greater modulus than less entangled PHD chains with their wider cross-section and shorter length.

For PHOe, the presence of double bonds stemming from its aliphatic appendages permits the formation of chemical cross-links between adjacent chains, thereby leading to a greater elastic modulus than the PHO and PHD polymers. In a previous report, researchers produced similar polyhydroxyalkanoate polymers synthesized from octane and octene and subjected them to varying intensities of electron-beam radiation to promote cross-linking[316]. Samples presumed to have a higher degree of cross-linking showed increased modulus values. Thus, in the melt phase where crystallinity does not contribute to the modulus, the network connectivity provided by cross-linking in the PHOe polymer is responsible for the higher G′ for PHOe and the onset of a rubbery plateau at low frequencies, compared to PHO and PHD which have lower values of modulus and display behavior characteristic of the terminal regime.

According to a report by Kazatchkov et al.[327] values observed for the crossover frequency, (ω_c), where the storage modulus (G′) is equal to the viscous modulus (G″),

show an inverse power-law dependence upon M_w, specifically $\omega_c = (M_w)^{-3.7}$ for LLDPE. In our case, ω_c was found to be ~70 rad/s for PHO and ~40 rad/s for PHOe. Data for G″ not shown. Both matrices had a similar value for the crossover modulus of ~1.5 Pa. This difference in ω_c values suggests that the M_w of PHOe is greater than that of PHO. But GPC results show that the M_w of PHO is 71K Da while that of PHOe is 54K Da. We interpret this as another indication of cross-linking in the PHOe matrix, thereby increasing the apparent M_w of linked polymer chains.

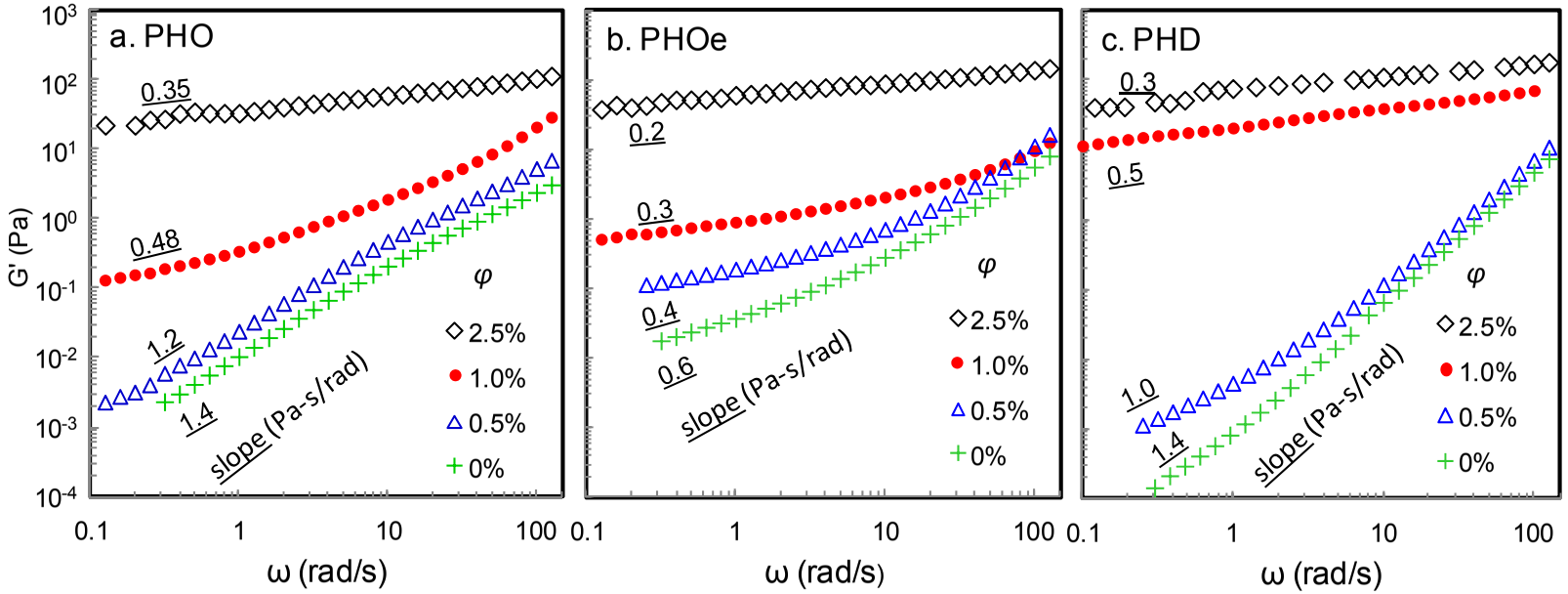

Figure 5.4 Frequency sweep profiles of PHA-graphene nanocomposites.
a.) PHO, **b.)** PHOe, **c.)** PHD, ϕ (graphene loading, %vol), G' (elastic storage modulus, Pa), ω (frequency of oscillation, rad/s) The number beside each curve is the calculated slope, Pa-s/rad, at low frequency.

In **Figure 5.4.a** data for the PHO-graphene composites is presented. As graphene loading increases, G′ increases and the slope of the G′ versus ω curve begins to decrease in the low frequency region. For purely elastic materials, G′ is invariant with respect to changes in the frequency of the applied strain, i.e. the slope of G' versus ω goes to zero . Thus, the reduction in slope of G′ versus ω at high graphene loadings indicates the emergence of elastic behavior due to the presence of a solid-like network structure within the composite. Similar results are obtained for PHOe and PHD, **Figures 4.4.b,c**. While there is a significant difference in G′ of the pure polymers, all three polymers begin to show a definite elastic response by 1% loading, and the differences in G′ are almost indistinguishable by 2.5% loading. This suggests that a network of particle-particle interactions dominates the rheology at high loadings while polymer-particle entanglements confer elasticity at lower loadings.

Values for storage modulus may also be used to predict the critical filler loading (φ_c) at which percolation of a pseudo-solid network first occurs. Using a hybrid, power-law model[328-329] of the form $G' = G'_g ((\varphi - \varphi_c)/(1 - \varphi_c))^{\nu}$, where G'_g is measured shear modulus of few-sheet graphene[330], we calculated the graphene loadings at which network percolation first occurs. See **Table 5.3**. Details of the calculations are presented in the Supporting Information. The negative signs for PHO and PHOe percolation limits arise from error on estimates of φ_c very near zero. Moreover, despite the negative signs, the numeric ordering of the values remains meaningful for predicting the relative sensitivity of each matrix to graphene inclusions. Practically, values for the percolation threshold $\leq$ 0 imply that increases in modulus are realized immediately, upon the smallest addition of filler. This makes sense given that virgin polymer matrices already form a network of entangled polymer chains, whereby stress created by the inclusion of one graphene particle may be transmitted to an adjacent particle, even if the two particles are not in direct contact. Because PHOe already contains a sample-spanning network of covalent cross-links, it is the most sensitive to graphene inclusions and has a φ_c lower than PHO. Alternatively, PHD, which is less likely to participate in molecular entanglements due to its greater packing length and reduced chain length, has a φ_c higher than PHO.

Table 5.3 Model Parameters for Power-law fit to Storage Modulus (G′) and Electrical Conductivity (σ) Data

		PHO	PHOe	PHD
G′	φ_c (vol.%)	-0.1	-0.8	0.33
	ν	6.0	6.3	5.0
	[a] r^2	0.999	0.999	0.979
σ	φ_c (vol.%)	0.48	0.40	0.44
	ν	4.3	5.0	5.0
	[a] r^2	0.999	0.991	0.995

[a] r^2 values from linear regression analysis.

Mechanical Properties

One of the most important benefits of graphene addition is its ability to enhance the mechanical properties of polymer matrices. At low graphene loadings below the percolation threshold, this enhancement is caused by the ability of the graphene particles to promote a greater level of polymer entanglement. At higher graphene loadings beyond the percolation threshold, a continuous graphene network begins to emerge which is capable of direct reinforcement of the polymer matrix. Both effects increase as the attractive molecular forces between the graphene particles and the polymer chains become stronger. **Figure 5.5.** shows stress-strain curves for the different composites, while tabular values for Young's modulus (E), ultimate strength (σ), and elongation at break (ε) are presented in **Table 5.4**.

The stress-strain profile of pure PHO, PHOe, and PHD is typical of elastomeric polymers and is characterized by three distinct regions: an initial high-modulus region (ε < ~10%), plastic deformation region (~10% < ε < ~50%), and a strain hardening region (~50% < ε < ~200-300%) before fracture at (ε > ~300-450%.) The increased strain at break observed for the pure PHO polymer, 450%, versus 325% for PHOe, and 275% PHD is likely due to the higher molecular weight of the PHO polymer, i.e. polymer chains must reptate further to break their initial entanglements.

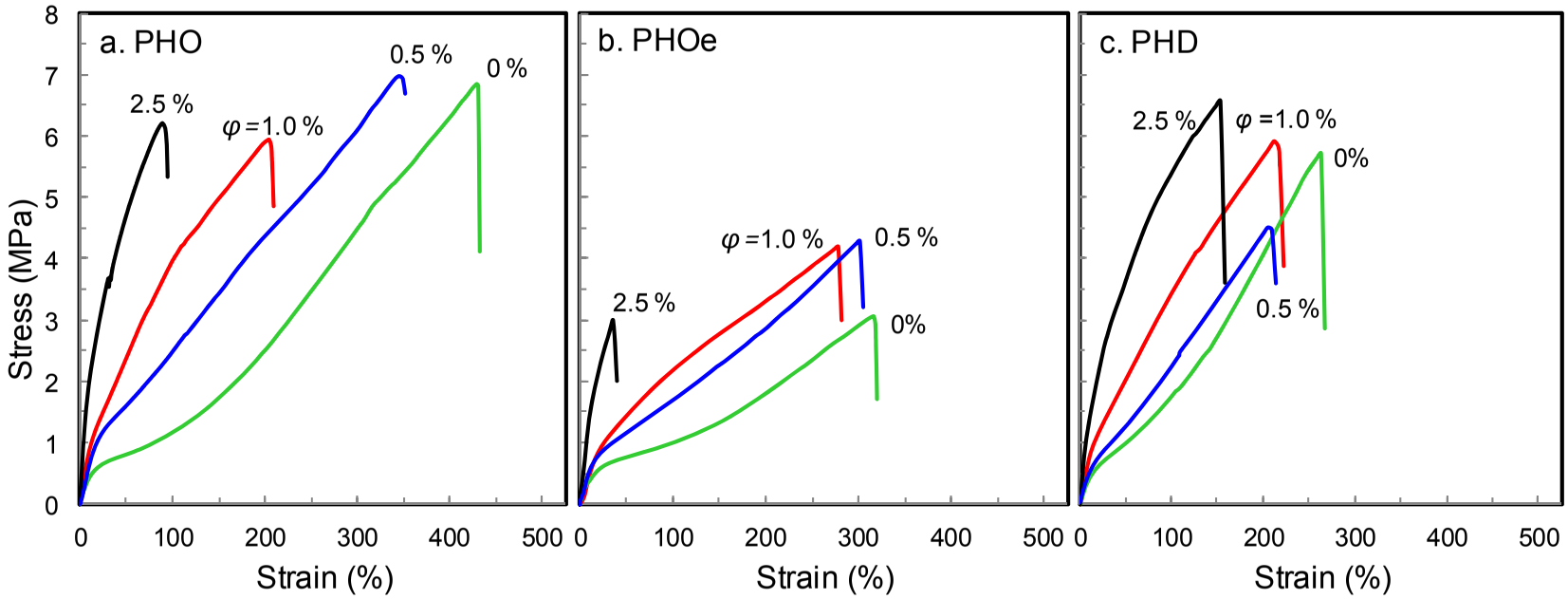

Figure 5.5 Stress-Strain curves for PHA-graphene nanocomposites.
a.) PHO, **b.)** PHOe, **c.)** PHD ϕ (graphene loading, vol.%)

Table 5.4. Mechanical properties of PHA-graphene nanocomposites.

TRG Loading	Young's Modulus E (MPa)			Ultimate Strength σ (MPa)			Elongation at Break ε (%)		
ϕ (% vol)	PHO	PHOe	PHD	PHO	PHOe	PHD	PHO	PHOe	PHD
0	4.5	6.3	5.3	6.4	4.2	5.7	425	316	263
0.5	7.2	6.9	5.7	7	4.3	4.5	346	302	209
1.0	10.9	8.5	11.8	5.6	3.9	5.9	204	293	212
2.5	31	18.8	20.1	6.7	3	6.6	105	34	155
Max. Chang	590%	200%	280%	9%	2%	16%	-75%	-89%	-41%

For composite samples, the addition of graphene leads to a significant increase in the Young's modulus. Normalization of modulus values as E_c / E_m, where E_c is the modulus of the composite and E_m is the modulus of the pure matrix, allows equal comparison among the different matrices. **Figure 5.10.a.** shows a plot of the normalized moduli for increasing graphene loadings. Modulus enhancement is greatest for PHO, 1.6 - 6.8, lower for PHD, 1.1 - 3.8, and lowest for PHOe 1.1 - 3.0. We discuss the disparity among the different matrices in a later section. On the other hand, changes in ultimate strength are less significant, and have minimal correlation with graphene loading. In contrast to modulus values, which increase with graphene loading, values for the elongation at break decrease by a maximum of 41-89% at the 2.5% loading. At this maximum loading, the PHD polymer permits the greatest strain before break, 155%, versus 105% for PHO and 34% for PHOe. We speculate that this may be due to the reduced packing length of the PHD polymer, which allows it to disentangle more easily before reaching its ultimate strength. Regardless of the decrease in elastic range, all composite samples experience a reasonable elongation before break such that they do not become brittle.

Interestingly, we note that as strain increases beyond the plastic deformation region, all composite samples extend with a modulus similar to that of their corresponding pure polymer. This implies that reptating chains eventually escape from their graphene-associated confinements by either disengaging their initial graphene

entanglements or by a strain-induced alignment of graphene sheets whereby sliding chains are less likely to encounter new graphene obstacles.

While graphene greatly enhances the modulus of the PHA polymers by 200 - 590% at 2.5% loading, the effect is even more significant if the decrease in crystallinity is considered. Given that the modulus of a polymer crystal is typically several orders of magnitude greater than the modulus of the amorphous material, the presence of small crystals can impart a significant enhancement in modulus similar to the effect of nanoparticle fillers[331-332]. At 2.5% loading, the relative crystallinity of PHO, PHOe, and PHD composites compared to the pure polymers is reduced to 0.79, 0.95, and 0.45, respectively; thus, by this effect we would expect the composites to have a lower modulus than the pure polymers.

By accounting for the effects of reduced crystallinity, we can make an alternate estimate of the modulus enhancement factor as $(E_c / E_m) / (x_c / x_p)$. Here we have made a conservative assumption of a 1:1 correlation between crystallinity and modulus; however, experimental studies in polyethylene suggest that the effect is likely greater[331]. **Figure 5.10.a** contains a plot of the normalized moduli versus graphene loading, with and without the correction for crystallinity. While there is a significant difference between PHO and PHD for the uncorrected modulus enhancement, the results are almost identical when crystallinity is considered. This alternative estimate suggests that the dispersion and molecular interactions of PHO and PHD with TRG are more similar than originally thought. For PHOe the effect of crystallinity on modulus enhancement is negligible.

Electrical Conductivity

Another important advantage of polymer-graphene composites is their potential for electrical conductivity. This conduction is possible via the overlap of sp^2 orbitals above the plane of the graphene monolayer. **Figure 5.6** shows the bulk resistivity (ρ) of PHA-graphene composites for various graphene loadings. Just before a graphene loading of 0.5%, the formation of a few, continuous, graphene pathways begins to produce a small drop in the resistivity of the composite. By $\varphi = 2.5\%$, the bulk resistivity in all three PHA matrices is decreased by >7 orders of magnitude.

To make a more accurate estimate of the electrical conductivity percolation threshold (φ_c), we employee a power-law model[329] of the form $\sigma = \sigma_g ((\varphi-\varphi_c)/(1- \varphi_c))^{\nu}$, where σ_g is the conductivity of few-layer graphene, and ν is the "universal constant" for which classical models specify a theoretical value of 2 for geometric percolation. Using this model, we calculated the graphene loading at which percolation of an electrically conducting network first occurs. See **Table 5.3**. The φ_c values for electrical conductivity are distinctly greater than those predicted for rheological percolation and are much more similar among the different polymer matrices. Details of the calculations are presented in the Supporting Information. In rheological and mechanical testing of nanocomposites, improvements in modulus may actually arise before formation of a continuous filler phase due to the aid of polymer entanglements that link distant particles[333]. For this reason, measurements of electrical conductivity are better indicators of geometric network percolation. However, the φ_c values predicted from conductivity data may still be below the threshold for true geometric percolation, as the corresponding estimates of ν are all greater than the classical value of 2. Such high ν values have been attributed to quantum tunneling effects, which can permit conductivity between proximal, but non-touching particles[329]. By analogy, the similarly high values of ν obtained from the rheology percolation models support the hypothesis that polymer entanglements between particles confer network structure well before geometric percolation. Moreover, the wide range of φ_c values for rheological percolation, -0.8-0.33 %vol, indicates significant variation in the molecular interactions of the TRG particles with the different PHA matrices.

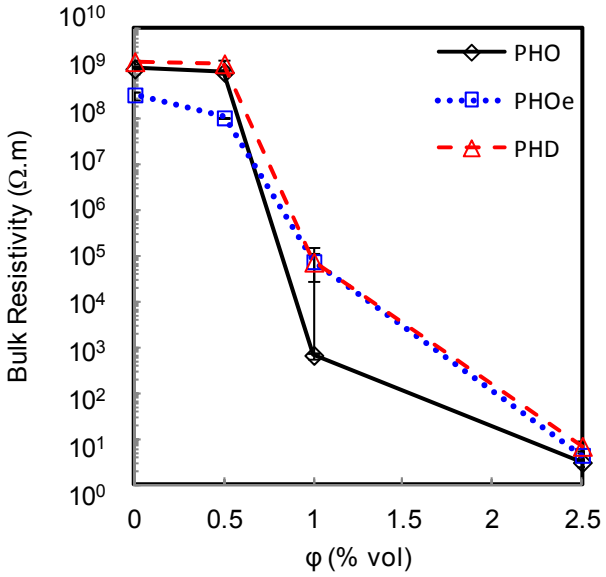

Figure 5.6 Bulk resistivity of PHA-graphene nanocomposites.
φ (graphene loading, % vol)

Estimation of A_f and Particle Dispersion from Electrical Conductivity

Nanocomposite structure may be described with respect to properties of the nanoparticles, e.g. size, aspect ratio, and dispersion, as well as properties of the polymer entanglements within the matrix, e.g. size and density of entanglements. Direct methods of evaluation include spectroscopy and microscopy while indirect methods use rheological, mechanical, or electrical conductivity measurements to infer structure.

According to percolation theory for electrically conducting networks, fillers with elongated or expanded geometry such as fibers or sheets possess a lower φ_c, because they can more readily form a continuous network in a polymer matrix[334-335]. Moreover, percolation arises most quickly when the particles are distributed in completely random orientations. Thus, φ_c for a composite system conveys information about the aspect ratio of the particles as well as their orientation. For a nanoparticle, the aspect ratio (A_f) is defined as the average diameter of the particle (d) divided by its thickness (t). Crumpling or breaking of graphene particles during exfoliation causes a direct reduction in A_f while particle aggregation, poor dispersion, and strain induced particle alignment during secondary processing can indirectly cause a reduction in the effective A_f.

Assuming a completely random orientation of the nanoparticles, several mathematical models have been proposed to relate φ_c to A_f. A semi-empirical estimation by Ren *et al.*[334] predicts the percolation loading as $\phi_c = \frac{3\ \phi_c^s}{2\ A_f}$, where ϕ_c^s is the percolation volume fraction of spherical particles ($\phi_c^s = 0.3$). A more rigorous model by Celzard *et al.*[335] predicts percolation loading to be bounded between $\phi_c = 1 - \exp\left(-\frac{3.6}{\pi A_f}\right)$ and $\phi_c = 1 - \exp\left(-\frac{5.6}{\pi A_f}\right)$ for an infinitesimally thin spheroid and a perfect sphere, respectively. On the other hand, a model used by Lu and Mai[336] predicts $\phi_c = \frac{2.154}{A_f}$. Using the values for φ_c obtained from conductivity data, values of A_f calculated from the different models are provided in **Table 5.5**. The average aspect ratios of all three models is $A_f^{PHO} = 288$, $A_f^{PHOe} = 345$ $A_f^{PHD} = 314$. The similarity in these values indicates that at low graphene loadings there is little difference in the geometry or dispersion of graphene in the three different matrices.

Table 5.5 Prediction of particle aspect ratio (A_f) from the percolation threshold (ϕ_c).

	ϕ_c	^aA_f			
	(%vol)	Ren	Celzard[b]	Lu	**Avg.**
PHO	0.48	94	238-370	449	**288**
PHOe	0.40	113	286-445	539	**345**
PHD	0.44	102	260-404	490	**314**

[a] Refer to the text for an explanation of the different models.
[b] Lower and upper bounds correspond to the oblate and spherical limits.

Transmission Electron Microscopy

TEM images can be used to visually assess nanofiller dispersion within the matrix. **Figure 5.7** shows TEM images of the each matrix for a filler loading of 0.5%. The best dispersion of graphene is seen in the PHO sample as is indicated by the existence of transparent, likely single layer, graphene sheets. The poorest dispersion is seen in the PHOe sample where the appearance of darkly contrasted and parallel edges is indicative of multilayer graphene aggregates. Similar dark edges are seen in the PHD sample, but the more diffuse coloration suggests better separation and more randomly oriented graphene layers than in the PHOe sample. As presented in the previous discussion on electrical conductivity, percolation of a continuous graphene phase was estimated to occur at between 0.4-0.5% for all three matrices.

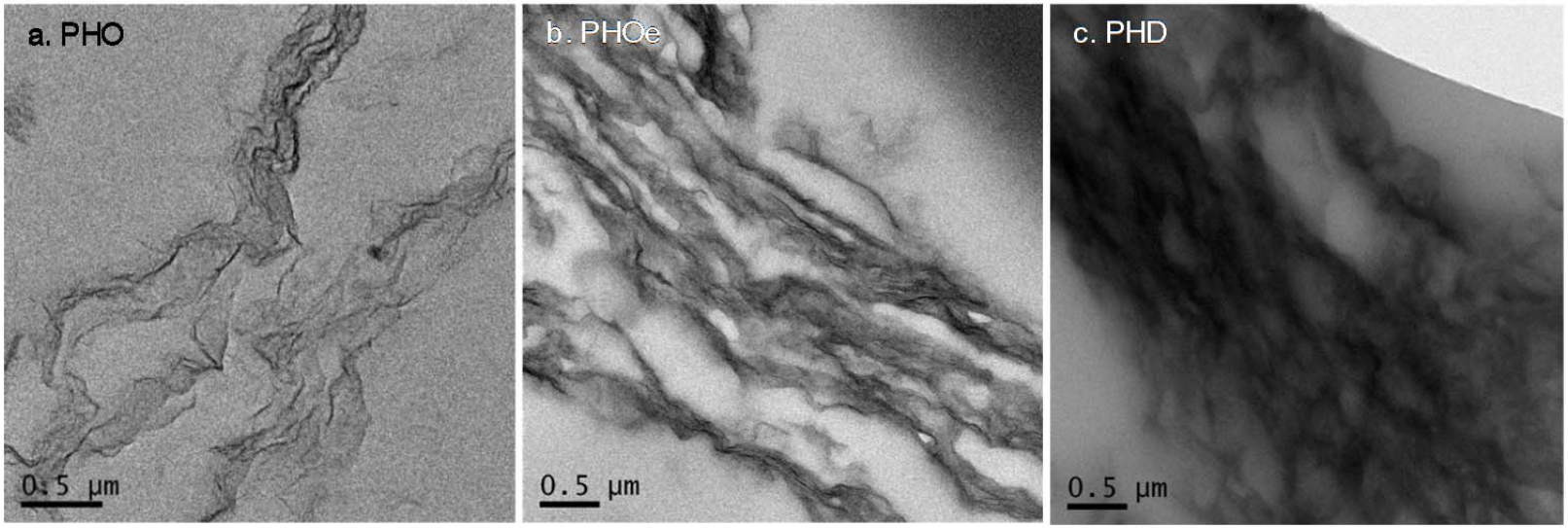

Figure 5.7 TEM micrographs of PHA-graphene nanocomposites.
a.) PHO, **b.)** PHOe, **c.** PHD, For all samples the graphene loading is 0.5 vol.%.

Scanning Electron Microscopy

Additionally, SEM images of fracture topology can be used to infer information about the entanglement structure of nanocomposites. See **Figure 5.8.** Images were taken from the fractured surfaces produced by DMA extension tests presented in **Figure 5.5**. When comparing among pure polymer samples only, i.e. 0% graphene loading, both the PHO and PHD samples show smooth surfaces while the PHOe sample is more textured. This surface roughness suggests inhomogeneity within the PHOe matrix, likely due the presence of cross-linking within the matrix.

With respect to graphene content, samples with increased filler loading tend to show greater surface roughness. We speculate that deeper cavities on the fracture surface, e.g. **Figure 5.8.a** PHO-0.5%, are caused by pull-out of more rigid, graphene-polymer entanglements from the softer, bulk matrix. This result indicates that even at a minimal filler loading of 0.5%, PHO molecules are capable of forming large entanglement masses with the graphene particles. We note that the characteristic size of features on the fracture surface are several μm in scale, yet the graphene particles used for reinforcement are on the order of tenths of μm in scale. Thus, the polymer entanglements that are induced by the presence of the graphene inclusions persist well beyond the characteristic size of the nanoparticles. The greatest variety of surface topology is seen for the PHO composites, which shows a strong correlation with the significant changes observed in the elongation at break values. See **Figure 5.5.a.** Interestingly, we find that the PHO-0.5% composite exhibits a greater surface roughness than the PHO-2.5% composite. Thus, it may be that as the number of graphene particles increases, the large entanglement masses that surround individual particles merge and create a more uniform entanglement density. For PHD composites shown in **Figure 5.8.c,** only a minimal increase in surface roughness is seen with graphene loading. This is consistent with the observation that the PHD composites all showed similar strain and modulus values just prior to fracture. See **Figure 5.5.c**. We interpret this to mean that at the point of fracture the presence of graphene nanoparticles had minimal influence on the entanglement structure of the polymer. It may be that a strain induced alignment of the particles and/or disentanglement of polymer chains from the graphene particles resulted

in greater homogeneity in the polymer cross section. Likewise, PHOe samples presented in **Figure 5.8.b** show little change in their fracture topology until the 2.5% graphene loading when the pull-out morphology appears. This again reflects the stress-strain trends seen in **Figure 5.5.b**. Thus, we infer that only at the 2.5% graphene loading do significant polymer-graphene entanglements form within the PHOe matrix. It is possible that the preexisting cross-links in the PHOe matrix prevented the formation of polymer entanglements with graphene particles until enough particles were present to significantly disrupt the cross-linked network. Ultimately, these images demonstrate that free PHO molecules engage in polymer entanglements more readily than PHD molecules or cross-linked PHOe molecules.

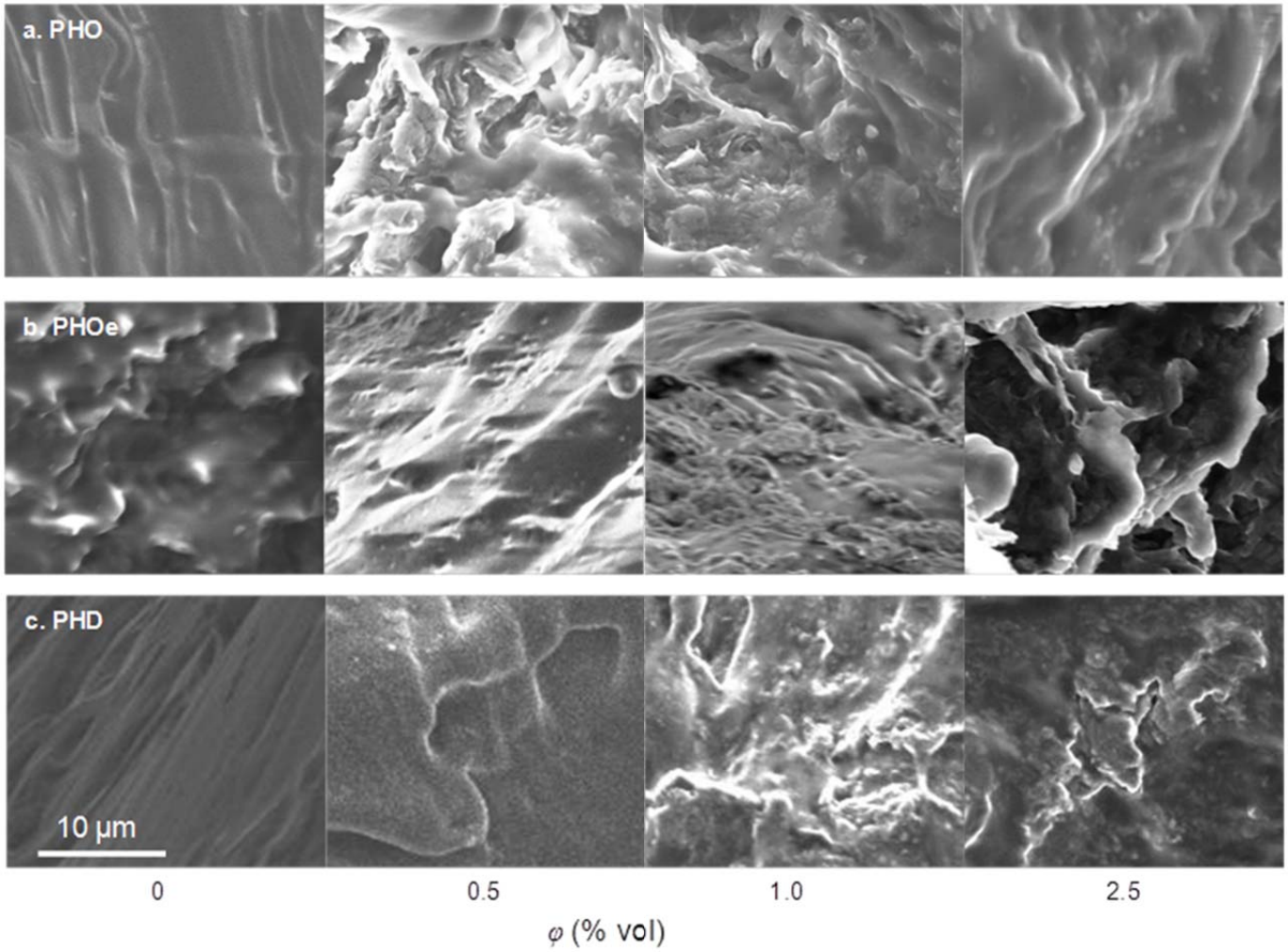

Figure 5.8 SEM micrograph of PHA-graphene nanocomposites.
Panels: **a.)** PHO, **b.)** PHOe, **c.)** PHD. Images are of fractured surfaces produced after DMA extensional testing.

Estimation of A_f and Particle Dispersion from Modulus Enhancement

According to micromechanical theory the enhancement of mechanical properties in composite materials[313, 337-338] is strongly impacted by both A_f as well as particle orientation[30, 62-63]. Particles with large aspect ratios, such as graphene sheets and carbon nanotubes, produce a greater increase in modulus than spherical ones. When a collection of randomly dispersed graphene particles are all oriented in the same direction, modulus enhancement is maximum and points in the direction normal to the graphene surface. Alternatively, when the orientation of particles is completely random, modulus enhancement is reduced, but the property becomes isotropic. Unlike the percolation of electrical conductivity, increases in modulus can occur even when reinforcing particles do not form a continuous network. An alternate technique to estimate the A_f and orientation of nanoparticles within a polymer matrix is by using the micromechanical equations of Tandon and Weng[313]. These equations based on earlier work by Mori and Tanaka[338] describe the enhancement in modulus of a polymer matrix due to the addition of small filler particles in the form of either oblate or prolate spheroids with varying degrees of A_f. The equations are used in conjunction with experimental data for E_c / E_m versus φ, where E_c is the composite modulus, E_m is the pure polymer modulus, and φ is the volume fraction of filler within the composite. Values for the filler modulus (E_f), and Poisson ratio of the matrix and the filler (ν_m , ν_f) are also required for the calculations. Details of the equations are presented in the Supporting Information. **Figure 5.10.a** is a plot of E_c / E_m versus φ for the composites in this study. Calculations with the Tandon-Weng equations predict: A_f^{PHO} = 309, A_f^{PHOe} = 97, A_f^{PHD} = 151. The value of A_f^{PHO} predicted by this method is similar to the ones predicted by percolation theory, while the values for A_f^{PHOe} and A_f^{PHD} are significantly smaller. However, when the modulus enhancement values are corrected for crystallinity, the resulting A_f values are, A_f^{PHO} = 435, A_f^{PHOe} = 106, A_f^{PHD} = 425. This suggests that the behavior of the PHO and PHD matrices are actually, very similar. For PHOe, the lower value of A_f predicted by modulus enhancement compared to percolation theory, suggests that the presence of covalent cross-links somehow prevents stress transmission to the graphene particle.

While the explanation of crystallinity seems to account of the difference in modulus between PHO and PHD, we note that the pull-out morphology seen in SEM images of PHO and PHOe fracture surfaces is not seen in PHD. Also, PHO and PHOe experience a 75% and 89% reduction in ε at 2.5% graphene loading, while for PHD the reduction in ε is only 41%. This suggests that under high stresses, PHD relinquishes its graphene entanglements more easily, possibly due a reduced interfacial attraction.

Effect of Particle-Polymer Interfacial Forces on Modulus Enhancement

Another important point when considering filler effects is the nature of the interfacial forces between the polymer and particle. In simulations it has been shown that attractive forces at the particle surface can result in a greater entanglement density surrounding the particle surface[308], thereby leading to increases in modulus. In choosing to compare the composites according to A_f values, we note that the Tandon and Weng equations, which assume perfect lamination between matrix and filler and a no-slip condition at the interface, do not account for variations in interfacial attraction and the phenomenon of entanglements. Alternatively, Lu et al. have developed a similar set of micro-mechanical equations that do account for the effects of entanglements caused by interfacial forces[339]. In their results, increasing the volume or modulus of the entanglement "interphase" surrounding each nanoparticle resulted in a linear increase in composite modulus similar to the linear trend seen with particle size. Thus, we assert that A_f values calculated from the basic Tandon and Weng equations are also an indicator of strong interfacial forces as well as particle geometry and the quality of dispersion.

Given the presence of epoxide, hydroxyl, and carbonyl groups on the TRG surface and ester linkages along the polyhydroxyalkanoate chain, the possibility does exist for the formation of polarity-based van der Waals attractions as well as hydrogen bonding. However, in PHA_{mcl} polymers the presence of long aliphatic extension from the polyester backbone would likely reduce the intensity of such interactions due to steric-hindrance of oxygen atoms along the polymer backbone. According to this hypothesis, we would expect that the PHO polymer with its shorter aliphatic appendages would be more available for bonding interactions with TRG particles than the PHD polymer. Thus,

PHO would exhibit a greater increase in the normalized modulus than PHD. In a related study of TRG composites, Kim *et al.*[340] demonstrated that functionalization of polyethylene with different polar moieties capable of hydrogen bonding resulted in greater enhancements of the Young's modulus compared to TRG composites of unmodified polyethylene. Furthermore, samples prepared by solvent blending had greater modulus enhancement than those prepared by melt blending, presumably due to better dispersion of the filler.

Modulus Enhancement in other Biodegradable, Polyester Nanocomposites

To further explore the relationships among polymer structure, particle size, and surface chemistry, we compared our results to other studies combining layered carbon fillers with biodegradable polyesters. All the studies we considered used some form of graphite-derived filler; however, variations in synthesis technique and exfoliation procedure resulted in different particle sizes, aspect ratio, and oxygen content of the nanoparticles. The systems considered include: poly(3-(*R*)-hydroxybutyrate)-co-poly(3-(*R*)-hydroxyhexanoate) (PHBH, 13% 3HH) with expanded graphite (EG)[322], poly(3-(*R*)-hydroxybutyrate)-co-poly(3-(*R*)-hydroxyvalerate) (PHBV, 13% 3HV) with microwave expanded graphite (MEG)[325], polylactide (PLA) with graphene nanoplatelets (GNP)[321], graphite oxide (GO)[321], or thermally reduced graphene (TRG)[341], poly(ε-caprolactone) with TRG[342] or GO[343], and polyglycolide-co-polylactide (PGLA, 50% lactide) with GO[344-345]. **Figure 5.9** shows the chemical structure of each polymer, and **Table 5.6** provides the details for each nanocomposite study. For a review of preparation and exfoliation techniques for graphene and graphite oxide see Kim *et al.*[304] and Dreyer *et al.*[315]. **Figure 5.10.b** provides a plot of E_c / E_m versus φ for the other nanocomposites in the literature, which was used to calculate A_f for each. In calculating the slopes of the E_c / E_m versus φ lines, we used only the first three loading fractions from each data set, including 0%, where dispersion is expected to be the best and the slope is a maximum. All the considered polymers have a similar polyoxoester backbone; however, they differ in the linear density of ester bonds and the size of aliphatic appendages stemming from the backbone. The Young's modulus of the polymers range on order from 1 to 1000 MPa

and include both glassy and semi-crystalline polymers. The equations of Tandon and Wang predict that for a given loading volume of filler, low modulus polymers will experience a proportionally greater enhancement in modulus than will high modulus polymers[304]. Thus, the calculation of A_f from the Tandon and Weng equations allows normalization of E_c / E_m versus ϕ data so that an equal comparison of reinforcement effects can be made.

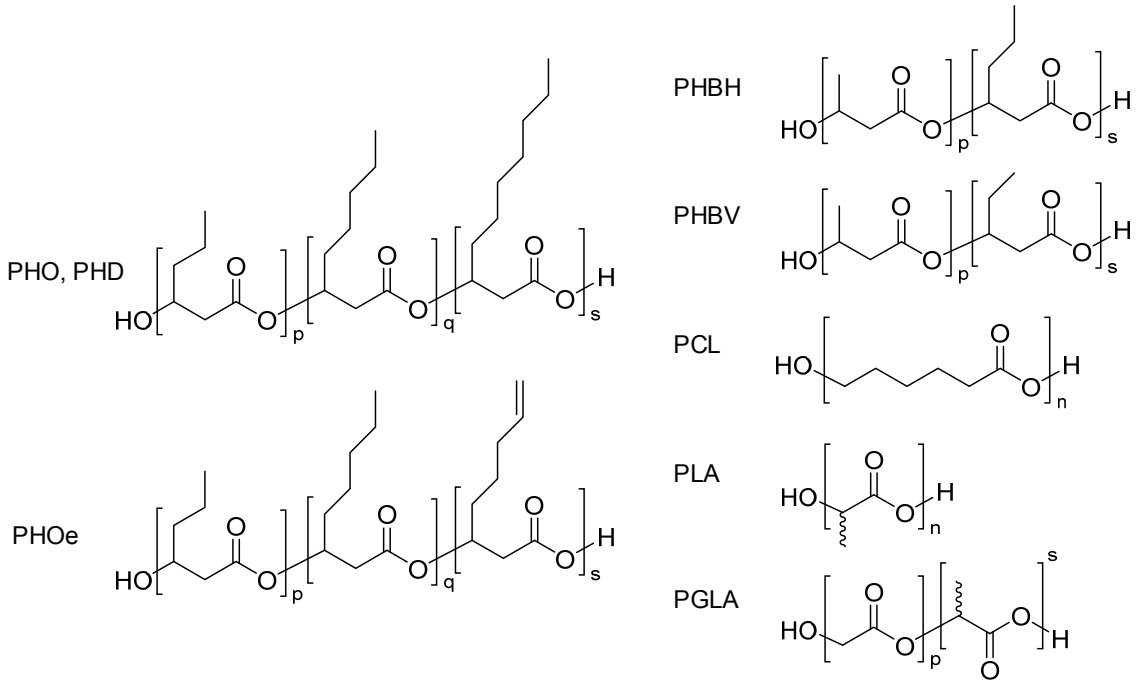

Figure 5.9 Structures of various biodegradable polyoxoesters.
Monomers < 1% (wt.) of polymer composition are not depicted in the structures.

We judge the quality of reinforcement for each system by comparing the value of A_f predicted from the Tandon and Weng equations to the A_f determined from particle measurements. In some cases measured A_f were taken from spectroscopy or microscopy data from the actual composite, and in others A_f values were determined from measurements of pure nanofiller.

Table 5.6 Properties of biodegradable polyoxoester-layered-carbon nanocomposites.

Polymer-Filler	Matrix Modulus E_m (MPa)	Particle Dia.[u] d (nm)	Aspect Ratio[v] Meas. A_f (d/t)	Aspect Ratio[v] Calc.	Oxygen Content C:O[w]	Dispr. Method[x]	Sonic. Time (hr)
[a]PHO- TRG	4.5	500[b]	700-1500[c]	309	10:1[d]	TCM	0.12
[a]PHOe -TRG	6.3	500[b]	700-1500[c]	97	10:1[d]	TCM	0.12
[a]PHD- TRG	5.3	500[b]	700-1500[c]	151	10:1[d]	TCM	0.12
[e]PHBH- EG	292	13000[f]	240-570[g]	325	58:1[346]	TCM	0.16
[i]PHBV- MEG	85.7	5000[j]	2500[j]	11	94:1[j]	TCM	0.16
[k]PLA- GNP	1800	5000[k]	600-900[k]	1110	22:1[l]	TCM	2
[m]PLA- TRG	3000	500[n]	700-1500[c]	81	10:1[d]	melt	0
[k]PLA- GO	1800	500[k]	300-800[o]	1405	2:1[d]	DMK/TCM	5
[p]PCL- TRG	107	500[n]	700-1500[c]	846	10:1	TCM	2
[q]PCL- GO	340	600[r]	400-900[o]	53	2:1[d]	DMF	24
[s]PLGA- GO	110	200[s]	150-300[o]	191	2:1[d]	DMF/DCM	24
[t]PLGA- GO	203	500[t]	300-800[o]	155	2:1[d]	DMF	1

[u] Particle diameter was usually given as a range: here we present an estimated median value.

[v] Aspect ratio (Meas.)was estimated by dividing the range of particle diameters by the estimated median value for particle thickness that was found in the specified references. Aspect ratio (Calc.) was determined from E_c / E_m versus φ data using the equations of Tandon and Weng.

[w] C:O (the ratio of carbon to oxygen atoms in the filler material)

[x] Solvents: TCM (chloroform), DCM (dichloromethane) DMK (acetone), DMF (N,N-dimethylformamide)

[a] Polymers in this study

References: [b] 265| [c] 265, 347 | [d] 348| [e] 322| [f] 349| [g] 350,351-352| [h] 346| [i] 325| [j] 353| [k] 321| [l] 348, 354-355| [m] 341| [n] 265| [o] 348, 355| [p] 342| [q] 343| [r] 356| [s] 345| [t] 344

Generally, the data show that the use of particles with a larger aspect ratio contributes to greater enhancements in the relative modulus. Polymers with small aliphatic appendages or none, e.g. PLA-GO, PLA-GNP, PHBH-EG, PCL-TRG, and PGLA-GO, tend to give values of A_f near or above the measured A_f, while PHO, PHOe, and PHD, all with longer aliphatic appendages, give values of A_f well below the A_f value measured from pure nanofiller. This is consistent with our hypothesis that steric hindrance from long aliphatic appendages may disrupt hydrogen bonding and other non-covalent interactions with oxygen molecules on the TRG surface. However, it is possible that use of a longer sonication period for the TRG used in our study could have resulted in increased value of A_f due to better exfoliation of multi-layer particles[356]. We also note that the highest value of A_f, 1405, occurs when PLA is paired with GO. Again this suggests that the additional interfacial attraction due to the presence of extra oxygen moieties on the surface of GO may give rise to strong reinforcement effects.

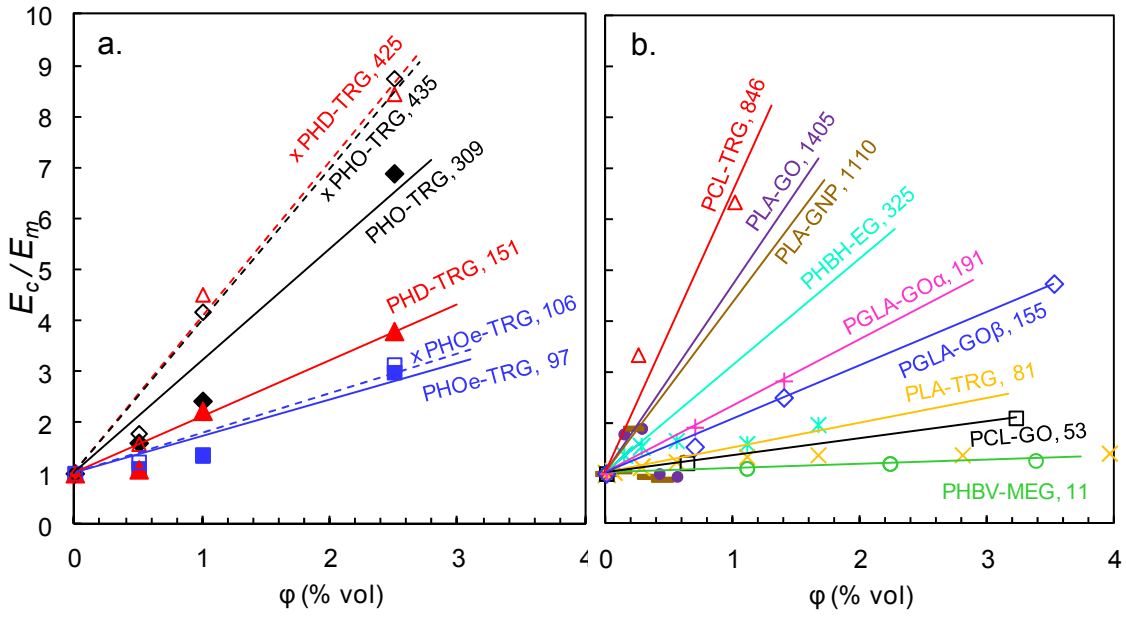

Figure 5.10 Modulus enhancement in various polyoxoester matrices.
Data is for various polyoxoester matrices containing some form of layered carbon nanofiller. E_c and E_m are the modulus for the composite and unfilled matrix, respectively. The number next to each polymer name is the filler's average aspect ratio (A_f) calculated using Tandon and Weng model. **a.**) Nanocomposites in this report: PHO-TRG (♦), PHOe-TRG (■), PHD-TRG (▲), xPHO-TRG (◊), xPHOe-TRG (□), xPHD-TRG (Δ). "x" before the abbreviation denotes data corrected for reduced crystallinity. **b.**) Nanocomposites in the literature: PLA-GO (●), PLA-GNP (▬), PHBH (*), PLA-TRG (x), PHBV-MEG (○), PGLA-GO$^{\alpha}$ (+), PGLA-GO$^{\beta}$ (◊), PCL-TRG (Δ), PCL-GO.

However, the data set does contain exceptions to these observations. The most conspicuous is the low modulus of PLA-TRG composites given that PLA-GO and PLA-GNP both show a much greater modulus enhancement. For PLA-TRG we attribute the low value of A_f to the melt blending technique used for graphene dispersion[340]. As a result of this process, the TRG received no sonication prior to mixing which likely resulted in poor exfoliation of graphene particles and a reduced aspect ratio. Furthermore, the viscosity of melt phase PLA is likely much higher than solvated PLA thus requiring greater mixing times for melt compounding.

The modulus enhancement for PHBV is also unexpectedly low given the much greater modulus enhancement for PHBH, which is structurally similar. Here we note that the oxygen content of the microwave expanded graphite used for PHBV (C:O = 94:1) is

the lowest among all filler materials. We speculate that reduced intermolecular attraction between the polymer and filler may have led to poor dispersion and minimal reinforcement effects.

Next, we draw attention to the result of the PCL-GO composites. Given the absence of any aliphatic appendages along the PCL backbone and the use of GO for filler, we expect the presence of strong interfacial adhesion in the composite, thus the minimal increase in modulus is an unexpected result. While the solvent used for this study, dimethylformamide (DMF), is a good solvent for graphite oxide[357] it is a poor solvent for PCL, especially as M_w increases beyond 65,000[358]: for the PCL-GO composite the M_w was 300,000. Thus, poor physical dispersion of the GO in PCL may have contributed to the low modulus enhancement.

For PGLA-GO, we obtained data from two, very similar studies; however, we do observe a small disparity in the degree of reinforcement. In the first study[345] which produced the highest calculated value of A_f, 191, we note that the researchers used a 24 hr sonication period to disperse the GO, and they dissolved the polymer in dichloromethane which is known to be a strong solvent for PGLA. In the second study[344] which produced a lower calculated value A_f, 155, the authors sonicated the GO for only 1 hour and dissolved the PGLA in dimethylformamide, a less effective solvent, thus requiring them to heat the polymer to 60 °C.

For several of the polymer systems including: PLA-GO, PLA-GNP, PLA-TRG, and PHBH, the modulus either remains constant or even decrease with increasing graphene loading beyond ~ 0.3 vol.%. This suggests a poor dispersion of graphene possibly induced by aggregation at higher graphene loadings.

Conclusions

The purpose of this study was to explore how variations in the molecular structure of elastomeric PHA_{mcl} polymers affect their performance in TRG nanocomposites. Depending on matrix type, the Young's modulus increased by 180-590%, and the elongation at break decreased by 41-89% at the 2.5% loading. However, it is likely that the magnitude of the modulus enhancements would have been higher if it were not for a decrease in matrix crystallinity by 15-55%.

Percolation of an electrically conducting, graphene, network was observed to occur between a volume loading of 0.4-0.5%, and an increase in electrical conductivity by > 10^7 orders was observed at 2.5% loading. Conversely, rheology data indicated that percolation of a pseudo-solid network based on graphene-polymer entanglements occurred at a distinctly lower graphene loading close to zero vol.%.

The addition of graphene to PHA_{mcl} also showed an effect on the thermal stability of the composites: for $T_{50\%}$ changes varied between an increase of 5.8°C and a decrease of -4.5°C. For the endothermic heat requirement at $T_{50\%}$, values varied between an increase of 60% and a decrease of -30%. Moreover, $E_{50\%}$ values showed a strong correlation with variation in the heat capacity of composites, likely due to changes in the entanglement structure of polymer chains.

Comparison of modulus improvements among the three different matrices was done by calculating values for A_f from normalized modulus data. Initially, the results indicated that reinforcement in PHO, $A_f^{PHO} = 309$, was more effective than in PHD, $A_f^{PHD} = 151$, but when the effects of crystallinity change were considered, PHO and PHD showed similar improvements in modulus, $A_f^{PHO} = 435$ and $A_f^{PHD} = 425$, respectively. Still, differences in the elongation at break and SEM fracture topology suggest that PHD may disentangle from the graphene particles more easily than PHO. We speculate this may be due to the longer packing length of PHD, i.e. its larger diameter, or a reduction in the interfacial attraction between PHD and TRG due to steric shielding of oxygen atoms along the polyester backbone.

In the covalently cross-linked PHOe matrix, $A_f^{PHOe} = 97$, modulus improvements were significantly lower than in the un-cross-linked PHO, $A_f^{PHO} = 309$, even when sample

crystallinity was considered. Presumably, the network structure of PHOe precludes the formation of strong entanglements with the graphene particles. This hypothesis is supported by SEM images of fractured surfaces following extension testing. The rough surface topology of the PHO-0.5% graphene composite suggests the formation of dense polymer-graphene entanglements. Only at 2.5% graphene loading does PHOe show a similarly rough, pull-out morphology. An interesting experiment would be to measure the reinforcement effects when matrix cross-linking is performed after graphene dispersion.

Our survey of other composite systems in the literature highlights the numerous factors, which can control the effectiveness of nanoparticle reinforcement. These include: polymer chemistry, particle aspect ratio, chemical modifications on the nanofiller surface, dispersion method (i.e. solvent versus melt), solvent choice for both graphene and polymer, and duration of sonication treatment for exfoliation. Comparison of our results against other, in-class, bio-polyesters gives support for our hypothesis that strong interfacial interactions can increase the degree of modulus enhancement in PHAs. Longer aliphatic appendages present in PHA_{mcl} polymers may preclude the formation of hydrogen bonds and other non-covalent interactions with the TRG nanoparticles compared to less bulky polymers such as PHB-co-PHH, PLA, PCL, and PGLA that showed greater improvements in relative modulus. The use of GO with its higher fraction of epoxide, hydroxyl, and carbonyl moieties may be a way to further improve interfacial attraction with PHA_{mcl}, similar to the way in which GO proved very effective with PLA[321] and PGLA[344] systems. Additionally PHA_{mcl} could itself be functionalized to promote hydrogen bonding, e.g. with the use of terminally substituted ω-hydroxy fatty acids[359] as monomer feedstocks.

Furthermore good dispersion technique is essential when preparing polymer graphene composites. The saturation of modulus enhancement with graphene loading seen in some composites is likely an indication of poor dispersion. While sonication can be a useful tool for exfoliation, which increases the aspect ratio of particles, it can also break graphene particles and lessen their aspect ratio when the duration of the treatment is extended[356]. Comparison among different studies in the field would benefit from a quantitative approach to this technique by detailed reporting of the graphene

concentration in the dispersant, duration of sonication times, and power density (power/volume) used for exfoliation. Furthermore, care should be taken to choose a solvent, which is effective at solubilizing both the nanoparticle and the polymer. In cases of high viscosity in either polymer melts or solutions, estimation of mixing time can help ensure proper dispersion, i.e. good micromixing at the length scale of the nanoparticles. The estimate of mixing time depends on filler density, solution viscosity, volumetric power density, and geometry of the mixing equipment.

We envision several practical applications for PHA-graphene composite technology. First, the significant improvements in polymer stiffness afforded by graphene reinforcement greatly expand the useful mechanical range of PHA elastomers. Second, the added property of electrical conductivity could allow the proliferation of PHA based materials into previously unrecognized applications. These may include for instance, biodegradable options for packaging of charge sensitive electronic circuit boards and charge dissipating floor coverings for use in static-sensitive manufacturing processes. Because polyhydroxyalkanoates are also biocompatible the possibility may exist for the use of these materials in implantable devices or as tissue scaffolds with electrical conductivity. However, what remains the most significant impediment to greater proliferation of PHA_{mcl} polymers is their low melting point, 45-55 °C, compared to PHB with a melting point of 175 °C. For PHO and PHD graphene addition resulted in a small increase in T_m by up to 3 °C but caused a reduction in T_m by as much as -8 °C for PHOe. Fortunately with the use of blends, copolymers, cross-linking, and more recently PHA block-copolymers, it is likely that a PHA_{mcl} material can be created with a melting temperature sufficiently high to meet the requirements of current engineering plastics.

Supporting Information

Thermal Stability of PHA-TRG Composites

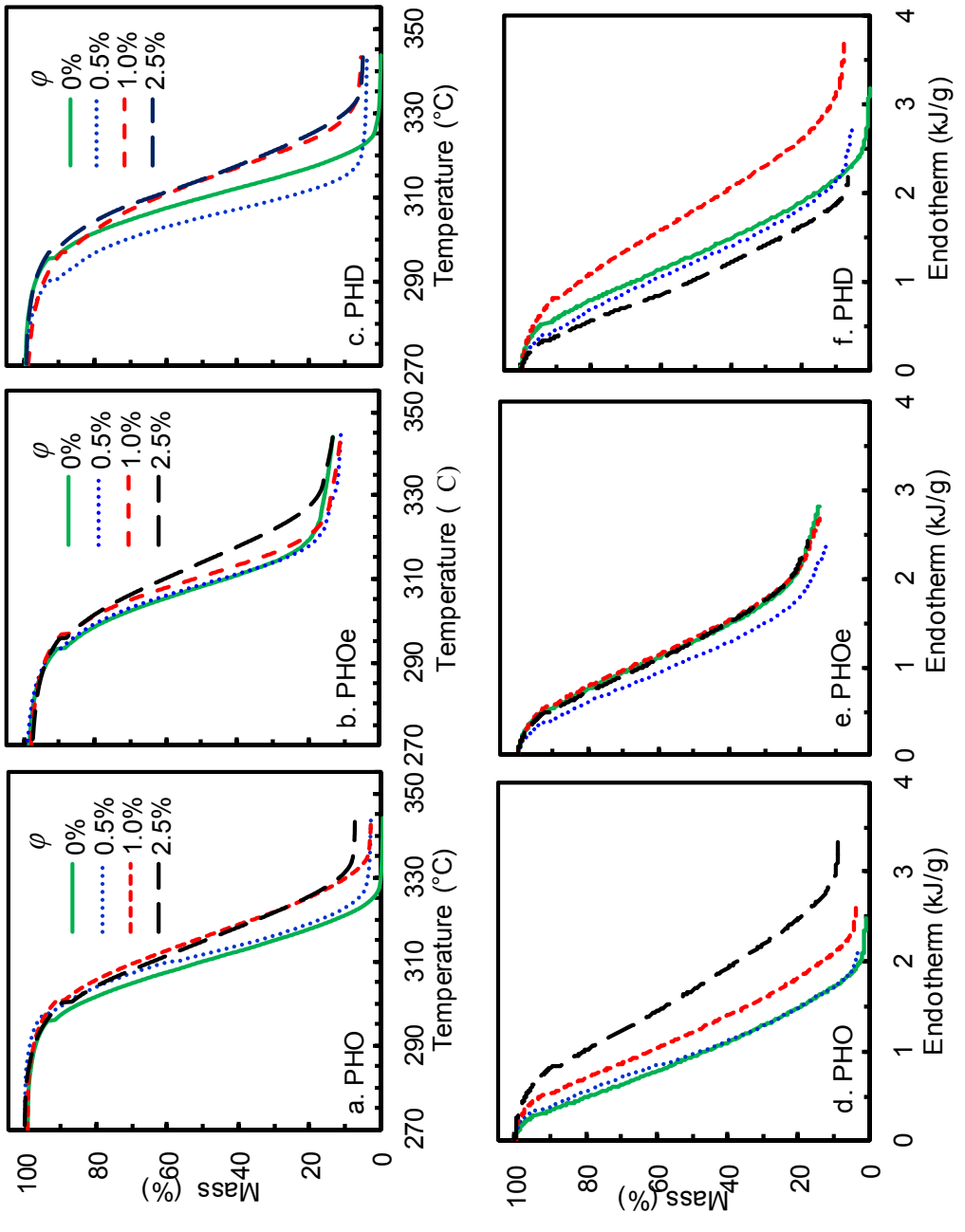

Figure 5.11 Mass-loss thermograms for thermal degradation of PHA-graphene nanocomposites. **a-c.** mass versus temperature, **d-f.** mass versus heat-flow.

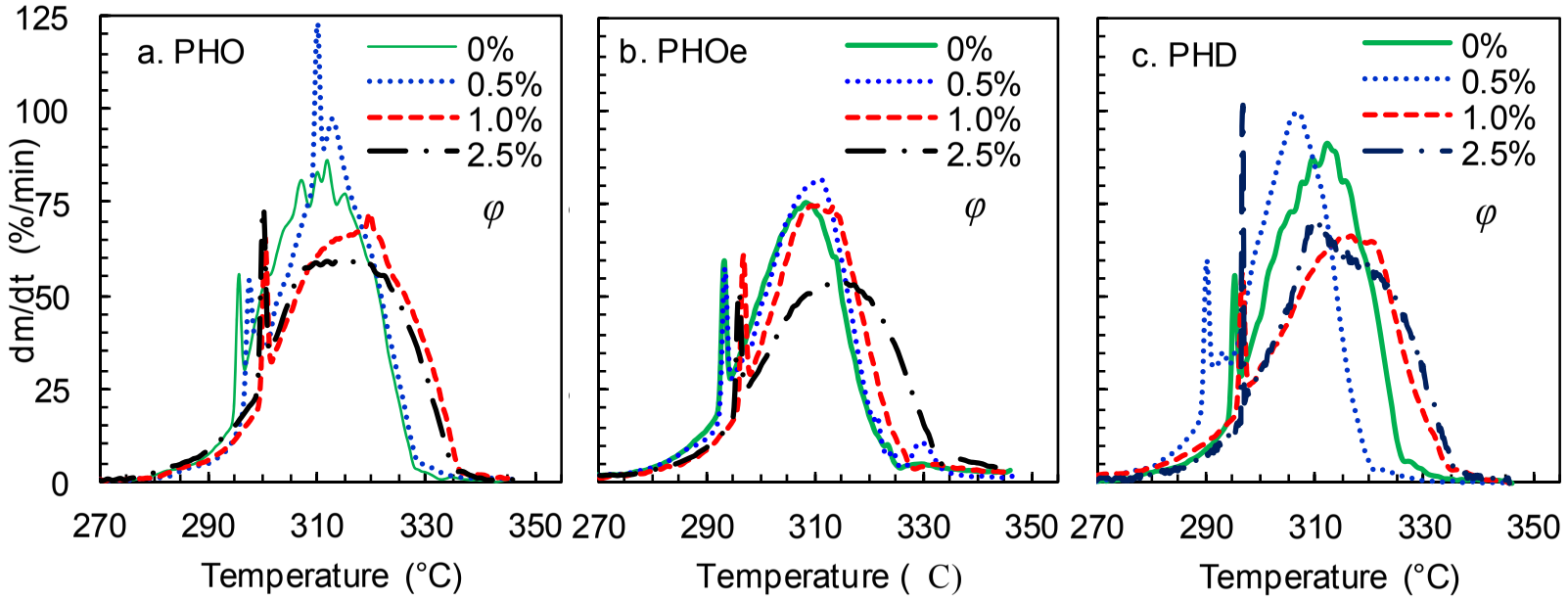

Figure 5.12 Mass-loss-rate thermograms for thermal degradation of PHA-graphene nanocomposites.
a-c. rate of mass-loss versus temperature.

Estimation of the Percolation Threshold from Rheology Data

Storage modulus (G′) data from rheology testing was used to predict the critical filler loading (φ_c) at which percolation of a pseudo-solid network first occurs. Commonly, an empirical model of the form $G' \propto (\varphi-\varphi_c)^{\nu}$ is used[304], where φ_c is the critical percolation threshold and ν is a power-law exponent. For our analysis we used the slightly modified equation $G' = G'_g ((\varphi - \varphi_c)/(1 - \varphi_c))^{\nu}$, which includes a boundary condition for the shear modulus of few-layer graphene (G'_g) (~$1x10^{11}$ Pa)[330]. Casting the model in this form makes it completely analogous to the power-law model we use later for estimating the percolation threshold from electrical conductivity data[329]. A plot of log(G′) versus $\log((\varphi - \varphi_c)/(1 - \varphi_c))$ for different graphene loadings yields estimates for φ_{perc} and ν. Moreover, forcing the models through G'_g improves the precision of the estimate and normalizes the models to a single, common value. While the G'_g value for few-layer graphene does not likely describe the storage modulus of a composite with 100%, randomly oriented, graphene sheets, we do expect that it is an appropriate constraint on composite behavior in the limit of sparse filler loadings. In obtaining the best fit we adjusted the value of φ_c to maximize the r^2 value of a least-squares, linear, regression model. From G′ measurements made at $\omega = 0.3$ rad/s we calculate that network percolation occurs at graphene loadings of -0.10, -0.80, and 0.33 %vol and ν values of 6.0, 6.3 and 5.0 for PHO, PHOe, and PHD respectively

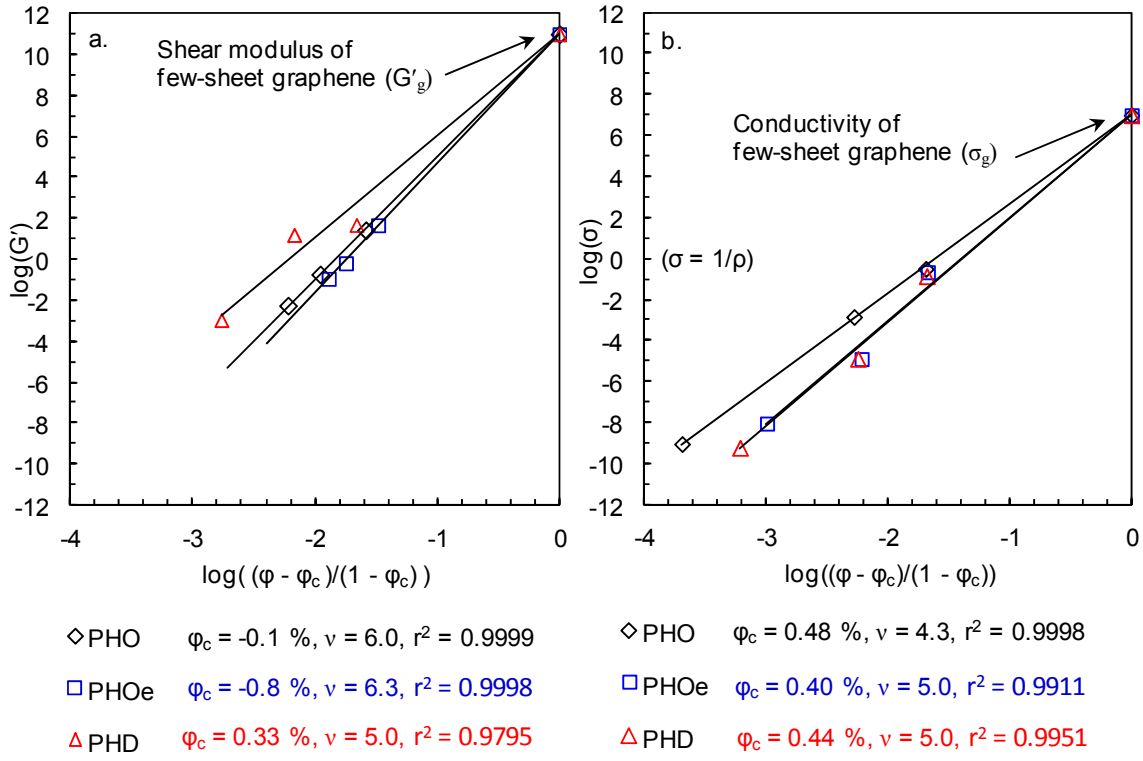

Figure 5.13 Estimation of the percolation threshold using a power-law model. **a.)** Rheology data fitted to the model $G' = G'_g ((\varphi - \varphi_c)/(1 - \varphi_c))^{\nu}$. G′ values correspond to a shear rate of ω = 0.3 rad/s. **b.)** Electrical conductivity data fitted to the model $\sigma = \sigma_g ((\varphi-\varphi_c)/(1- \varphi_c))^{\nu}$

Estimation of the Percolation Threshold from Electrical Conductivity Data

The percolation threshold (φ_c) for electrical conductivity ($\sigma = 1/\rho$) can be estimated using a power-law model of the form $\sigma = \sigma_g ((\varphi-\varphi_c)/(1- \varphi_c))^{\nu}$, where σ_g is the conductivity of few-layer graphene ($\sim 1\text{x}10^7$ $(\Omega\text{-m})^{-1}$) and ν is the "universal constant" for which classical models specify a theoretical value of 2 for geometric percolation[329]. Calculations were made via the same linear regression procedure used for the rheological model. Using this method we estimate that percolation of an electrically conducting network occurs at filler loadings of 0.48, 0.40, and 0.44 %vol with ν values of 4.3, 5.0, and 5.0 for PHO, PHOe, and PHD, respectively.

Calculating A_f using Tandon and Weng Micromechanical Model

A theoretical model for determining the average stress in a composite matrix with misfitting inclusions was first proposed by Mori and Tanaka[338] utilizing the transformation tensor for a single inclusion derived previously by Eshlby[360-361]. Based on these results Tandon and Weng[313] derived analytical expressions for the longitudinal (E_{11}) and traverse (E_{22}) moduli of a composite matrix for the hypothetical case of perfectly aligned inclusions. In addition to the general case of spherical inclusions, they expanded their derivation to include the effect of both oblate spheroids, e.g. graphene nanoparticles, and prolate spheroids, e.g. graphene nanotubes, of varying aspect ratio (A_f). In the hypothetical case of perfectly aligned inclusions, the longitudinal modulus (E_{11}), which points in the direction normal to the flat plane of an oblate nanoparticle, takes on a maximum, and the traverse modulus (E_{22}) assumes a minimum. Thus when a collection of nanoparticles is dispersed in a completely random orientation, the traverse modulus (E_{22}) takes on a maximum value and becomes equal to E_{11}. According to Tandon and Weng, the traverse modulus of the composite is a function of the loading volume of filler particles (φ), their aspect ratio (A_f), and the Young's modulus (E) and Poisson ratio (ν) for both the filler particles and the matrix (E_m and E_f) and (ν_m and ν_f).

$$\frac{E_{22}}{E_m} = \frac{1}{1 + \dfrac{\varphi[-2\nu_m A_3 + (1-\nu_m)A_4 + (1+\nu_m)A_5 A]}{2A}}$$

The contributions of these parameters are contained within the coefficients, A, A_3 A_4 and A_5, the formulas for which are quite detailed and may be found in the original article by Tandon and Weng[313]. For purpose of calculations E_{22} is assigned value of Young's modulus measured for the composite (E_c) Thus, using the slope obtained from a plot of E_c / E_m versus φ , an estimate can be made for the value of A_f .

For most reports in the literature, graphene content was given in wt%; thus, estimates for the filler and matrix mass desnsities (ρ_f and ρ_m) were used to calculate the corresponding loading volume in vol%. For graphene oxide (GO) a value of ρ_f = 1.8 kg/m^3 was used[362]. For all other nanofillers the density assumed was that of graphite, ρ_f=

2.28 kg/m^3. Mechanical properties of the nanofillers were assumed to be the same as those of pristine graphene, E_f =1060 GPa[302] and a Poisson ratio of, v_f = 0.186[363]. When possible, values for the Posisson ratio of the matrix (v_m) were obtained from the literature. For PHO, PHOe, and PHD a value of v_m = 0.49 was assumed based on a Poisson ratio of 0.5 corresponding to a perfect elastomer. For PGLA a value of v_m = 0.33 was assumed based on the similar value of v_m = 0.36 for PLA.

For each composite system data for E_c / E_m versus φ was fitted to a linear model using least-squares regression. In most cases reinforcement effects were best at low filler loadings, but plateaued at higher levels, likely due to difficulty in dispersing the filler particles at higher volume loadings. Thus, to obtain a maximum value of A_f, slopes of E_c / E_m versus φ were calculated using only the first three data points of each set, including the 0% loading. In some cases additional data points were included if doing so resulted in a higher estimate of slope. Computations were performed using a Matlab code. The calculated values of A_f for each composite and the parameter values used in the calculations are presented in **Table 5.7**.

Table 5.7 Parameters used for calculation of aspect ratio (A_f)

Polymer	Graph. Type	Matrix Modulus E_m(MPa)	Matrix Density ρ_m (g/mL)	Matrix Poisson Ratio v_m	Slope m	Calculated Aspect Ratio A_f
†PHO	TRG	4.5	1.02[364]	0.49	3.193	309
†PHOe	TRG	6.3	1.02[364]	0.49	1.714	97
†PHD	TRG	5.3	1.02[364]	0.49	2.099	151
[322]PHBH	EG	292	1.22[365]	0.39[366]	3.104	325
[325]PHBV	MEG	85.7	1.22[365]	0.39[366]	1.089	11
[321]PLA	GNP	1800	1.25[367]	0.36[367]	4.339	1110
[341]PLA	TRG	3000	1.25[367]	0.36[367]	1.496	81
[321]PLA	GO	1800	1.25[367]	0.36[367]	4.676	1405
[342]PCL	TRG	107	1.14[368]	0.47[368]	6.513	846
[343]PCL	GO	340	1.14[368]	0.47[368]	1.389	53
[345]PLGA	GO	110	1.35[369]	0.33	2.302	191
[344]PLGA	GO	203	1.35[369]	0.33	2.049	155

Correction of the Modulus Enhancement Factor for Changes in Crystallinity

The derivation used by Tandon and Weng to describe the effect of nanoparticle inclusions assumes 1.) that the mechanical properties of the bulk polymer matrix are completely homogeneous and 2.) that particle inclusion do not alter the mechanical properties of the bulk matrix e.g., by changing the crystallinity or entanglement density. However, the decreases in ΔH_m that is seen with graphene addition indicates that crystallinity is indeed affected by graphene addition.

Estimation of A_f using the equations of Tandon and Weng involves estimating an average modulus enhancement factor $(E_c/E_m)_{avg}$ by fitting modulus enhancement data to a linear approximation dependent on the dimensionless, volumetric, filler fraction, φ.

$$E_c/E_m = \varphi * (E_c/E_m)_{avg.} + 1$$

By recognizing the physical analogy between reinforcement with nanofiller and reinforcement with polymer crystals, we have adopted a similar model of crystal reinforcement assuming a linear expression of the form:

$$E_c / E_m = (x_c/x_m)*(1-(E_a / E_m)) + (E_a / E_m)$$

dependent on a dimensionless, relative crystallinity (x_c/x_m) and the modulus of the purely amorphous polymer (E_a). While the quantity E_a/E_m is specific for each polymer system, in the case of $E_a/E_m << 1$ the relation becomes independent of polymer type, giving the simplified form:

$$E_c/E_m \approx (x_c/x_m)$$

Results presented in a previous report showed that for a similar PHO polymer the measured E_m for a semi-crystalline matrix was more than 100x > than the corresponding E_a of the amorphous material[370]. From our own measurements we report similar values of E_m of 4.5 MPa and 5.3 MPa for PHO and PHD respectively. Based on this and the similar composition between PHO and PHD we assume that E_a/E_m for PHD is of the same, negligible magnitude. Furthermore x-ray crystallography performed on PHO and PHD polymers showed a very similar crystalline structure[293], which supports our assumption that reinforcement effects by PHO and PHD crystals are similar. Thus we expect that our linear approximation for crystallinity imparts minimal inaccuracy for comparing PHO and PHD.

Because the relative modulus enhancement is proportional to both graphene content as well as crystal content we can use a combination model of the form:

$$E_c / E_m = (\varphi * (E_c / E_m)_{avg.} + 1) * (x_c / x_m)$$

Note, the model gives the correct value of $E_c/E_m = 1$ when $\varphi = 0$ and $x_c = x_m$. Thus, the modulus enhancement factor corrected for crystallinity becomes.

$$(E_c / E_m)/(x_c / x_m) = (\varphi * (E_c / E_m)_{avg.} + 1)$$

While a more rigorous derivation can certainly be made, this simplified model highlights the important effects that changes in matrix crystallinity can have on modulus enhancement when using nanofiller reinforcements.

Chapter 6. Process Control of Mixotrophic Biosyntheses for the Production of PHB-b-(PHB-co-PHV) Block-Copolymers and the CO_2-neutral Conversion of Heterotrophic Substrates

Overview

The mechanical toughness of poly(3-(*R*)-hydroxybutyrate) (PHB) homopolymer is known to be enhanced by the incorporation of 3-(*R*)-hydroxyvalerate (PHV) monomers along the polymer chain, especially when these PHV monomers are segregated within block domains. In this article we demonstrate the synthesis of both random and block-copolymers of PHB and PHV using CO_2 and valeric acid as monomer precursors, respectively. We perform this conversion via the mixotrophic capabilities of *Ralstonia eutropha,* which permit the simultaneous utilization of catabolic pathways to degrade heterotrophic substrates along with anabolic cycles for CO_2 fixation.

Our understanding of the dynamic interplay of these two metabolic modes is enhanced via the use of real-time, mass-spectroscopy data from biosynthesis off-gas, thereby, allowing us to interrogate the metabolic state of the cell as it responds to changes in the availability of different substrates. Furthermore, the sensitivity of this measurement technique allows us to make predictions for both the molecular size and composition of PHV-rich block domains, which affect the bulk mechanical properties of the block-copolymers.

As a product of our mass-spectroscopy measurements, we demonstrate how process control of a mixotrophic bioprocess can be used to achieve the CO_2-neutral conversion of a heterotrophic substrate. By continuous monitoring of the culture's metabolic state via off-gas composition data, we are able to maximize the feed rate of a heterotrophic substrate while preventing the production of waste CO_2 and minimizing the requirement for added hydrogen.

Lastly, we bring additional insight to our study using a metabolic model to estimate maximum substrate yields for autotrophic growth and predict the process operating points needed to produce pure PHV homopolymer.

Background

In light of the growing concern for the economic and environmental liabilities associated with petroleum feedstocks, both consumers and manufactures have expressed interest in plastics, fuels, and chemicals derived from alternative feedstocks that are both sustainable and environmentally friendly. *Ralstonia eutropha* with its ability to grow on a wide range of renewable substrates including sugars, vegetable oils, volatile organic acids, industrial and municipal waste streams, and even carbon dioxide is an attractive organism for the development of sustainable manufacturing processes. Moreover, the known correlation of global warming with CO_2 emissions, make the autotrophic assimilation of CO_2 by *R. eutropha* an especially promising biosynthesis route with the possible benefit of environmental remediation. Already *R. eutropha* has demonstrated significant utility for its ability to synthesize polyhydroxbutyrate (PHB), a renewable bioplastic that is strong, rigid, and valued for its biodegradability.

PHB, which is formed from monomers of 3-(R)-hydroxbutyryl-CoA (C_4), is a simple polyoxoester and among the larger class of polyhydroxyalkanoates (PHAs) for which more than 120 types have been identified[4]. Variation among PHAs arises from the size and type of appendages that extend from their polyester backbone. With an ultimate strength of 40 MPa and a Young's modulus of 3.5-4 GPa, PHB is strong and stiff; however with an elongation at break of only 3-8%, it is also brittle[292]. Alternatively, copolymers which contain modest fractions of other PHA types have reduced strength and modulus but greater flexibility[270]. Furthermore, the application of block-copolymer technology to PHAs has been shown to greatly improve mechanical toughness when compared to random copolymers of similar composition[20-21, 215]. Hence, PHA plastics, with their large selection of unique monomers and demonstrated processes for block-copolymer synthesis, show strong potential for the development of an array of new materials to fill the diversity of applications currently served by petroleum polymers. Thus, PHAs are logical products with which to build upon for the development of *R. eutropha* as a platform organism for autotrophic biosyntheses.

Already research has been conducted to explore the feasibility of autotrophic biosynthesis with *R. eutropha*[269, 371-372], which presents a challenge because of the

requirement of hydrogen gas to supply the energy for carbon fixation. The challenge of using hydrogen is due to both its poor solubility in water as well as its liability for explosive reaction with oxygen gas, which must be co-fed to support autotrophic respiration. Nevertheless, researchers have achieved success in utilizing CO_2 for PHB[83] production, and others have built on this work to develop related processes in which both CO_2 and heterotrophic carbons sources are co-fed (i.e. mixotrophic metabolism) to make unique PHA copolymers[38, 373-374].

However, the application of process technology for the synthesis of PHA block-copolymers from CO_2 has not yet been demonstrated. Herein we describe a process for the synthesis of block-copolymers of PHB (C_4) and PHV (polyhydroxyvalerate, C_5) using CO_2 and valeric acid (VA) as monomer precursors. CO_2 which is fixed via the Calvin cycle, using energy supplied from hydrogen oxidation, is primarily routed to the formation of 3-*R*-(hydroxybutyryl-CoA (3HB-CoA) monomers used for PHB synthesis. Valeric acid which is degraded via β-oxidation, produces monomers of 3-(*R*)-hydroxyvaleryl-CoA (3HV-CoA) used for PHV synthesis as well as some 3HB-CoA monomers. Because VA is added in periodic doses, the copolymer molecules formed are expected to contain blocks of PHB homopolymer covalently bonded to blocks of PHB-*co*-PHV random copolymer, i.e. block-copolymers of PHB-*b*-(PHB-*co*-PHV).

Using online mass-spectroscopy to measure the composition of biosynthesis off-gas, we are able to closely monitor the metabolic response of cultures to VA additions during autotrophic growth. This allows us to carefully control the duration and frequency of periodic VA additions, which affect the microstructure of the block-copolymers. Moreover, we are interested in exploring how the fraction of PHV in the block-copolymers correlates with the physical and mechanical properties of the bulk materials. We compare our results against a PHB homopolymer, and three, PHB-co-PHV, random copolymers, which were also produced autotrophically.

In an earlier study conducted by our laboratory[375], results showed that heterotrophic metabolism of valeric acid resulted in a copolymer of both PHB and PHV; however, when hydrogen was supplied to the culture, a pure PHV homopolymer was obtained. The ability to synthesize block-copolymer domains of pure PHV, as compared

to domains of PHB-co-PHV, may allow for the creation of a new class of PHA block-copolymer molecules with unique properties. With interest in these novel polymers, we present data from three different mixotrophic biosyntheses designed to explore the process conditions under which pure, PHV homopolymer can be produced. To facilitate our discussion we present simulation results using elementary mode analysis (EMA) to model the behavior of mixotrophic metabolism.

Lastly, using the off-gas composition data we collected, we demonstrate how controlled feeding of a heterotrophic carbon source (e.g. valeric acid) during autotrophic cultivation in *Ralstonia eutropha* can be used to conduct biosyntheses that achieve 100% conversion of the heterotrophic carbon. The benefits of such a mixotrophic process are two-fold: 1.) in eliminating the CO_2 emissions typically associated with bioconversion of heterotrophic feedstocks and 2.) in offsetting the amount of gaseous hydrogen required for fully autotrophic biosyntheses.

Results and Discussion

Optimization of Autotrophic Growth

At the onset of our study, a significant challenge was in developing a reliable process for preparing inoculum in autotrophic shake-flasks. Often we observed that cultures entered a prolonged lag-phase (> 12 h) following inoculation of flasks from cells grown on gas-plates. To study this we tested the effects on growth rate of both inoculum density and oxygen composition in the substrate gas. The tests were performed in 500-ml shake-flasks, with inoculum for the cultures taken from a fresh gas-plate. **Figure 6.1.a** shows the effect of inoculum density of cell growth. The substrate gas used in the experiment was H_2:O_2:CO_2 = 70:20:10. The data reveal a slight lag phase beginning at ~6 hr batch age and lasting for a period of ~2-4 hr, with the duration of the lag phase lasting longer at lower inoculum density. However, after the lag is over, a correlation is seen in which low density cultures demonstrate a higher maximum growth rate than high-density cultures. **Figure 6.1.b** shows the effect of oxygen fraction in the substrate gas. For the substrate gas the fraction of CO_2 was held at 10%, while the amount of O_2 and H_2 was varied to achieve the desired O_2 fraction. Results show that the use of a 5% O_2 fraction promotes maximum growth and produces no lag-phase; however, the maximum OD_{600} is stoichiometrically limited at 6. When 20% O_2 is used, the culture is delayed by ~6 h but reaches a higher OD_{600} of 12. This result is consistent with an earlier report[376], which demonstrated a trend of increasing specific growth rate as the oxygen partial pressure in the gas was reduced below 0.2 atm, with a maximum, specific growth rate of 0.42 h^{-1} occurring at 0.05 atm.

Ultimately we chose to use 10 mol% O_2 in the seed flask to strike a balance between growth rate and maximum biomass accumulation. However, once the seed was transferred to the production stage vessel, DO was immediately set to 25% to maximize the rate of cell growth.

A peculiar phenomenon we sometimes observed was that of cell-clumping, in which low-density, liquid cultures would form visible, cell clumps shortly after inoculation. As the culture progressed, the clumps continued to increase in size, often for more than 12 h, until at some critical point the clumps rapidly disintegrated, and the cells

resumed normal growth. We speculate that the clumping behavior may be a mechanism used by the cells in order to alter the local concentration of some critical substrate within the cell, e.g. by increasing the concentration of some paracrine growth factor, or by decreasing the local DO concentration due to reduced diffusion inside the clump.

Another important factor for preventing the occurrence of an extend lag-phase was the use of a freshly cultivated gas-plate for inoculations. While 5 mol% O_2 produced the fastest growth rate in liquid cultures, the substrate gas we used to cultivate gas-plates was H_2:O_2:CO_2 = 70:20:10. This was done to provide sufficient oxygen for biomass accumulation while ensuring that CO_2 would be the limiting reactant in the chamber, in order to prevent PHB accumulation[377]. We suspected that cells, which contained large stores of PHB, might instead begin degrading PHB rather than continuing in autotrophic metabolism, especially if the gas-plate had been removed from the autotrophic atmosphere for too long. In another report, Repaske et al.[378] observed that a lag in exponential growth occurred when cells were transferred between two medias with unequal concentrations of bicarbonate ion.

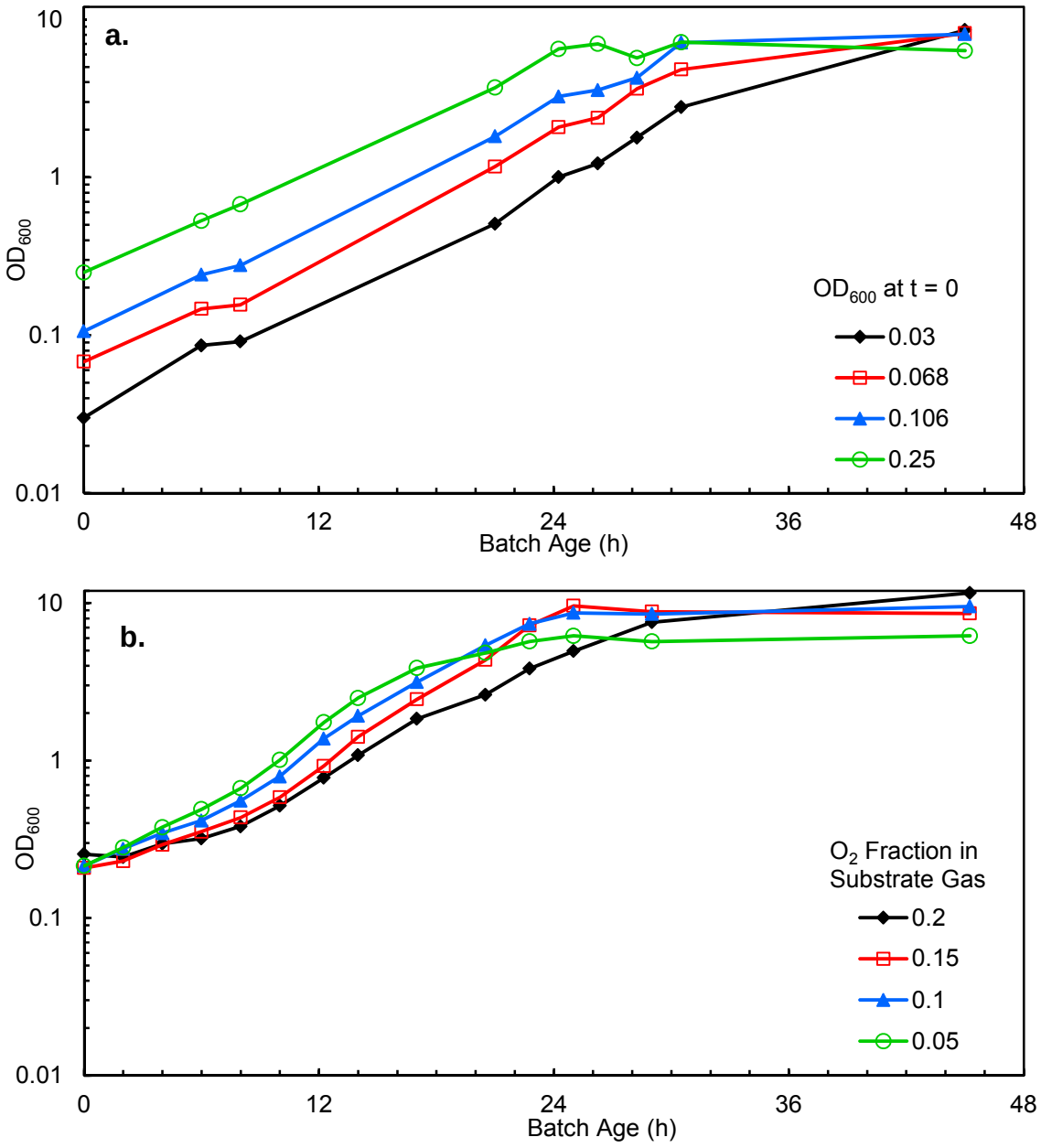

Figure 6.1 Autotrophic growth in 500-mL shake-flasks.
Data shows how cell growth (measured as OD_{600}) is affected by **a.**) variation in inoculum density and **b.**) variation in the oxygen fraction of the substrate gas. For **a**, H_2:O_2:CO_2 = 70:20:10 % vol. For **b**, the fraction of CO_2 is held constant at 10% vol. while H_2 and O_2 fractions are adjusted to obtain the desired composition.

Mixotrophic Metabolism

In heterotrophic mode, *Ralstonia eutropha* is capable of growth on a variety of substrates including: sugars, oils, and volatile fatty acids. When growth is restricted by either oxygen, nitrogen, or phosphorous, the organism accumulates the biopolymer poly(3-(*R*)-hydroxybutyrate) (PHB) as a storage mechanism for excess carbon and reducing equivalents in the form of NADPH. When valeric acid or propionic acid are supplied as precursors the accumulated polymer contains a random distribution of both poly(3-*R*-hydroxyvalerate) (PHV) and PHB.

During autotrophic metabolism *R. eutropha* utilizes energy derived from the oxidation of hydrogen to drive the fixation of carbon dioxide via the Calvin cycle. Just as in heterotrophic growth, PHB accumulation occurs under conditions of nutrient limitation when both H_2 and CO_2 are in excess. During growth on certain heterotrophic substrates, the activities of genes responsible for the uptake of H_2 and CO_2 are absent, but for other heterotrophic substrates, the activities of key autotrophic genes are elevated to levels similar to those seen under purely autotrophic conditions[379-380], thus, suggesting the possibility for simultaneous uptake of both CO_2 and heterotrophic carbon. Indeed, studies have reported this capacity for mixotrophic growth with numerous substrates including fructose[375, 381], lactic acid[380], various alkanoic acids (C_4, C_5, C_6, C_7, and C_8)[373-374], as well as γ-butryolactone[374].

When alkanoic acids were used to supplement autotrophic growth, cells produced PHA copolymers comprised of PHB along with higher chain-length 3-(*R*)-hydroxyalkynoate monomers[373, 375]. The co-feeding of γ-butryolactone[374] produced copolymers of 3-(*R*)-hydroxybutyrate and 4-(*R*)-hydroxybutyrate. In 2006 Pederson et al. demonstrated a process using *R. eutropha* for the biosynthesis of PHB-*b*-(PHB-*co*-PHV) block-copolymers from the combination of heterotrophic substrates fructose and valeric acid[21]. To synthesize these materials the authors administered small, periodic doses of valeric acid to produce PHV monomers while simultaneously feeding fructose as a source of PHB monomers. Based on the author's report that block-copolymers showed superior mechanical toughness versus random copolymers of a similar PHV fraction, we set out to

develop an analogous process by which PHA block-copolymers could be produced using CO_2 as the primary carbon source.

Process Description

To achieve this conversion of CO_2 we employed the mixotrophic capabilities of *R. eutropha* using CO_2 as a precursor for PHB and valeric acid as a precursor for PHV. The process utilizes a fed-batch biosynthesis in which H_2, O_2, and CO_2 are supplied continuously to a bioreactor containing minimal media with no heterotrophic carbon. Upon inoculation of the production culture, cells grow exponentially for ~24 h. See **Figure 6.2.** We avoided the occurrence of a post-inoculation lag-phase by transferring the seed culture just before the onset of stationary phase, and by controlling the DO concentration in the production reactor at 25%. (Note: 100% DO = air-saturated media at 30 °C.) The 25% DO set-point was enforced immediately upon inoculation and was maintained throughout biomass accumulation by intermittently increasing both oxygen content in the feed gas (from 5-10% v/v) and agitation speed (from 250-1200 RPM), until the maximum OTR was reached. After ~24 h, limitation by nitrogen and / or oxygen leads to a reduction in the rate of biomass accumulation and the onset of PHB production. The average specific growth rate measured during the exponential phase was ~0.22 h^{-1}. Interestingly, this value is significantly below the value of 0.42 h^{-1} reported by Ishizaki et al.[376] for the cultivation of Alcaligenese eutrophus 1769^T under the same DO concentration.

Gas consumption data for batch BC_14 is shown in **Figure 6.3.a.** The data show that gas consumption of all three substrate gases increase exponentially until ~24 h. At 26 h a small dose of valeric acid was administered to the culture to prime the cells for valeric acid uptake before total nitrogen depletion. Then, beginning at 27 hr periodic doses of 100 μL of valeric acid were made every hour until the end of the biosynthesis. Due to the nature of the PhbC synthase enzyme, the processes of chain initiation and termination occur throughout the polymer accumulation phase. Thus, in order to maximize the yield of di-block molecules, valeric acid must be supplied at regular intervals throughout the entire biosynthesis[209]. For the block-copolymer batches in this study, valeric acid additions were made hourly which is the same order as time-scale of

average chain life, ~38 minutes for a PHB chain and ~19 minutes a 50:50 PHB-co-PHV chain.[40]

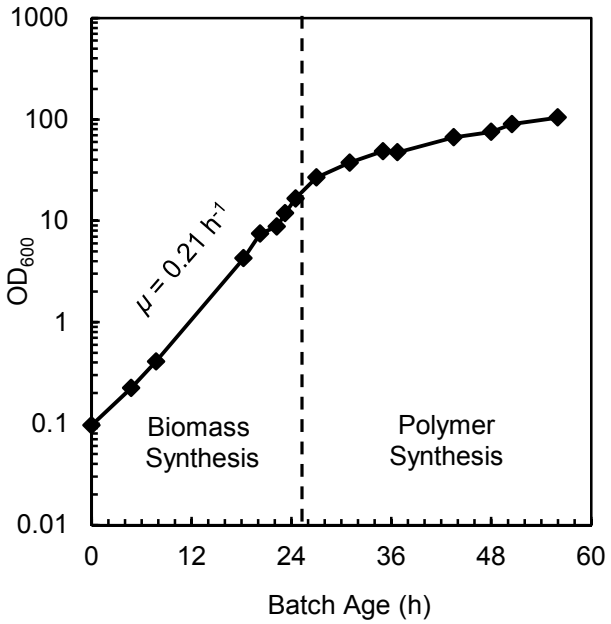

Figure 6.2 Cell growth profile of *R. eutropha* under autotrophic conditions in a controlled bioreactor.

Cell concentration (g/mL) is proportional to OD_{600}. Following inoculation, cells grow exponentially for ~24 hr at a specific growth rate of 0.21 h^{-1}. After limitation by oxygen and / or nitrogen, polymer accumulation begins, exhibiting linear synthesis kinetics until PHA content reaches ~70-80% of total cell mass. Autotrophic cultivation was performed in a stirred bioreactor, containing 1-L of minimal media (carbon-free) at 30 °C with substrate gas, H_2:O_2:CO_2:Ar = 80:5:10:5 %vol., supplied at 1 vvm. Oxygen concentration was intermittently increased up to 10% vol. (with H_2 concentration reduced accordingly), and agitation was automatically ramped from 250-1200 RPM in order to maintain a DO set-point of 25%. Media pH (initially 6.9) was allowed to drop naturally to 6.0 before beginning addition of NaOH to maintain pH at that level. Data shown is for BC_14.

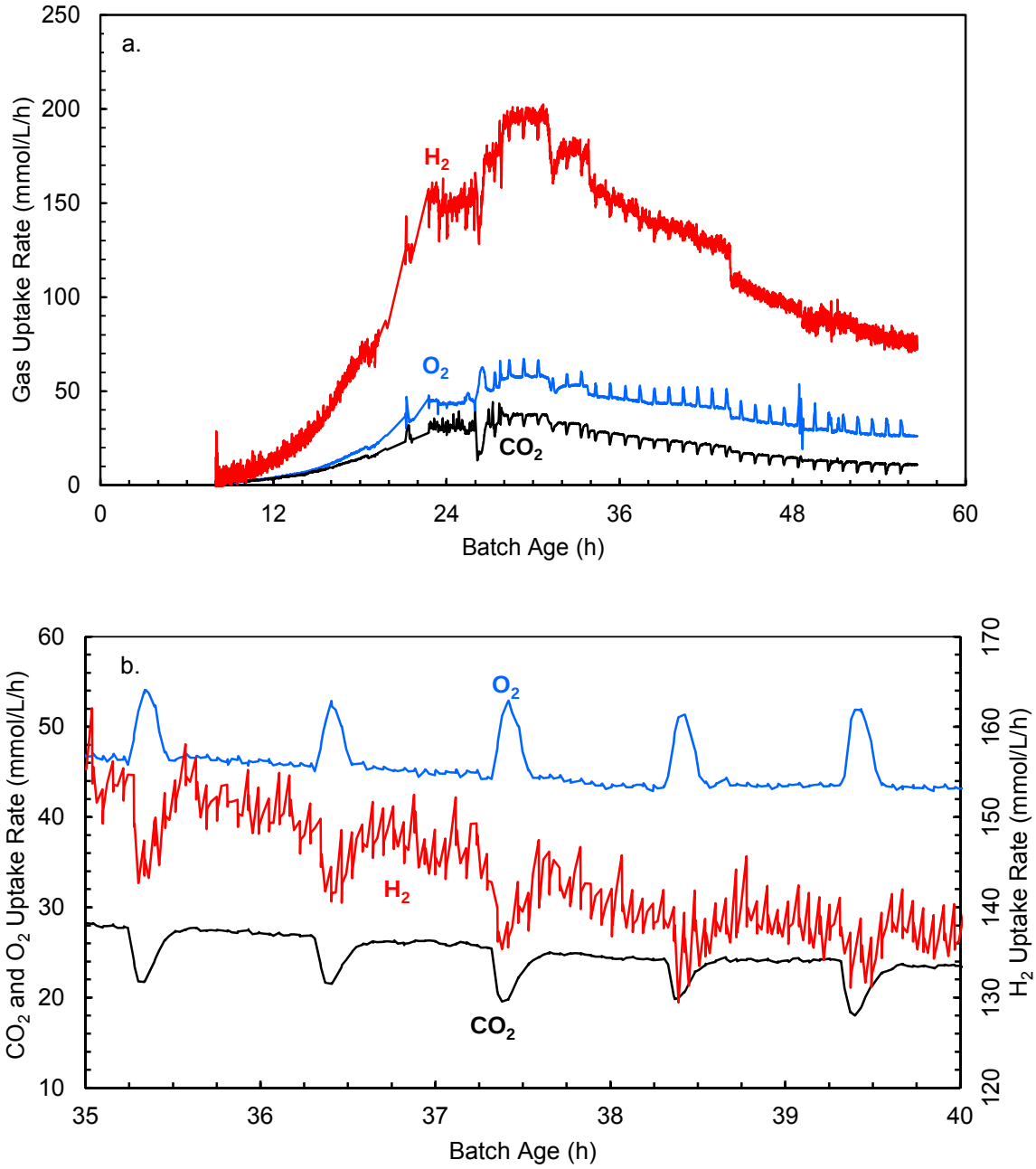

Figure 6.3 Gas uptake rates during mixotrophic block-copolymer synthesis. CO_2 consumed via autotrophic metabolism is used for PHB synthesis, while molecular domains rich in PHV are synthesized by the addition of small shots of valeric acid. **a.** Gas uptake rates for H_2, O_2, and CO_2 (mmol/L/h). **b.** Close up view of **a.** between 35-40 h. The spikes in gas uptake occur when small doses of valeric acid (100 µL) are added to the batch. Data shown is for batch BC_14.

Monitoring Valeric Acid Uptake via Real-time Off-gas Analysis

Due to the short period between valeric acid additions, monitoring of the substrate concentration by off-line analytical methods e.g., HPLC or GC is not practical. Instead, transient changes in the gas consumption profile of the batch may be used as a proxy for the depletion of valeric acid. **Figure 6.3.b** shows a closer view of the gas consumption profile seen in **Figure 6.3.a,** between 35-40 h. The addition of valeric acid to the batch causes a temporary decrease in the uptake rates of CO_2 and H_2 while the uptake rate of O_2 increases. In order to achieve the target PHV fraction in the copolymer, the valeric acid additions, which must be delivered over ~30 shots, are very small, between 30-100 μL or 28-93 mg/L after dilution in the batch. Thus, off-gas analysis provides a very sensitive method for detecting the consumption of valeric acid in the batch.

Batch Productivity

Batch productivity data for BC_14 is presented in **Figure 6.4.a**. The onset of rapid accumulation of PHA, including both PHB and PHV, begins at ~24 h which corresponds to the change in gas uptake evident in **Figure 6.3.a**. Although the batch growth rate rate begins to slow after 24 h, the accumulation of residual biomass by the culture continues until ~36 hr. By the end of the batch at 56 h, the PHA content of the cells was 79 wt.% with a PHV composition of 14 wt.% of the total polymer.

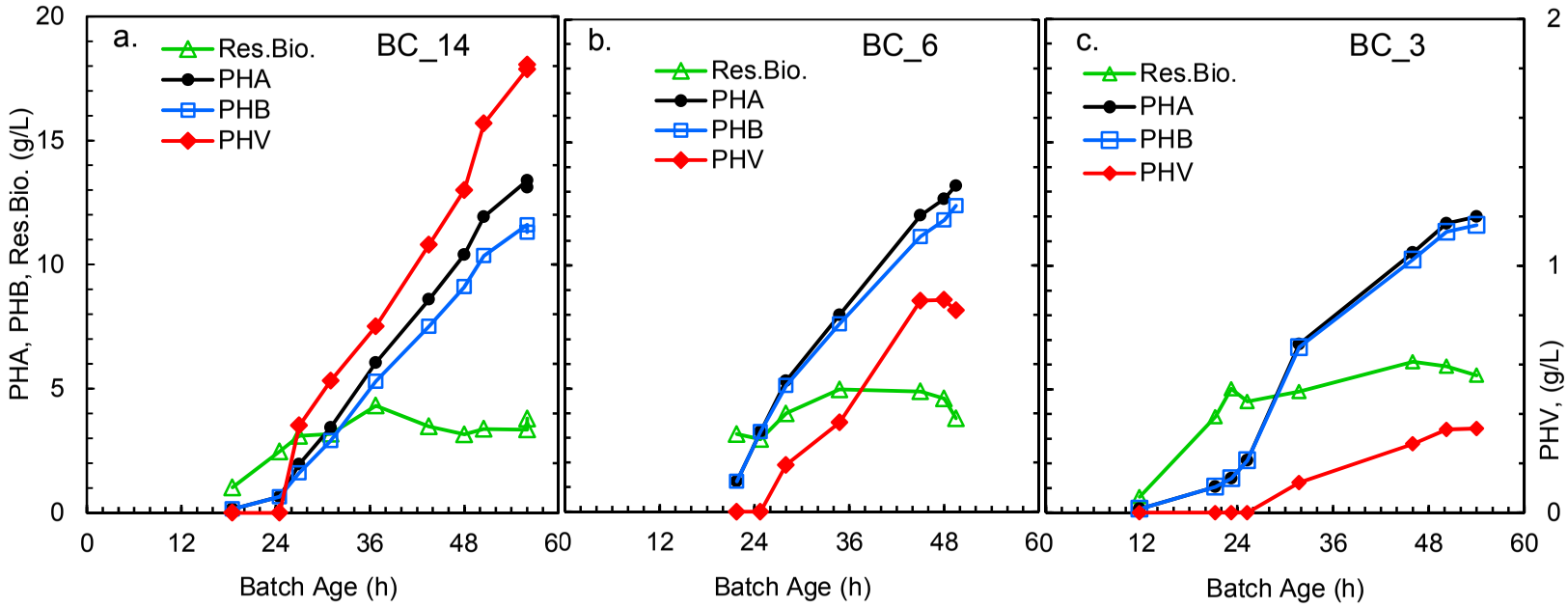

Figure 6.4 Productivity data for block-copolymer batches.
a.) BC_14, **b.)** BC_6, **c.)** BC_3.

In order to test the effect of PHV fraction on the copolymer properties we prepared three different batches by the same biosynthesis procedure. BC_14 received shots of 100 μL valeric acid, BC_6 received shots of 60 μL, and BC_3 received shots of 30 μL. Productivity data for BC_6 and BCP_3 are also shown in **Figure 6.4** In **Table 6.1,** values for the specific, mass productivity of polymer synthesis ($\bar{P}$ [=] g PHA/ g Residual Biomass / h) are averaged for the period of polymer synthesis beginning with the onset of valeric acid addition through the end of the batch. Values for the volumetric, mass productivity (P_v [=] g PHA/L/h) are calculated as the maximum PHA titer produced divided by the batch age at that value The values for polymer composition are given in units of wt.% and represent the polymer composition measured for the highest PHA titer.

In a related study Tanaka et al.[382] demonstrated autotrophic production of PHB in a high cell-density cultivation, achieving 91 g/L of CDW and 61 g/L of PHB in 40 h. The 1-L culture was fed using a gas mixture in which O_2 was maintained below 6 mol% and employed a doughnut-shaped, wire basket to create turbulence inside the vessel. At conditions of 700 RPM and 2 L/min gas feed-rate, the reactor produced a maximum $K_l a$ = 2970 h^{-1}. While the volumetric, mass productivity reported by Tanaka et al. , P_v = 1.55 g PHB/L/h , is much greater than the values observed in our system, P_v = 0.22-0.36, the specific, mass productivity $\bar{P}$ = 0.10 g PHB/g Residual Biomass/h of their batch is very similar to values that we report, $\bar{P}$ = 0.06 – 0.13.

Table 6.1 Productivity data for all autotrophic batches.

	VA Shots	VA Feed	Final Age	CDW	PHA	Res. Bio.	PHA Content	PHA Composition		PHA Productivity	
								y_{PHB}	y_{PHV}	P_{vol}	$\bar{P}$
	(µL (#)	$\left(\frac{\mu L}{h}\ (h)\right)$	(h)	(g/L)	(g/L)	(g/L)	$\left(\frac{g\ PHA}{g\ CDW}\right)$	$\left(\frac{g\ PHB}{g\ PHA}\right)$	$\left(\frac{g\ PHV}{g\ PHA}\right)$	$\left(\frac{g\ PHA}{L \cdot h}\right)$	$\left(\frac{g\ PHA}{g\ Res.\ Bio. \cdot h}\right)$
HP_0	–	–	48.5	23.1	17.5	6.7	0.76	1.0	0.0	0.36	0.10
BC_3	30 (30)	–	54	17.6	12.0	5.6	0.68	0.97	0.03	0.22	0.06
BC_6	60 (30)	–	50.5	17.0	13.2	3.8	0.78	0.94	0.06	0.26	0.11
BC_14	100 (30)	–	56	16.8	13.2	3.6	0.79	0.86	0.14	0.24	0.12
RC_9	–	100	54	20.4	17.1	3.3	0.84	0.91	0.09	0.31	0.13
RC_49	–	793	51	20.3	15.7	4.6	0.78	0.51	0.49	0.31	0.12
RC_55	–	600	55	19.4	14.3	5.1	0.73	0.45	0.55	0.26	0.09
RC_45	–	830	27.5	6.4	2.3	4.1	0.36	0.55	0.45	0.08	0.07

Inferring Polymer Structure via Analysis of Off-gas Composition

According to the modeling prediction of Mantzaris et al., when the time span of VA co-feeding is 33% of the polymer synthesis period, the resulting polymer contains equal length blocks of both PHB homopolymer and PHB-co-PHV copolymer with the PHB-co-PHV blocks containing ~50 mol% PHV. In the block copolymers synthesized by Pederson et al. the authors maintained this 33% VA feeding ratio, but adjusted the length of the overall dosing cycles, e.g. 24 min, 30 min, 42 min, or 96 min. This was done to control the fractional composition of distinct polymer chains, which Mantzaris et. al predicted would include di-block copolymes, tri-block copolymers, and separate chains of both PHB homopolymer and PHB-co-PHV random copolymer.

In contrast, our experiment was designed to produce an equivalent distribution of polymer types (i.e. same fraction of homopolymer, di-block, and tri-block copolymers) in each material by conducting each batch with the same 60-min dosing cycle. Instead we intended to vary the fractional length of the PHV-co-PHB blocks by administering different sized shots of valeric acid, e.g. 30 uL, 60 uL, and 100 uL, at the start of each cycle. This resulted in copolymers with PHV wt. fractions of 0.03, 0.06, and 0.14. Ideally, our goal was to synthesize each block-copolymer so that the composition of the PHV-co-PHB domains would be identical for all three materials, with variation only in the relative length of their PHV-co-PHB block domains. **Figure 6.5**. shows the size and duration of oxygen-uptake spikes produced during valeric acid shots for each of the three block-copolymer batches. While the batch productivity data in **Figure 6.4** implies that PHV fraction increases continuously throughout the biosynthesis, the discrete nature of the off-gas peaks indicates that valeric acid metabolism occurs for only a few minutes following each shot. Peak statistics for each batch are presented in **Table 6.2**.

For analysis of the data we define the following variables. $\Delta h_v^{O_2}$, $w_v^{O_2}$, and $\Delta a_v^{O_2}$ describe the average height [mmol O_2/L/h], width [min], and area [mmol O_2/L], respectively, of the oxygen uptake spikes produced during the consumption of valeric acid shots. More accurately, $\Delta h_v^{O_2}$ and $\Delta a_v^{O_2}$ are the changes in the total OUR

height and area taken in reference to the baseline OUR value at the time of the shot (hence their designation as Δ values). The baseline value is calculated as an average of the OUR values observed immediately before and after the peak. Within each valeric acid shot cycle, w_{pv} [min] represents the time period during which valeric acid is not present in the media. This period starts when the valeric acid of the first shot is totally consumed and ends with the dosing of the subsequent shot. For all three block-copolymer batches prepared in this study $w_v + w_{pv} = 60$ min. If we define N_{tot} as the average, degree of polymerization of block-copolymer chains, and N_{PHBV} as the number of monomer units within a sub-domain of PHB-co-PHV, then $f_{PHBV} = N_{PHBV}/N_{tot}$ [molecule/molecule] denotes the average, length fraction of the PHB-co-PHV block within the entire polymer chain. x_{PHV}^{bulk} is the mole fraction of PHV in the bulk polymer, estimated experimentally by GC-FID, and x_{PHV}^{block} is the mole fraction of PHV within individual block domains of PHB-co-PHV. The estimation of is described below.

If information for the simultaneous, molar synthesis rates of each polymer type is known then it is possible to estimate the value of x_{PHV}^{block}. Kelley et al. showed that when both fructose and valeric acid are present in the media, the molar synthesis of PHB and PHV in *R. eutropha* are approximately equal, but when valeric acid is absent and only fructose is present, PHV synthesis stops but the molar synthesis rate of PHB is unchanged[177]. In Kelley's work synthesis rates were measured during extended periods of VA uptake; however, we note that due to the short time period over which valerate addtions are made (< 15 min) it may be that the kinetics of PHV synthesis do not reach the same steady stave values observed under prolonged feeding. Thus to calculate the polymer synthesis rates during short-time does, we perform a mass balance including the mass of VA added for each shot, the corresponding change in CO_2 uptake during this period, and the average molar synthesis rates of PHB and PHV determined over the entire shot period. Furthermore, with knowledge of the simultaneous molar synthesis rates of each polymer type it is also possible to estimate the fractional length of PHB-co-PHV domains within the block-copolymer molecule.

Values for f_{PHBV}, x_{PHV}^{bulk}, and x_{PHV}^{block} are given in **Table 6.2**, and a corresponding graphical illustration of the block-copolymer molecules in each batch is given in **Figure 6.6.** While BC_14 and BC_6 have are estimated to have similar values of x_{PHV}^{block} of 30 mol% PHV, the x_{PHV}^{block} estimated for BC_3 is much smaller at 16 mol% PHV. We see that as the size of the valeric acid doses decreases, the value of x_{PHV}^{block} also decreases. To explain this disparity, we speculate that for BC_3 the concentration of valeric acid in the media was so low that the uptake rate fell below the V_{max} (concentration-invariant limit) of the uptake system. Because the uptake rate is presumably lower, a greater amount of time is required to consume the smaller doses, thereby reducing the value of x_{PHV}^{block}. Additionally, numerical integration of the area under each oxygen-uptake peak gives information about the stoichiometry of valeric acid conversion, indicating that ~1 mole of oxygen is consumed per 1 mole of valeric acid.

For future studies, controlling the PHV fraction with the copolymer domains could be better accomplished by administering VA shots as small periods of continuous feeding within each hourly cycle, e.g. 10 μL/min for 10, 6, or 3, thereby providing an equal VA concentration to all batches. Physical and mechanical properties of the different block-copolymers are presented in a subsequent section.

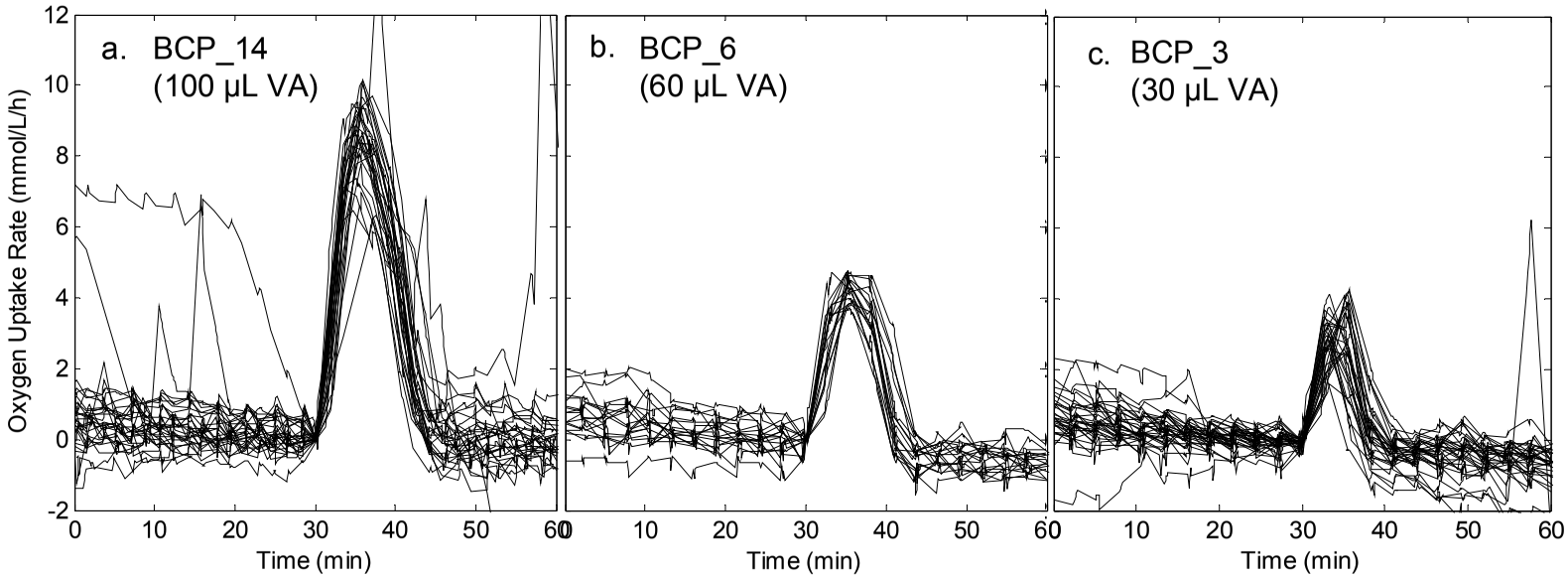

Figure 6.5 Collection of oxygen uptake spikes for each block-copolymer batch.
The data shows the oxygen-uptake peaks produced during valeric acid addition to block-copolymer batches. **a.** BC_14, **b.** BC_6, **c.** BC_3. (shot size (µL) of valeric acid (VA))

Table 6.2 Statistics of Oxygen Uptake Peaks from Valeric Acid Doses

	VA Shots	O_2 uptake spikes			CO_2 evolution spikes	Post-VA CO_2 Uptake Rate	Post-VA Period	Avg PHB Rate	Avg PHV Rate	PHBV Length Fraction	PHV Mole Fraction	
	Batch Conc.	$\Delta h_v^{O_2}$	$w_v^{O_2}$	$\Delta a_v^{O_2}$	$\Delta a_v^{CO_2}$	$h_{pv}^{CO_2}$	w_{pv}	N_{avg}^{PHB}	N_{avg}^{PHV}	f_{PHBV}	x_{PHV}^{bulk}	x_{PHV}^{block}
	$\left(\frac{mmol}{L}\right)$	$\left(\frac{mmol}{L \cdot h}\right)$	(min)	$\left(\frac{mmol}{L}\right)$	$\left(\frac{mmol}{L}\right)$	$\left(\frac{mmol}{L \cdot h}\right)$	(min)	$\left(\frac{mmol}{L \cdot h}\right)$	$\left(\frac{mmol}{L \cdot h}\right)$	$\left(\frac{\#\ PHBV}{\#\ PHA}\right)$	$\left(\frac{mol\ PHV}{mol\ PHA}\right)$	$\left(\frac{mol\ PHV}{mol\ PHA}\right)$
BC_3	0.27	3.2 ±0.7	9 ±2	0.26 ±0.07	0.07 ±0.04	20.9	51	4.0	0.13	0.17	0.026	0.16
BC_6	0.54	4.3 ±0.4	12 ±1	0.51 ±0.05	0.14 ±0.05	19.2	48	4.2	0.40	0.26	0.052	0.30
BC_14	0.91	8.6 ±1.1	15 ±1	1.11 ±0.15	0.64 ±0.17	20.4	45	4.0	0.51	0.29	0.123	0.30
[a]BC_17†	na	na	8	na	na	na	16	na	na	0.5	0.15	0.50
[a]BC_25†	na	na	32	na	na	na	64	na	na	0.5	0.23	0.50

[a] References: [20, 210]

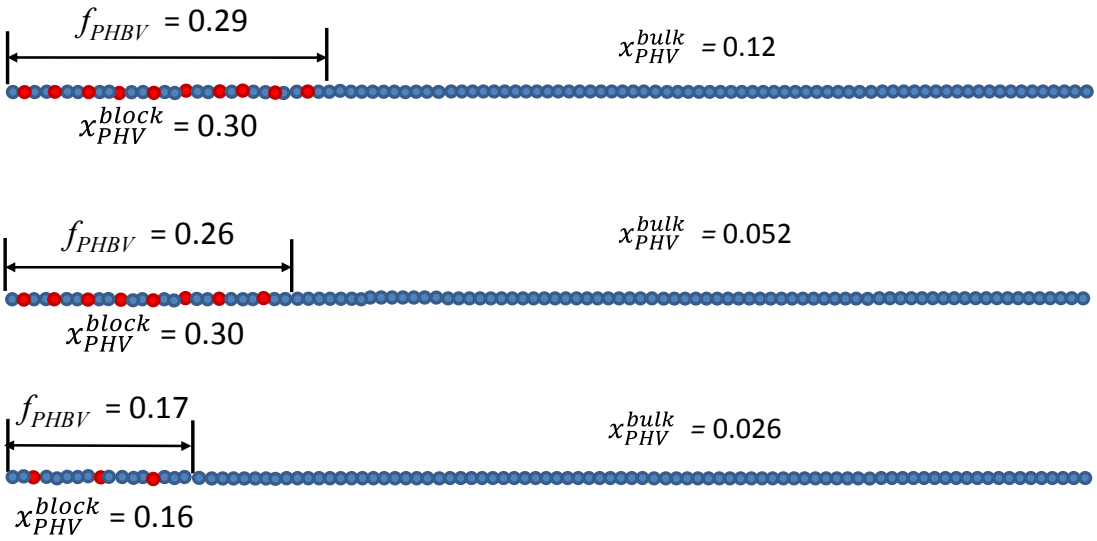

Figure 6.6. Illustration of Polymer Structures Predicted from Oxygen-Uptake Peaks

A reduction in the size of valeric acid shots causes a decrease in both the predicted size and composition of the PHB-co-PHV domains of the block-copolymers. Illustrations are drawn to scale with respect to both l_f and x_{PHV}^{block} . a.) BC_14, b.) BC_6, and c.) BC_3 In this illustration, PHB-co-PHV domains are shown to exist at the terminus of the molecule; however, due to the continual occurrence of polymer termination and re-initiation that occur throughout the batch, a distribution of molecules is expected in which the average position of the center of the PHB-co-PHV domain is located at center of the polymer molecule.

Synthesis of Random Copolymers and PHV Homopolymer

In order to understand how monomer composition can affect the behavior of block-copolymers, it is important to first understand its effects in simple, random copolymers. For comparison with block-copolymer batches, we synthesized the random copolymer RC_9 by feeding the same total volume of valeric acid used for BC_14, but with a constant feed rate during the entire polymer synthesis phase, i.e. 100 µL/hr between 24-54 h. Despite having the same average feeding rates, the PHV composition of RC_1 was only 9 wt.% versus 14 wt.% for BC_1. This suggests that when the media concentration of valeric acid is lower, the fraction that is converted to PHV is decreased.

In batches RC_49, RC_55, and RC_45 we wanted to synthesize random copolymers with a higher fraction of PHV similar to the compositions we predicted for the PHV-co-PHB block-domains of BC_14. More specifically, we were interested in the types of polymer formed when valeric acid was used as the primary carbon substrate. In a related study involving *R. eutropha*, Jackson and Srienc[375] reported the synthesis of PHA with 88 mol% PHV using valeric acid as the sole carbon source, in nitrogen-free media, under an atmosphere of H_2:O_2 = 80:20. Conversely, when an atmosphere of air was used, the polymer produced from VA contained only 43 mol% PHV. However, when nitrogen was present in the media, Doi et al.[383] reported a much higher PHV fraction of 75% in the presence of air, using valeric acid as the sole carbon source. Additionally, Volova et al.[373] reported the synthesis of PHA with up to 88 mol% PHV by supplying valeric acid under an atmosphere of H_2:O_2 = 66:22:11. With the variety of results reported, we wanted to better understand how the interplay VA feed-rate and the availability of CO_2 and O_2 gases affected the PHV composition of the copolymers, with the ultimate goal of identifying process conditions for the synthesis of PHV homopolymer.

As an initial target for the VA feed rate we calculated the value in order to match the molar synthesis rate observed for PHB in batch HP_0, ~7.7 mmol/L/h. While this value was used as an initial target, our intended plan was to actively control the feed-rate of VA in order to maintain the net CO_2 uptake rate at zero during the PHA production

phase. As a result, the instantaneous feed-rate of VA was adjusted at several times during the batch.

Figure 6.7shows the productivity data for the three different random copolymer batches. Tabular values of polymer composition and productivity are given in **Table 6.1.** In **Table 6.3** we give data for the molar, volumetric productivity (N_V [=] mmol / L /h) of each polymer type during the time-period when the rate of PHV synthesis was at its maximum. Based on the relative rates we can estimate the molar PHV fraction (z_{PHV}^{bulk}) of the copolymer produced during this time ($z_{PHV}^{bulk} = N_V^{PHV}/(N_V^{PHV} + N_V^{PHB})$). However, because PHB synthesis often started a few hours before the onset of VA addition, and because the relative PHB/PHV synthesis rates did not remain constant throughout the batch, the molar composition of PHA calculated in **Table 6.3** is not equivalent to the molar composition in **Table 6.2.**

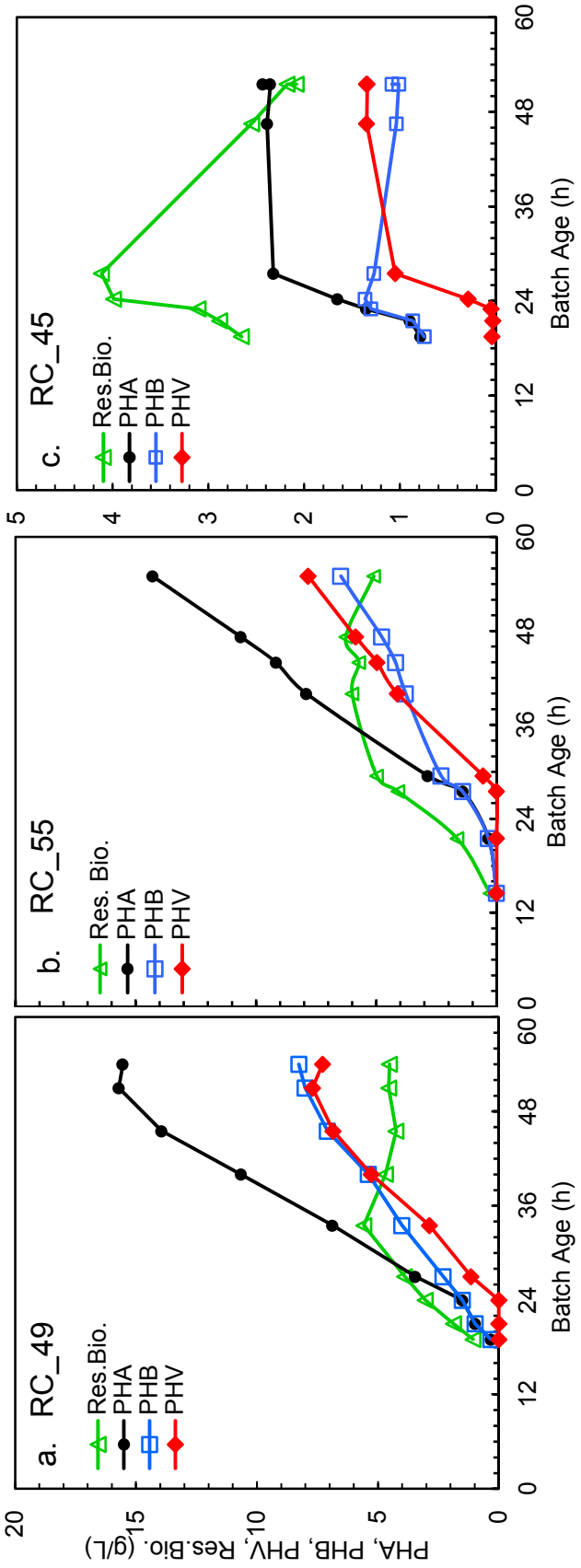

Figure 6.7 Productivity data for random copolymer batches
a. RC_49, **b.** RC_55, **c.** RC_45

Table 6.3 Polymer Synthesis Rates under Varying Process Conditions

	Avg. Feed Rate Valeric Acid	Gas Composition		Time Period	Polymer Synthesis Rates		[a]PHV Fraction
		CO_2	O_2		N_V^{PHB}	N_V^{PHV}	z_{PHV}^{bulk}
	$\left(\frac{mmol\ VA}{L \cdot h}\right)$	mol %		h	$\left(\frac{mmol}{L \cdot h}\right)$	$\left(\frac{mmol}{L \cdot h}\right)$	$\left(\frac{mol\ PHV}{mol\ PHA}\right)$
HP_0	0	10	10	28-49	7.7	0	0.0
RC_9	0.9	10	10	24-35	6.7	0.8	0.11
RC_49	7.2	10	10	24-46	3.0	3.2	0.51
RC_55	5.5	0	10	28-44	1.5	3.3	0.68
RC_45	7.6	0	<5	23-28	0	2.2	1.0

[a] PHV mole fraction (relative rate of PHV synthesis) : $z_{PHV}^{bulk} = N_V^{PHV}/(N_V^{PHV} + N_V^{PHB})$

Impact of Substrate Degree of Reduction on Copolymer Composition

In batch RC_49 the feed rate of VA was maximized while the composition of O_2 and CO_2 in the feed gas was kept the same as in batch RC_9. Adjustments in the VA feed-rate were made to maintain the maximum rate of addition, while avoiding CO_2 emissions due to overfeeding. Under these conditions, the relative PHV fraction (z_{PHV}^{bulk}) was 51 mol %. In an ideal conversion the molar synthesis rate of PHV should be equal or close to the feed rate of valeric acid. However, the numbers in **Table 6.3** indicate that for RC_49 more than half of the valeric acid supplied was degraded and presumably converted into precursors for PHB. Compared to RC_9, the rate of PHB synthesis in RC_49 is cut by more than 50%, simply by increasing the feed rate of valeric acid, thus indicating that when co-feeding high levels of VA under autotrophic conditions, the cell must reduce its rate of PHB synthesis to accommodate the increase in PHV synthesis. This non-additive quality of copolymer production implies the presence of a flux limitation in some reaction that is common to both polymer synthesis pathways e.g., PhbA, PhbB, PhbC, or the oxidative phosphorylation pathway. However, Kelley and Srienc[177] observed that when valeric acid was depleted from heterotrophic media containing both valeric acid and fructose, the accumulation of PHV ceased but the rate of PHB synthesis was unchanged, thus indicating that the rates of PhbA, PhbB, and PhbC were not limiting in the presence of the additional 3HV-CoA flux.

Because PHV is more electrically reduced than PHB, the conversion of valeric acid, which is more highly reduced than PHV, into PHB requires that either more CO_2 or O_2 must be consumed to absorb the excess electrons produced. This is compared to the alternative in which the excess reducing power is stored primarily in the form of PHV. Thus, we speculated that by limiting the supply of electron acceptors from either CO_2 or O_2 we might force the cells to convert more of the valeric acid to PHV.

In batch RC_55, we tested this hypothesis by eliminating the supply of CO_2 concurrent with the start of VA feeding. While this manipulation did not create a significant increase in the molar synthesis rate of PHV, it did decrease the rate of PHB synthesis by ~50%; thus, z_{PHV}^{bulk} was increased to 68 mol%.

In batch RC_45 we further restricted the supply of electron acceptors during VA feeding by eliminating CO_2 and reducing the composition of O_2 in the feed gas to ~4 mol% after 24 h. Note: under normal operation, O_2 in the feed-gas was set at 5 mol% at the start of the batch but was quickly raised to 10 mol% and left at this level for the remainder of the batch. Before the restriction of gas supply, PHB synthesis occurred rapidly, but afterward the extreme deprivation of electron acceptors resulted in a total cessation of PHB synthesis. Conversely, the production of PHV still occurred, albeit at a reduced rate of ~67% compared to conditions of normal O_2 composition. This period of PHV homopolymer synthesis continued for ~4.5 h until we further reduced the O_2 composition to 2.4 mol%. This change had the unintended consequence of drastically and irreparably reducing all cell growth, despite an attempt one hour later to resuscitate the culture by increasing the O_2 composition back above 4 mol%.

Taken together, these five batches suggest that under mixotrophic conditions a negative correlation exists between the redox potential of the feed substrates and the rate of PHB synthesis by the cells. An increase in the redox potential of the feed substrates can be made by either increasing the supply of H_2 or VA or by decreasing the supply of CO_2 or O_2. However, a strong correlation between increasing redox potential and the rate of PHV synthesis is not observed. Furthermore, the maximum synthesis rate observed for PHB is N_V^{PHB} = 7.6 mmol/L/h, is more than double the maximum synthesis rate observed for PHV is N_V^{PHV} = 3.3 mmol/L/h. If this disparity were a sign of kinetic limitation at an enzyme common in both polymer synthesis pathways e.g. PhbA, PhbB, or PhbC, we would expect to see a clear, negative correlation between N_V^{PHB} and N_V^{PHV} at every point, but this is not the case. Rather, the plateau seen in N_V^{PHV}, even as N_V^{PHB} continues to decrease, suggests that the limitation in PHV synthesis occurs either in the fatty-acid degredation pathway or in the electron transport chain that must oxidize the extra $FADH_2$ produced from VA. Ultimately, the data indicate that under mixotrophic conditions, production of a PHV homopolymer can be achieved by increasing N_V^{PHV} with VA feeding while at the same time reducing the rate of N_V^{PHB} by restricting the availability of O_2 and CO_2 in the feed gas.

One caveat to our line of experimentation is that we did not probe for the possibility that O_2 limitation alone might yield PHV homopolymer. We expect that under conditions of high redox potential, the conversion of CO_2 to PHV, instead of PHB, would be the preferred pathway for maintaining a balanced redox state within the cell.

Polymer Properties

Physical and mechanical properties for the different polymer samples are presented in **Table 6.4**. Among the eight different polymer batches conducted for this study, seven of them were extracted and purified: RC_45 was not processed past biosynthesis due to its low yield. Given that the reported tensile strength of PHV homopolymer[215] is 37% that of PHB homopolymer and that both polymers are similarly brittle, it is not intuitive that a combination of these two monomer types should yield an enhanced material. The behavior of these homopolymers is attributed mainly to their ability to form highly crystalline matrices, which imparts great strength but also brittleness.

Compared to the PHB homopolymer HP_0, all three random copolymers show reduced modulus (*E*) and ultimate strength (U) but improved elongation at break (ε_b). In RC_9 a small amount of PHV commoner produces a small increase in the elongation of the polymer (6%), but when the PHV content is near 50% as in RC_49 and RC_55 the elongation at break is increased dramatically (1568% and 960% respectively). This is consistent with the known effect of comonomer incorporation leading to a reduction in polymer crystallinity[270]. With the increases in molecular heterogenity, the polymer becomes more amorphous, thereby changing the nature of the material from one dominated by crystallinity and brittleness to one dominated by a network of polymer entanglements and viscous deformation upon yielding.Another indication of the reduced crystallinity in RC_49 and RC_55 is their greater optical transparency, when compared to the other polymer samples.

As a caveat to the data, we note that the the molecular weight of the HP_0 sample is significantly lower than all the other polymer samples tested. For polymer polymer extraction lyophilized cell pellet was continually stirred in chloroform at 25 °C for 12 hours; however, HP_0 was extracted at 60 °C for 48 h, likely leading to polymer degradation. If the molecular weight of HP_0 had been more similar to that of the other polymers, it is likely that both its U and ε_b would have been higher.

For the block-copolymer samples, a different effect is observed. Similar to the random copolymers, the addition of PHV comonomer causes a reduction in *E* and an

increase in ε_b; however, unlike the random copolymers, both BC_3 and BC_14 show a noticeable increase in U. We attribute this effect to the presence of the distinct polymer heterodomains within the block-copolymers, which allow for the simultaneous existence of crystalline PHB domains along with more amorphous domains of PHB-co-PHV copolymer. Thus, the block-copolymer arcthitecture permits combination of high-strength PHB domains along with elastic PHB-co-PHV domains. For BC_6, which has a high *E* but low U and ε_b, we speculate that this polymer sample may contain an especially high fraction of PHB homopolymer blended with the block-copolymer molecules. This is based on inspection of productivity data for BC_6 in **Figure 6.4.b** that shows the accumulation of a significant amount of PHB before the onset of PHV synthesis as well as a second period of PHB-only synthesis at the end of the batch. Based on this data we estimate that BC_6 may contain up to 33 wt.% of PHB homopolymer, which could explain the high modulus and smaller elongation at break for this sample.

Also shown in **Table 6.4** are the mechanical properties of PHB-co-PHV polymers prepared by Pederson et al.[210] and further evaluated by McChalicher and Srienc[20]. These include two random copolymers, RC_9† and RC_32†, and two block-copolymers, BC_17† and BC_25†. (Here, the symbol † is used to denote the prior study.) Compared to the block-copolymers synthesized in the present study, BC_17† and BC_25† show reduced values for *E* but with much greater values for ε_b. For example between BC_14 and BC_17† , the *E* values differ by 3.9x, but the ε_b of BC_17† is 9.5x larger. One explanation for this difference could simply be that the added PHV content in these samples leads to a material that is more amorphous an hence more elastic, similar to RC_49. However, it peculiar that the RC_9 in the present study has a modulus value that is 3.5x higher (0.760 GPa) than RC_9† (0.220 GPa) even though both polymers have the same PHV content. In addition, both samples show the same value for ultimate strength (19 MPa), even though the reported molecular weight (M_n) is >3x higher for RC_9† than for RC_9—typically ultimate strength increases as the polymer chain length increases. Concerning this disparity, we note that the polymer films prepared by McChalicher and Srienc were prepared from solution using 1,2,4-trichlorobenze (TCB) (bp. 214 °C) as the solvent followed by a 1-h annealing period at 135 °C. In the present study, films were

prepared by melt-press at temperatures between 170-180 °C followed by rapid cooling. Prior to this, the polymers were precipitated in chlorform (bp. 60 °C) / methanol (bp 65 °C) (1:7 v/v) and dried in a vacuum oven over-night to ensure the removal of excess solvent. Thus, given the low volatility of TCB, thereby making it more difficult remove from the polymer films, we question if some residual solvent may have acted as a plasticizer in the these films, thereby softening the polymers and increasing their ε_b. Furthermore, others have also reported that solution-cast films exhibit higher values of ε_b when compared to melt-pressed films.[384]

For random copolymers, the mol% PHV in individual polymer chains is expected to be the same as in the bulk material (x_{PHV}^{bulk}). However, for block-copolymer molecules the measured value of x_{PHV}^{bulk} is expected to significantly underrepresent the mol% of PHV within the PHV-co-PHB domains (x_{PHV}^{block}) (An explanation for the calculation of x_{PHV}^{block} was presented in **Table 6.2**) Consequently, we expect the physical and mechanical properties of the block-copolymer to be more of a reflection of x_{PHV}^{block} than of x_{PHV}^{bulk}. Given the very large values of ε_b observed for RC_49 and RC_55 it seems logical that block copolymers with x_{PHV}^{block} values approaching 50 mol% would show the greatest elongation before break.

Table 6.4 Physical and Mechanical Properties of PHA Polymers

	x_{PHV}^{bulk}	M_w	M_n	PDI	T_g	T_m	t_a	Film Type[a]	x_{PHV}^{block}	E	U	ε_b	Clarity[b]
	$\left(\frac{mol\ PHV}{mol\ PHA}\right)$	(kDa)	(kDa)	$\left(\frac{M_w}{M_n}\right)$	(°C)	(°C)	(days)	–	$\left(\frac{mol\ PHV}{mol\ PHA}\right)$	(GPa)	(MPa)	(%)	–
HP_0	0.0	51	21	2.47	5.9	178.5	?	melt	0.0	1.5	23	2.6	opq
BC_3	0.026	115	33	3.53	4.2	171.8	19	melt	0.10	0.493	31	9	opq
BC_6	0.052	126	30	4.21	1.4	167.2	19	melt	0.16	0.769	21	5	opq
BC_14	0.123	170	47	3.59	1.2	166.1	19	melt	0.31	0.613	32	11	opq
BC_17[c]	0.15	198	99	2.0	-8, 7	142	19	soln.	0.30	0.215	22	105	–
BC_25[c]	0.23	224	107	2.1	-5, 6	125	19	soln.	0.46	0.110	14	170	–
RC_9	0.08	112	30	3.70	1.5	159.5	19	melt	0.08	0.760	19	6	opq
RC_49	0.45	149	51	2.95	-6.3	71.7, 172.5	19	melt	0.45	0.072	11	1568	tpt
RC_55	0.51	162	45	3.64	-8.1	68.0, 181.3	19	melt	0.51	0.114	11	960	tlt
RC_9[c]	0.08	216	108	2.0	10	151	19	soln.	0.08	0.220	19	10	–
RC_32[c]	0.29	198	99	2.0	-10	87	19	soln.	0.29	0.190	17	15	–

Symbols: x_{PHV}^{bulk} (fraction of PHV in the bulk sample), x_{PHV}^{block} (fraction of PHV in PHV-co-PHB block), M_w and M_n (weight and number average molecular weight), PDI (polydispersity index = M_w/M_n), T_g (glass transition temp.), T_m (melting temp.), t_a (sample age time) *E* (Young's modulus), U (ultimate strength), ε_b (elongation at break),

[a] Films prepared by either melt-press or solution-casting.

[b] Clarity: opaque (opq), transparent (tpt), semi-transparent / translucent (tlt)

[c] Reference: [20, 210]

Metabolic Model

To better understand the metabolic factors affecting the balance of PHB and PHV biosynthesis during mixotrophic growth we constructed a simplified metabolic model based on reactions known to occur in *R. eutroha*. The model includes reactions for hydrogen uptake, carbon fixation via the Calvin cycle, the TCA cycle, oxidative phosphorylation, valeric acid degradation, PHB/PHV synthesis, and various other fermentation byproducts. Details of the model are included in the Supporting Information. More specifically, we were interested in exploring the question of how the conversion of valeric acid to PHV occurs differently between purely heterotrophic conditions versus mixotrophic conditions. To study this we prepared two versions of the model, one which included the Calvin cycle for carbon fixation and hydrogenase reactions for consuming hydrogen, and one in which these reactions were deleted.

Elementary Mode Analysis

We investigated the model using the framework of elementary mode analysis[274]. An "elementary mode" describes one, unique, overall, reaction that converts a specific stoichiometry of external reactants, e.g. H_2 O_2, CO_2, NH_3, and valeric acid, to a specific stoichiometry of external products, e.g. biomass, PHB, PHV, CO_2, acetic acid, lactic acid, etc. While each elementary mode is formed from a linear combination of internal reaction equations, the elementary modes themselves are a minimal set of linearly-independent vectors. Thus, the product metabolites synthesized by a cell, given any set of reactant metabolites, can be computed from a linear combination of elementary modes.

Of all the elementary modes that can be computed for a reaction network, not all modes may be relevant to the question at hand. In evaluating each mode for selection, we considered only modes that 1.) produce PHV, PHB, or both, 2.) consume valeric acid, and 3.) produce no biomass. We then analyzed the modes according to their PHV mol% (PHV/(PHV+PHB), versus their relative consumption of H_2, O_2, and CO_2. **Figures 5.8.a,b,c** show data for the mixotrophic model, while **Figures 5.8.d,e,f** show data for a simulated heterotrophic conditions in which the Calvin cycle and hydrogenase reactions

are removed. The figures convey both the PHV mol% of each mode as well as its location in the space of H_2, O_2, and CO_2 uptake rates. Because mixotrophic conversion combines the autotrophic capacity for CO_2 uptake with the heterotrophic capacity for CO_2 generation from valeric acid degredation, scaling the individual gas rates according to the corresponding VA rate is necessary for understanding the relative balance between the two types of carbon cycles. In **Figures 5.8.c,f** we see that both the mixtotrophic and the heterotrophic models contain modes that produce PHV homopolymer in addition to PHB homopolymer as well as modes, which simultaneously produce both polymer types. As a result, copolymer synthesis can occur either by a single "mixed" mode or from a combination of PHB and PHV homopolymer modes. Comparing **Figures 5.8.a,b** to **Figures 5.8.d,e** we see that the main effect of adding hydrogen to the metabolism is in creating a 3-dimensional synthesis space versus the 2-dimensional synthesis space of the heterotrophic case. Due to the dense clustering of both PHB and PHV modes seen in **Figures 5.8.d,e** the production of a PHV homopolymer is less likely to occur at a particular operating location. However, in **Figure 6.8.a** we see that under mixotrophic conditions a new grouping of modes emerges which shows strong separation in the H_2-versus-CO_2 space; thus, it becomes possible to find PHV homopolymer modes which are more isolated from the effects of PHB producing modes. Especially interesting is the large group of densely clustered PHV modes that occur at ~2 mol CO_2 / mol VA. We expect that with a greater mode density, PHV production should be even more robust to small deviations in process conditions. Moreover, in **Figures 5.8.a,b** we see that with the addition of hydrogen, the PHV homopolymer modes that show good separation in the O_2-versus-CO_2 space gain even greater separation from PHB homopolymer modes with their extension into the H_2-versus-CO_2 space.

Using a less mathematical explanation: the addition of hydrogen during valeric acid consumption allows for the creation of a more highly reduced redox state, especially when the concentration of oxygen acceptors like CO_2 or O_2 are controlled at low levels. As a result, the synthesis of PHV, which is a more highly reduced compound than PHB, becomes a better alternative on an electron-per-carbon basis for regulating the redox state of the cell.

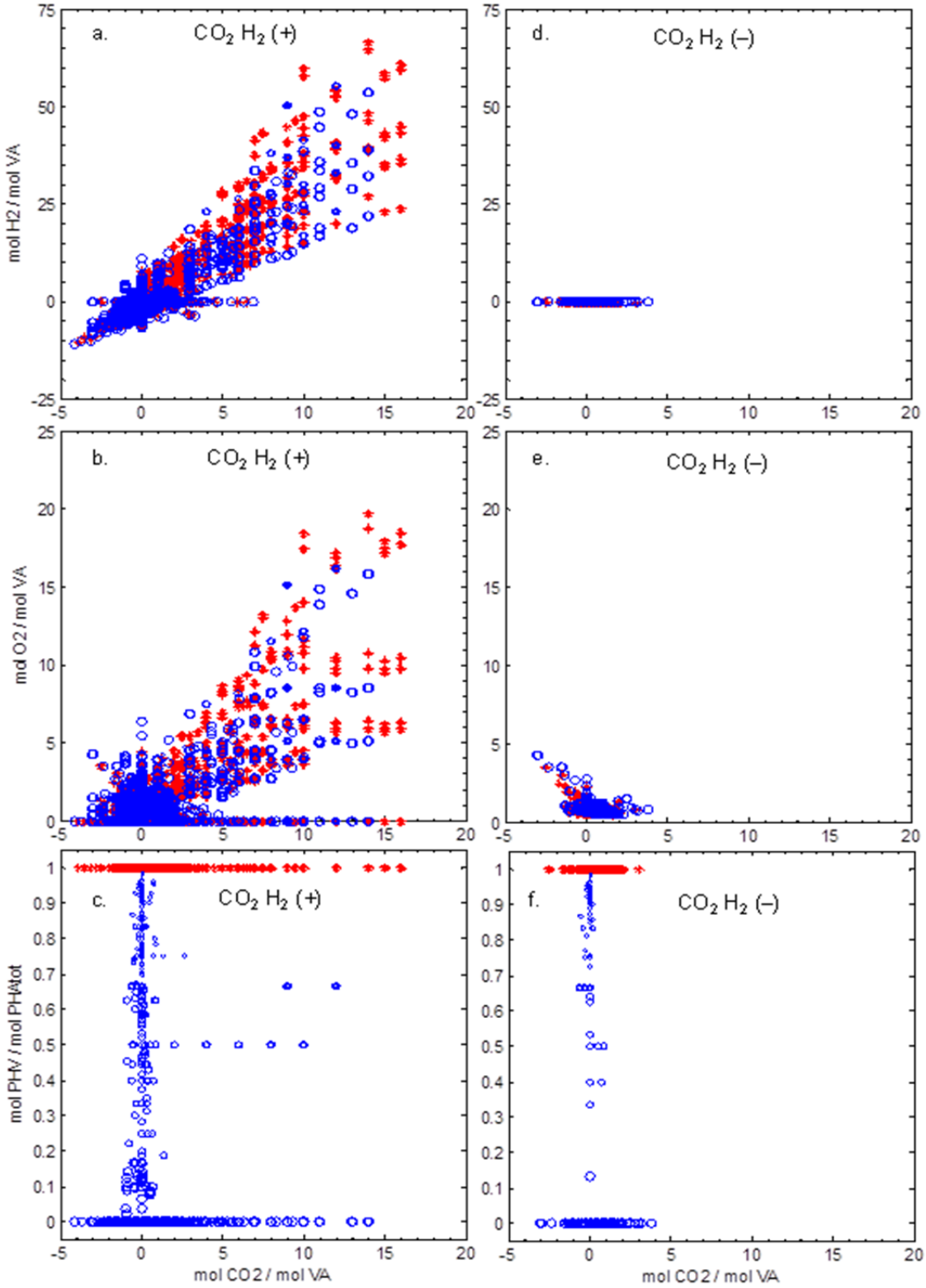

Figure 6.8 Variation in the PHV fraction of polymer produced by specific elementary modes.

Figure 6.8 Variation in the PHV fraction of polymer produced by specific elementary modes.
(see previous page) PHV fraction is given in mol% of total PHA produced. All selected modes satisfy the criteria for 1.) polymer production, from 2.) valeric acid, with 3.) no biomass accumulation. PHV fraction is shown with respect to the relative uptake rates of H_2, O_2, CO_2. All gas uptake rates are normalized by their simultaneous valeric acid uptake rate. The x-axis for all plots shows variation with respect to CO_2 fixation. a.b.c.) Data for the full mixotrophic model. d.e.f.) Data for the mixotrophic model with Calvin cycle and hydrogenase reactions deleted. a.b.) Variation with respect to hydrogen supply. c.d.) Variation with respect to oxygen supply. e.f.) Detailed data for PHV fraction. Modes which produce polymer with 100 mol% PHV(*). Modes which produce polymer with < 100 mol% PHV (o). The perimeter of each (o) marker is proportional to the PHB mol% of the polymer. Positive values indicate gas consumption while negative values indicate gas production.

Stoichiometry of Autotrophic Biosynthesis

Off-gas composition data obtained using online mass-spectroscopy may also be used for determining the stoichiometry and yield of autotrophic conversions. Data for the molar composition of the gas consumed in batch BC_3 is shown in **Figure 6.9**. Variability in the data near 8 h is caused by imprecision in measuring the very small changes in composition between the feed-gas and the off-gas when total gas uptake of the batch is very small due to low cell density. Based on the molar composition data, relative stoichiometries of gaseous substrates are presented in **Table 6.5.** Also included in the table are the estimated, maximum efficiencies for hydrogen utilization (mol H_2 / mol CO_2) computed from the metabolic model we constructed. Values are given for autotrophic growth under both aerobic and anaerobic conditions. For comparison, we have listed the stoichiometry values reported for other studies of autotrophic metabolism in *R. eutropha.*

Anaerobic growth of *Ralstonia eutropha* has been reported, but only with the addition of nitrate and nitrite[385] as external electron acceptors. Nonetheless, our metabolic model suggests that *R. eutropha* does have the potential for anaerobic growth without external electron acceptors. For this to occur, the membrane-bound hydrogenase protein (Mbh), which is highly expressed during autotrophic growth, must be present. This enzyme catalyzes the reversible transfer of reducing equivalents from H_2 to some

form of periplasmic electron carrier. The exact identity of the membrane-bound electron carriers is not known; however, reports have given evidence supporting the utilization of the ubiquinol- ubiquinone (UQH_2-UQ) system[386-387]. In our model we represent the Mbh reaction as $UQ + H_2 \leftrightarrow UQH_2$ which allows anaerobic regeneration of UQ, while relying solely on the soluble hydrogenase (Sh) for the generation of cellular reducing equivalents with the reaction $H_2 + NAD \leftrightarrow NADH$. Normally, under aerobic respiration, the reactions of oxidative phosphorylation, UQ-cytochrome c reductase (Complex III) and cytochrome c oxidase (Complex IV), are coupled to produce the net conversion $UQH_2 + \frac{1}{2} O_2 \rightarrow UQ + 6\ H_{ATP}^{+}$. In this reaction, the 6 H_{ATP}^{+} are periplasmic protons used for energy generation by ATP synthase with the stoichiometry 3 H_{ATP}^{+} + ADP ↔ ATP. Under anaerobic conditions, H_{ATP}^{+} and hence, ATP, are still produced via the electron transport chain using Complex I in the reaction $UQ + NADH \leftrightarrow UQH_2 + 4\ H_{ATP}^{+}$.

Furthermore, a simple species balance shows that anaerobic production of biomass and PHB in *R. eutropha* is indeed feasible using only H_2, CO_2, and NH_3 as substrates. The reaction for biomass[83] is $8.71\ H_2 + 4.09\ CO_2 + 0.76\ NH_3 \rightarrow C_{4.09}H_{7.13}O_{1.84}N_{0.76} + 6.29\ H_2O$, and the reaction for PHB is $9\ H_2 + 4\ CO_2 \rightarrow C_4H_6O_2 + 6\ H_2O$. Moreover, the negative values predicted for the free energy of reaction (ΔG_r) [388-389] indicate that both reactions are thermodynamically favorable at ambient conditions.

Interestingly, the fraction of both O_2 and CO_2 in **Figure 6.9** show significant variation over the course of the batch while that of hydrogen remains essentially constant at ~ 0.66. This observation suggests that during autotrophic metabolism the cell maintains a constant uptake of high-energy, electron donors while adjusting the ratio of electron acceptors O_2/ CO_2 to maximize carbon consumption in the face of increasing energy demands. In the first part of the batch biomass is the predominant product, but upon nitrogen depletion PHB becomes the major product. However, in **Table 6.5** we see that under aerobic conditions, at maximum H_2 efficiency, the CO_2/O_2 ratio for PHB and biomass is the same. Thus, biomass and PHB require the same amount of ATP to drive their synthesis. Nevertheless, the rising ratio of O_2/CO_2 as the batch progresses reflects a

greater energy demand by the cells. We speculate that this is due in part to the increasing amount of PV-work required for polymer production as the intracellular volume becomes more tightly packed with PHB. In addition, the conversion of ATP to polyphosphate, another energy-storing compound utilized by *R. eutropha*, may also contribute to the increasing energy demand. Even under the various conditions of substrate limitation reported by Bongers[372], the fraction of H_2 in the gas consumed showed minimal deviation from the value 0.66.

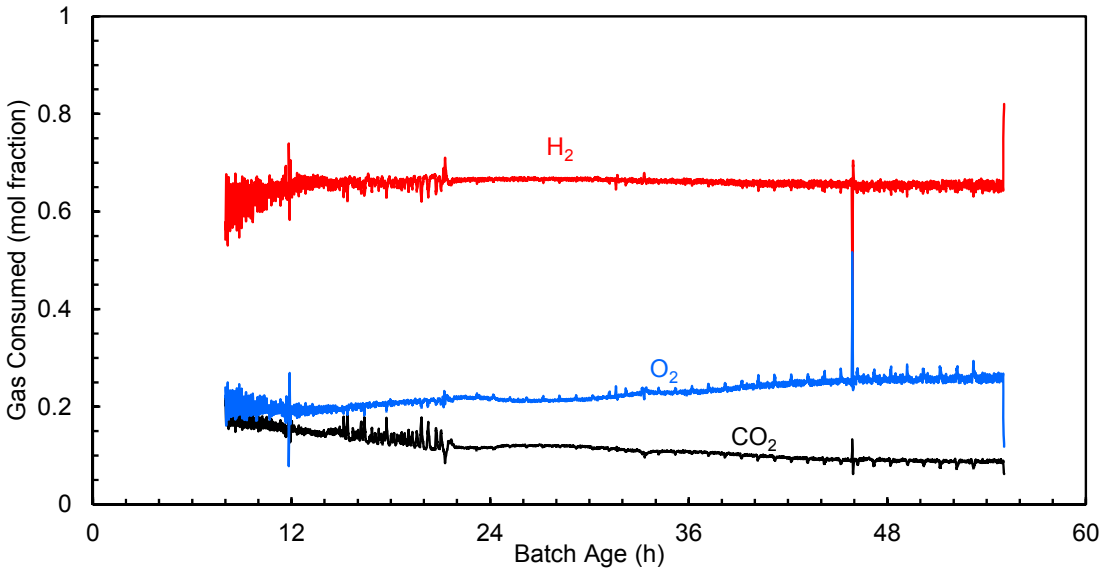

Figure 6.9 Molar composition of gas consumed during mixotrophic biosynthesis. The data shown is for in BC_3. Using this information we can estimate the stoichiometry during synthesis periods for both biomass (10h) and PHB (26 h, 54 h). Values were selected for periods in which VA was not present in the system.

Table 6.5 Stoichiometry of Gas Consumption for Autotrophic Conversions.

	Reactant Stoichiometry			Hydrogen Fraction
Product	H_2	O_2	CO_2	mol %
Biomass[a] (CO_2 limited)	9.3	3.55	1	0.673
Biomass[b] (max)	6.6	1.90	1	0.695
Biomass[a] (H_2 limited)	5.4	1.58	1	0.670
Biomass[c]	5.2	1.52	1	0.674
Biomass[a] (O_2 limited)	5.0	1.56	1	0.661
Biomass[b] (min)	4.5	1.18	1	0.674
Biomass[d] (BC_3, 10 h)	4.4	1.23	1	0.666
Biomass[a] (unlimited)	4.4	1.20	1	0.668
Biomass[e] (max aerobic eff.)	3.4	0.54	1	0.690
Biomass [e](max anaerobic eff.)	2.3	0	1	0.700
PHB[c]	8.2	3.00	1	0.673
PHB [d] (BC_3, 54 h)	7.5	2.86	1	0.660
PHB [d] (BC_3, 26 h)	5.5	1.75	1	0.668
PHB [e] (max aerobic eff.)	3.3	0.54	1	0.683
PHB [e](max anaerobic eff.)	2.2	0	1	0.692

[a]Bongers [372] The author observed different stoichiometries depending on which gaseous substrate was limiting.
[b]Amman et al. [371] The authors observed a range of stoichiometries during continuous operation of an autotrophic chemostat.
[c]Ishizaki et al. [83]
[d]This study: determined from mass spectroscopy measurements collected at different times during the batch
[e]This study: computed using metabolic model for conditions with and without oxygen.

Figure 6.10 shows the correlation of CDW (g/L) with the total moles of each gas consumed over the course of the batch (mmol/L) . To aid in comparison, gas values are normalized in proportion to the stoichiometry observed for biomass synthesis in BC_3 at 10 h. Refer to **Table 6.5**. **Figure 6.10.a** shows the data for batch BC_3. Before the slow-down in biomass synthesis at ~23 h, all three gas rates show a similar correlation to the CDW data. As the biosynthesis continues, CO_2 consumption continues to show close correlation with CDW; however, the proportionality of H_2 and O_2 consumed per CDW increases significantly. This reflects the increasing energy demand as the cells begin to fill with PHB. By fitting the CO_2 consumption data to the CDW data, we computed the following stoichiometric ratio: $\frac{1750\ mmol\ CO_2}{30\ g\ CDW} = \frac{2.56\ g\ CO_2}{g\ CDW}$, which remains essentially constant throughout biomass and PHB production. For H_2 this ratio varies between 0.52-0.88 $\frac{g\ H_2}{g\ CDW}$, and for O_2 the ratio varies between 2.29-5.33 $\frac{g\ O_2}{g\ CDW}$, the limits for which correspond to the end of biomass synthesis at 10 h and the end of the batch at 54 h, respectively.

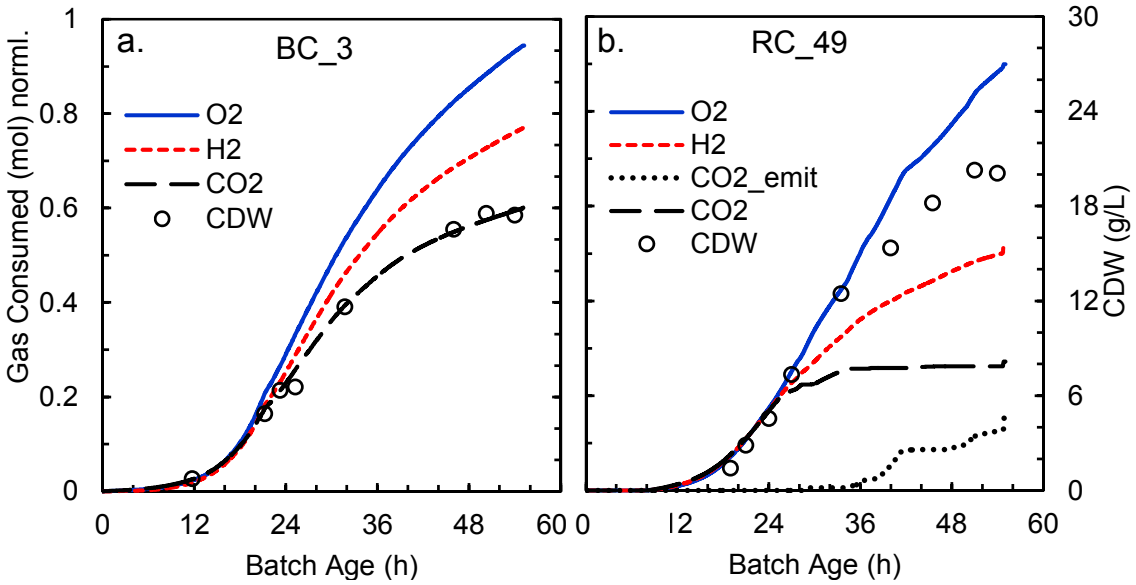

Figure 6.10 Total moles of gas consumed versus CDW.
a. Data for BC_3. **b.** Data for RC_49. The total moles of each gas consumed are normalized by the following values: H_2 (7781 mmol/L), O_2 (2152 mmol/L), and CO_2 (1750 mmol/L). These scaling factors represent the gas amounts required to synthesize 30 g/L of CDW. The normalization factor for CO_2 was chosen to give the best fit to the CDW data. The factors for H_2 and O_2 were scaled to the factor for CO_2 in proportion to the biomass stoichiometry estimated from BC_3 at 10 h. The axes for both **a.** and **b.** are scaled by the same factors.

CO_2-Neutral Conversion of a Heterotrophic Substrate

The autotrophic capacity of *Ralstonia eutropha* to grow using CO_2 as its sole carbon source has significant potential to reshape the industries for liquid fuels, polymers, and commodity chemicals. The most significant benefit to these industries is in reducing their dependence on petroleum feedstocks, which are unsustainable and have been cited as the prime suspect in global warming. Alternatively, hydrogen gas provides the energy for autotrophic bioprocesses. An ideal source of H_2 gas is via the electrolysis of water using electricity generated from solar, wind, tidal, or even nuclear power sources. In addition, concentrated streams of hydrogen and carbon dioxide can be obtained from various sources of lignocellulosic biomass including: corn stover, sugar bagasse, forest residues, grass crops, and dried municipal waste. This conversion is accomplished via

the production of synthesis gas from either steam reforming or catalytic partial oxidation. The syngas, which contains predominantly H_2 and CO, can be further reacted via the water-gas-shift reaction to increase the hydrogen yield while oxidizing the CO to CO_2.

While the use of hydrogen gas is attractive for its reduced environmental impact, the scale-up and economic feasibility of such processes are hindered by the use of hydrogen gas. Due to the low solubility of H_2 in water (0.7 mM/atm at 30°C) compared to that of O_2 (1.1 mM/atm) and CO_2 (28.4 mM/atm), continuous mass-transfer of H_2 from the gas to liquid phase requires a significant amount of energy. One way to reduce the consumption of hydrogen gas during autotrophic growth is by supplementing the bioreactor with a heterotrophic carbon source, similar to the way in which we produced copolymers from CO_2 and valeric acid. Presently, heterotrophic bioprocesses are the predominant route for the conversion of refined feedstocks such as sugars and plant oils. As a byproduct, these processes often produce CO_2 emissions of >40 mol% of the molecular carbon contained within in the feedstock. Thus, the use of *R. eutropha* for mixotrophic process in which a feedstock such as fructose, glycerol, or some organic acid is co-fed with hydrogen gas could have multiple benefits.

Benefits of Mixotrophic Metabolism

First, the addition of heterotrophic substrates, which supply both carbon and energy, would reduce the need for gaseous CO_2 and H_2 . As a result, the maximum K_la needed so sustain the culture at its peak growth rate would be reduced[390], thus, allowing for a reduction in both the capital costs and operating costs associated with mass-transfer equipment e.g., electrolysis units, gas storage tanks, compressors, agitators, and bubble-towers. Second, because of their high solubility heterotrophic substrates are not affected by the same mass-transfer limitations that encumber hydrogen uptake. Thus, with the ability to supply energy simultaneously from both the heterotrophic substrate and hydrogen gas, it may be possible to increase the specific productivity of the cultivations. Third, the use of plant-derived heterotrophic substrates greatly improves the energy efficiency of mixotrophic processes compared to a purely autotrophic process. By utilizing solar energy via photosynthesis, plants act as scrubbers to collect and

concentrate dilute CO_2 from the air. Furthermore, plants improve the efficiency of the $CO_2 \rightarrow$Product conversion by pre-fixing the carbon with added reducing equivalents. As a result, the use of hydrogen in a mixotrophic biosynthesis is only necessary to recapture and fix the waste CO_2 molecules released from the heterotrophic conversion. Hence, mixotrophic growth allows for the possibility of a carbon-neutral conversion of heterotrophic substrates. Finally, results of elementary mode analysis suggest the possibility of a synergistic effect in mixotrophic metabolism whereby the residual energy from the catabolism of hetrotrophic carbon i.e., ATP, NADH, NADPH, and $FADH_2$, is used to increase the CO_2/H_2 yield of anabolic carbon fixation, relative to the yield of a purely autotrophic conversion.

Process Control of a Mixotrophic Biosynthesis

Figure 6.11.a shows the gas uptake profile of batch RC_49 in which an average of 793 μL/h of valeric acid was fed to the batch between 26-55 h. During this period, the levels of CO_2 and O_2 were both kept at 10 mol%, while the VA feed rated was periodically adjusted. Arrows in **Figure 6.11.a** show when and how the VA feed rate was adjusted. Similar to the behavior seen in the block-copolymer batches, the addition of valeric acid causes an increase in the O_2 uptake of the cells while the H_2 and CO_2 uptake rates decline. If the feed rate of valeric acid is sufficiently large, the amount of CO_2 generated from VA catabolism exceeds the anabolic rate of CO_2 fixation by the Calvin cycle. This results in a net emission of CO_2 from the culture, indicated by negative-valued CO_2 uptake rate. During the course of the batch we periodically manipulated the feed rate of valeric acid in order to shift the batch between states of CO_2 consumption and CO_2 evolution.

Figure 6.11.b shows the molar composition of the gas consumed. The trends shows that for periods when CO_2 uptake is positive, the mole fraction of H_2 in the gas remains fairly close to the value 0.66, but during periods of CO_2 emission this fraction drops significantly. Nevertheless hydrogen uptake does not cease during these periods of CO_2 emission.

A critical result of this experiment is that despite the drop in H_2 consumption with increasing VA feed-rate, once the feed-rate is reduced, the rates of H_2 and CO_2 uptake quickly return to their previous levels. This resumption in autotrophic carbon fixation is observed even when the cells are in a state of net CO_2 evolution. These results indicate that below some maximum level of VA co-feeding, which we have not determined, the capacity for simultaneous autotrophic carbon fixation is not significantly diminished, thus allowing the possibility of a carbon neutral conversion of VA.

Process Robustness During Mixotrophic Cultivation

The significance of the above mentioned result is understood light of an earlier report by Friedrich et al.[379], which demonstrated that growth on pyruvate, succinate, or acetate resulted in a reduction in the activity of soluble hydrogenases (Sh) , membrane-bound hydrogenases (Mbh), and carbon fixing enzymes ribulose-5-phosphate kinase (RuPK) and ribulose bisphosphate carboxylase (RuBC). Conversely, they observed much higher activity levels for growth on formate, glycerol, fructose, and gluconate. Thus, CO_2-neutral conversion may be more difficult to obtain for some substance than others. Substance for which mixotrophich growth in *R. eutropha* has been clearly demonstrated include: fructose[381], lactic acid[380], γ-caprolactone[374], and other fatty-acids[373-374].

The rapid resumption of CO_2 and H_2 uptake that is seen following a reduction in the VA feed rate suggest that the concentrations of autotrophic enzymes may not be significantly reduced during valeric acid metabolism. Rather, the drop in H_2 uptake is likely caused by other reasons such as feedback inhibition of enzyme activity by downstream metabolites or a drop in autotrophic flux due to reactions operating close to equilibrium. As both hydrogenases, Mbh and Sh, are known to be reversible, an increase in the availability of reducing equivalents NADH and $FADH_2$ from VA catabolism could easily produce a drop in the H_2 flux.

The net effect of valeric acid feeding during batch RC_49 is shown in **Figure 6.10.b.** While the total amount of CDW formed in RC_49 is similar to that of BC_3 shown in **Figure 6.10.a.**, the amount of CO_2 consumed by RC_49 is significantly lower.

As a result of the reducing equivalents supplied by the VA feed, the total amount of H_2 consumed by the batch is also much lower. Given that the immediate response of the culture to VA addition is a noticeable uptick in OUR, we find it peculiar that the total amount of O_2 consumed by batch RC_49 is quite similar to that of batch BC_3. It may be the case that the immediate increase in OUR seen upon VA dosage is more of a transient effect due to temporary overflow of reducing equivalents in the cell, and that as the cells restore their redox balance by reducing hydrogen uptake, so the OUR decreases. Moreover, because the polymer from RC_49 was synthesized using a significant quantity of valeric acid, less CO_2 was used, requiring less energy for carbon fixation, and hence less O_2.

Net CO_2 Emissions

Due to our imperfect control of the VA feed rate in batch RC_49, a significant quantity of CO_2 was emitted from the batch. See **Figure 6.10.b**. Nevertheless, the total CO_2 consumed by batch RC_49 was greater than the total CO_2 produced, resulting in a CO_2-negative bioconversion. Moreover, we have shown how controlling the relative balance of heterotrophic catabolism and autotrophic anabolism determines the net CO_2 produced by the batch, and how the measurement of off-gas composition is critical for maximizing the efficiency of carbon utilization.

An alternative process for achieving a carbon-neutral process would be to rely on a heterotrophic substrate to support the maximum growth rate during biomass accumulation, followed by a period of purely autotrophic metabolism during the slower product synthesis phase, as was done by Tanaka and Ishizaki[390]. In this way CO_2 emitted during the first phase of the batch would be fixed during the second phase. However, such a process would not constitute a mixotrophic conversion because the heterotrohic substrate is not fed concurrent with the hydrogen feeding. Furthermore, the efficiency of the bioconversion would be reduced because of the chemical potential wasted by allowing the CO_2 gas to leave the liquid phase during the heterotrophic portion of the batch.

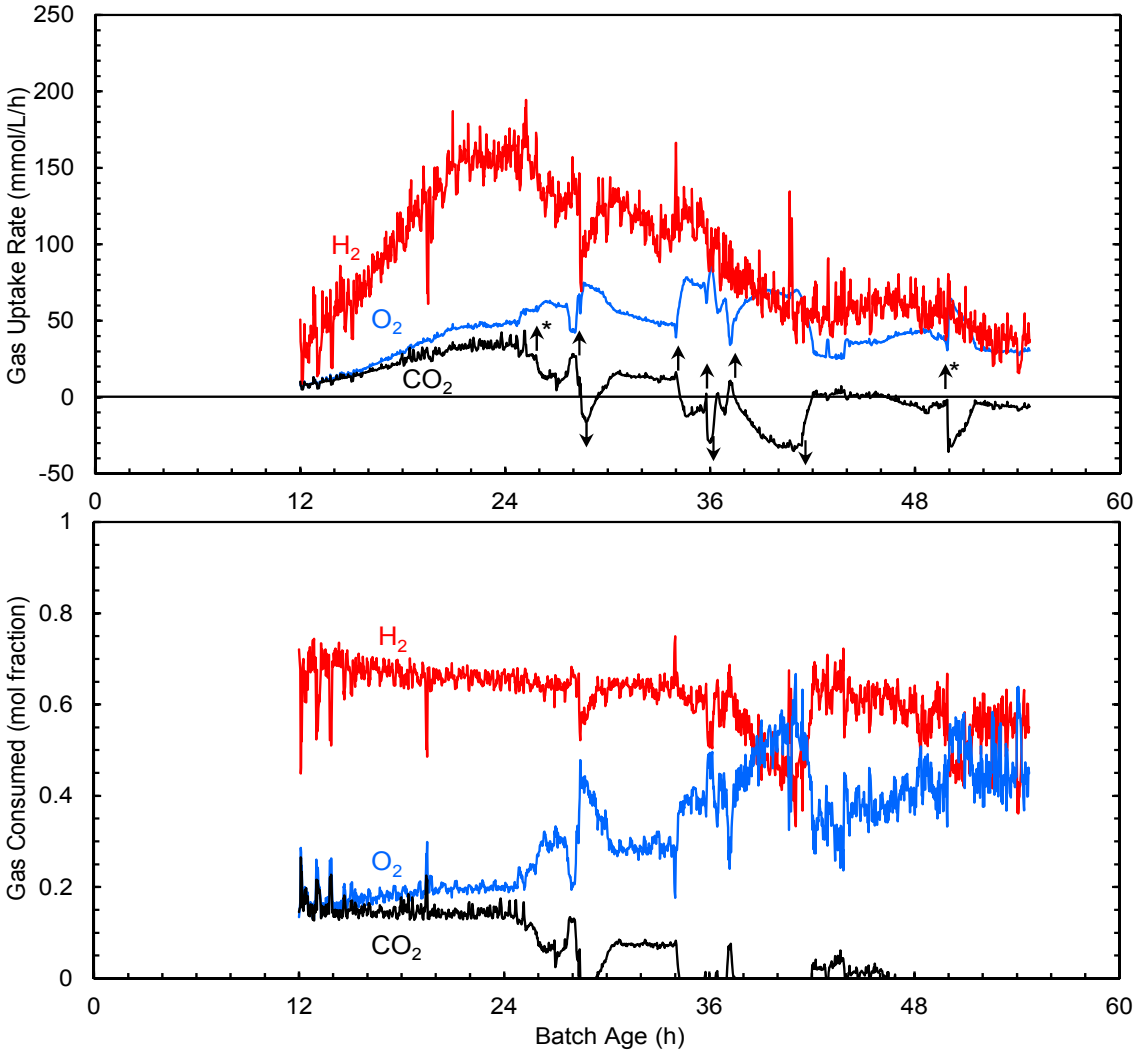

Figure 6.11 Control of CO_2 evolution from a mixotrophic biosynthesis.
The evolution and consumption of CO_2 gas is controlled by adjusting the valeric acid feed rate. Data is shown for batch RC_49 **a.** Gas uptake rates of H_2, O_2, and CO_2 (mmol/L/h). Negative values of CO_2 uptake represent net CO_2 evolution. Feeding of valeric acid was initiated at 26 h and continued until the end of the batch. An average of 23 ml of valeric acid was fed over 29 h. Arrows indicate when the feed rate of valeric acid was increased (↑) or decreased (↓). The asterisk (*) at 26 h indicates that valeric acid was added as a shot. The * at 50 h indicates an accidental dump of valeric acid. **b.** Molar composition of the gas consumed. During periods of net CO_2 evolution, the mol% of H_2 consumed by the cell decreases significantly below the typical value of 0.66.

Conclusions

Autotrophic and mixotrophic conversions using *Ralstonia eutropha* are promising biosynthesis routes for the production of liquid fuels, polymers, and commodity chemicals. Whether using bio-derived synthesis gas, flu-gas from a fossil fuel combustion facility, or refined sources of heterotrophic carbon, these processes, which utilize clean hydrogen gas for energy, have real potential to offset the CO_2 emissions and petroleum consumption typically required for such products.

While autotrophic processes rely totally on gaseous CO_2, mixotrophic processes can derive part or all of their carbon from heterotrophic substrates, using H_2 only to capture and fix the waste CO_2 emissions. In this paper we have shown how the co-feeding of a heterotrophic substrate, valeric acid, can be used to reduce the consumption of H_2 gas for autotrophic conversions. By monitoring the off-gas composition via real-time mass-spectroscopy, we were able to control the rate of substrate feeding in order to decrease hydrogen consumption while minimizing the CO_2 emissions that would typically occur with a purely heterotrophic conversion. Below a certain maximum feed rate, valeric acid could be fed with no net CO_2 emissions. Moreover, the autotrophic cycles of H_2 and CO_2 uptake were robust and dynamically stable to transient periods of valeric acid over-feeding when CO_2 emission was positive. Thus, by careful control of the substrate feed rate we have demonstrated the feasibility of a CO_2-neutral process, whereby a significant quantity of heterotrophic carbon may be converted to a useful product, PHV-co-PHB polymer, with no net CO_2 emission. Similar processes should also be feasible for other heterotrophic substrates of *Ralstonia eutropha* including fructose, glycerol, gluconate, formic acid, lactic acid, and other fatty-acids. If high levels of hydrogenase and Calvin cycle enzymes are induced first, during a period of purely autotrophich growth, it may even be possible to feed substrates, such as acetate and succinate that show minimal activity of autotrophic enzymes, at rates low enough so that H_2 and CO_2 fixation cycles are maintained without significant downregulation of the autotrophic enzymes.

From the off-gas data we collected, we were also able to compute the stoichiometric ratio of gas uptake during synthesis of both biomass and PHB. The stoichiometry we calculated for biomass production is similar to other values reported in the literature.;

however, for PHB production we report a greater CO_2/H_2 efficiency than that reported by Ishizaki et al.[83]. Moreover, at the initial start of PHB accumulation, when PHB content within the cells is still low, the CO_2/H_2 yield is 35% higher compared to the end of the batch when the PHB content approaches 80%.

Using a stoichiometric model of autotrophic metabolism we have predicted the existence of certain elementary modes for biomass and PHB production which have CO_2/H_2 efficiencies that are significantly greater than those observed experimentally. Furthermore, our model predicts that the most efficient modes for biomass and PHB production are a small set of anaerobic modes that consume only H_2 and O_2, reactions, which are in fact thermodynamically favorable. Such predictions could be used to guide the application of genome knockouts and enzyme overexpression to maximize growth rate and product yields.

With the highly sensitive measurements provided by mass-spectroscopy, we are able to monitor the consumption of valeric acid doses as low as 275 μM with a time resolution as precise as 1 minute. This type of information allows us to make estimates for both the length fraction and molar composition of PHV-co-PHB block domains within block-copolymer molecules. Based on these predictions of molecular structure, we speculate that the reason BC_14 possesses superior toughness compared to that of BC_6 and BC_3 is, not because its PHV-co-PHB domains are slightly longer, but because its copolymer domains are made of 50% PHV. In support of this hypothesis, manual testing of RC_49 and RC_55, which both contain close to 50% PHV, indicated that these random copolymers are more amorphous and have much more elasticity than those, reported in our study and elsewhere, that contain < 30% PHV. This may explain why BC_6 and BC_3, which contain random copolymer domains of 26 mol% and 16 mol%, respectively, show no improvement in strength or toughness compared to PHB homopolymer.

Given the effect that PHV composition is known to have on copolymer properties, we were interested in exploring how adjustments in the feed rates of H_2, O_2, and CO_2 relative to that of valeric acid might be used to control polymer composition. When VA is supplied in excess, PHV synthesis is maximized, but PHB expression still occurs. When

CO_2 is removed from the feed, the rate of PHB synthesis is reduced, which further increases the PHV/PHB ratio. When O_2 supply is restricted in addition to CO_2 elimination, PHB synthesis is completely eliminated, and it is becomes possible to produce a pure PHV homopolymer.

To gain additional insight into the synthesis of PHV-co-PHB polymers under mixotrophic conditions, we performed elementary mode analysis (EMA) using a stoichiometric model of cell metabolism. Our intuitive rationale was that during valeric acid consumption, shifting the redox balance of the cell, either by increasing the supply of H_2 or by restricting the supply of CO_2 and O_2, might force cells to preferentially produce PHV in order to restore their redox balance. The EMA we performed sheds light on this theory by contrasting the landscape of PHV-producing modes observed for heterotorphic versus mixotrophic metabolism. Under simulated heterotrophic conditions, modes for pure PHV synthesis do exist, but they are closely surrounded by modes of impure PHV production. The main benefit of adding reactions for H_2 and CO_2 uptake, is in the creation of new elementary modes which not only produce PHV polymer but are further separated from modes of impure PHV production. Moreover the separation distances are even greater due to the addition of H_2 to the state space. However, the model does not support our simplified intuition that merely reducing O_2 or CO_2 consumption should result in a linear increase in PHV fraction. On the contrary, operating conditions, in the region where the uptake of both O_2 and CO_2 are close to zero, give rise to a very dense population of modes producing both PHV and PHB. Rather, once the maximum supply rate of H_2 is constrained e.g., by mass transfer limitations, both the valeric acid and oxygen supply rates must be carefully adjusted to focus the metabolism over conditions of PHV homopolymer synthesis.

By developing tools with which we can control both the size and composition of the molecular domains of PHA block-copolymers, we hope to encourage the commencement of new studies that will thoroughly explore the correlation between polymer structure and material properties. As a result, we anticipate the creation of more useful materials that will exploit the full potential of this valuable class of renewable polymers.

Supporting Information

R. eutropha Metabolic Model

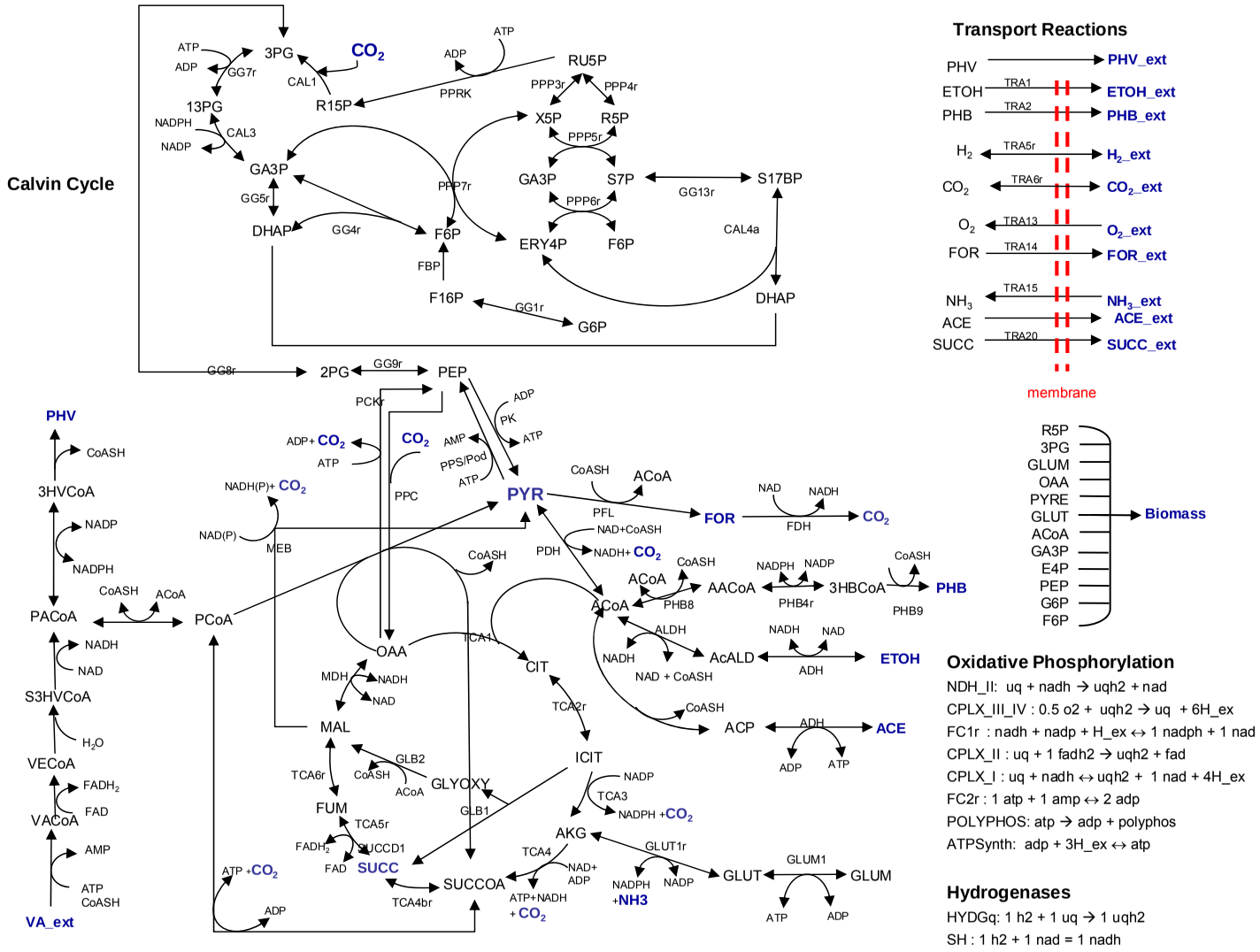

Figure 6.12 R. eutropha Metabolic Model used for Elementary Mode Analysis

Chapter 7. Summary and Recommendations for Future Work

Polyhydroxyalkanoates are a valuable class of polymer materials due to their rapid biodegradation and potential for synthesis from a variety of renewable feedstocks. Ultimately the commercial success of these materials will be based on their ability to compete with petroleum-based polymers in respect to both price and performance. The goal of this thesis was to develop solutions to improve both the cost effectiveness of PHA production and the material properties of the purified polymers.

Technology to Reduce the Price of PHA Plastics

Reducing the price of PHA production can be achieved in numerous ways, two of which are with the utilization of cheap raw materials and by increasing the yield of feedstock-to-polymer conversion. In this thesis we utilized elementary mode analysis to design an *E. coli* knock-out mutant, TCS010, capable of converting glycerol to PHB with a yield of 99% compared to 77% for the wild-type, MG1655. Moreover, a market surplus of glycerol, caused by its generation as a waste product from biodiesel synthesis, has made glycerol a low-price substrate.

Another abundant waste product that can be used as a feed-stock for PHA production is CO_2. Furthermore, the economics of CO_2 utilization are improved when the gas is obtained from concentrated sources such as the off-gas of an ethanol fermentation facility or from the flue-gas of a coal-fired power plant. The conversion of CO_2 to PHA is achieved via the carbon-fixation pathways of the microorganism *Ralstonia eutropha*. While CO_2 may be an abundant feed-stock, the hydrogen gas used by *R. eutropha* for autotrophic growth is not a low-cost substrate. Furthermore, the high mass-transfer coefficients needed to sustain autotrophic bathes during peak growth can require a large capital investment in gas-supply equipment and additional energy costs.

Alternatively, the mixotrophic capabilities of *R. eutropha,* which permit the simultaneous uptake of hydrogen gas along with a heterotrophic carbon feedstock, can be used to offset the requirements for both hydrogen gas and high mass-transfer capabilities. Instead, these processes get their extra energy from the reducing equivalents already present in the heterotrophic feedstock. In this thesis we have demonstrated how real-time monitoring of the off-gas composition can be used to regulate the feed rate of a

heterotrophic substrate in order to prevent the emission of CO_2 from the fermentation while minimizing the amount of hydrogen required.

Further Studies to Explore Mixotrophic Metabolism

Given the success of our mass-spec-based control method, we recommend that similar mixotrophic experiments be conducted using alternative substrates such as fructose, glycerol, and acetate. A major goal of these experiments should be to make a more quantitative analysis of the correlation between the feed-rate of each heterotrophic substrate and the level of CO_2 uptake by the cells. One critical metric would be the specific feed-rate at which the culture switches from net CO_2 uptake to net CO_2 emission. Such studies would be a source of interesting science in studying how *R. eutropha* regulates the balance between heterotrophic catabolism and autotrophic anabolism when substrates with different redox potentials are supplied. Furthermore, we expect that the differences in the levels of autotrophic enzyme expression that was reported by Friedrich et al may affect the relative balance between heterotrophic and autotrophic cycles as well as the dynamic stability of the mixotrophic state. In addition, the study should also assess if an increase in the rate of biomass and product syntheses or an increase in the substrate-to-product yield can be achieved under mixotrophic growth. With the utilization of elementary mode analysis in the study, it may be possible to predict the existence of any possible yield increase by mixotrophic growth and suggest possible gene deletions to improve the efficiency of hydrogen utilization.

Autotrophic Biosynthesis of PHA Block-Copolymers using *Ralstonia eutropha*

In polyhydroxyalkanoates as well as other polymer types, mechanical toughness is a highly desirable property. For the case of PHB-*b*-(PHV-co-PHB) block-copolymers, the origin of their enhanced toughness comes, presumably, from the development of a heterogeneous microstructure within the bulk polymer. Indeed, such behavior is a hallmark of block-copolymers. As a result of the phase separation that is known to occur between dissimilar polymer segments, we speculate the emergence of an ordered

structure in which the elastomeric domains of PHV-co-PHB copolymer are embedded within a matrix of the more rigid PHB homopolymer. Thus, the brittle fracture that occurs with PHB homopolymer is prevented by transmission of the excess stress to the more elastomeric PHV-co-PHB domains.

Initially, our interest in improving the material properties of PHA polymers was inspired by the seminal works of Mantzaris, Pederson, and McChalicher who developed the process technology for producing PHA block-copolymers and demonstrated their superior mechanical properties. As part of this thesis we developed an analogous process whereby random and block-copolymers of PHB and PHV can be produced using CO_2 and valeric acid as feedstocks.

By observing the variation in the length of oxygen-uptake spikes, we were able to estimate the fractional length of PHB-co-PHV domains with the block-copolymer molecules; however, based on the molar composition of the bulk polymer samples we predicted that the mol% of PHV in the PHV-co-PHB domains was different for each block-copolymer. While BC_14 showed a noticeable improvement in mechanical toughness, BC_6 and BC_3 were weak and brittle. Ultimately, we conclude that the improved properties of BC_14 are due to it containing PHV-co-PHB domains of 50 mol% PHV, as opposed to BC_6 and BC_3 which are estimated to contain copolymer domains with a lower PHV fraction. Indeed, the random copolymers we produce which contained ~50 mol% PHV showed obvious elasticity and toughness.

Synthesis of PHB-co-PHA$_{mcl}$ Copolymers using Recombinant *E. coli*

Given the positive results observed for block-copolymers containing PHB and PHV, we were also interested in what properties might result from block-copolymers that combine PHB with monomers of PHA$_{mcl}$, which are more molecularly dissimilar. This was the motivation that led us to purse the development of a mutant, *P. oleovorans* PhaC1 synthase capable of accepting both monomer types. To further increase the productivity of PHB-co-PHA$_{mcl}$ copolymers we constructed the *E. coli* knock-out strain JSBS01, and added expression of the *R*-specific enoyl-CoA hydratase gene PhaJ of *Pseudomonas oleovorans.* When cultured in shake-flasks with optimized conditions of

buffering, glucose, and dodecanoic acid levels, the mutant polymerase showed a significant improvement in both the PHB fraction of the polymer and the total amount of PHA produced, when compared to the wt. *P. oleovorans* polymerase.

Under controlled conditions in a stirred bioreactor we confirmed that the synthesis pathways of PHB and PHA_{mcl} do indeed operate simultaneously. However, we observed dual monomer accumulation only during the period of biomass synthesis: when biomass synthesis began to diminish so did the accumulation of PHA_{mcl}. In addition, we also observed that when *E. coli* are cultivated on glucose as the primary carbon source, the addition of small doses of dodecanoic acid produces distinct spikes in the oxygen uptake-rate similar to the behavior of *R. eutropha* when cultivated on fructose and valeric acid. Thus, we have demonstrated a basic process whereby the production of PHB-co-PHA_{mcl} block copolymers is feasible. The current challenge that impedes the future development of this process is finding a way to sustain the production of PHA_{mcl} monomers throughout the entire coursed of the batch. Otherwise, purified polymer from the batch would be expected to contain a large fraction of PHB homopolymer mixed with the block-copolymer molecules.

Further Studies in PHA Block-Copolymer and Novel Homopolymer Biosyntheses

With the addition of the current study to the field of PHA block-copolymer synthesis, it has become clearly evident that real-time monitoring of cell metabolism during polymer biosynthesis has the potential to be a very useful tool for controlling the molecular properties of PHA block-copolymers produced *in vivo*. These properties include block length, block composition, and the fractional composition of different molecule types within the polymer mixture.

In the block-copolymer molecules produced in our study as well as in the ones produced by Pederson et al., the PHB-co-PHV domains all contained <=50 mol% PHV. But as we have demonstrated, under the correct process conditions of CO_2 and O_2 availability, it is possible to produce PHV-co-PHB copolymers with a PHV fraction > 50% and conceivably even PHV homopolymer. Furthermore, using elementary mode analysis we have shown that the production of polymer segments with a high PHV

fraction is promoted by the simultaneous supply of hydrogen gas. Thus, we can envision a variety of future experiments to explore the correlation between the size and composition of block-domains with the material properties of PHA block-copolymers.

When a reliable process for synthesizing PHB-co-PHA_{mcl} block copolymers is finally realized, the opportunities for scientific and technological advancement in the field of PHAs will expanded tremendously. If the properties of these PHB-*b*-(PHB-co-PHA_{mcl}) polymers are found to be desirable, we envision a future project in which the mutant $PhaC1_{mut}$ synthase and PhaJ enzymes of *P. oleovornas* are recombinantly expressed in *R. eutropha,* thereby allowing the synthesis of these polymer under mixotrophic conditions. Already, some preliminary success with this project has been achieved in a Master's thesis completed by Dan Rouse of the Srienc lab.

Because the results of our elementary mode calculations have suggested that the synthesis of PHV homopolymer is promoted in the presence of hydrogen gas, the possibility exists for a novel synthesis route for the production of PHA_{mcl} homopolymers of higher chain-length, e.g. polyhydroxyoctanoate (PHO) and polyhydroxydecanoate (PHD).

PHA-Graphene Nanocomposites

By a technique that is opposite but analogous to the toughening of PHAs via block-copolymer structures, we can also achieve greater toughness by starting with a low-modulus, elastomeric polymer and creating within it microstructures that are more rigid. This is the approach we took when creating nanocomposites of elastomeric PHA_{mcl} reinforced with rigid graphene nanoparticles. By the phenomenon of polymer entanglement, the graphene particles serve as entanglement attractors that create microstructured regions of more densely entangled polymer chains. As stress is applied to the polymer, the deformation that occurs throughout the bulk PHA_{mcl} matrix is retarded when it crosses the more densely entangled PHA-graphene structures. For the PHA_{mcl} – graphene nanocomposites we created, the modulus was increased by up to 590% for PHO. However, for PHOe the presence of a preexisting network of molecular cross-links was the apparent cause of poor reinforcement by graphene nanoparticles. Essentially, the

graphene nanoparticles and polymer chains were unable to form the rigid entanglements necessary to boost modulus.

From our comparison between PHO and PHD nanocomposites along with our review of other polyoxoester nanocomposites in the literature, we found evidence that indicated the importance of the molecular affinity between the polymer matrix and the nanoparticle filler, i.e modulus enhancement was improved when the attractive interaction between polymer and filler was thought to be higher. Nevertheless, when experimentalists used fabrication techniques that were not conducive to good graphene dispersion, e.g. poor solvents and melt blending, the modulus enhancement of the nanocomposites was poorer.

Further Studies in PHA-Graphene Nanocomposites

From our initial investigation, two ideas for future study emerge. Given the significant impact that molecular cross-linking in the PHOe matrix was seen to have on graphene dispersion, we would be interested in making a more quantitative assessment of this effect. In a report by de Konig et al. the authors showed that greater cross-linking within the PHOe matrix increased the modulus of the material, but our results show that the presence of a gel network with the matrix hinders graphene reinforcement. Our initial hypothesis of reduced polymer-graphene entanglements could be substantiated by varying the composition of unsaturated polyhydroxyoctene residues within the PHO-co-PHOe copolymer thereby altering the gel fraction of the matrix. Presumably, polymers with a higher gel fraction would be less conducive to entanglement formation with the graphene particles, thereby resulting in a lower modulus enhancement. In addition, it would be telling of the underlying phenomenon to measure the modulus improvement when polymer cross-linking was performed after the addition of graphene nanoparticles, i.e. after first allowing the PHA chains to entangle with the graphene particles. Moreover, if vulcanization were initiated after graphene addition it could be possible to create covalent bonds between the unsaturated carbons of graphene and those of the PHOe residues, which could actually boost modulus enhancement.

A second study, which we would do if we had more money and more graduate students, could further explore the effects of interfacial attraction between the polymer and graphene surface. Control of this interfacial interaction can be achieved by varying either the monomer chemistry of the PHA matrix or the surface chemistry of the graphene particles themselves. The surface chemistry of graphene particles can be controlled most easily by varying the oxygen content of the nanofiller. While TRG has a C:O ratio of 10:1, graphite oxide has a C:O ratio of 2:1. If our hypothesis on the role of non-covalent bonding between the oxygen species on TRG and the polyester backbone of PHA is correct, then we expect that even greater improvements in modulus can be achieved by using graphite oxide as a nanofiller. Improvements in non-covalent bonding could also be achieved by altering the monomer composition along the polymer backbone to include side chains with hydroxyl, carbonyl, amine, or cyano moities that could further promote hydrogen bonding. Given that more than 120 different monomer types have been reported for PHA polymers, the creation of such functionalized PHA chains is likely achievable. Moreover, it is also conceivable that appropriately functionalized PHAs and graphene particles could be covalently linked, either by reaction in the bulk matrix or by a secondary processing step whereby PHA polymers or oligomers are covalently grafted onto the graphene surface before dispersal in a bulk polymer matrix. Another possibility for forming PHA grafted nanoparticles is by *in vitro* polymerization of PHA from initiators on the graphene surface. Indeed, several routes to for *in vitro* PHA synthesis have already been described.

While copolymers that contain high fractions of PHB have T_m values > 150°C, copolymers of PHA_{mcl} have much lower T_m values < 70°C, which continues to be the predominant factor that hinders their proliferation into technological applications. Therefore, developing a useful PHA elastomer with a high T_m above 100°C (or either no T_m), remains a worthwhile goal for motivating the continued study of PHA_{mcl}-based materials.

Bibliography

1. Reis, M. A. M.; Serafim, L. S.; Lemos, P. C.; Ramos, A. M.; Aguiar, F. R.; Van Loosdrecht, M. C. M., Production of polyhydroxyalkanoates by mixed microbial cultures. *Bioprocess Biosystems Eng.* **2003,** *25* (6), 377-385.

2. Mayer, F.; Hoppert, M., Determination of the thickness of the boundary layer surrounding bacterial PHA inclusion bodies, and implications for models describing the molecular architecture of this layer. *J. Basic Microbiol.* **1997,** *37* (1), 45-52.

3. Rehm, B. H. A., Polyester synthases: natural catalysts for plastics. *Biochem. J.* **2003,** *376* (1), 15-33.

4. Steinbüchel, A.; Valentin, H. E., Diversity of bacterial polyhydroxyalkanoic acids. *FEMS Microbiology Letters* **1995,** *128* (3), 219-228.

5. Slater, S.; Gallaher, T.; Dennis, D., Production of poly-(3-hydroxybutyrate-co-3-hydroxyvalerate) in a recombinant Escherichia coli strain. *Appl. Environ. Microbiol.* **1992,** *58* (4), 1089-1094.

6. Lageveen, R. G.; Huisman, G. W.; Preusting, H.; Ketelaar, P.; Eggink, G.; Witholt, B., Formation of Polyesters by Pseudomonas oleovorans: Effect of Substrates on Formation and Composition of Poly-(R)-3-Hydroxyalkanoates and Poly-(R)-3-Hydroxyalkenoates. *Appl. Environ. Microbiol.* **1988,** *54* (12), 2924-2932.

7. Fukui, T.; Doi, Y., Cloning and analysis of the poly(3-hydroxybutyrate-co-3- hydroxyhexanoate) biosynthesis genes of Aeromonas caviae. *J. Bacteriol.* **1997,** *179* (15), 4821-4830.

8. Li, R.; Zhang, H.; Qi, Q., The production of polyhydroxyalkanoates in recombinant Escherichia coli. *Bioresour. Technol.* **2007,** *98* (12), 2313-2320.

9. Matsusaki, H.; Manji, S.; Taguchi, K.; Kato, M.; Fukui, T.; Doi, Y., Cloning and Molecular Analysis of the Poly(3-hydroxybutyrate) and Poly(3-hydroxybutyrate-co-3-hydroxyalkanoate) Biosynthesis Genes in Pseudomonas sp. Strain 61-3. *J. Bacteriol.* **1998,** *180* (24), 6459-6467.

10. Reddy, S.; Thirumala, M.; Mahmood, S., A novel Bacillus sp. accumulating poly (3-hydroxybutyrate-co-3-hydroxyvalerate) from a single carbon substrate. *J. Ind. Microbiol. Biotechnol.* **2009,** *36* (6), 837-843.

11. Sheu, D.-S.; Lee, C.-Y., Altering the Substrate Specificity of Polyhydroxyalkanoate Synthase 1 Derived from Pseudomonas putida GPo1 by Localized Semirandom Mutagenesis. *Journal of bacteriology* **2004,** *186* (13), 4177-4184.

12. Takase, K.; Taguchi, S.; Doi, Y., Enhanced Synthesis of Poly(3-hydroxybutyrate) in Recombinant Escherichia coli by Means of Error-Prone PCR Mutagenesis, Saturation Mutagenesis, and In Vitro Recombination of the Type II Polyhydroxyalkanoate Synthase Gene. *J Biochem* **2003,** *133* (1), 139-145.

13. Ram, A., *Fundamentals of Polymer Engineering*. Plenum Press: New York, 1997.

14. Sim, S. J.; Snell, K. D.; Hogan, S. A.; Stubbe, J.; Rha, C.; Sinskey, A. J., PHA synthase activity controls the molecular weight and polydispersity of polyhydroxybutyrate in vivo. *Nat Biotech* **1997,** *15* (1), 63-67.

15. Quagliano Javier, C.; Miyazaki Silvia, S., Microbial Production of the Biodegradable Polyester Poly-3-Hydroxybutyrate (PHB) from Azotobacter Chroococcum 6B: Relation between PHB Molecular Weight, Thermal Stability and Tensile Strength. In *Applied Microbiology*, 2002; pp 135-140.

16. van der Walle, G.; de Koning, G.; Weusthuis, R.; Eggink, G., Properties, Modifications and Applications of Biopolyesters. In *Biopolyesters*, 2001; pp 263-291.

17. Doi, Y., *Microbial Polyesters*. VCH Publishers Inc.: New York, 1990.

18. de Koning, G. J. M.; Scheeren, A. H. C.; Lemstra, P. J.; Peeters, M.; Reynaers, H., Crystallization phenomena in bacterial poly[(R)-3-hydroxybutyrate]: 3. Toughening via texture changes. *Polymer* **1994,** *35* (21), 4598-4605.

19. Hocking, P. J.; Marchessault, R. H., Polyhydroxyalkanoates. In *Biopolymers from Renewable Resources*, Kaplan, D. L., Ed. Springer: Verlag Berlin Heidelberg New York, 1998; pp 220-248.

20. McChalicher, C. W. J.; Srienc, F., Investigating the structure-property relationship of bacterial PHA block copolymers. *J. Biotechnol.* **2007,** *132* (3), 296-302.

21. Pederson, E. N.; McChalicher, C. W.; Srienc, F., Bacterial synthesis of PHA block copolymers. *Biomacromolecules* **2006,** *7* (6), 1904-11.

22. Holmes, P., Biologically Produced (R)-3-hydroxyalkanoate Polymers and Copolymers. In *Development in Crystaline Polymers*, Basset, C. D., Ed. Elsevier: London, 1988; Vol. 2, pp 1-65.

23. Verhoogt, H.; Ramsay, B. A.; Favis, B. D., Polymer blends containing poly(3-hydroxyalkanoate)s. *Polymer* **1994,** *35* (24), 5155-5169.

24. Gagnon, K. D.; Lenz, R. W.; Farris, R. J.; Fuller, R. C., Crystallization behavior and its influence on the mechanical properties of a thermoplastic elastomer produced by Pseudomonas oleovorans. *Macromolecules* **1992,** *25* (14), 3723-3728.

25. Mark, J. E., *Polymer Data Handbook (2nd Edition)*. Oxford University Press: 2009.

26. Kaplan, W. A., *Modern Plastics Encyclopedia '99*. McGraw-Hill: New York, 1998.

27. Parulekar, Y.; Mohanty, A. K., Extruded Biodegradable Cast Films from Polyhydroxyalkanoate and Thermoplastic Starch Blends: Fabrication and Characterization. *Macromolecular Materials and Engineering* **2007,** *292* (12), 1218-1228.

28. Bhatt, R.; Shah, D.; Patel, K. C.; Trivedi, U., PHA-rubber blends: Synthesis, characterization and biodegradation. *Bioresour. Technol.* **2008,** *99* (11), 4615-4620.

29. Schreck, K. M.; Hillmyer, M. A., Block copolymers and melt blends of polylactide with Nodax(TM) microbial polyesters: Preparation and mechanical properties. *J. Biotechnol.* **2007,** *132* (3), 287-295.

30. Noda, I.; Satkowski, M. M.; Dowrey, A. E.; Marcott, C., Polymer Alloys of Nodax Copolymers and Poly(lactic acid). *Macromol. Biosci.* **2004,** *4* (3), 269-275.

31. Chen, G. X.; Hao, G. J.; Guo, T. Y.; Song, M. D.; Zhang, B. H., Structure and mechanical properties of poly(3-hydroxybutyrate-co-3-hydroxyvalerate) (PHBV)/clay nanocomposites. *J. Mater. Sci. Lett.* **2002,** *21* (20), 1587-1589.

32. Yun, S. I.; Lo, V.; Noorman, J.; Davis, J.; Russell, R. A.; Holden, P. J.; Gadd, G. E., Morphology of composite particles of single wall carbon nanotubes/biodegradable polyhydroxyalkanoates prepared by spray drying. *Polym. Bull.* **2010,** *64* (1), 99-106.

33. Yu, L.; Dean, K.; Li, L., Polymer blends and composites from renewable resources. *Prog. Polym. Sci.* **2006,** *31* (6), 576-602.

34. Meuler, A. J.; Hillmyer, M. A.; Bates, F. S., Ordered Network Mesostructures in Block Polymer Materials. *Macromolecules* **2009,** *42* (19), 7221-7250.

35. Eggink, G.; van der Wal, H.; Huijberts, G. N. M.; de Waard, P., Oleic acid as a substrate for poly-3-hydroxyalkanoate formation in Alcaligenes eutrophus and Pseudomonas putida. *Industrial Crops and Products* **1992,** *1* (2-4), 157-163.

36. Qiu, Y.-Z.; Han, J.; Chen, G.-Q., Metabolic engineering of Aeromonas hydrophila for the enhanced production of poly(3-hydroxybutyrate- co-3-hydroxyhexanoate). *Applied Microbiology & Biotechnology* **2006,** *69* (5), 537-542.

37. Matsusaki, H.; Abe, H.; Doi, Y., Biosynthesis and Properties of Poly(3-hydroxybutyrate-co-3-hydroxyalkanoates) by Recombinant Strains of Pseudomonas sp. 61-3. *Biomacromolecules* **2000,** *1* (1), 17-22.

38. Volova, T. G.; Kalacheva, G. S., The synthesis of hydroxybutyrate and hydroxyvalerate copolymers by the bacterium Ralstonia eutropha. *Microbiology* **2005,** *74* (1), 54-59.

39. Pereira, S. M. F.; Sánchez, R. J.; Rieumont, J.; Cabrera, J. G., Synthesis of biodegradable polyhydroxyalcanoate copolymer from a renewable source by alternate feeding. *Polymer Engineering & Science* **2008,** *48* (10), 2051-2059.

40. Mantzaris, N. V.; Kelley, A. S.; Daoutidis, P.; Srienc, F., A population balance model describing the dynamics of molecular weight distributions and the structure of PHA copolymer chains. *Chem. Eng. Sci.* **2002,** *57* (21), 4643-4663.

41. Jurasek, L.; Marchessault, R. H., Polyhydroxyalkanoate (PHA) granule formation in Ralstonia eutropha cells: a computer simulation. *Applied Microbiology & Biotechnology* **2004,** *64* (5), 611-617.

42. Iadevaia, S.; Mantzaris, N. V., Genetic network driven control of PHBV copolymer composition. *Journal of Biotechnology* **2006,** *122* (1), 99-121.

43. Iadevaia, S.; Mantzaris, N. V., Synthesis of PHBV block copolymers driven by an oscillatory genetic network. *Journal of Biotechnology* **2007,** *128* (3), 615-637.

44. Witholt, B.; Kessler, B., Perspectives of medium chain length poly(hydroxyalkanoates), a versatile set of bacterial bioplastics. *Current Opinion in Biotechnology* **1999,** *10* (3), 279-285.

45. Matsumoto, K. i.; Nakae, S.; Taguchi, K.; Matsusaki, H.; Seki, M.; Doi, Y., Biosynthesis of Poly(3-hydroxybutyrate-co-3-hydroxyalkanoates) Copolymer from Sugars by Recombinant Ralstonia eutropha

Harboring the phaC1Ps and the phaGPs Genes of Pseudomonas sp. 61-3. *Biomacromolecules* **2001,** *2* (3), 934-939.

46. Rehm, B. H. A.; Kruger, N.; Steinbüchel, A., A New Metabolic Link between Fatty Acid de NovoSynthesis and Polyhydroxyalkanoic Acid Synthesis. *J. Biol. Chem.* **1998,** *273* (37), 24044-24051.

47. Schubert, P.; Steinbüchel, A.; Schlegel, H. G., Cloning of the Alcaligenes eutrophus genes for synthesis of poly-beta-hydroxybutyric acid (PHB) and synthesis of PHB in Escherichia coli. *J. Bacteriol.* **1988,** *170* (12), 5837-5847.

48. Peoples, O. P.; Sinskey, A. J., Poly-beta-hydroxybutyrate (PHB) biosynthesis in Alcaligenes eutrophus H16. Identification and characterization of the PHB polymerase gene (phbC). *J. Biol. Chem.* **1989,** *264* (26), 15298-15303.

49. Choi, J.-i.; Lee, S. Y.; Han, K., Cloning of the Alcaligenes latus Polyhydroxyalkanoate Biosynthesis Genes and Use of These Genes for Enhanced Production of Poly(3-hydroxybutyrate) in Escherichia coli. *Appl. Environ. Microbiol.* **1998,** *64* (12), 4897-4903.

50. Taguchi, K.; Aoyagi, Y.; Matsusaki, H.; Fukui, T.; Doi, Y., Over-expression of 3-ketoacyl-ACP synthase III or malonyl-CoA-ACP transacylase gene induces monomer supply for polyhydroxybutyrate production in Escherichia coli HB101. *Biotechnol. Lett* **1999,** *21* (7), 579-584.

51. Taguchi, K.; Aoyagi, Y.; Matsusaki, H.; Fukui, T.; Doi, Y., Co-expression of 3-ketoacyl-ACP reductase and polyhydroxyalkanoate synthase genes induces PHA production in Escherichia coli HB101 strain. *FEMS Microbiol. Lett.* **1999,** *176* (1), 183-190.

52. Timm, A.; Steinbüchel, A., Cloning and molecular analysis of the poly(3-hydroxyalkanoic acid) gene locus of Pseudomonas aeruginosa PAO1. *Eur. J. Biochem.* **1992,** *209* (1), 15-30.

53. Qi, Q.; Rehm, B. H. A.; Steinbüchel, A., Synthesis of poly(3-hydroxyalkanoates) in Escherichia coli expressing the PHA synthase gene phaC2 from Pseudomonas aeruginosa: comparison of PhaC1 and PhaC2. *FEMS Microbiol. Lett.* **1997,** *157* (1), 155-162.

54. Langenbach, S.; Rehm, B. H.; Steinbuchel, A., Functional expression of the PHA synthase gene phaC1 from Pseudomonas aeruginosa in Escherichia coli results in poly(3-hydroxyalkanoate) synthesis. *FEMS Microbiol Lett* **1997,** *150* (2), 303-9.

55. Qi, Q.; Steinbüchel, A.; Rehm, B. H. A., Metabolic routing towards polyhydroxyalkanoic acid synthesis in recombinant Escherichia coli (fadR): inhibition of fatty acid ß-oxidation by acrylic acid. *FEMS Microbiol. Lett.* **1998,** *167* (1), 89-94.

56. Tsuge, T.; Fukui, T.; Matsusaki, H.; Taguchi, S.; Kobayashi, G.; Ishizaki, A.; Doi, Y., Molecular cloning of two (R)-specific enoyl-CoA hydratase genes from Pseudomonas aeruginosa and their use for polyhydroxyalkanoate synthesis. *FEMS Microbiol. Lett.* **2000,** *184* (2), 193-198.

57. Fiedler, S.; Steinbüchel, A.; Rehm, B., The role of the fatty acid β-oxidation multienzyme complex from Pseudomonas oleovorans in polyhydroxyalkanoate biosynthesis: molecular characterization of the fadBA operon from P. oleovorans and of the enoyl-CoA hydratase genes phaJ from P. oleovorans and Pseudomonas putida. *Archives of Microbiology* **2002,** *178* (2), 149-160.

58. Park, S. J.; Lee, S. Y., Identification and Characterization of a New Enoyl Coenzyme A Hydratase Involved in Biosynthesis of Medium-Chain-Length Polyhydroxyalkanoates in Recombinant Escherichia coli. *J. Bacteriol.* **2003,** *185* (18), 5391-5397.

59. Tsuge, T.; Taguchi, K.; Seiichi; Taguchi; Doi, Y., Molecular characterization and properties of (R)-specific enoyl-CoA hydratases from Pseudomonas aeruginosa: metabolic tools for synthesis of polyhydroxyalkanoates via fatty acid ß-oxidation. *Int. J. Biol. Macromol.* **2003,** *31* (4-5), 195-205.

60. Rehm, B. H. A.; Mitsky, T. A.; Steinbüchel, A., Role of Fatty Acid De Novo Biosynthesis in Polyhydroxyalkanoic Acid (PHA) and Rhamnolipid Synthesis by Pseudomonads: Establishment of the Transacylase (PhaG)-Mediated Pathway for PHA Biosynthesis in Escherichia coli. *Appl. Environ. Microbiol.* **2001,** *67* (7), 3102-3109.

61. Rehm, B. H. A.; Steinbüchel, A., Heterologous expression of the acyl-acyl carrier protein thioesterase gene from the plant Umbellularia californica mediates polyhydroxyalkanoate biosynthesis in recombinant Escherichia coli. *Applied Microbiology & Biotechnology* **2001,** *55* (2), 205-209.

62. Lu, X.-Y.; Wu, Q.; Zhang, W.-J.; Zhang, G.; Chen, G.-Q., Molecular Cloning of Polyhydroxyalkanoate Synthesis Operon from Aeromonas hydrophila and Its Expression in Escherichia coli. *Biotechnol. Prog.* **2004,** *20* (5), 1332-1336.

63. Fukui, T.; Shiomi, N.; Doi, Y., Expression and Characterization of (R)-Specific Enoyl Coenzyme A Hydratase Involved in Polyhydroxyalkanoate Biosynthesis by Aeromonas caviae. *J. Bacteriol.* **1998,** *180* (3), 667-673.

64. Takase, K.; Matsumoto, K. i.; Taguchi, S.; Doi, Y., Alteration of Substrate Chain-Length Specificity of Type II Synthase for Polyhydroxyalkanoate Biosynthesis by in Vitro Evolution: in Vivo and in Vitro Enzyme Assays. *Biomacromolecules* **2004,** *5* (2), 480-485.

65. Nomura, C. T.; Taguchi, K.; Taguchi, S.; Doi, Y., Coexpression of Genetically Engineered 3-Ketoacyl-ACP Synthase III (fabH) and Polyhydroxyalkanoate Synthase (phaC) Genes Leads to Short-Chain-Length-Medium-Chain-Length Polyhydroxyalkanoate Copolymer Production from Glucose in Escherichia coli JM109. *Appl. Environ. Microbiol.* **2004,** *70* (2), 999-1007.

66. Nomura, C. T.; Taguchi, K.; Gan, Z.; Kuwabara, K.; Tanaka, T.; Takase, K.; Doi, Y., Expression of 3-Ketoacyl-Acyl Carrier Protein Reductase (fabG) Genes Enhances Production of Polyhydroxyalkanoate Copolymer from Glucose in Recombinant Escherichia coli JM109. *Appl. Environ. Microbiol.* **2005,** *71* (8), 4297-4306.

67. Nomura, C. T.; Tanaka, T.; Eguen, T. E.; Appah, A. S.; Matsumoto, K. i.; Taguchi, S.; Ortiz, C. L.; Doi, Y., FabG Mediates Polyhydroxyalkanoate Production from Both Related and Nonrelated Carbon Sources in Recombinant Escherichia coli LS5218. *Biotechnol. Prog.* **2008,** *24* (2), 342-351.

68. Park, S. J.; Lee, S. Y., New fadB homologous enzymes and their use in enhanced biosynthesis of medium-chain-length polyhydroxyalkanoates in <I>fadB</I> mutant <I>Escherichia coli</I>. *Biotechnol. Bioeng.* **2004,** *86* (6), 681-686.

69. Leaf, T. A.; Peterson, M. S.; Stoup, S. K.; Somers, D.; Srienc, F., Saccharomyces cerevisiae expressing bacterial polyhydroxybutyrate synthase produces poly-3-hydroxybutyrate. *Microbiology* **1996,** *142* (5), 1169-1180.

70. Carlson, R.; Srienc, F., Effects of recombinant precursor pathway variations on poly[(R)-3-hydroxybutyrate] synthesis in Saccharomyces cerevisiae. *J. Biotechnol.* **2006,** *124* (3), 561-573.

71. Zhang, B.; Carlson, R.; Srienc, F., Engineering the Monomer Composition of Polyhydroxyalkanoates Synthesized in Saccharomyces cerevisiae. *Appl. Environ. Microbiol.* **2006,** *72* (1), 536-543.

72. Poirier, Y.; Dennis, D. E.; Klomparens, K.; Somerville, C., Polyhydroxybutyrate, a Biodegradable Thermoplastic, Produced in Transgenic Plants. *Science* **1992,** *256* (5056), 520-523.

73. Bohmert, K.; Balbo, I.; Kopka, J.; Mittendorf, V.; Nawrath, C.; Poirier, Y.; Tischendorf, G.; Trethewey, R. N.; Willmitzer, L., Transgenic Arabidopsis plants can accumulate polyhydroxybutyrate to up to 4% of their fresh weight. *Planta* **2000,** *211* (6), 841-845.

74. Somleva, M. N.; Snell, K. D.; Beaulieu, J. J.; Peoples, O. P.; Garrison, B. R.; Patterson, N. A., Production of polyhydroxybutyrate in switchgrass, a value-added co-product in an important lignocellulosic biomass crop. *Plant Biotechnol. J.* **2008,** *6* (7), 663-678.

75. Purnell, M. P.; Petrasovits, L. A.; Nielsen, L. K.; Brumbley, S. M., Spatio-temporal characterization of polyhydroxybutyrate accumulation in sugarcane. *Plant Biotechnol. J.* **2007,** *5* (1), 173-184.

76. Houmiel, K. L.; Slater, S.; Broyles, D.; Casagrande, L.; Colburn, S.; Gonzalez, K.; Mitsky, T. A.; Reiser, S. E.; Shah, D.; Taylor, N. B.; Tran, M.; Valentin, H. E.; Gruys, K. J., Poly(ß-hydroxybutyrate) production in oilseed leukoplasts of Brassica napus. *Planta* **1999,** *209* (4), 547-550.

77. Hahn, J. J.; Eschenlauer, A. C.; Sleytr, U. B.; Somers, D. A.; Srienc, F., Peroxisomes as Sites for Synthesis of Polyhydroxyalkanoates in Transgenic Plants. *Biotechnol. Prog.* **1999,** *15* (6), 1053-1057.

78. Mooney, B. P., The second green revolution? Production of plant-based biodegradable plastics. *Biochem. J* **2009,** *418*, 219-232.

79. Choi, J.; Lee, S. Y., Factors affecting the economics of polyhydroxyalkanoate production by bacterial fermentation. *Appl. Microbiol. Biotechnol.* **1999,** *51* (1), 13-21.

80. DiGregorio, B. E., Biobased Performance Bioplastic: Mirel. *Chem. Biol.* **2009,** *16* (1), 1-2.

81. Kim, S.; Dale, B. E., Energy and Greenhouse Gas Profiles of Polyhydroxybutyrates Derived from Corn Grain: A Life Cycle Perspective. *Environ. Sci. Technol.* **2008,** *42* (20), 7690-7695.

82. Castilho, L. R.; Mitchell, D. A.; Freire, D. M. G., Production of polyhydroxyalkanoates (PHAs) from waste materials and by-products by submerged and solid-state fermentation. *Bioresour. Technol.* **2009,** *100* (23), 5996-6009.

83. Ishizaki, A.; Tanaka, K.; Taga, N., Microbial production of poly-D-3-hydroxybutyrate from CO2. *Appl Microbiol Biotechnol* **2001,** *57* (1-2), 6-12.

84. Kadouri, D.; Jurkevitch, E.; Okon, Y.; Castro-Sowinski, S., Ecological and Agricultural Significance of Bacterial Polyhydroxyalkanoates. *Crit. Rev. Microbiol.* **2005,** *31* (2), 55-67.

85. Wallen, L. L.; Rohwedder, W. K., Poly-ß-hydroxyalkanoate from activated sludge. *Environ. Sci. Technol.* **1974,** *8* (6), 576-579.

86. Bengtsson, S.; Werker, A.; Christensson, M.; Welander, T., Production of polyhydroxyalkanoates by activated sludge treating a paper mill wastewater. *Bioresour. Technol.* **2008,** *99* (3), 509-516.

87. Liu, W.-T.; Mino, T.; Matsuo, T.; Nakamura, K., Isolation, characterization and identification of polyhydroxyalkanoate-accumulating bacteria from activated sludge. *J. Biosci. Bioeng.* **2000,** *90* (5), 494-500.

88. Satoh, H. I., Y.; Mino, T.; Matsuo, T., Activated sludge as a possible source of biodegradable plastic. *Water Sci. Technol.* **1998,** *32* (2), 103-109.

89. Dias, J. M. L.; Lemos, P. C.; Serafim, L. S.; Oliveira, C.; Eiroa, M.; Albuquerque, M. G. E.; Ramos, A. M.; Oliveira, R.; Reis, M. A. M., Recent Advances in Polyhydroxyalkanoate Production by Mixed Aerobic Cultures: From the Substrate to the Final Product. *Macromol. Biosci.* **2006,** *6* (11), 885-906.

90. Johnson, K.; Jiang, Y.; Kleerebezem, R.; Muyzer, G.; van Loosdrecht, M. C. M., Enrichment of a Mixed Bacterial Culture with a High Polyhydroxyalkanoate Storage Capacity. *Biomacromolecules* **2009,** *10* (4), 670-676.

91. Dionisi, D.; Beccari, M.; Gregorio, S. D.; Majone, M.; Papini, M. P.; Vallini, G., Storage of biodegradable polymers by an enriched microbial community in a sequencing batch reactor operated at high organic load rate. *Journal of Chemical Technology & Biotechnology* **2005,** *80* (11), 1306-1318.

92. de Koning, G. J. M.; Lemstra, P. J., The amorphous state of bacterial poly[(R)-3-hydroxyalkanoate]in vivo. *Polymer* **1992,** *33* (15), 3292-3294.

93. Noel, B. J. Process for preparing poly-beta-hydroxybutyric acid. 3044942, 1962.

94. Lafferty, R. M., Heinzle, Elmar Cyclic carbonic acid esters as solvents for poly-(ß-hydroxybutyric acid. 4101533, 1978.

95. McChalicher, C. W. J.; Srienc, F.; Rouse, D. P., Solubility and degradation of polyhydroxyalkanoate biopolymers in propylene carbonate. *AICHE J.* **2010,** *56* (6), 1616-1625.

96. Traussnig, H.; Kloimstein, E.; Kroath, H.; Estermann, R. Extracting agents for poly-D(-)-3-hydroxybutyric acid. 4968611, 1990.

97. Zinn, M.; Weilenmann, H.-U.; Hany, R.; Schmid, M.; Egli, T., Tailored Synthesis of Poly([R]-3-hydroxybutyrate-co-3-hydroxyvalerate) (PHB/HV) in Ralstonia eutropha DSM 428. *Acta Biotechnol.* **2003,** *23* (2-3), 309-316.

98. Hanggi, U. J., Pilot scale production of P(3HB) with Alcaligenes latus. In *Novel Biodegradable Microbial Polymers*, Dawes, E. A., Ed. Dordrecht Kluwer: 1990; pp 65-70.

99. Jacquel, N.; Lo, C.-W.; Wei, Y.-H.; Wu, H.-S.; Wang, S. S., Isolation and purification of bacterial poly(3-hydroxyalkanoates). *Biochem. Eng. J.* **2008,** *39* (1), 15-27.

100. Lee, K. M.; Chang, H. N.; Chang, Y. K.; Kim, B. S.; Hahn, S. K., The lysis of gram-negative Alcaligenes eutrophus and Alcaligenes latus by palmitoyl carnitine. *Biotechnol. Tech.* **1993,** *7* (4), 295-300.

101. Kim, M.; Cho, K.-S.; Ryu, H. W.; Lee, E. G.; Chang, Y. K., Recovery of poly(3-hydroxybutyrate) from high cell density culture of Ralstonia eutropha by direct addition of sodium dodecyl sulfate. *Biotechnol. Lett* **2003,** *25* (1), 55-59.

102. Berger, E.; Ramsay, B. A.; Ramsay, J. A.; Chavarie, C.; Braunegg, G., PHB recovery by hypochlorite digestion of non-PHB biomass. *Biotechnol. Tech.* **1989,** *3* (4), 227-232.

103. Holmes, P. A.; Lim, G. B. Separation process. 4910145, 1990.

104. Kapritchkoff, F. M.; Viotti, A. P.; Alli, R. C. P.; Zuccolo, M.; Pradella, J. G. C.; Maiorano, A. E.; Miranda, E. A.; Bonomi, A., Enzymatic recovery and purification of polyhydroxybutyrate produced by Ralstonia eutropha. *J. Biotechnol.* **2006,** *122* (4), 453-462.

105. de Koning, G. J. M.; Witholt, B., A process for the recovery of poly(hydroxyalkanoates) from Pseudomonads Part 1: Solubilization. *Bioprocess Biosystems Eng.* **1997,** *17* (1), 7-13.

106. Yasotha, K.; Aroua, M. K.; Ramachandran, K. B.; Tan, I. K. P., Recovery of medium-chain-length polyhydroxyalkanoates (PHAs) through enzymatic digestion treatments and ultrafiltration. *Biochem. Eng. J.* **2006,** *30* (3), 260-268.

107. Tamer, I. M.; Moo-Young, M.; Chisti, Y., Disruption of Alcaligenes latus for Recovery of Poly(ß-hydroxybutyric acid): Comparison of High-Pressure Homogenization, Bead Milling, and Chemically Induced Lysis. *Industrial & Engineering Chemistry Research* **1998,** *37* (5), 1807-1814.

108. Hwang, K.-J. Y., Shao-Fu; Don, Trong-Ming, Disruption kinetics of bacterial cells during purification of poly-.beta.-hydroxyalkanoate using ultrasonication. *J. Chin. Inst. Chem. Eng,* **2006,** *37* (3), 209-216.

109. Ghatnekar, M S.; Pai, J S.; Ganesh, M., Production and recovery of poly-3-hydroxybutyrate from Methylobacterium sp V49. *Journal of Chemical Technology & Biotechnology* **2002,** *77* (4), 444-448.

110. Resch, S.; Gruber, K.; Wanner, G.; Slater, S.; Dennis, D.; Lubitz, W., Aqueous release and purification of poly(ß-hydroxybutyrate) from Escherichia coli. *J. Biotechnol.* **1998,** *65* (2-3), 173-182.

111. Gerngross, T. U.; Martin, D. P., Enzyme-catalyzed synthesis of poly[(R)-(-)-3-hydroxybutyrate]: formation of macroscopic granules in vitro. *Proceedings of the National Academy of Sciences* **1995,** *92* (14), 6279-6283.

112. Satoh, Y.; Murakami, F.; Tajima, K.; Munekata, M., Enzymatic synthesis of poly(3-hydroxybutyrate-co-4-hydroxybutyrate) with CoA recycling using polyhydroxyalkanoate synthase and acyl-CoA synthetase. *J. Biosci. Bioeng.* **2005,** *99* (5), 508-511.

113. Jaipuri, F. A.; Bower, B. D.; Pohl, N. L., Protic acid-catalyzed polymerization of ß-lactones for the synthesis of chiral polyesters. *Tetrahedron: Asymmetry* **2003,** *14* (20), 3249-3252.

114. Tokiwa, Y.; Ugwu, C. U., Biotechnological production of (R)-3-hydroxybutyric acid monomer. *J. Biotechnol.* **2007,** *132* (3), 264-272.

115. Matsumura, S.; Suzuki, Y.; Tsukada, K.; Toshima, K.; Doi, Y.; Kasuya, K.-i., Lipase-Catalyzed Ring-Opening Polymerization of ß-Butyrolactone to the Cyclic and Linear Poly(3-hydroxybutyrate). *Macromolecules* **1998,** *31* (19), 6444-6449.

116. Gorke, J. T.; Okrasa, K.; Louwagie, A.; Kazlauskas, R. J.; Srienc, F., Enzymatic synthesis of poly(hydroxyalkanoates) in ionic liquids. *J. Biotechnol.* **2007,** *132* (3), 306-313.

117. Drumright, R. E.; Gruber, P. R.; Henton, D. E., Polylactic Acid Technology. *Adv. Mater.* **2000,** *12* (23), 1841-1846.

118. Tsai, S.; Coleman, R.; Moon, S.; Schneider, K.; Millard, C., Strain screening and development for industrial lactic acid fermentation. *Appl. Biochem. Biotechnol.* **1993,** *39-40* (1), 323-335.

119. Yoo, D. K. K., Dukjoon; Lee, Doo Sung., Synthesis of lactide from oligomeric PLA: effects of temperature, pressure, and catalyst. *Macromolecular Research* **2006,** *14* (5), 510-516.

120. Mehta, R.; Kumar, V.; Bhunia, H.; Upadhyay, S. N., Synthesis of Poly(Lactic Acid): A Review. *Journal of Macromolecular Science: Polymer Reviews* **2005,** *45* (4), 325-349.

121. Williams, C. K.; Hillmyer, M. A., Polymers from Renewable Resources: A Perspective for a Special Issue of Polymer Reviews. *Polymer Reviews* **2008,** *48* (1), 1-10.

122. Spassky, N.; Wisniewski, M.; Pluta, C.; Borgne, A. L., Highly stereoelective polymerization of rac-(D,L)-lactide with a chiral schiff's base/aluminium alkoxide initiator. *Macromol. Chem. Phys.* **1996,** *197* (9), 2627-2637.

123. Hormnirun, P.; Marshall, E. L.; Gibson, V. C.; White, A. J. P.; Williams, D. J., Remarkable Stereocontrol in the Polymerization of Racemic Lactide Using Aluminum Initiators Supported by Tetradentate Aminophenoxide Ligands. *J. Am. Chem. Soc.* **2004,** *126* (9), 2688-2689.

124. Tsuji, H., Poly(lactide) Stereocomplexes: Formation, Structure, Properties, Degradation, and Applications. *Macromol. Biosci.* **2005,** *5* (7), 569-597.

125. Zhang, D.; Hillmyer, M. A.; Tolman, W. B., Catalytic Polymerization of a Cyclic Ester Derived from a "Cool" Natural Precursor. *Biomacromolecules* **2005,** *6* (4), 2091-2095.

126. Wanamaker, C. L.; Bluemle, M. J.; Pitet, L. M.; Leary, L. E.; Tolman, W. B.; Hillmyer, M. A., Consequences of Polylactide Stereochemistry on the Properties of Polylactide-Polymenthide-Polylactide Thermoplastic Elastomers. *Biomacromolecules* **2009,** *10* (10), 2904-2911.

127. Taguchi, S.; Yamada, M.; Matsumoto, K. i.; Tajima, K.; Satoh, Y.; Munekata, M.; Ohno, K.; Kohda, K.; Shimamura, T.; Kambe, H.; Obata, S., A microbial factory for lactate-based polyesters using a lactate-polymerizing enzyme. *Proceedings of the National Academy of Sciences* **2008,** *105* (45), 17323-17327.

128. Yamada, M.; Matsumoto, K. i.; Nakai, T.; Taguchi, S., Microbial Production of Lactate-Enriched Poly[(R)-lactate-co-(R)-3-hydroxybutyrate] with Novel Thermal Properties. *Biomacromolecules* **2009,** *10* (4), 677-681.

129. Yang, T. H.; Kim, T. W.; Kang, H. O.; Lee, S.-H.; Lee, E. J.; Lim, S.-C.; Oh, S. O.; Song, A.-J.; Park, S. J.; Lee, S. Y., Biosynthesis of polylactic acid and its copolymers using evolved propionate CoA transferase and PHA synthase. *Biotechnology and Bioengineering* **2010,** *105* (1), 150-160.

130. Jung, Y. K.; Kim, T. Y.; Park, S. J.; Lee, S. Y., Metabolic engineering of Escherichia coli for the production of polylactic acid and its copolymers. *Biotechnol. Bioeng.* **2010,** *105* (1), 161-171.

131. Auras, R.; Harte, B.; Selke, S., An Overview of Polylactides as Packaging Materials. *Macromol. Biosci.* **2004,** *4* (9), 835-864.

132. Seebach, D. B., Albert K.; Breitschuh, Richard; Job, Kurt, Direct degradation of the biopolymer poly[(R)-3-hydroxybutyric acid] to (R)-3-hydroxybutanoic acid and its methyl ester. *Organic Syntheses* **1993,** (71).

133. Ren, Q.; Grubelnik, A.; Hoerler, M.; Ruth, K.; Hartmann, R.; Felber, H.; Zinn, M., Bacterial Poly(hydroxyalkanoates) as a Source of Chiral Hydroxyalkanoic Acids. *Biomacromolecules* **2005,** *6* (4), 2290-2298.

134. Lee, S. Y.; Lee, Y.; Wang, F., Chiral compounds from bacterial polyesters: Sugars to plastics to fine chemicals. *Biotechnol. Bioeng.* **1999,** *65* (3), 363-368.

135. Misra, S. K.; Valappil, S. P.; Roy, I.; Boccaccini, A. R., Polyhydroxyalkanoate (PHA)/Inorganic Phase Composites for Tissue Engineering Applications. *Biomacromolecules* **2006,** *7* (8), 2249-2258.

136. Russell, R. A.; Holden, P. J.; Garvey, C. J.; Wilde, K. L.; Hammerton, K. M.; Foster, L. J., Investigation of the phase morphology of bacterial PHA inclusion bodies by contrast variation SANS. *Physica B: Condensed Matter* **2006,** *385-386* (Part 2), 859-861.

137. Dennis, D.; Liebig, C.; Holley, T.; Thomas, K. S.; Khosla, A.; Wilson, D.; Augustine, B., Preliminary analysis of polyhydroxyalkanoate inclusions using atomic force microscopy. *FEMS Microbiol. Lett.* **2003,** *226* (1), 113-119.

138. Jendrossek, D., Polyhydroxyalkanoate Granules Are Complex Subcellular Organelles (Carbonosomes). *J. Bacteriol.* **2009,** *191* (10), 3195-3202.

139. Banki, M. R.; Gerngross, T. U.; Wood, D. W., Novel and economical purification of recombinant proteins: Intein-mediated protein purification using in vivo polyhydroxybutyrate (PHB) matrix association. *Protein Sci.* **2005,** *14* (6), 1387-1395.

140. Barnard, G. C.; McCool, J. D.; Wood, D. W.; Gerngross, T. U., Integrated Recombinant Protein Expression and Purification Platform Based on Ralstonia eutropha. *Appl. Environ. Microbiol.* **2005,** *71* (10), 5735-5742.

141. Wang, Z. W., H.; Chen, J.; Zhang, J.; Yao, Y.; Chen, G.-Q., A novel self-cleaving phasin tag for purification of recombinant proteins based on hydrophobic polyhydroxyalkanoate nanoparticles. *Lab on a Chip* **2008,** (8), 1957-1962.

142. Atwood, J.; Rehm, B., Protein engineering towards biotechnological production of bifunctional polyester beads. *Biotechnol. Lett* **2009,** *31* (1), 131-137.

143. Yao, Y.-C.; Zhan, X.-Y.; Zhang, J.; Zou, X.-H.; Wang, Z.-H.; Xiong, Y.-C.; Chen, J.; Chen, G.-Q., A specific drug targeting system based on polyhydroxyalkanoate granule binding protein PhaP fused with targeted cell ligands. *Biomaterials* **2008,** *29* (36), 4823-4830.

144. Bates, F. S.; Fredrickson, G. H., Block copolymers—designer soft materials. *Physics today* **2008,** *52* (2), 32-38.

145. Hadjichristidis, N.; Pitsikalis, M.; Iatrou, H., Synthesis of Block Copolymers. In *Block Copolymers I*, Abetz, V., Ed. Springer Berlin Heidelberg: 2005; Vol. 189, pp 1-124.

146. Hiemenz, P. C.; Lodge, T. P., *Polymer Chemistry*. 2nd ed.; CRC Press: 2007.

147. Matsen, M. W., Polydispersity-induced macrophase separation in diblock copolymer melts. *Phys Rev Lett* **2007,** *99* (14), 148304.

148. Lynd, N. A.; Meuler, A. J.; Hillmyer, M. A., Polydispersity and block copolymer self-assembly. *Progress in Polymer Science* **2008,** *33* (9), 875-893.

149. Schacher, F. H.; Rupar, P. A.; Manners, I., Functional Block Copolymers: Nanostructured Materials with Emerging Applications. *Angewandte Chemie International Edition* **2012,** *51* (32), 7898-7921.

150. Holmberg, A. L.; Reno, K. H.; Wool, R. P.; Epps, I. I. I. T. H., Biobased building blocks for the rational design of renewable block polymers. *Soft Matter* **2014**.

151. O'Reilly, R. K.; Hawker, C. J.; Wooley, K. L., Cross-linked block copolymer micelles: functional nanostructures of great potential and versatility. *Chemical Society Reviews* **2006,** *35* (11), 1068-1083.

152. Amalvy, J. I.; Unali, G. F.; Li, Y.; Granger-Bevan, S.; Armes, S. P.; Binks, B. P.; Rodrigues, J. A.; Whitby, C. P., Synthesis of Sterically Stabilized Polystyrene Latex Particles Using Cationic Block Copolymers and Macromonomers and Their Application as Stimulus-Responsive Particulate Emulsifiers for Oil-in-Water Emulsions. *Langmuir* **2004,** *20* (11), 4345-4354.

153. Pederson, E. N.; Srienc, F., Mass Spectrometry Feedback Control for Synthesis of Polyhydroxyalkanoate Granule Microstructures in Ralstonia eutropha. *Macromolecular Bioscience* **2004,** *4* (3), 243-254.

154. Yang, L.; Sun, P.; Yang, H.; Qi, D.; Wu, M., A feasible method of preparation of block copolymer latex films with stable microphase separation structures. *Progress in Organic Coatings* **2014,** *77* (2), 305-314.

155. Dean, J. M.; Lipic, P. M.; Grubbs, R. B.; Cook, R. F.; Bates, F. S., Micellar structure and mechanical properties of block copolymer-modified epoxies. *Journal of Polymer Science Part B: Polymer Physics* **2001,** *39* (23), 2996-3010.

156. Zou, J.; Liu, L.; Chen, H.; Khondaker, S. I.; McCullough, R. D.; Huo, Q.; Zhai, L., Dispersion of Pristine Carbon Nanotubes Using Conjugated Block Copolymers. *Advanced Materials* **2008,** *20* (11), 2055-2060.

157. Zheng, X.; Xu, Q.; He, L.; Yu, N.; Wang, S.; Chen, Z.; Fu, J., Modification of Graphene Oxide with Amphiphilic Double-Crystalline Block Copolymer Polyethylene-b-poly(ethylene oxide) with Assistance of Supercritical CO2 and Its Further Functionalization. *The Journal of Physical Chemistry B* **2011,** *115* (19), 5815-5826.

158. Tsukruk, V., Nanocomposite polymer layers for molecular tribology. *Tribology Letters* **2001,** *10* (1-2), 127-132.

159. Ndoni, S.; Jannasch, P.; Larsen, N. B.; Almdal, K., Lubricating Effect of Thin Films of Styrene−Dimethylsiloxane Block Copolymers. *Langmuir* **1999,** *15* (11), 3859-3865.

160. Raviv, U.; Giasson, S.; Kampf, N.; Gohy, J.-F.; Jerome, R.; Klein, J., Lubrication by charged polymers. *Nature* **2003,** *425* (6954), 163-165.

161. Li, Y.; Rojas, O. J.; Hinestroza, J. P., Boundary Lubrication of PEO-PPO-PEO Triblock Copolymer Physisorbed on Polypropylene, Polyethylene, and Cellulose Surfaces. *Industrial & Engineering Chemistry Research* **2012,** *51* (7), 2931-2940.

162. Meuler, A. J.; Fleury, G.; Hillmyer, M. A.; Bates, F. S., Structure and Mechanical Properties of an O70 (Fddd) Network-Forming Pentablock Terpolymer. *Macromolecules* **2008,** *41* (15), 5809-5817.

163. Topham, P. D.; Parnell, A. J.; Hiorns, R. C., Block copolymer strategies for solar cell technology. *Journal of Polymer Science Part B: Polymer Physics* **2011,** *49* (16), 1131-1156.

164. Yang, X.; Loos, J., Toward High-Performance Polymer Solar Cells: The Importance of Morphology Control. *Macromolecules* **2007,** *40* (5), 1353-1362.

165. Orilall, M. C.; Wiesner, U., Block copolymer based composition and morphology control in nanostructured hybrid materials for energy conversion and storage: solar cells, batteries, and fuel cells. *Chemical Society Reviews* **2011,** *40* (2), 520-535.

166. Rothemund, P. W. K., Folding DNA to create nanoscale shapes and patterns. *Nature* **2006,** *440* (7082), 297-302.

167. Horowitz, D. M.; Sanders, J. K. M., Amorphous, biomimetic granules of polyhydroxybutyrate: preparation, characterization, and biological implications. *Journal of the American Chemical Society* **1994,** *116* (7), 2695-2702.

168. Curley, J. M.; Lenz, R. W.; Fuller, R. C., Sequential production of two different polyesters in the inclusion bodies of Pseudomonas oleovorans. *International Journal of Biological Macromolecules* **1996,** *19* (1), 29-34.

169. Shi, F.; Gross, R. A.; Rutherford, D. R., Microbial Polyester Synthesis: Effects of Poly(ethylene glycol) on Product Composition, Repeat Unit Sequence, and End Group Structure†. *Macromolecules* **1996,** *29* (1), 10-17.

170. Shi, F.; Ashby, R.; Gross, R. A., Use of Poly(ethylene glycol)s To Regulate Poly(3-hydroxybutyrate) Molecular Weight during Alcaligenes eutrophus Cultivations. *Macromolecules* **1996,** *29* (24), 7753-7758.

171. Ashby, R. D.; Shi, F.; Gross, R. A., Use of poly(ethylene glycol) to control the end group structure and molecular weight of poly(3-hydroxybutyrate) formed by Alcaligenes latus DSM 1122. *Tetrahedron* **1997,** *53* (45), 15209-15223.

172. Kim, Y. B.; Rhee, Y.-H.; Lenz, R. W.; Fuller, R. C., Poly(3-hydroxyalkanoate)s Produced by Pseudomonas oleovorans Grown by Feeding Nonanoic and 10-Undecenoic Acids in Sequence. *Polym J* **1997,** *29* (11), 894-898.

173. Kelley, A. S.; Jackson, D. E.; Macosko, C.; Srienc, F., Engineering the composition of co-polyesters synthesized byAlcaligenes eutrophus. *Polymer Degradation and Stability* **1998,** *59* (1–3), 187-190.

174. Madden, L. A.; Anderson, A. J.; Asrar, J., Synthesis and Characterization of Poly(3-hydroxybutyrate) and Poly(3-hydroxybutyrate-co-3-hydroxyvalerate) Polymer Mixtures Produced in High-Density Fed-Batch Cultures of Ralstonia eutropha (Alcaligenes eutrophus). *Macromolecules* **1998,** *31* (17), 5660-5667.

175. Kawaguchi, Y.; Doi, Y., Kinetics and mechanism of synthesis and degradation of poly(3-hydroxybutyrate) in Alcaligenes eutrophus. *Macromolecules* **1992,** *25* (9), 2324-2329.

176. Steinbüchel, A.; Aerts, K.; Liebergesell, M.; Wieczorek, R.; Babel, W.; Föllner, C.; Madkour, M. H.; Mayer, F.; Pieper-Fürst, U.; Pries, A.; Valentin, H. E., Considerations on the structure and biochemistry of bacterial polyhydroxyalkanoic acid inclusions. *Canadian Journal of Microbiology* **1995,** *41* (13), 94-105.

177. Kelley, A. S.; Srienc, F., Production of two phase polyhydroxyalkanoic acid granules in Ralstonia eutropha. *International Journal of Biological Macromolecules* **1999,** *25* (1–3), 61-67.

178. Kelley, A. S.; Mantzaris, N. V.; Daoutidis, P.; Srienc, F., Controlled Synthesis of Polyhydroxyalkanoic (PHA) Nanostructures in R. eutropha. *Nano Letters* **2001,** *1* (9), 481-485.

179. Su, L.; Lenz, R. W.; Takagi, Y.; Zhang, S.; Goodwin, S.; Zhong, L.; Martin, D. P., Enzymatic polymerization of (R)-3-hydroxyalkanoates by a bacterial polymerase. *Macromolecules* **2000,** *33* (2), 229-231.

180. Jia, Y.; Yuan, W.; Wodzinska, J.; Park, C.; Sinskey, A. J.; Stubbe, J., Mechanistic Studies on Class I Polyhydroxybutyrate (PHB) Synthase from Ralstonia eutropha: Class I and III Synthases Share a Similar Catalytic Mechanism†. *Biochemistry* **2000,** *40* (4), 1011-1019.

181. Wodzinska, J.; Snell, K.; Rhomberg, A.; Sinskey, A.; Biemann, K.; Stubbe, J., Polyhydroxybutyrate synthase: evidence for covalent catalysis. *Journal of the American Chemical Society* **1996,** *118* (26), 6319-6320.

182. Gerngross, T. U.; Snell, K. D.; Peoples, O. P.; Sinskey, A. J.; Csuhai, E.; Masamune, S.; Stubbe, J., Overexpression and Purification of the Soluble Polyhydroxyalkanoate Synthase from Alcaligenes eutrophus: Evidence for a Required Posttranslational Modification for Catalytic Activity. *Biochemistry* **1994,** *33* (31), 9311-9320.

183. Yuan, W.; Jia, Y.; Tian, J.; Snell, K. D.; Müh, U.; Sinskey, A. J.; Lambalot, R. H.; Walsh, C. T.; Stubbe, J., Class I and III Polyhydroxyalkanoate Synthases from Ralstonia eutropha and Allochromatium vinosum: Characterization and Substrate Specificity Studies. *Archives of Biochemistry and Biophysics* **2001,** *394* (1), 87-98.

184. Jia, Y.; Kappock, T. J.; Frick, T.; Sinskey, A. J.; Stubbe, J., Lipases Provide a New Mechanistic Model for Polyhydroxybutyrate (PHB) Synthases: Characterization of the Functional Residues in Chromatium vinosum PHB Synthase†. *Biochemistry* **2000,** *39* (14), 3927-3936.

185. Bhubalan, K.; Chuah, J.-A.; Shozui, F.; Brigham, C. J.; Taguchi, S.; Sinskey, A. J.; Rha, C.; Sudesh, K., Characterization of the Highly Active Polyhydroxyalkanoate Synthase of Chromobacterium sp. Strain USM2. *Applied and Environmental Microbiology* **2011,** *77* (9), 2926-2933.

186. Zhang, S.; Kolvek, S.; Goodwin, S.; Lenz, R. W., Poly(hydroxyalkanoic acid) Biosynthesis in Ectothiorhodospira shaposhnikovii: Characterization and Reactivity of a Type III PHA Synthase. *Biomacromolecules* **2003,** *5* (1), 40-48.

187. Qi, Q.; Steinbuchel, A.; Rehm, B. H., In vitro synthesis of poly(3-hydroxydecanoate): purification and enzymatic characterization of type II polyhydroxyalkanoate synthases PhaC1 and PhaC2 from Pseudomonas aeruginosa. *Appl Microbiol Biotechnol* **2000,** *54* (1), 37-43.

188. Ushimaru, K.; Sangiambut, S.; Thomson, N.; Sivaniah, E.; Tsuge, T., New insights into activation and substrate recognition of polyhydroxyalkanoate synthase from Ralstonia eutropha. *Appl Microbiol Biotechnol* **2013,** *97* (3), 1175-1182.

189. Tian, J.; Sinskey, A. J.; Stubbe, J., Class III Polyhydroxybutyrate Synthase: Involvement in Chain Termination and Reinitiation†. *Biochemistry* **2005,** *44* (23), 8369-8377.

190. Müh, U.; Sinskey, A. J.; Kirby, D. P.; Lane, W. S.; Stubbe, J., PHA Synthase from Chromatium vinosum: Cysteine 149 Is Involved in Covalent Catalysis†. *Biochemistry* **1998,** *38* (2), 826-837.

191. Pfeiffer, D.; Jendrossek, D., PhaM Is the Physiological Activator of Poly(3-Hydroxybutyrate) (PHB) Synthase (PhaC1) in Ralstonia eutropha. *Applied and Environmental Microbiology* **2014,** *80* (2), 555-563.

192. Cho, M.; Brigham, C. J.; Sinskey, A. J.; Stubbe, J., Purification of Polyhydroxybutyrate Synthase from Its Native Organism, Ralstonia eutropha: Implications for the Initiation and Elongation of Polymer Formation in Vivo. *Biochemistry* **2012,** *51* (11), 2276-2288.

193. Byrom, D., Polyhydroxyalkanoates. In *Plastics from Microbes: microbial synthesis of polymers and polymer precursors.*, Mobley, D. P., Ed. Hanser: Munich, 1994; pp 5-33.

194. Preusting, H.; Nijenhuis, A.; Witholt, B., Physical characteristics of poly(3-hydroxyalkanoates) and poly(3-hydroxyalkenoates) produced by Pseudomonas oleovorans grown on aliphatic hydrocarbons. *Macromolecules* **1990,** *23* (19), 4220-4224.

195. Brandl, H.; Gross, R. A.; Lenz, R. W.; Fuller, R. C., Pseudomonas oleovorans as a Source of Poly(β-Hydroxyalkanoates) for Potential Applications as Biodegradable Polyesters. *Applied and Environmental Microbiology* **1988,** *54* (8), 1977-1982.

196. Choi, J.-i.; Lee, S., High level production of supra molecular weight poly (3-hydroxybutyrate) by metabolically engineeredEscherichia coli. *Biotechnol. Bioprocess Eng.* **2004,** *9* (3), 196-200.

197. Kusaka, S.; Abe, H.; Lee, S. Y.; Doi, Y., Molecular mass of poly[(R)-3-hydroxybutyric acid] produced in a recombinant Escherichia coli. *Appl Microbiol Biotechnol* **1997,** *47* (2), 140-143.

198. Shah, D. T.; Tran, M.; Berger, P. A.; Aggarwal, P.; Asrar, J.; Madden, L. A.; Anderson, A. J., Synthesis and Properties of Hydroxy-Terminated Poly(hydroxyalkanoate)s. *Macromolecules* **2000,** *33* (8), 2875-2880.

199. Tsuge, T.; Ko, T.; Tago, M.; Abe, H., Effect of glycerol and its analogs on polyhydroxyalkanoate biosynthesis by recombinant Ralstonia eutropha: A quantitative structure-activity relationship study of chain transfer agents. *Polymer Degradation and Stability* **2013,** *98* (9), 1586-1590.

200. Madden, L. A.; Anderson, A. J.; Shah, D. T.; Asrar, J., Chain termination in polyhydroxyalkanoate synthesis: involvement of exogenous hydroxy-compounds as chain transfer agents. *International Journal of Biological Macromolecules* **1999,** *25* (1–3), 43-53.

201. Shimizu, H.; Tamura, S.; Shioya, S.; Suga, K.-i., Kinetic study of poly-d(−)-3-hydroxybutyric acid (PHB) production and its molecular weight distribution control in a fed-batch culture of Alcaligenes eutrophus. *Journal of Fermentation and Bioengineering* **1993,** *76* (6), 465-469.

202. Anderson, A. J.; Williams, D. R.; Taidi, B.; Dawes, E. A.; Ewing, D. F., Studies on copolyester synthesis by Rhodococcus ruber and factors influencing the molecular mass of polyhydroxybutyrate accumulated by Methylobacterium extorquens and Alcaligenes eutrophus. *FEMS Microbiology Letters* **1992,** *103* (2-4), 93-101.

203. Matsumoto, K. i.; Takase, K.; Aoki, E.; Doi, Y.; Taguchi, S., Synergistic Effects of Glu130Asp Substitution in the Type II Polyhydroxyalkanoate (PHA) Synthase: Enhancement of PHA Production and Alteration of Polymer Molecular Weight. *Biomacromolecules* **2004,** *6* (1), 99-104.

204. Matsumoto, K. i.; Aoki, E.; Takase, K.; Doi, Y.; Taguchi, S., In Vivo and in Vitro Characterization of Ser477X Mutations in Polyhydroxyalkanoate (PHA) Synthase 1 from Pseudomonas sp. 61−3: Effects of Beneficial Mutations on Enzymatic Activity, Substrate Specificity, and Molecular Weight of PHA. *Biomacromolecules* **2006,** *7* (8), 2436-2442.

205. Normi, Y. M.; Hiraishi, T.; Taguchi, S.; Abe, H.; Sudesh, K.; Najimudin, N.; Doi, Y., Characterization and Properties of G4X Mutants of Ralstonia eutropha PHA Synthase for Poly(3-hydroxybutyrate) Biosynthesis in Escherichia coli. *Macromolecular Bioscience* **2005,** *5* (3), 197-206.

206. Zheng, Z.; Li, M.; Xue, X.-J.; Tian, H.-L.; Li, Z.; Chen, G.-Q., Mutation on N-terminus of polyhydroxybutyrate synthase of Ralstonia eutropha enhanced PHB accumulation. *Appl Microbiol Biotechnol* **2006,** *72* (5), 896-905.

207. Koizumi, F.; Abe, H.; Doi, Y., Molecular weight of poly (3-hydroxybutyrate) during biological polymerization in Alcaligenes eutrophus. *Journal of Macromolecular Science, Part A: Pure and Applied Chemistry* **1995,** *32* (4), 759-774.

208. Hori, K.; Soga, K.; Doi, Y., Effects of culture conditions on molecular weights of poly (3-hydroxyalkanoates) produced byPseudomonas putida from octanoate. *Biotechnology letters* **1994,** *16* (7), 709-714.

209. Mantzaris, N. V.; Kelley, A. S.; Srienc, F.; Daoutidis, P., Optimal carbon source switching strategy for the production of PHA copolymers. *AIChE Journal* **2001,** *47* (3), 727-743.

210. Pederson, E. N.; McChalicher, C. W. J.; Srienc, F., Bacterial Synthesis of PHA Block Copolymers. *Biomacromolecules* **2006,** *7* (6), 1904-1911.

211. Gardner, T. S.; Cantor, C. R.; Collins, J. J., Construction of a genetic toggle switch in Escherichia coli. *Nature* **2000,** *403* (6767), 339-342.

212. Elowitz, M. B.; Leibler, S., A synthetic oscillatory network of transcriptional regulators. *Nature* **2000,** *403* (6767), 335-338.

213. Hu, D.; Chung, A.-L.; Wu, L.-P.; Zhang, X.; Wu, Q.; Chen, J.-C.; Chen, G.-Q., Biosynthesis and Characterization of Polyhydroxyalkanoate Block Copolymer P3HB-b-P4HB. *Biomacromolecules* **2011,** *12* (9), 3166-3173.

214. Li, S.; Cai, L.; Wu, L.; Zeng, G.; Chen, J.; Wu, Q.; Chen, G.-Q., Microbial Synthesis of Functional Homo-, Random, and Block Polyhydroxyalkanoates by β-Oxidation Deleted Pseudomonas entomophila. *Biomacromolecules* **2014,** *15* (6), 2310-2319.

215. Li, S.; Dong, C.; Wang, S.; Ye, H.; Chen, G.-Q., Microbial production of polyhydroxyalkanoate block copolymer by recombinant Pseudomonas putida. *Appl Microbiol Biotechnol* **2011,** *90* (2), 659-669.

216. Li, Z.; Yang, X.; Wu, L.; Chen, Z.; Lin, Y.; Xu, K.; Chen, G.-Q., Synthesis, Characterization and Biocompatibility of Biodegradable Elastomeric Poly(ether-ester urethane)s Based on Poly(3-hydroxybutyrate-co-3-hydroxyhexanoate) and Poly(ethylene glycol) via Melting Polymerization. *Journal of Biomaterials Science, Polymer Edition* **2009,** *20* (9), 1179-1202.

217. Tripathi, L.; Wu, L.-P.; Chen, J.; Chen, G.-Q., Synthesis of Diblock copolymer poly-3-hydroxybutyrate-block-poly-3-hydroxyhexanoate [PHB-b-PHHx] by a beta-oxidation weakened Pseudomonas putida KT2442. *Microbial Cell Factories* **2012,** *11*, 44.

218. Tripathi, L.; Wu, L.-P.; Meng, D.; Chen, J.; Chen, G.-Q., Biosynthesis and Characterization of Diblock Copolymer of P(3-Hydroxypropionate)-block-P(4-hydroxybutyrate) from Recombinant Escherichia coli. *Biomacromolecules* **2013,** *14* (3), 862-870.

219. Wang, Q.; Yang, P.; Xian, M.; Liu, H.; Cao, Y.; Yang, Y.; Zhao, G., Production of Block Copolymer Poly(3-hydroxybutyrate)-block-poly(3-hydroxypropionate) with Adjustable Structure from an Inexpensive Carbon Source. *ACS Macro Letters* **2013,** *2* (11), 996-1000.

220. Randall, J. C., *Polymer Sequence Determination*. Academic: New York, 1977.

221. Kamiya, N.; Yamamoto, Y.; Inoue, Y.; Chujo, R.; Doi, Y., Microstructure of bacterially synthesized poly(3-hydroxybutyrate-co-3-hydroxyvalerate). *Macromolecules* **1989,** *22* (4), 1676-1682.

222. Romeu, C.; Denise, F. S. P.; Michael, J.; Luiz, H. C., Block Copolymers Containing (R)-3-Hydroxybutyrate and Isosorbide Succinate or (S)-Lactic Acid Mers. **2009**.

223. Alicata, R.; Barbuzzi, T.; Giuffrida, M.; Ballistreri, A., Characterization of poly[(R)-3-hydroxybutyrate-co-ε-caprolactone] copolymers by matrix-assisted laser desorption/ionization time-of-flight and electrospray ionization mass spectrometry. *Rapid Communications in Mass Spectrometry* **2006,** *20* (4), 568-576.

224. Abe, H.; Doi, Y.; Kumagai, Y., Synthesis and Characterization of Poly[(R,S)-3-hydroxybutyrate-b-6-hydroxyhexanoate] as a Compatibilizer for a Biodegradable Blend of Poly[(R)-3-hydroxybutyrate] and Poly(6-hydroxyhexanoate). *Macromolecules* **1994,** *27* (21), 6012-6017.

225. Andrade, A. P.; Neuenschwander, P.; Hany, R.; Egli, T.; Witholt, B.; Li, Z., Synthesis and Characterization of Novel Copoly(ester−urethane) Containing Blocks of Poly-[(R)-3-hydroxyoctanoate] and Poly-[(R)-3-hydroxybutyrate]. *Macromolecules* **2002,** *35* (13), 4946-4950.

226. Li, X.; Loh, X. J.; Wang, K.; He, C.; Li, J., Poly(ester urethane)s Consisting of Poly[(R)-3-hydroxybutyrate] and Poly(ethylene glycol) as Candidate Biomaterials: Characterization and Mechanical Property Study. *Biomacromolecules* **2005,** *6* (5), 2740-2747.

227. Liu, K. L.; Choo, E. S. G.; Wong, S. Y.; Li, X.; He, C. B.; Wang, J.; Li, J., Designing Poly[(R)-3-hydroxybutyrate]-Based Polyurethane Block Copolymers for Electrospun Nanofiber Scaffolds with Improved Mechanical Properties and Enhanced Mineralization Capability. *The Journal of Physical Chemistry B* **2010,** *114* (22), 7489-7498.

228. Liu, K. L.; Goh, S. H.; Li, J., Controlled synthesis and characterizations of amphiphilic poly[(R,S)-3-hydroxybutyrate]-poly(ethylene glycol)-poly[(R,S)-3-hydroxybutyrate] triblock copolymers. *Polymer* **2008,** *49* (3), 732-741.

229. Zhao, Q.; Cheng, G., Preparation of biodegradable poly(3-hydroxybutyrate) and poly(ethylene glycol) multiblock copolymers. *Journal of Materials Science* **2004,** *39* (11), 3829-3831.

230. Zhao, Q.; Cheng, G.; Li, H.; Ma, X.; Zhang, L., Synthesis and characterization of biodegradable poly(3-hydroxybutyrate) and poly(ethylene glycol) multiblock copolymers. *Polymer* **2005,** *46* (23), 10561-10567.

231. Li, Z.; Cheng, S.; Li, S.; Liu, Q.; Xu, K.; Chen, G.-Q., Novel amphiphilic poly(ester-urethane)s based on poly[(R)-3-hydroxyalkanoate]: synthesis, biocompatibility and aggregation in aqueous solution. *Polymer International* **2008,** *57* (6), 887-894.

232. Ravenelle, F.; Marchessault, R. H., One-Step Synthesis of Amphiphilic Diblock Copolymers from Bacterial Poly([R]-3-hydroxybutyric acid). *Biomacromolecules* **2002,** *3* (5), 1057-1064.

233. Mochizuki, M.; Hirano, M.; Kanmuri, Y.; Kudo, K.; Tokiwa, Y., Hydrolysis of polycaprolactone fibers by lipase: Effects of draw ratio on enzymatic degradation. *Journal of Applied Polymer Science* **1995,** *55* (2), 289-296.

234. Reeve, M. S.; McCarthy, S. P.; Gross, R. A., Preparation and characterization of (R)-poly(.beta.-hydroxybutyrate)-poly(.epsilon.-caprolactone) and (R)-poly(.beta.-hydroxybutyrate)-poly(lactide) degradable diblock copolymers. *Macromolecules* **1993,** *26* (5), 888-894.

235. Chen, C.; Fei, B.; Peng, S.; Wu, H.; Zhuang, Y.; Chen, X.; Dong, L.; Feng, Z., Synthesis and characterization of poly(β-hydroxybutyrate) and poly(ϵ-caprolactone) copolyester by transesterification. *Journal of Polymer Science Part B: Polymer Physics* **2002,** *40* (17), 1893-1903.

236. Impallomeni, G.; Giuffrida, M.; Barbuzzi, T.; Musumarra, G.; Ballistreri, A., Acid Catalyzed Transesterification as a Route to Poly(3-hydroxybutyrate-co-ε-caprolactone) Copolymers from Their Homopolymers. *Biomacromolecules* **2002,** *3* (4), 835-840.

237. Kim, B. O.; Woo, S. I., Compatibilizing capability of poly(β-hydroxybutyrate-,co-ε-caprolactone) in the blend of poly(β-hydroxybutyrate) and poly(ε-caprolactone). *Polymer Bulletin* **1998,** *41* (6), 707-712.

238. Dai, S.; Li, Z., Enzymatic Preparation of Novel Thermoplastic di-Block Copolyesters Containing Poly[(R)-3-hydroxybutyrate] and Poly(ϵ-Caprolactone) Blocks via Ring-Opening Polymerization. *Biomacromolecules* **2008,** *9* (7), 1883-1893.

239. Liu, Q.; Shyr, T.-W.; Tung, C.-H.; Deng, B.; Zhu, M., Block copolymers containing poly (3-hydroxybutyrate-co-3-hydroxyvalerate) and poly (ε-caprolactone) units: Synthesis, characterization and thermal degradation. *Fibers Polym* **2011,** *12* (7), 848-856.

240. Hirt, T. D.; Neuenschwander, P.; Suter, U. W., Synthesis of degradable, biocompatible, and tough block-copolyesterurethanes. *Macromolecular Chemistry and Physics* **1996,** *197* (12), 4253-4268.

241. Anderson, K. S.; Schreck, K. M.; Hillmyer, M. A., Toughening Polylactide. *Polymer Reviews* **2008,** *48* (1), 85-108.

242. Schreck, K. M.; Hillmyer, M. A., Block copolymers and melt blends of polylactide with Nodax™ microbial polyesters: Preparation and mechanical properties. *Journal of Biotechnology* **2007,** *132* (3), 287-295.

243. Hiki, S.; Miyamoto, M.; Kimura, Y., Synthesis and characterization of hydroxy-terminated [RS]-poly(3-hydroxybutyrate) and its utilization to block copolymerization with l-lactide to obtain a biodegradable thermoplastic elastomer. *Polymer* **2000,** *41* (20), 7369-7379.

244. Aluthge, D. C.; Xu, C.; Othman, N.; Noroozi, N.; Hatzikiriakos, S. G.; Mehrkhodavandi, P., PLA–PHB–PLA Triblock Copolymers: Synthesis by Sequential Addition and Investigation of Mechanical and Rheological Properties. *Macromolecules* **2013,** *46* (10), 3965-3974.

245. Hazer, B., Poly(β-hydroxynonanoate) and polystyrene or poly(methyl methacrylate) graft copolymers: microstructure characteristics and mechanical and thermal behavior. *Macromolecular Chemistry and Physics* **1996,** *197* (2), 431-441.

246. Eroğlu, M. S.; Çaykara, T.; Hazer, B., γ-Ray induced graft copolymerization of methyl methacrylate onto poly(β-hydroxynonanoate). *Polymer Bulletin* **1998,** *41* (1), 53-60.

247. Ceccorulli, G.; Scandola, M.; Adamus, G., Compatibilizing effect of a graft copolymer on bacterial poly(3-hydroxybutyrate)/poly(methyl methacrylate) blends. *Journal of Polymer Science Part B: Polymer Physics* **2002,** *40* (13), 1390-1399.

248. Kann, Y.; Padwa, A. R., Methods for branching pha using thermolysis. Google Patents: 2011.

249. Krishnaswamy, R. K.; Van, W. J.; Peoples, O. P.; Shabtai, Y.; Padwa, A. R., Biobased rubber modified biodegradable polymer blends. Google Patents: 2013.

250. Li, J.; Li, X.; Ni, X.; Leong, K. W., Synthesis and Characterization of New Biodegradable Amphiphilic Poly(ethylene oxide)-b-poly[(R)-3-hydroxy butyrate]-b-poly(ethylene oxide) Triblock Copolymers. *Macromolecules* **2003,** *36* (8), 2661-2667.

251. Barrett, J. S. F.; Abdala, A. A.; Srienc, F., Poly(hydroxyalkanoate) Elastomers and Their Graphene Nanocomposites. *Macromolecules* **2014,** *47* (12), 3926-3941.

252. Durner, R.; Witholt, B.; Egli, T., Accumulation of Poly[(R)-3-Hydroxyalkanoates] in Pseudomonas oleovorans during Growth with Octanoate in Continuous Culture at Different Dilution Rates. *Applied and Environmental Microbiology* **2000,** *66* (8), 3408-3414.

253. Andrade, A. P.; Witholt, B.; Hany, R.; Egli, T.; Li, Z., Preparation and Characterization of Enantiomerically Pure Telechelic Diols from mcl−Poly[(R)-3-hydroxyalkanoates]. *Macromolecules* **2001,** *35* (3), 684-689.

254. Ausubel, F. M.; Brent, R.; Kingston, R.; Moore, D.; Seidman, J.; Smith, J.; Struhl, K., Short Protocols in Molecular Biology, 1995. *Greene & Wiley-Interscience, New York*.

255. Baba, T.; Ara, T.; Hasegawa, M.; Takai, Y.; Okumura, Y.; Baba, M.; Datsenko, K. A.; Tomita, M.; Wanner, B. L.; Mori, H., Construction of Escherichia coli K-12 in-frame, single-gene knockout mutants: the Keio collection. *Molecular systems biology* **2006,** *2* (1).

256. Posfai, G.; Koob, M. D.; Kirkpatrick, H. A.; Blattner, F. R., Versatile insertion plasmids for targeted genome manipulations in bacteria: isolation, deletion, and rescue of the pathogenicity island LEE of the Escherichia coli O157: H7 genome. *Journal of bacteriology* **1997,** *179* (13), 4426-4428.

257. Trinh, C. T.; Srienc, F., Metabolic Engineering of Escherichia coli for Efficient Conversion of Glycerol to Ethanol. *Applied and Environmental Microbiology* **2009,** *75* (21), 6696-6705.

258. Jackson, J. K. Recombinant modulation of the phbCAB operon copy

number inRalstonia eutropha and modification of the precursor selectivity of

the Pseudomonas oleovorans polymerase I. . Universtiy of Minnesota, St. Paul, 1998.

259. Vick, J. E.; Johnson, E. T.; Choudhary, S.; Bloch, S. E.; Lopez-Gallego, F.; Srivastava, P.; Tikh, I. B.; Wawrzyn, G. T.; Schmidt-Dannert, C., Optimized compatible set of BioBrick™ vectors for metabolic pathway engineering. *Appl Microbiol Biotechnol* **2011,** *92* (6), 1275-1286.

260. Bubeck, P.; Winkler, M.; Bautsch, W., Rapid cloning by homologous recombination in vivo. *Nucleic acids research* **1993,** *21* (15), 3601.

261. Inoue, H.; Nojima, H.; Okayama, H., High efficiency transformation of< i> Escherichia coli</i> with plasmids. *Gene* **1990,** *96* (1), 23-28.

262. Rand, K. N., Crystal violet can be used to visualize DNA bands during gel electrophoresis and to improve cloning efficiency. *Technical Tips Online, Elseivier* **1996,** *1*, 23-24.

263. Riis, V.; Mai, W., Gas chromatographic determination of poly- beta-hydroxybutyric acid in microbial biomass after hydrochloric acid propanolysis. *Journal of Chromatography A* **1988,** *445* (1), 285-289.

264. Chaurasia, C. S.; Williams, T. D.; Judson, C. M.; Hanzlik, R. P., Quantitation of fatty acids and hydroxy fatty acids by gas chromatography/mass spectrometry. Predictively useful correlations of relative response factors with empirical formula. *Journal of Mass Spectrometry* **1995,** *30* (7), 1018-1022.

265. McAllister, M. J.; Li, J.-L.; Adamson, D. H.; Schniepp, H. C.; Abdala, A. A.; Liu, J.; Herrera-Alonso, M.; Milius, D. L.; Car, R.; Prud'homme, R. K.; Aksay, I. A., Single Sheet Functionalized Graphene by Oxidation and Thermal Expansion of Graphite. *Chem. Mater.* **2007,** *19* (18), 4396-4404.

266. Prud'homme, R. K.; Aksay, I. A.; Adamson, D.; Abdala, A. Thermally exfoliated graphite oxide and polymer nanocomposites. US7658901B2, 2010.

267. Staudenmaier, L., Method for the preparation of graphitic acid. *Ber. Dtsch. Chem. Ges.* **1898,** *31*, 1481-1487.

268. Ramsay, B. A.; Lomaliza, K.; Chavarie, C.; Dube, B.; Bataille, P.; Ramsay, J. A., Production of poly-(beta-hydroxybutyric-co-beta-hydroxyvaleric) acids. *Appl Environ Microbiol* **1990,** *56* (7), 2093-8.

269. Repaske, R.; Mayer, R., Dense autotrophic cultures of Alcaligenes eutrophus. *Appl Environ Microbiol* **1976,** *32* (4), 592-7.

270. Noda, I.; Green, P. R.; Satkowski, M. M.; Schechtman, L. A., Preparation and Properties of a Novel Class of Polyhydroxyalkanoate Copolymers†. *Biomacromolecules* **2005,** *6* (2), 580-586.

271. Takase, K.; Matsumoto, K. i.; Taguchi, S.; Doi, Y., Alteration of Substrate Chain-Length Specificity of Type II Synthase for Polyhydroxyalkanoate Biosynthesis by in Vitro Evolution: in Vivo and in Vitro Enzyme Assays. *Biomacromolecules* **2004,** *5* (2), 480-485.

272. Shen, X.-W.; Shi, Z.-Y.; Song, G.; Li, Z.-J.; Chen, G.-Q., Engineering of polyhydroxyalkanoate (PHA) synthase PhaC2Ps of Pseudomonas stutzeri via site-specific mutation for efficient production of PHA copolymers. *Appl Microbiol Biotechnol* **2011,** *91* (3), 655-665.

273. da Silva, G. P.; Mack, M.; Contiero, J., Glycerol: a promising and abundant carbon source for industrial microbiology. *Biotechnology advances* **2009,** *27* (1), 30-39.

274. Trinh, C.; Wlaschin, A.; Srienc, F., Elementary mode analysis: a useful metabolic pathway analysis tool for characterizing cellular metabolism. *Appl Microbiol Biotechnol* **2009,** *81* (5), 813-826.

275. Carlson, R.; Wlaschin, A.; Srienc, F., Kinetic Studies and Biochemical Pathway Analysis of Anaerobic Poly-(R)-3-Hydroxybutyric Acid Synthesis in Escherichia coli

10.1128/AEM.71.2.713-720.2005. *Appl. Environ. Microbiol.* **2005,** *71* (2), 713-720.

276. Park, S. J.; Lee, S. Y., Biosynthesis of poly (3-hydroxybutyrate-co-3-hydroxyalkanoates) by metabolically engineered Escherichia coli strains. *Applied biochemistry and biotechnology* **2004,** *114* (1-3), 335-346.

277. Black, P. N.; Dirusso, C. C., Molecular and biochemical analyses of fatty acid transport, metabolism, and gene regulation in Escherichia coli. *Biochimica et Biophysica Acta (BBA) - Lipids and Lipid Metabolism* **1994,** *1210* (2), 123-145.

278. Kimata, K.; Takahashi, H.; Inada, T.; Postma, P.; Aiba, H., cAMP receptor protein-cAMP plays a crucial role in glucose-lactose diauxie by activating the major glucose transporter gene in Escherichia coli. *Proceedings of the National Academy of Sciences of the United States of America* **1997,** *94* (24), 12914-9.

279. Nichols, N. N.; Dien, B. S.; Bothast, R. J., Use of catabolite repression mutants for fermentation of sugar mixtures to ethanol. *Applied Microbiology & Biotechnology* **2001,** *56* (1/2), 120-125.

280. Li, Q.; Chen, Q.; Li, M. J.; Wang, F. S.; Qi, Q. S., Pathway engineering results the altered polyhydroxyalkanoates composition in recombinant Escherichia coli. *New biotechnology* **2011,** *28* (1), 92-5.

281. Li, R.; Chen, Q.; Wang, P. G.; Qi, Q., A novel-designed Escherichia coli for the production of various polyhydroxyalkanoates from inexpensive substrate mixture. *Appl Microbiol Biotechnol* **2007,** *75* (5), 1103-9.

282. Campbell, J. W.; Morgan-Kiss, R. M.; E. Cronan, J., A new Escherichia coli metabolic competency: growth on fatty acids by a novel anaerobic β-oxidation pathway. *Molecular Microbiology* **2003,** *47* (3), 793-805.

283. Snell, K. D.; Feng, F.; Zhong, L.; Martin, D.; Madison, L. L., YfcX enables medium-chain-length poly(3-hydroxyalkanoate) formation from fatty acids in recombinant Escherichia coli fadB strains. *Journal of bacteriology* **2002,** *184* (20), 5696-705.

284. Vemuri, G. N.; Altman, E.; Sangurdekar, D. P.; Khodursky, A. B.; Eiteman, M. A., Overflow Metabolism in Escherichia coli during Steady-State Growth: Transcriptional Regulation and Effect of the Redox Ratio. *Applied and Environmental Microbiology* **2006,** *72* (5), 3653-3661.

285. Malpica, R.; Franco, B.; Rodriguez, C.; Kwon, O.; Georgellis, D., Identification of a quinone-sensitive redox switch in the ArcB sensor kinase. *Proceedings of the National Academy of Sciences of the United States of America* **2004,** *101* (36), 13318-13323.

286. Nizam, S. A.; Shimizu, K., Effects of arcA and arcB genes knockout on the metabolism in Escherichia coli under anaerobic and microaerobic conditions. *Biochemical Engineering Journal* **2008,** *42* (3), 229-236.

287. van Wegen, R. J.; Lee, S. Y.; Middelberg, A. P., Metabolic and kinetic analysis of poly(3-hydroxybutyrate) production by recombinant Escherichia coli. *Biotechnol Bioeng* **2001,** *74* (1), 70-80.

288. Valgepea, K.; Adamberg, K.; Nahku, R.; Lahtvee, P.-J.; Arike, L.; Vilu, R., Systems biology approach reveals that overflow metabolism of acetate in Escherichia coli is triggered by carbon catabolite repression of acetyl-CoA synthetase. *BMC systems biology* **2010,** *4* (1), 166.

289. Sigüenza, R.; Flores, N.; Hernández, G.; Martínez, A.; Bolivar, F.; Valle, F., Kinetic characterization in batch and continuous culture of Escherichia coli mutants affected in phosphoenolpyruvate metabolism: differences in acetic acid production. *World Journal of Microbiology and Biotechnology* **1999,** *15* (5), 587-592.

290. Chou, C. H.; Bennett, G. N.; San, K. Y., Effect of modified glucose uptake using genetic engineering techniques on high-level recombinant protein production in escherichia coli dense cultures. *Biotechnology and Bioengineering* **1994,** *44* (8), 952-960.

291. Lee, S. Y.; Lee, Y. K.; Chang, H. N., Stimulatory effects of amino acids and oleic acid on poly(3-hydroxybutyric acid) synthesis by recombinant Escherichia coli. *Journal of Fermentation and Bioengineering* **1995,** *79* (2), 177-180.

292. Barrett, J. S. F.; Srienc, F. In *Green chemistry for the production of biodegradable, biorenewable, and biocompatible polymers*, John Wiley & Sons, Inc.: 2011; pp 329-359.

293. Gross, R. A.; DeMello, C.; Lenz, R. W.; Brandl, H.; Fuller, R. C., The biosynthesis and characterization of poly(β-hydroxyalkanoates) produced by Pseudomonas oleovorans. *Macromolecules* **1989,** *22* (3), 1106-1115.

294. Liu, W.; Chen, G. Q., Production and characterization of medium-chain-length polyhydroxyalkanoate with high 3-hydroxytetradecanoate monomer content by fadB and fadA knockout mutant of Pseudomonas putida KT2442. *Appl. Microbiol. Biotechnol.* **2007,** *76* (5), 1153-9.

295. Fernandes, E. G.; Pietrini, M.; Chiellini, E., Bio-Based Polymeric Composites Comprising Wood Flour as Filler. *Biomacromolecules* **2004,** *5* (4), 1200-1205.

296. Botana, A.; Mollo, M.; Eisenberg, P.; Torres Sanchez, R. M., Effect of modified montmorillonite on biodegradable PHB nanocomposites. *Appl. Clay Sci.* **2010,** *47* (3–4), 263-270.

297. Maiti, P.; Batt, C. A.; Giannelis, E. P., New Biodegradable Polyhydroxybutyrate/Layered Silicate Nanocomposites. *Biomacromolecules* **2007,** *8* (11), 3393-3400.

298. Xu, C.; Qiu, Z., Crystallization behavior and thermal property of biodegradable poly(3-hydroxybutyrate)/multi-walled carbon nanotubes nanocomposite. *Polym. Adv. Technol.* **2011,** *22* (5), 538-544.

299. Li, B.; Zhong, W.-H., Review on polymer/graphite nanoplatelet nanocomposites. *J. Mater. Sci.* **2011,** *46* (17), 5595-5614.

300. Byrne, M. T.; Gun'ko, Y. K., Recent Advances in Research on Carbon Nanotube–Polymer Composites. *Adv. Mater.* **2010,** *22* (15), 1672-1688.

301. Verdejo, R.; Bernal, M. M.; Romasanta, L. J.; Lopez-Manchado, M. A., Graphene filled polymer nanocomposites. *J. Mater. Chem.* **2011,** *21* (10), 3301-3310.

302. Lee, C.; Wei, X.; Kysar, J. W.; Hone, J., Measurement of the Elastic Properties and Intrinsic Strength of Monolayer Graphene. *Science* **2008,** *321* (5887), 385-388.

303. Bunch, J. S.; Verbridge, S. S.; Alden, J. S.; van, d. Z. A. M.; Parpia, J. M.; Craighead, H. G.; McEuen, P. L., Impermeable Atomic Membranes from Graphene Sheets. *Nano Lett.* **2008,** *8* (8), 2458-2462.

304. Kim, H.; Abdala, A. A.; Macosko, C. W., Graphene/Polymer Nanocomposites. *Macromolecules* **2010,** *43* (16), 6515-6530.

305. Everaers, R.; Sukumaran, S. K.; Grest, G. S.; Svaneborg, C.; Sivasubramanian, A.; Kremer, K., Rheology and microscopic topology of entangled polymeric liquids. *Science* **2004,** *303* (5659), 823-6.

306. de Gennes, P. G., Reptation of a Polymer Chain in the Presence of Fixed Obstacles. *J. Chem. Phys.* **1971,** *55* (2), 572-579.

307. Sarvestani, A. S., Modeling the solid-like behavior of entangled polymer nanocomposites at low frequency regimes. *Eur. Polym. J.* **2008,** *44* (2), 263-269.

308. Kabanemi, K. K.; Hétu, J.-F., A reptation-based model to the dynamics and rheology of linear entangled polymers reinforced with nanoscale rigid particles. *J. Non-Newtonian Fluid Mech.* **2010,** *165* (15–16), 866-878.

309. Toepperwein, G. N.; Karayiannis, N. C.; Riggleman, R. A.; Kröger, M.; de Pablo, J. J., Influence of Nanorod Inclusions on Structure and Primitive Path Network of Polymer Nanocomposites at Equilibrium and Under Deformation. *Macromolecules* **2011,** *44* (4), 1034-1045.

310. Schneider, G. J.; Nusser, K.; Willner, L.; Falus, P.; Richter, D., Dynamics of Entangled Chains in Polymer Nanocomposites. *Macromolecules* **2011,** *44* (15), 5857-5860.

311. Riggleman, R. A.; Toepperwein, G.; Papakonstantopoulos, G. J.; Barrat, J.-L.; de Pablo, J. J., Entanglement network in nanoparticle reinforced polymers. *J. Chem. Phys.* **2009,** *130* (24), 244903-6.

312. Knauert, S. T.; Douglas, J. F.; Starr, F. W., The effect of nanoparticle shape on polymer-nanocomposite rheology and tensile strength. *J. Polym. Sci., Part B: Polym. Phys.* **2007,** *45* (14), 1882-1897.

313. Tandon, G. P.; Weng, G. J., The effect of aspect ratio of inclusions on the elastic properties of unidirectionally aligned composites. *Polym. Compos.* **1984,** *5* (4), 327-333.

314. Masnada, E.; Merabia, S.; Couty, M.; Barrat, J.-L., Entanglement-induced reinforcement in polymer nanocomposites. *Soft Matter* **2013,** *9* (44), 10532-10544.

315. Dreyer, D. R.; Park, S.; Bielawski, C. W.; Ruoff, R. S., The chemistry of graphene oxide. *Chem. Soc. Rev.* **2010,** *39* (1), 228-240.

316. de Koning, G. J. M.; van Bilsen, H. M. M.; Lemstra, P. J.; Hazenberg, W.; Witholt, B.; Preusting, H.; van der Galiën, J. G.; Schirmer, A.; Jendrossek, D., A biodegradable rubber by crosslinking poly(hydroxyalkanoate) from Pseudomonas oleovorans. *Polymer* **1994,** *35* (10), 2090-2097.

317. Kokta, B. V.; Valade, J. L.; Hornof, V.; Law, K. N., Effect of molecular weight of polystyrene on heat capacity and thermal transitions. *Thermochim. Acta* **1976,** *14* (1–2), 71-86.

318. Kashiwagi, T.; Du, F.; Douglas, J. F.; Winey, K. I.; Harris, R. H.; Shields, J. R., Nanoparticle networks reduce the flammability of polymer nanocomposites. *Nat. Mater.* **2005,** *4* (12), 928-933.

319. Kim, K.; Regan, W.; Geng, B.; Alemán, B.; Kessler, B. M.; Wang, F.; Crommie, M. F.; Zettl, A., High-temperature stability of suspended single-layer graphene. *physica status solidi (RRL) – Rapid Research Letters* **2010,** *4* (11), 302-304.

320. Wilkie, C. A.; Morgan, A. B., *Fire retardancy of polymeric materials*. CRC Press: 2010.

321. Pinto, A. M.; Cabral, J.; Tanaka, D. A. P.; Mendes, A. M.; Magalhães, F. D., Effect of incorporation of graphene oxide and graphene nanoplatelets on mechanical and gas permeability properties of poly(lactic acid) films. *Polym. Int.* **2013,** *62* (1), 33-40.

322. Lin, G.; Noda, I.; Mark, J. E., Synthesis and Properties of Graphene-Basead Nanocomposites in a Biodegradable Polymer. In *Graphite, Graphene, and their Polymer Nanocomposites*, Mukhopadhyay, P.; Gupta, R. K., Eds. CRC Press: 2013; pp 423-446.

323. Li, Y.; Kröger, M.; Liu, W. K., Nanoparticle Effect on the Dynamics of Polymer Chains and Their Entanglement Network. *Phys. Rev. Lett.* **2012,** *109* (11), 118001.

324. Miloaga, D. G.; Hosein, H.-A. A.; Misra, M.; Drzal, L. T., Crystallization of poly(3-hydroxybutyrate) by exfoliated graphite nanoplatelets. *J. Appl. Polym. Sci.* **2007,** *106* (4), 2548-2558.

325. Sridhar, V.; Lee, I.; Chun, H. H.; Park, H., Graphene reinforced biodegradable poly(3-hydroxybutyrate-co-4-hydroxybutyrate) nano-composites. *eXPRESS Polym. Lett.* **2013,** *7* (4), 320-328.

326. Bordes, P.; Pollet, E.; Bourbigot, S.; Avérous, L., Structure and Properties of PHA/Clay Nano-Biocomposites Prepared by Melt Intercalation. *Macromol. Chem. Phys.* **2008,** *209* (14), 1473-1484.

327. Kazatchkov, I. B.; Hatzikiriakos, S. G.; Bohnet, N.; Goyal, S. K., Influence of molecular structure on the rheological and processing behavior of polyethylene resins. *Polym. Eng. Sci.* **1999,** *39* (4), 804-815.

328. Vermant, J.; Ceccia, S.; Dolgovskij, M.; Maffettone, P.; Macosko, C., Quantifying dispersion of layered nanocomposites via melt rheology. *J. Rheol. (1978 - present)* **2007,** *51* (3), 429-450.

329. McLachlan, D. S.; Sauti, G., The AC and DC Conductivity of Nanocomposites. *J. Nanomater.* **2007,** *2007*.

330. Liu, X.; Metcalf, T. H.; Robinson, J. T.; Houston, B. H.; Scarpa, F., Shear Modulus of Monolayer Graphene Prepared by Chemical Vapor Deposition. *Nano Lett.* **2012,** *12* (2), 1013-1017.

331. Crist, B.; Fisher, C. J.; Howard, P. R., Mechanical properties of model polyethylenes: tensile elastic modulus and yield stress. *Macromolecules* **1989,** *22* (4), 1709-1718.

332. Halpin, J.; Kardos, J., Moduli of crystalline polymers employing composite theory. *J. Appl. Phys.* **1972,** *43* (5), 2235-2241.

333. Du, F.; Scogna, R. C.; Zhou, W.; Brand, S.; Fischer, J. E.; Winey, K. I., Nanotube Networks in Polymer Nanocomposites: Rheology and Electrical Conductivity. *Macromolecules* **2004,** *37* (24), 9048-9055.

334. Ren, J.; Silva, A. S.; Krishnamoorti, R., Linear Viscoelasticity of Disordered Polystyrene−Polyisoprene Block Copolymer Based Layered-Silicate Nanocomposites. *Macromolecules* **2000,** *33* (10), 3739-3746.

335. Celzard, A.; McRae, E.; Deleuze, C.; Dufort, M.; Furdin, G.; Marêché, J. F., Critical concentration in percolating systems containing a high-aspect-ratio filler. *Phys. Rev. B: Condens. Matter Mater. Phys.* **1996,** *53* (10), 6209-6214.

336. Lu, C.; Mai, Y.-W., Influence of Aspect Ratio on Barrier Properties of Polymer-Clay Nanocomposites. *Phys. Rev. Lett.* **2005,** *95* (8), 088303.

337. Halpin, J. C.; Kardos, J. L., The Halpin-Tsai equations: A review. *Polym. Eng. Sci.* **1976,** *16* (5), 344-352.

338. Mori, T.; Tanaka, K., Average stress in matrix and average elastic energy of materials with misfitting inclusions. *Acta Metall.* **1973,** *21* (5), 571-574.

339. Lu, P.; Leong, Y. W.; Pallathadka, P. K.; He, C. B., Effective moduli of nanoparticle reinforced composites considering interphase effect by extended double-inclusion model – Theory and explicit expressions. *Int. J. Eng. Sci.* **2013,** *73* (0), 33-55.

340. Kim, H.; Kobayashi, S.; AbdurRahim, M. A.; Zhang, M. J.; Khusainova, A.; Hillmyer, M. A.; Abdala, A. A.; Macosko, C. W., Graphene/polyethylene nanocomposites: Effect of polyethylene functionalization and blending methods. *Polymer* **2011,** *52* (8), 1837-1846.

341. Kim, I.-H.; Jeong, Y. G., Polylactide/exfoliated graphite nanocomposites with enhanced thermal stability, mechanical modulus, and electrical conductivity. *J. Polym. Sci., Part B: Polym. Phys.* **2010,** *48* (8), 850-858.

342. Zhang, J.; Qiu, Z., Morphology, Crystallization Behavior, and Dynamic Mechanical Properties of Biodegradable Poly(ε-caprolactone)/Thermally Reduced Graphene Nanocomposites. *Ind. Eng. Chem. Res.* **2011,** *50* (24), 13885-13891.

343. Kai, W.; Hirota, Y.; Hua, L.; Inoue, Y., Thermal and mechanical properties of a poly(ϵ-caprolactone)/graphite oxide composite. *J. Appl. Polym. Sci.* **2008,** *107* (3), 1395-1400.

344. Park, J. J.; Yu, E. J.; Lee, W.-K.; Ha, C.-S., Mechanical properties and degradation studies of poly(D,L-lactide-co-glycolide) 50:50/graphene oxide nanocomposite films. *Polym. Adv. Technol.* **2013,** *25* (1), 48-54.

345. Yoon, O.; Sohn, I.; Kim, D.; Lee, N.-E., Enhancement of thermomechanical properties of poly(D,L-lactic-co-glycolic acid) and graphene oxide composite films for scaffolds. *Macromol. Res.* **2012,** *20* (8), 789-794.

346. Li, J.; Kim, J.-K.; Lung Sham, M., Conductive graphite nanoplatelet/epoxy nanocomposites: Effects of exfoliation and UV/ozone treatment of graphite. *Scripta Mater.* **2005,** *53* (2), 235-240.

347. Burnett, T. L.; Yakimova, R.; Kazakova, O., Identification of epitaxial graphene domains and adsorbed species in ambient conditions using quantified topography measurements. *J. Appl. Phys.* **2012,** *112* (5), 054308-7.

348. Schniepp, H. C.; Li, J.-L.; McAllister, M. J.; Sai, H.; Herrera-Alonso, M.; Adamson, D. H.; Prud'homme, R. K.; Car, R.; Saville, D. A.; Aksay, I. A., Functionalized Single Graphene Sheets Derived from Splitting Graphite Oxide. *J. Phys. Chem. B* **2006,** *110* (17), 8535-8539.

349. Celzard, A.; Marêché, J. F.; Furdin, G., Surface area of compressed expanded graphite. *Carbon* **2002,** *40* (14), 2713-2718.

350. Chen, G.; Weng, W.; Wu, D.; Wu, C.; Lu, J.; Wang, P.; Chen, X., Preparation and characterization of graphite nanosheets from ultrasonic powdering technique. *Carbon* **2004,** *42* (4), 753-759.

351. Celzard, A.; Marêché, J. F.; Furdin, G.; Puricelli, S., Electrical conductivity of anisotropic expanded graphite-based monoliths. *J. Phys. D: Appl. Phys.* **2000,** *33* (23), 3094.

352. Zhang, X.; Lin, G.; Abou-Hussein, R.; Allen, W. M.; Noda, I.; Mark, J. E., Biodegradable Nanocomposites Based on the Polyester Poly(3-hydroxybutyrate-co-3-hydroxyhexanoate) and Layered Silicate or Expanded Graphite. *J. Macromol. Sci., Part A: Pure Appl.Chem.* **2008,** *45* (6), 431-439.

353. Sridhar, V.; Jeon, J.-H.; Oh, I.-K., Synthesis of graphene nano-sheets using eco-friendly chemicals and microwave radiation. *Carbon* **2010,** *48* (10), 2953-2957.

354. Szatkowski, C., Personal communication. Personal communication ed.; XG Sciences, Inc.: Lansing, MI, **2013**.

355. Stankovich, S.; Dikin, D. A.; Piner, R. D.; Kohlhaas, K. A.; Kleinhammes, A.; Jia, Y.; Wu, Y.; Nguyen, S. T.; Ruoff, R. S., Synthesis of graphene-based nanosheets via chemical reduction of exfoliated graphite oxide. *Carbon* **2007,** *45* (7), 1558-1565.

356. Botas, C.; Pérez-Mas, A. M.; Álvarez, P.; Santamaría, R.; Granda, M.; Blanco, C.; Menéndez, R., Optimization of the size and yield of graphene oxide sheets in the exfoliation step. *Carbon* **2013,** *63* (0), 576-578.

357. Paredes, J. I.; Villar-Rodil, S.; Martínez-Alonso, A.; Tascón, J. M. D., Graphene Oxide Dispersions in Organic Solvents. *Langmuir* **2008,** *24* (19), 10560-10564.

358. Bordes, C.; Fréville, V.; Ruffin, E.; Marote, P.; Gauvrit, J. Y.; Briançon, S.; Lantéri, P., Determination of poly(ε-caprolactone) solubility parameters: Application to solvent substitution in a microencapsulation process. *Int. J. Pharm.* **2010,** *383* (1–2), 236-243.

359. Lu, W.; Ness, J. E.; Xie, W.; Zhang, X.; Minshull, J.; Gross, R. A., Biosynthesis of Monomers for Plastics from Renewable Oils. *J. Am. Chem. Soc.* **2010,** *132* (43), 15451-15455.

360. Eshelby, J. D., The Determination of the Elastic Field of an Ellipsoidal Inclusion, and Related Problems. *Proc. R. Soc. London, Ser. A* **1957,** *241* (1226), 376-396.

361. Eshelby, J. D., The elastic field outside an ellipsoidal inclusion. *Proc. R. Soc. London, Ser. A* **1959,** *252* (1271), 561-569.

362. Dikin, D. A.; Stankovich, S.; Zimney, E. J.; Piner, R. D.; Dommett, G. H.; Evmenenko, G.; Nguyen, S. T.; Ruoff, R. S., Preparation and characterization of graphene oxide paper. *Nature* **2007,** *448* (7152), 457-460.

363. Liu, F.; Ming, P.; Li, J., Ab initio calculation of ideal strength and phonon instability of graphene under tension. *Phys. Rev. B* **2007,** *76* (6), 064120.

364. Van de Velde, K.; Kiekens, P., Biopolymers: overview of several properties and consequences on their applications. *Polym. Test.* **2002,** *21* (4), 433-442.

365. Barker, P. A.; Mason, F.; Barham, P. J., Density and crystallinity of poly (3-hydroxybutyrate/3-hydroxyvalerate) copolymers. *J. Mater. Sci.* **1990,** *25* (4), 1952-1956.

366. Owen, A. J.; Koller, I., A note on the young's modulus of isotropic two-component materials. *Polymer* **1996,** *37* (3), 527-530.

367. Jamshidian, M.; Tehrany, E. A.; Imran, M.; Jacquot, M.; Desobry, S., Poly-Lactic Acid: Production, Applications, Nanocomposites, and Release Studies. *Compr. Rev. Food Sci. F.* **2010,** *9* (5), 552-571.

368. Chen, B.; Evans, J. R. G., Poly(ε-caprolactone)−Clay Nanocomposites: Structure and Mechanical Properties. *Macromolecules* **2005,** *39* (2), 747-754.

369. Mikos, A. G.; Sarakinos, G.; Leite, S. M.; Vacant, J. P.; Langer, R., Laminated three-dimensional biodegradable foams for use in tissue engineering. *Biomaterials* **1993,** *14* (5), 323-330.

370. Dufresne, A.; Kellerhals, M. B.; Witholt, B., Transcrystallization in Mcl-PHAs/Cellulose Whiskers Composites. *Macromolecules* **1999,** *32* (22), 7396-7401.

371. Ammann, E. C.; Reed, L. L.; Durichek, J. E., Jr., Gas consumption and growth rate of Hydrogenomonas eutropha in continuous culture. *Appl Microbiol* **1968,** *16* (6), 822-6.

372. Bongers, L., Energy generation and utilization in hydrogen bacteria. *J Bacteriol* **1970,** *104* (1), 145-51.

373. Volova, T. G.; Kalacheva, G. S.; Kozhevnikov, I. V.; Steinbüchel, A., Biosynthesis of multicomponent polyhydroxyalkanoates by Wautersia eutropha. *Microbiology* **2007,** *76* (6), 704-711.

374. Volova, T. G.; Zhila, N. O.; Kalacheva, G. S.; Sokolenko, V. A.; Sinskey, A. J., [Synthesis of 3-hydroxybutyrate-CO-4-hydroxybutyrate copolymers by hydrogen-oxidizing bacteria]. *Prikl Biokhim Mikrobiol* **2011,** *47* (5), 544-50.

375. Jackson, D. E.; Srienc, F., Novel Methods to Synthesize Polyhydroxyalkanoatesa. *Annals of the New York Academy of Sciences* **1994,** *745* (1), 134-148.

376. Ishizaki, A.; Tanaka, K., Batch culture of Alcaligenes eutrophus ATCC 17697T using recycled gas closed circuit culture system. *Journal of Fermentation and Bioengineering* **1990,** *69* (3), 170-174.

377. Volova, T. G.; Zhila, N. O.; Kalacheva, G. S.; Brigham, C. J.; Sinskey, A. J., Effects of intracellular poly(3-hydroxybutyrate) reserves on physiological-biochemical properties and growth of Ralstonia eutropha. *Res Microbiol* **2013,** *164* (2), 164-71.

378. Repaske, R.; Ambrose, C. A.; Repaske, A. C.; De Lacy, M. L., Bicarbonate requirement for elimination of the lag period of Hydrogenomonas eutropha. *J Bacteriol* **1971,** *107* (3), 712-7.

379. Friedrich, C. G.; Friedrich, B.; Bowien, B., Formation of Enzymes of Autotrophic Metabolism During Heterotrophic Growth of Alcaligenes eutrophus. *Journal of General Microbiology* **1981,** *122* (1), 69-78.

380. Rittenberg, S. C.; Goodman, N. S., Mixotrophic growth of Hydrogenomonas eutropha. *J Bacteriol* **1969,** *98* (2), 617-22.

381. Cook, D. W.; Tischer, R. G.; Brown, L. R., CARBOHYDRATE METABOLISM IN HYDROGENOMONAS EUTROPHA. *Canadian Journal of Microbiology* **1967,** *13* (6), 701-709.

382. Tanaka, K.; Ishizaki, A.; Kanamaru, T.; Kawano, T., Production of poly(D-3-hydroxybutyrate) from CO(2), H(2), and O(2) by high cell density autotrophic cultivation of Alcaligenes eutrophus. *Biotechnol Bioeng* **1995,** *45* (3), 268-75.

383. Doi, Y.; Tamaki, A.; Kunioka, M.; Soga, K., Production of copolyesters of 3-hydroxybutyrate and 3-hydroxyvalerate by Alcaligenes eutrophus from butyric and pentanoic acids. *Appl Microbiol Biotechnol* **1988,** *28* (4-5), 330-334.

384. Laycock, B.; Halley, P.; Pratt, S.; Werker, A.; Lant, P., The chemomechanical properties of microbial polyhydroxyalkanoates. *Progress in Polymer Science* **2013,** *38* (3–4), 536-583.

385. Tiemeyer, A.; Link, H.; Weuster-Botz, D., Kinetic studies on autohydrogenotrophic growth of Ralstonia eutropha with nitrate as terminal electron acceptor. *Appl Microbiol Biotechnol* **2007,** *76* (1), 75-81.

386. Bernhard, M.; Benelli, B.; Hochkoeppler, A.; Zannoni, D.; Friedrich, B., Functional and Structural Role of the Cytochrome b Subunit of the Membrane-Bound Hydrogenase Complex of Alcaligenes Eutrophus H16. *European Journal of Biochemistry* **1997,** *248* (1), 179-186.

387. Cramm, R., Genomic view of energy metabolism in Ralstonia eutropha H16. *J Mol Microbiol Biotechnol* **2009,** *16* (1-2), 38-52.

388. Sandler, S. I.; Orbey, H., On the thermodynamics of microbial growth processes. *Biotechnology and Bioengineering* **1991,** *38* (7), 697-718.

389. Grosz, R.; Stephanopoulos, G., Statistical mechanical estimation of the free energy of formation of E. coli biomass for use with macroscopic bioreactor balances. *Biotechnol Bioeng* **1983,** *25* (9), 2149-63.

390. Tanaka, K.; Ishizaki, A., Production of poly-d-3-hydroxybutyric acid from carbon dioxide by a two-stage culture method employing Alcaligenes eutrophus ATCC 17697T. *Journal of Fermentation and Bioengineering* **1994,** *77* (4), 425-427.